



IntechOpen

Ethanol and Glycerol Chemistry

Production, Modelling, Applications,
and Technological Aspects

*Edited by Rampal Pandey, Israel Pala-Rosas,
José L. Contreras and José Salmones*



Ethanol and Glycerol
Chemistry - Production,
Modelling, Applications,
and Technological Aspects

*Edited by Rampal Pandey, Israel Pala-Rosas,
José L. Contreras and José Salmones*

Published in London, United Kingdom

Ethanol and Glycerol Chemistry – Production, Modelling, Applications, and Technological Aspects

<http://dx.doi.org/10.5772/intechopen.102260>

Edited by Rampal Pandey, Israel Pala-Rosas, José L. Contreras and José Salmenes

Contributors

Patrick U. Okoye, Estefania Duque-Brito, Diego R. Lobata-Peralta, Jude A. Okolie, Dulce M. Arias, Joseph P. Sebastian, Lethiwe D. Mthembu, Anele Sibeko, Rishi Gupta, Nirmala Deenadayalu, Guilherme D. Machado, Jacqueline M. Ortega Bacicheti, Fábio Nishiyama, Vladimir F. Cabral, Donato Aranda, Manikandan Kanagasabai, Babu Elango, Preetha Balakrishnan, Jayachitra Jayabalan, Israel Pala-Rosas, Jose L. Contreras, José Salmenes, Ricardo López-Medina, Beatriz Zeifert, Naomi N. González-Hernández, Chakali Ayyanna, Kuppusamy Sujatha, Sujit Kumar Mohanthy, Jayaraman Rajangam, B. Naga Sudha, H. G. Raghavendra, Pietro Salvatori, Ali Amoushahi, Steven W. Stogner

© The Editor(s) and the Author(s) 2023

The rights of the editor(s) and the author(s) have been asserted in accordance with the Copyright, Designs and Patents Act 1988. All rights to the book as a whole are reserved by INTECHOPEN LIMITED. The book as a whole (compilation) cannot be reproduced, distributed or used for commercial or non-commercial purposes without INTECHOPEN LIMITED's written permission. Enquiries concerning the use of the book should be directed to INTECHOPEN LIMITED rights and permissions department (permissions@intechopen.com).

Violations are liable to prosecution under the governing Copyright Law.



Individual chapters of this publication are distributed under the terms of the Creative Commons Attribution 3.0 Unported License which permits commercial use, distribution and reproduction of the individual chapters, provided the original author(s) and source publication are appropriately acknowledged. If so indicated, certain images may not be included under the Creative Commons license. In such cases users will need to obtain permission from the license holder to reproduce the material. More details and guidelines concerning content reuse and adaptation can be found at <http://www.intechopen.com/copyright-policy.html>.

Notice

Statements and opinions expressed in the chapters are those of the individual contributors and not necessarily those of the editors or publisher. No responsibility is accepted for the accuracy of information contained in the published chapters. The publisher assumes no responsibility for any damage or injury to persons or property arising out of the use of any materials, instructions, methods or ideas contained in the book.

First published in London, United Kingdom, 2023 by IntechOpen

IntechOpen is the global imprint of INTECHOPEN LIMITED, registered in England and Wales, registration number: 11086078, 5 Princes Gate Court, London, SW7 2QJ, United Kingdom

British Library Cataloguing-in-Publication Data

A catalogue record for this book is available from the British Library

Additional hard and PDF copies can be obtained from orders@intechopen.com

Ethanol and Glycerol Chemistry – Production, Modelling, Applications, and Technological Aspects

Edited by Rampal Pandey, Israel Pala-Rosas, José L. Contreras and José Salmenes

p. cm.

Print ISBN 978-1-80355-717-5

Online ISBN 978-1-80355-718-2

eBook (PDF) ISBN 978-1-80355-719-9

We are IntechOpen, the world's leading publisher of Open Access books Built by scientists, for scientists

6,700+

Open access books available

180,000+

International authors and editors

195M+

Downloads

156

Countries delivered to

Our authors are among the
Top 1%

most cited scientists

12.2%

Contributors from top 500 universities



WEB OF SCIENCE™

Selection of our books indexed in the Book Citation Index
in Web of Science™ Core Collection (BKCI)

Interested in publishing with us?
Contact book.department@intechopen.com

Numbers displayed above are based on latest data collected.
For more information visit www.intechopen.com



Meet the editors



Dr. Rampal Pandey is currently a senior Assistant professor in the Department of Chemistry, National Institute of Technology Uttarakhand. He has been a DST Inspire Faculty member for the Department of Science and Technology (DST) under “Innovation in Science Pursuit for Inspired Research” (INSPIRE) program, a Research Associate, and a junior (JRF) and senior research fellow (SRF). He obtained BSc and MSc degrees from APS University, India, and a Ph.D. from Banaras Hindu University (BHU), India. He has more than 15 years of teaching and research experience. He has research/academic projects worth ~50 Lakhs (INR) and thirteen awards/recognitions/appreciations to his credit, including an Inspired Teacher Award. Dr. Pandey has published more than fifty-five papers and has been granted two patents. He has delivered many invited lectures at national and international seminars/Faculty Development Programmes (FDPs)/Short Term Courses (STCs). Dr. Pandey serves as a coordinator for Massive Open Online Courses (MOOCs) and a content writer for the e-PG-Pathshala programme of the Ministry of Education. He is a member of the American Chemical Society, Royal Society of Chemistry, Society of Material Chemistry, Solar Energy Society of India, and Indian Society of Chemists and Biologists. He is a section and academic editor as well as a reviewer for several journals. He is also a Ph.D. supervisor.



Israel Pala-Rosas is a biochemical engineer. He obtained a master's degree in Chemical Engineering from the Benemérita Universidad Autónoma de Puebla, México, and a Ph.D. in Chemical Engineering Science from the School of Chemical Engineering and Extractive Industries, Instituto Politécnico Nacional, México. Dr. Pala-Rosas has experience in production and quality in the canned food and beverage industry, as well as in the processing of triglycerides for the production of soap and biodiesel. He has been a professor at different universities and a thesis co-director for undergraduate and master's students at Universidad Autónoma Metropolitana, México. His interests include the research and development of catalytic and biotechnological processes for the transformation of biomass-derived molecules to compounds of technological and industrial interest. He focuses his work on the synthesis, characterization, and testing of catalysts, as well as the design and analysis of chemical and biochemical reactors. Areas related to the catalytic processes, such as chemical thermodynamics, unit operations, and economics, are also under his scope. Dr. Pala-Rosas has published research articles on the use of zeolites for the synthesis of pyridine bases from acrolein and ammonia, the catalytic dehydration of glycerol to acrolein, heterogeneous catalysts for biodiesel synthesis, and biomaterials. He is the author of a book chapter dealing with the production of acrolein from glycerol and the editor of the book *Current Drying Processes*.



José Luis Contreras Larios obtained a Ph.D. in Sciences from the Universidad Autónoma Metropolitana- Iztapalapa, México, as well as master's and engineering degrees in Chemical Engineering from the School of Chemical Engineering and Extractive Industries, Instituto Politécnico Nacional, México. Dr. Contreras has more than 40 years of industrial and research experience in heterogeneous catalysis. Currently, he is a research professor and head of the Chemical Industry Processes curriculum of the Chemical Engineering Program, Energy Department, Universidad Autónoma Metropolitana-Azcapotzalco, México, where he teaches undergraduate and postgraduate courses on catalytic materials, chemical reactors, transport phenomena, unit operations, and process engineering. He has also directed undergraduate and postgraduate theses on chemical engineering topics such as chemical reactors, catalysis, and process and environmental engineering. Dr. Contreras is the author of several patents and internationally indexed articles. His research and application areas are focused on the synthesis and characterization of catalysts for processes in chemical and environmental engineering, such as the production of niacinamide from glycerol, hydrogen synthesis by bioethanol and glycerol reforming, fixation of CO₂ emissions from thermoelectric power plants using algae, and the design of catalytic converters for diesel and gasoline machines. He is a level I member of the National System of Researchers in Mexico.



José Salmenes obtained a master's in Chemical Engineering and a doctorate in Science from the Universidad Autónoma Metropolitana-Iztapalapa, México. He obtained a degree in chemical engineering from the Universidad Veracruzana, México. Dr. Salmenes has taught countless courses in the Postgraduate Studies and Research Section of the School of Chemical Engineering and Extractive Industries of the Instituto Politécnico Nacional, México, since 2004. Previously, he held various positions at the Instituto Mexicano del Petróleo and at the Universidad Autónoma Metropolitana. He is the author of sixty-five internationally indexed articles, co-author of a published book, author of two book chapters and twenty-seven registered patents. He has 217 papers in national and international forums to his credit. He has supervised eighteen bachelor's, ten master's, and two doctorate theses. He is a level II member of the National System of Researchers in Mexico. His current research deals with the synthesis and application of catalysts and nanostructured materials for the synthesis and storage of hydrogen and carbon dioxide.

Contents

Preface	XI
Section 1	
Production of Ethanol and Glycerol	1
Chapter 1	3
Ethanol Production from Bioresources and Its Kinetic Modeling: Optimization Methods <i>by Manikandan Kanagasabai, Babu Elango, Preetha Balakrishnan and Jayachitra Jayabalan</i>	
Chapter 2	17
Catalysis for Glycerol Production and Its Applications <i>by Anele Sibeko, Lethiwe D. Mthembu, Rishi Gupta and Nirmala Deenadayalu</i>	
Chapter 3	37
Bioethanol Production <i>by Chakali Ayyanna, Kuppusamy Sujatha, Sujit Kumar Mohanthy, Jayaraman Rajangam, B. Naga Sudha and H.G. Raghavendra</i>	
Section 2	
Conversion of Glycerol into Aromatic Compounds	47
Chapter 4	49
Sustainable Synthesis of Pyridine Bases from Glycerol <i>by Israel Pala-Rosas, José L. Contreras, José Salmenes, Ricardo López-Medina, Beatriz Zeifert and Naomi N. González Hernández</i>	
Chapter 5	65
Catalytic Conversion of Glycerol to Bio-Based Aromatics <i>by Patrick U. Okoye, Estefania Duque-Brito, Diego R. Lobata-Peralta, Jude A. Okolie, Dulce M. Arias and Joseph P. Sebastian</i>	

Section 3	
Applications	83
Chapter 6	85
Ethanol Inhalation in Treatment and Prevention of Coronavirus Disease (COVID-19)	
<i>by Ali Amoushahi</i>	
Chapter 7	99
Nebulized Ethanol: An Old Treatment for a New Disease	
<i>by Steven W. Stogner</i>	
Chapter 8	117
Theoretical Bases for the Disinfection of the SARS-CoV-2-Contaminated Airways by Means of Ethanol Inhalation	
<i>by Pietro Salvatori</i>	
Chapter 9	135
Ethanol as a Subgroup of the UNIFAC Model in the Prediction of Liquid-Liquid Equilibrium in Food and Fuel Systems	
<i>by Jacqueline M. Ortega Bacicheti, Guilherme D. Machado, Fábio Nishiyama, Vladimir F. Cabral and Donato Aranda</i>	

Preface

In the wake of more stringent health and environment concerns, the world requires more and clearer awareness about the production of valuable chemicals from bio-resources or natural products as well as the use of these natural products in areas of health and environment. With this objective in mind, *Ethanol and Glycerol Chemistry – Production, Modelling, Applications, and Technological Aspects*, discusses the green production of ethanol and glycerol by feasible methods and their possible applications in medical sciences and for environmentally friendly fuel production via a practical approach and appropriate modelling.

The book is organized into three sections and nine chapters contributed by authors from around the globe. Section 1, “Production of Ethanol and Glycerol”, is an introductory section that includes three chapters. Chapter 1 by Manikandan Kanagasabai et al., focuses on the production of ethanol from bioresources. Chapter 2 by Chakali Ayyanna et al., discusses the production of bioethanol. Chapter 3 by Lethiwe D. Mthembu et al., illustrates the catalyzed production and applications of glycerol.

Section 2, “Conversion of Glycerol into Aromatic Compounds”, focuses on the transformation of glycerol into valuable organic products and includes two chapters. Chapter 4 by Israel Pala-Rosas et al., describes the synthesis of pyridine bases from glycerol using sustainable methods. Chapter 5 by Patrick U. Okoye et al., deals with the preparation of bio-based aromatics via catalytic transformation of glycerol.

Section 3, “Applications”, includes four chapters on applications of ethanol in medical sciences. Chapter 6 by Ali Amoushahi et al., illustrates the utility of ethanol inhalation in the treatment and prevention of COVID-19. Chapter 7 by Steven W. Stogner et al., focuses on the use of an old treatment, nebulized ethanol, for a new disease. Chapter 8 by Pietro Salvatori et al., theoretically describes the utility of ethanol inhalation for the disinfection of SARS-COV-2-contaminated airways. Finally, Chapter 9 contributed by Guilherme D. Machado et al., illustrates the modelling of Ethanol to predict the Liquid-Liquid Equilibrium in Food and Fuel Systems.

We congratulate all the authors for providing quality data, research, and analysis and participating in this volume. We would like to thank the staff at IntechOpen, especially Author Service Managers Ms. Marija Nezirovic, Ms. Martina Ivancic, Ms. Nika Karamatic, and Ms. Ana Javor.

Dr. Rampal Pandey
Department of Chemistry,
National Institute of Technology Uttarakhand,
Srinagar (Garhwal), Uttarakhand, India

Israel Pala-Rosas and José Salmones
Higher School of Chemical Engineering and Extractive Industries,
National Polytechnic Institute,
Mexico City, Mexico

José L. Contreras
CBI-Energy,
Autonomous Metropolitan University-Azcapotzalco,
Mexico City, Mexico

Section 1

Production of Ethanol and Glycerol

Chapter 1

Ethanol Production from Bioresources and Its Kinetic Modeling: Optimization Methods

*Manikandan Kanagasabai, Babu Elango,
Preetha Balakrishnan and Jayachitra Jayabalan*

Abstract

Ethanol is viable alternative fuel and its substitute to fossil fuel has gained importance with rise in fuel prices. The chapter elaborates about methods of production from different types of bio resources like molasses, starch and cellulose commercially. The chapter also details about different methods of pretreatment for cellulosic and starchy raw materials. This also includes hydrolysis using acid and enzymes. The modes of ethanol fermentation using bioreactors like batch fed batch and continuous operation will be discussed. The growth kinetics models like monod logistic model will be elaborated. The product formation growth associated models like Leudiking pirt model and parameter estimation methods will be described. Optimization of process variables using response surface methodology and media optimization using PB design will be elaborated. The application of ANN in modeling will be described.

Keywords: ethanol production, growth and product kinetics, optimization response, surface methodology, PB design ANN

1. Introduction

Biomass energy can contribute to sustainable development and plays a significant role in reducing greenhouse gas emissions. In addition, application of agro-industrial residues in bioprocesses not only provide alternative substrates but also helps solve their disposal problem. The transfer of crude oil-based refinery to biomass-based bio refinery has attracted strong scientific interest which focuses on the development of bioethanol as an alternative transportation fuel to petroleum fuels. A huge ethanol demand will come in the near future, forcing the ethanol production to be fast and have high capacity. [1, 2]. Green fuel from bioresources is gaining more importance to meet the increasing demand of fuel supply and reduced emission of pollutant gases like sulfur dioxide [3]. The major biomass resources that can be converted into biofuels are classified into three major types of carbohydrates namely glucose, starch and cellulose [4]. Pre-treatment steps are more vital in conversion of starchy and

cellulosic substrates that are cheaper and available in plenty. Optimization techniques like artificial neural network, response surface methodology can be effectively used to improve the yield of biofuel from these substrates.

The biggest challenge of the conversion comes from the recalcitrant structure of lignocellulosic biomass. To improve the biomass digestibility, a pre-treatment step is required to break up the lignocellulosic matrix, thus making the carbohydrate fraction more accessible to hydrolytic enzymes for fermentable sugar production. Pre-treatment of lignocelluloses is intended to disorganize the crystalline structure of macro- and microfibrils, in order to release the polymer chains of cellulose and hemicellulose to improve its digestibility and easy access for microbial attack [5] and/or modify the pores in the material to allow the enzymatic hydrolysis [6]. This leads to the fractionation of three components and opening of cellulose structure. It results in enlargement of the inner surface area of substrate particles, accomplished by partial solubilization and/or degradation of hemicellulose and lignin [7].

The bioconversion of starchy substrates like corn, cassava, potatoes, involves pre-treatment with fungal α amylase at suitable temperature followed by saccharification and fermentation. The last two steps can also be carried out in a single fermenter by a process called simultaneous saccharification and fermentation using amylolytic enzyme and yeast at optimum conditions of pH and temperature. This process reduces substrate inhibition and maximum utilization of glucose formed by amylolytic enzymes. Cellulose from different biomass like paper pulp, sulfite waste liquor etc. must undergo pre-treatment with mineral acids or alkali to remove lignin and hemicellulose. Cellulose can be converted into simple sugars by the action of cellulase enzyme and can readily ferment them to ethanol by the action of yeast. [8]. Although lignocellulosic biomass is a very promising alternative feedstock for ethanol production, its conversion to ethanol is more difficult than that of sugar or starch.

Mathematical models are tools that can be applied to biotechnological processes operating at many different levels, from the action of an enzyme within a cell, to the growth of that cell within a commercial scale bioreactor [9]. Unstructured kinetic models give the most fundamental observations concerning microbial metabolic processes and can be considered a good approximation when the cell composition is time dependent or when the substrate concentration is high compared to the saturation constant [10]. In addition to kinetic models describing the behavior of microbiological systems, artificial neural network (ANN) and Response Surface Methodology (RSM) are effectively used for the optimization of process variables for the fermentation of bioethanol [11, 12].

This chapter will focus on the current status of available ethanol production technologies including chemistry, applications, technological aspects and the kinetics and modeling of biotechnological processes and it especially provides essential evidence for the future scale-up conversion studies.

2. Industrial ethanol production

2.1 Ethanol production from corn

Corn is the most viable source for industrial ethanol production as it contains 70% starch. 5% of annual food grains produced can be effectively diverted to ethanol production [13]. The major threat that poses corn as an effective substrate is the horny endosperm that makes it difficult for pretreatment with α amylase enzyme with

low conversion. Floury endosperm is easy to digest with enzymes and has high swelling when compared with horny endosperm.

The steps involved in the industrial production are

- i. Milling of corn grains to remove oil from germs and the hull that reduces the activity of amylase enzyme in pre-treatment step.
- ii. Liquefaction of milled corn starch using alpha amylase enzyme at optimum conditions of pH and temperature.
- iii. Saccharification of liquified starch using glucoamylase enzyme to convert dextrin to glucose which is primary substrate for ethanol producing yeast.
- iv. Fermentation of saccharified starch using *Saccharomyces cerevisiae* yeast at optimum conditions of pH and temperature with suitable initial substrate concentration to yield ethanol.
- v. Distillation of the product to yield 95% ethanol which forms an azeotrope with water. Azeotropic distillation is employed to separate water and to form 100% pure industrial alcohol.

2.2 Milling of grains

The two main processes that are employed in milling of grains are wet milling and dry milling of corn grains.

2.2.1 Wet milling process

The wet milling of corn grains is a very expensive process as it is highly energy consuming. The valuable by-products can be obtained in this process and it is generally used in biorefineries. The by-products obtained from the wet milling process are corn oil from germs, hull, fibers and gluten. Gluten along with corn meal is used as high protein content animal feed [14]. The main product starch solution obtained from this process is used as raw material for saccharification and fermentation processes. The ethanol yield from this process is about 10 liters per 100 kg of corn used as substrate.

2.2.2 Dry milling

Dry grinding process is currently employed in industries as it is less energy intensive when compared with wet milling process [15]. Corn grains are powdered using a hammer mill to pass through a 30 mesh screen and mixed with water to form mash. The mash is first liquefied using alpha amylase enzyme at an initial pH 6 and temperature of 90°C then saccharified with glucoamylase enzyme and fermented with yeast to produce ethanol [16]. The fermented liquid is distilled to produce industrial grade ethanol. The by-product obtained is distiller's grain used as an animal feed stock and carbon dioxide.

2.3 Liquefaction

Starchy substrates cannot be utilized directly by yeast, and they are to be converted into maltose and dextrin in the first pretreatment step. A thermostable

alpha-amylase enzyme is usually employed for converting the starch to dextrin quickly and randomly by hydrolyzing alpha 1–4 bonds of starch molecule. The optimum temperature and pH greatly depends upon the source of alpha amylase enzymes [17]. Microbial sources of alpha amylase includes both bacteria and fungus. Alpha amylase derived from fungi are mostly employed as they are more active at higher temperature in range of 80 to 90°C [18]. The optimum pH is in the range of 5.5- as the activity of the enzyme is maximum. The higher temperature favors the liquefaction of starch by rupturing the molecules and aiding the enzyme molecules to cleave the branching bonds of it. This process is carried out in holding tubes by adding fungal diastase enzyme in excess for a period of 30 minutes.

2.4 Saccharification and fermentation of starch

Liquified starch is converted into simple sugars by saccharification process. Glucoamylase enzyme is generally employed for this process. The optimum temperature is usually 50 to 55°C and pH is 4.5. Glucoamylase attacks the linear chain 1–6 linkages of dextrin and convert them into simple sugars [19]. Saccharified starch is suitable substrate for fermentative production of ethanol by yeast. Thermotolerant yeast can be used for carrying out saccharification and fermentation process in a single step. Optimization of process variables and nutrients is most important to maximize the ethanol yield. Response surface methodology can be employed to carry out optimization statistically by carefully designing the experiments. The RSM yields best combination of pH, temperature, initial starch concentration and enzyme concentration that give maximum ethanol concentration in the fermenter [20]. The interactive effects of process variables can be analyzed very effectively in the single step simultaneous saccharification and fermentation process. Optimization is essential because enzymes are active in a range of temperature and pH that may or may not favor the growth of yeast [21, 22]. Generally, thermotolerant yeast can withstand the temperature that favors optimum activity of glucoamylase enzyme that can produce simple sugars from dextrin and are consumed by yeast to produce ethanol. Optimum pH and temperature for this process are generally pH 5 and 37°C respectively as reported by many researchers [23, 24]. High temperature also favors reduced contamination of fermentation broth. They also reduces the inhibitive effect of high glucose concentration for yeast as it is simultaneously consumed giving 8 to 10% concentration of ethanol in the broth.

2.5 Modes of ethanol fermentation

Three different modes of fermentation that are generally used in commercial production are batch, fed batch and continuous operation. Ethanol production is usually carried out in batch fermenters [25]. The advantages of batch fermentation are mainly effective sterilization of medium and fermenter vessel, reduced contamination risk, maintaining required concentration of microbes for fermentation, effective control of process parameters like pH, temperature agitation speed to maximize the ethanol concentration in the broth. The usual fermentation time for ethanol production using yeast is about 48 hours. The additional feature is simultaneous saccharification and fermentation can be carried out most effectively in a single fermenter in batch mode by controlling the process variables at optimum conditions of pH, temperature and agitation speed. Continuous mode of operation is also employed for production of ethanol using beer still, by maintaining the microbes

inside the still using high aspect ratio. The yeast concentration is more at the bottom of the still and the main advantage is that agitation is not required and continuous production of ethanol is feasible [26].

2.6 Production of absolute alcohol

Distillation is the process of separating the ethanol from the solids and water in the mash. The difference in boiling point of alcohol and water allows water to be separated from ethanol by heating in a distillation column. The maximum ethanol concentration in the top product of distillation column is 95% ethanol and 5% water. Azeotropic extractive distillation using benzene as third component produce absolute alcohol. Modern dry grind ethanol plants use a molecular sieve system to produce absolute (100%, or 200 proof) ethanol.

The bottom product containing fiber, oil, and protein components of the grain, as well as the non-fermented starch is used as feed stock for animals. Bottom product is further processed to remove insoluble solids using centrifuges or extruders. The liquid is decanted and part of it is recycled to the still. The remaining liquor is further concentrated by evaporation and mixed with solids and used as feed stock. The block diagram for ethanol production from corn is shown in **Figure 1**.

2.7 Ethanol production from molasses

Sugarcane is grown primarily for sucrose and molasses production. The crop may be harvested over an extended period of time due to its long growing season. Black

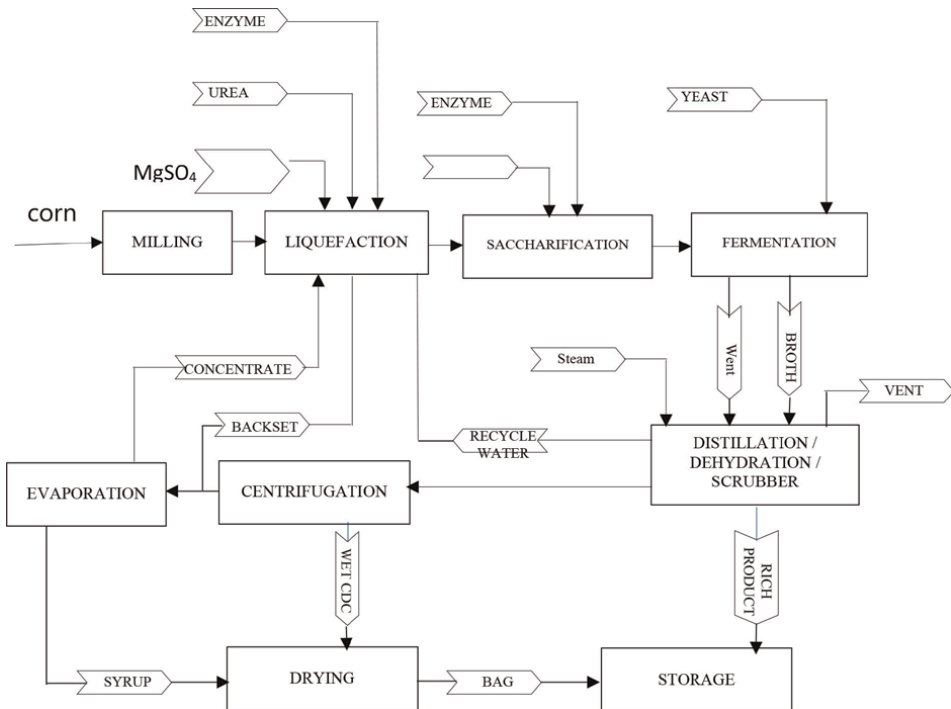


Figure 1.
Ethanol production from corn.

strap molasses is the by- product obtained from sugar mill and can be stored and easily diluted to a concentration of 10% reducing sugars [27]. The total sugar content of molasses is generally in the range of 50 to 60%. The fermentation of diluted molasses is carried out in batch fermenters using yeast as inoculum. The fermentation time is generally 20–24 and rate of ethanol production decreases as sugar utilized by the yeast is about 90–95%. The ethanol concentration in the broth is about 10% and does not increase above it as ethanol inhibits the yeast growth. The additional nitrogen nutrients like ammonium sulphate and micronutrients like magnesium sulfate, potassium hydrogen phosphate is added to favor the growth of yeast [28]. Ethanol production is always growth associated fermentation and hence it is desirable to optimize the process variables like temperature pH and agitation to maximize the yeast concentration and ethanol production. The overall productivity for this process is about 1.8–2.5 kg ethanol produced per m³ fermenter volume per hour [29]. **Figure 2** illustrates the steps required to produce ethanol from cane juice molasses.

2.8 Ethanol production from cellulose

Cellulose-based ethanol production is attractive as an alternative fuel in the transportation sector. Extensive research in the past 20 years on fuel-grade ethanol fermentation has answered most of the major challenges on the road to commercialization and also open the door for novel technological development [30].

The first step in this process is primarily removal of lignin and hemi cellulose present in the wood wastes by digestion using steam at very high pressure followed by hydrolysis of cellulosic substrate into glucose using sulfuric acid [31]. The final step is fermentation of the reducing sugar solution in a fermenter using yeast. Hydrolysis of

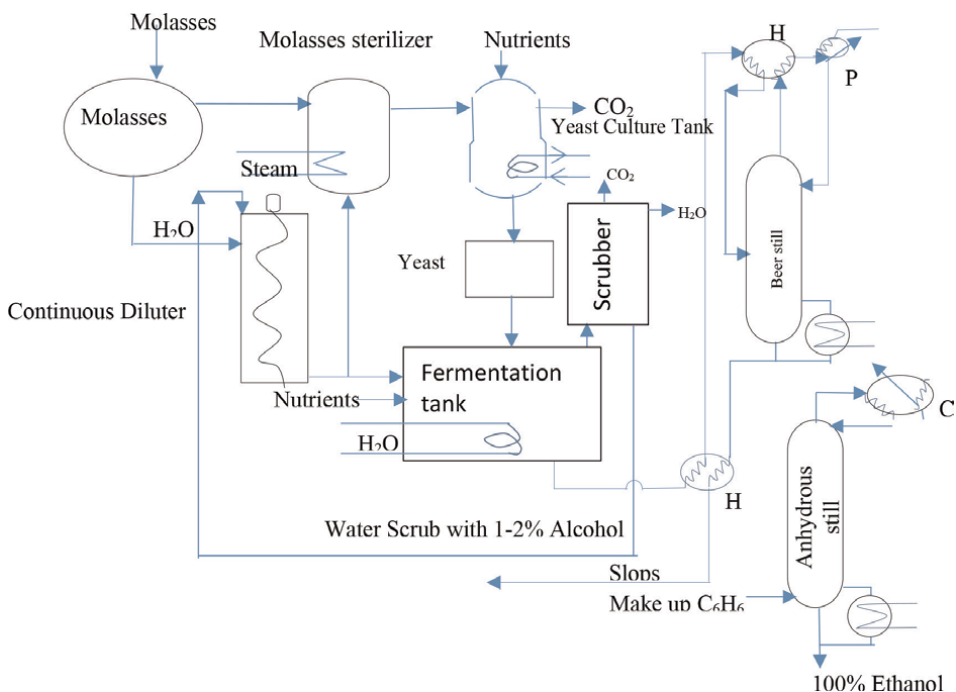


Figure 2.
Ethanol production from cane molasses.

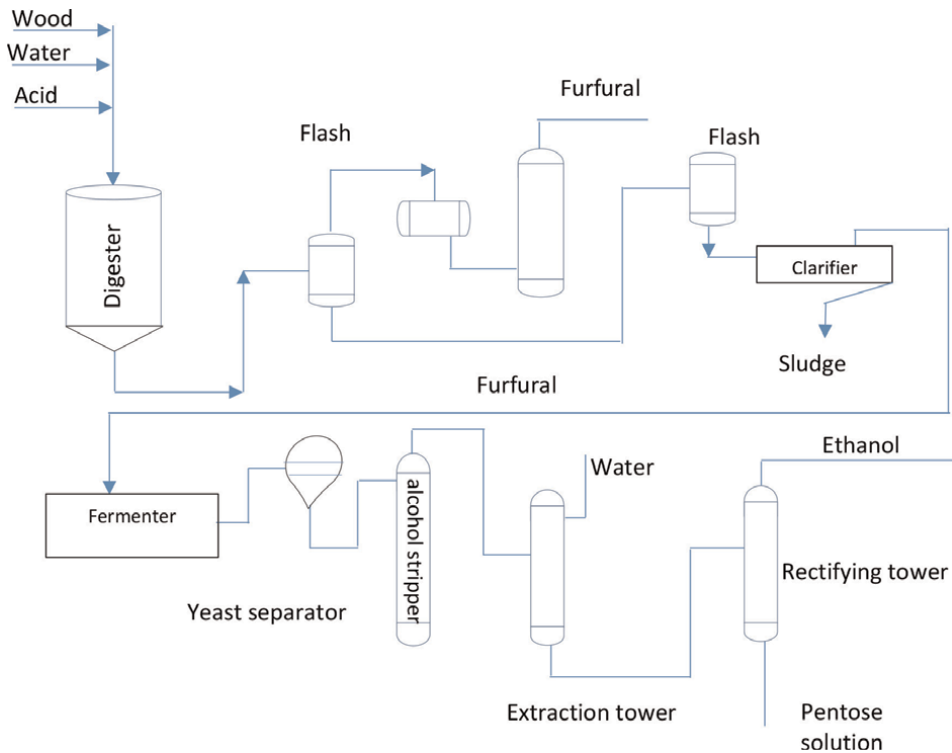


Figure 3.
Ethanol production from cellulose.

wood waste is carried out using sulfuric acid and steam at a temperature of 200°C and at a very high pressure of 1500 kPa. Lignin rich residue is removed as the bottom product and hydrolysate solution containing methanol and furfural is separated from the condenser of the flash vaporization process carried out in two different stages of different operating pressure, i.e., the first stage operating at 456.0 kPa and the second stage is at atmospheric pressure. The underflow of the second stage flash vaporizer is reducing sugar solution and it is diluted to desired concentration and fermented to ethanol using yeast. Methanol and furfural are separated using two stages of distillation.

The sugar rich solution is neutralized using lime and the precipitate is removed as sludge. The clarified liquid is added with additional micronutrients and fermented in a batch fermenter using yeast, The recovered yeast from an earlier fermentation is added to neutralized liquor and sent to fermentation tanks. The fermented liquor is filtered or centrifuged to remove the yeast content. Ethanol is separated from the distillation column as top product containing 95 vol.%. The bottom product contains unfermented pentoses. **Figure 3** shows the flow sheet of industrial ethanol production form cellulose.

3. Modeling

Mathematical models are very much useful to describe the performance of enzymatic and fermentation processes. They can be applied to study the kinetics of

enzyme catalyzed reactions, microbial growth in batch fermentation and product formation. These models fit the experimental data and can be modified effectively to find out the inhibiting parameters that affects the growth of microbes or activity of enzymes or rate of product formation [32]. The kinetic models are used in designing the batch fermenter suitable for ethanol production. In addition to kinetic models describing the behavior of microbiological systems, modeling based on combining the effects of various parameters namely time, temperature, and concentration into one single parameter is also used to develop a linear model expressing the relationship between ethanol production and variables like pH, temperature, and initial concentration of substrate. Artificial Neural Network (ANN) and Response Surface Methodology (RSM) are used for the optimization of process variables for the production of bioethanol [33].

3.1 Kinetic models

Kinetic models describing the behavior of microbiological systems can be a highly appreciated tool and can reduce tests to eliminate extreme possibilities. The kinetic parameters are obtained from the concentrations of biomass, products, and substrates consumed during the fermentation.

$$\mu = \frac{\mu_{\max} S}{K_s + S} \quad (1)$$

where μ_{\max} and K_s are the maximum specific growth rate and the Monod constant respectively.

3.1.1 Logistic growth model

$$x = \frac{x_o e^{kt}}{1 - \beta x_o (1 - e^{kt})} \quad (2)$$

Where x_o is the initial biomass concentration (g/l) and t is time (h).

3.1.2 Leudeking-Piret kinetic model - product formation kinetics

The rate of product formation is well described by an unstructured model. The kinetic expression, Leudeking-Piret equation, does fit the kinetic data of ethanol formation. Ethanol production is a growth associated product kinetics with significant α , the growth associated term [34].

$$p(t) - p_o - \beta \left(\frac{x_s}{k} \right) \left[1 - \frac{x_o}{x_s} (1 - e^{kt}) \right] = \alpha [x(t) - x_o] \quad (3)$$

3.1.3 Substrate utilization kinetics

$$-\frac{ds}{dt} = \frac{1}{Y_{x/s}} \frac{dx}{dt} + \frac{1}{Y_{p/s}} \frac{dp}{dt} + k_e x \quad (4)$$

where $Y_{x/s}$ and $Y_{p/s}$ are the yield coefficient for the biomass and product, respectively and K_e is the specific maintenance coefficient.

3.1.4 Yield of growth

To evaluate the model parameters and to relate the changes in substrate, cell mass and product concentrations, a Yield coefficient is introduced. The yield coefficients are related by the equation [35].

$$Y_{p/s} = Y_{x/s} Y_{p/x} \quad (5)$$

3.2 Experimental design, analysis and optimization using response surface methodology (RSM)

RSM is an empirical statistical technique employed for multiple regression analysis by using quantitative data obtained from properly designed experiments to solve multivariate equations simultaneously. The response surface, which is a two-dimensional graphic representation of the system's behavior, is used to determine the individual and cumulative effects of the variables and the mutual interactions between the variables on the dependent variable [36]. The graphic representations of the regression equation called the response surfaces. The quality of fit of the second order equation is expressed by the coefficient of determination R^2 , and its statistical significance is determined by F-test. The significance of each coefficient is determined using Student's t-test.

The application of statistical experimental design techniques in ethanol fermentation process development can result in improved production yields, reduced process variability, closer conformance of the output response (Ethanol yield) to nominal and target requirements and reduced development time and overall costs. The statistical design of experiments using central composite design can be effectively used to optimize the process variables like pH, temperature initial reducing sugar concentration to maximize the ethanol concentration [37]. The chosen independent variables used in this experiment are coded according to the Eq. (6):

$$x_i = \frac{X_i - X_o}{\Delta x} \quad (6)$$

where x_i is the coded value of the i^{th} variable, X_i is the uncoded value of the i^{th} test variable and X_o is the uncoded value of the i^{th} test variable at the centre point. The behavior of the system is explained by the following second-degree polynomial Eq. (7):

$$Y = \beta_o + \sum_{i=1}^k \beta_i X_i + \sum_{i=1}^k \beta_{ii} X_i^2 + \sum_{i=1}^{k-1} \sum_{j=2}^k \beta_{ij} X_i X_j \quad (7)$$

where Y is the predicted response, β_o is the offset term, β_i is the coefficient of linear effect, β_{ii} is the coefficient of squared effect and β_{ij} is the coefficient of interaction effect.

3.3 Artificial neural network analysis

Artificial Neural Network (ANN) is another important tool that has also been effectively used in modeling biotechnological process, majorly reduces time and

experimental readings required for modeling [38]. It is used to predict the degree of non-linearity and to learn complex analyses in various fields. RSM is used to analyze the data with least experimental data and gives a mathematical relation while ANN is a machine learning statistical approach that can be applied in a wide range of data analysis including optimization thereby estimates the response based on the trained data [39].

3.3.1 Analysis of model predictability in artificial neural network

Eqs. (8) and (9) indicates the Mean Squared Error (MSE) and RMSE, a widespread measure for model predictability in which the ANN output error between the actual and the predicted output can be evaluated [40]:

$$MSE = \frac{1}{n} \sum_{i=1}^n (y_i - y_{di})^2 \quad (8)$$

$$RMSE = MSE^{1/2} \quad (9)$$

where, n is the number of points, y_i is the predicted value obtained from the neural network model, y_{di} is the actual value.

The closer the R^2 value is to 1, the better the model fits to the actual data:

$$R^2 = 1 - \sum_{i=1}^n \left(\frac{(y_i - y_{di})^2}{(y_{di} - y_m)^2} \right) \quad (10)$$

where, n is the number of points, y_i is the predicted value from neural network model, y_{di} is the actual value, and y_m is the average of the actual values.

Absolute Average Deviation (AAD) in Eq. (11) is another significant index to evaluate the ANN output error between the actual and the predicted output:

$$\text{Absolute Average Deviation (AAD)} = \left\{ \left[\sum_{i=1}^n (|y_i - y_{di}| / y_{di}) \right] / n \right\} \times 100 \quad (11)$$

where, y_i and y_{di} are the predicted and actual responses, respectively, and n is the number of the points.

4. Conclusion

Industrial production of ethanol is viable from cheaper substrates like biomass, corn and molasses. The molasses from sugar manufacturing unit can be used as a raw material for ethanol production by fermentation. The starch present in the corn is also used as substrate after liquefaction and saccharification using enzymes. The cellulosic raw materials are cheaper but it is essential to pre-treat the biomass residue by digesting the lignin and hemicellulose using sulfuric acid before fermentation to ethanol. Optimization of process variables like pH, temperature substrate concentration and agitation speed for maximum ethanol production is effectively done using statistical tool response surface methodology and artificial neural network. The modeling and kinetics of ethanol production is the most important to design the suitable bioreactors. Microbial growth kinetics, product formation kinetics and substrate utilization kinetics are enumerated.

Author details


Manikandan Kanagasabai^{1*}, Babu Elango¹, Preetha Balakrishnan¹
and Jayachitra Jayabalan²

1 Faculty of Engineering and Technology Annamalai University, Department of Chemical Engineering, Bioprocess Laboratory, Annamalainagar, Tamilnadu, India

2 Faculty of Agriculture, Department of Agricultural Microbiology, Annamalai University, Annamalainagar, Tamilnadu, India

*Address all correspondence to: kmchemical_27@yahoo.co.in

IntechOpen

© 2022 The Author(s). Licensee IntechOpen. This chapter is distributed under the terms of the Creative Commons Attribution License (<http://creativecommons.org/licenses/by/3.0>), which permits unrestricted use, distribution, and reproduction in any medium, provided the original work is properly cited. 

References

- [1] Lynd LR, Wang MQ. A product nonspecific framework for evaluating the potential of biomass based products to displace fossil fuels. *Journal of Industrial Ecology*. 2004;**7**:17-32
- [2] Wang PY, Shopsis C, Schneider H. Fermentation of pentose by yeast. *Biochemical and Biophysical Research Communications*. 1980;**94**:248
- [3] Logsdon JE. Ethanol. In: Kirk RE, Othmer DF, et al., editors. *Encyclopedia of Chemical Technology*. New York: John Wiley & Sons, Inc.; 2006
- [4] Lin Y, Tanaka S. Ethanol fermentation from biomass resources: Current State and prospects. *Applied Microbiology and Biotechnology*. 2006; **69**:627-642
- [5] Alani F, Smith JE. Effect of chemical pretreatment on the fermentation and ultimate digestibility of bagasse by *Phanerochaete chrysosporium*. *Journal of the Science of Food and Agriculture*. 1988;**42**:19-28
- [6] Gable M, Zacchi G. A review of the production of ethanol from softwood. *Applied Microbiology and Biotechnology*. 2002;**59**(6):618-628
- [7] Pandey A, Soccol CR, Nigam P, Soccol VT. Biotechnological potential of agro-industrial residues. I Sugarcane bagasse. *Bioresource Technology*. 2006; **74**:69-80
- [8] Adams MR, Little CL, Easter MC. Modelling the effect of pH, acidulant and temperature on the growth rate of *Yersinia enterocolitica*. *The Journal of Applied Bacteriology*. 1991;**71**:65-71
- [9] Anjum MF, Tasadduq I, Al-Sultan K. Response surface methodology: A neural network approach. *European Journal of Operational Research*. 1997;**101**:65-73
- [10] Bailey JE. Kinetics of substrate utilization, product formation and biomass production in cell cultures. In: Bailey JE, editor. *Biochemical Engineering Fundamentals*. 3rd ed. New York: McGraw Hill Book Company; 1986
- [11] Goudar CT, Delvin JF. Nonlinear estimation of microbial and enzyme kinetic parameters from progress curve data. *Water Environment Research*. 2001;**73**:260-265
- [12] Shapouri HJ, Duffield A, Graboski MS. Energy balance of corn ethanol revisited. In: ASAE (ed) *Conference proceedings liquid fuel conference*. ASAE, St. Joseph. 1996. pp. 253-259
- [13] Chandel AK, Es C, Rudravaram R, Narasu ML, Rao LV, Ravindra P. Economics and environmental impact of bioethanol production technologies: An appraisal. *Biotechnology and Molecular Biology Reviews*. 2007;**2**: 14-32
- [14] Duggleby RG, Wood C. Analysis of progress curves for enzyme catalyzed reactions. *The Biochemical Journal*. 1989;**258**:397
- [15] Contois DE. Kinetics of bacterial growth: Relationship between population density and specific growth of continuous culture. *Journal of General Microbiology*. 1959;**21**:40-50
- [16] Chen H, Jin S. Effect of ethanol and yeast on cellulase activity and hydrolysis of crystalline cellulose. *Enzyme and Microbial Technology*. 2006;**39**: 1430-1432

- [17] Egli T. The ecological and physiological significance of the growth of heterotrophic microorganisms with mixture of substrates. In: Jones JG, editor. *Advances in Microbial Ecology*. Vol. 14. New York: Plenum Press; 1995. pp. 305-386
- [18] Gibson AM, Bratchell N, Roberts TA. The effects of sodium chloride and temperature on the rate and extent of growth of *Clostridium botulinum* type A in pasteurized pork slurry. *The Journal of Applied Bacteriology*. 1987;**62**: 479-490
- [19] Hahn-Hagerdal B, Galbe M, Gorwa-Grauslund MF, Liden G, Zacchi G. Bio-ethanol the fuel of tomorrow from the residues of today. *Trends in Biotechnology*. 2006;**24**: 549-556
- [20] Kanagasabai M, Maruthai K, Thangavelu V. Simultaneous saccharification and fermentation and factors influencing ethanol production in SSF process. In: *Alcohol Fuels - Current Technologies and Future Prospect*. London, United Kingdom: IntechOpen; 2019 [Online]. Available from: <https://www.intechopen.com/chapters/67972>. DOI: 10.5772/intechopen.86480
- [21] Manikandan K, Rengadurai S, Babu E, Sothivanan S. Optimization studies in simultaneous saccharification and fermentation of wheat bran flour into ethanol. *Food and Nutrition Sciences*. 2022;**13**:463-470. DOI: 10.4236/fns.2022.135034
- [22] Hamelinck CN, van Hooijdonk G, Faaij APC. Ethanol from lignocellulosic biomass: Techno-economic performance in short-middle and long-term. *Biomass and Bioenergy*. 2005;**28**:384-410
- [23] McMeekin TA, Chandler RE, Doe PE, Garland CD, Olley J, Putro S, et al. Model for combined effect of temperature and salt concentration/water activity on the growth rate of *Staphylococcus xylosus*. *Journal of Applied Bacteriology*. 1987;**62**: 543-550
- [24] Keim CR. Technology and economics of fermentation alcohol - An update. *Enzyme and Microbial Technology*. 1983;**5**:103-114
- [25] Haykin S. *Neural networks: A comprehensive foundation*. New Jersey: Prentice Hall; 1994
- [26] Rittmann BE, McCarty PL. Evaluation of steady-state-biofilm kinetics. *Biotechnology and Bioengineering*. 1980;**22**:2359-2373
- [27] Jeffries TW, Jin YS. Ethanol and thermotolerance in the bioconversion of xylose by yeasts. *Advances in Applied Microbiology*. 2000;**47**:221-268
- [28] Kovarova-Kovar K, Egli T. Growth kinetics of suspended microbial cells: From single-substrate-controlled growth to mixed substrate kinetics. *Microbiology and Molecular Biology Reviews*. 1998;**62**:646-666
- [29] Nielson J, Villadsen J. Structured modelling of a microbial system. III. Growth on mixed substrates. *Biotechnology and Bioengineering*. 1991;**38**:24
- [30] Penfold W, Norris D. The relation of concentration of food supply to generation time bacteria. *The Journal of Hygiene*. 1912;**12**:527-531
- [31] Schmidt SK, Alexander M, Shuler ML. Predicting threshold concentrations of organic substrates for bacterial growth. *Journal of Theoretical Biology*. 1985;**114**:1-8

- [32] Simkins S, Alexander M. Nonlinear estimation of the parameters of monod kinetics that best described mineralization of several substrate concentrations by dissimilar bacterial densities. *Applied and Environmental Microbiology*. 1985;**50**:816-824
- [33] Smith MR, Ewing M, Ratledge C. The interactions of various aromatic substrates degraded by *Pseudomonas* sp. NCIB 10643: Synergistic inhibition of growth by two compounds that serve as growth substrates. *Applied Microbiology and Biotechnology*. 1991;**34**:536-538. DOI: 10.1007/BF00180584
- [34] Sutherland JP, Bayliss AJ, Roberts TA. Predictive modelling of growth of *Staphylococcus aureus*: The effects of temperature, pH and sodium chloride. *International Journal of Food Microbiology*. 1994;**12**:217-236
- [35] Tan Y, Wang Z, Marshall KC. Modelling substrate inhibition of microbial growth. *Biotechnology and Bioengineering*. 1996;**52**:602
- [36] Tros ME, Schraa G, Zehnder AJB. Transformation of low concentrations of 3-chlorobenzoate by *Pseudomonas* sp. strain B13: Kinetics and residual concentrations. *Applied and Environmental Microbiology*. 1996;**62**:437-442
- [37] Wang M, Saricks C, Wu M. FUEL-cycle Fossil Energy Use and Greenhouse Gas Emissions of Fuel Ethanol Produced from U.S Midwest Corn. Argonne: Argonne National Laboratory for Illinois Department of Commerce and Community Affairs; 1997. pp. 24-28
- [38] Wijtzes T, McClure PJ, Zwietering MH, Roberts TA. Modelling bacterial growth as a function of water activity, pH and temperature. *International Journal of Food Microbiology*. 1992;**18**:139-149
- [39] Overend RP, Chornet E. Fractionation of lignocellulosics by steam-aqueous pretreatments. *Philosophical Transactions of the Royal Society of London*. 1987;**321**:523-536
- [40] Arellano-Plaza M, Herrera-López EJ, Díaz-Montaño DM, Moran A, Ramírez-Córdova JJ. Unstructured kinetic model for tequila batch fermentation. *International Journal of Mathematics and Computers in Simulation*. 2007; **1**(1):1-6

Chapter 2

Catalysis for Glycerol Production and Its Applications

*Anele Sibeko, Lethiwe D. Mthembu, Rishi Gupta
and Nirmala Deenadayalu*

Abstract

Globally, there is a climate change due to greenhouse gases, hence the production processes for chemicals should comply with green chemistry principles to decrease the impact it has on the climate. This book chapter focuses on the catalytic production of glycerol, which is a platform chemical that is widely used in the manufacture of various industrially important chemicals and derivatives, namely 2,3-dihydroxypropanal, glycerol ether, glycerol ester, acrolein, 1,2-propanediol and glycidol. The literature reviewed compares the production of glycerol using homogeneous and heterogeneous catalysts, to determine efficient and environmentally benign glycerol catalysts and to study glycerol as a platform chemical and its value in application.

Keywords: catalysis, homogenous catalysts, heterogeneous catalysts, value-added compounds, glycerol production

1. Introduction

The enormous growth in demand for fuels, along with growing environmental concerns and limited raw oil sources has increased the use of renewable energy. Biodiesel is one of the potential alternatives, and renewable fuels, has gained popularity in recent years, and their production capacity have grown significantly.

It is produced through various methods such as the transesterification of non-edible and waste vegetable oils with methanol and efforts are also being made to utilise the glycerol by-product to compensate the production cost of biodiesel to make it commercially viable, yielding quite significant percentage of a glycerol by-product which lowers the production cost and makes it commercially available. For every 4 litres of biodiesel generated [1].

Around 500 grams of glycerol is made, this equates to approximately 11,500 tons of 99.9% pure glycerine produced by a plant with a capacity of 113,562,354 million litres per year. The resulting oversupply of raw glycerol from biodiesel production can influence the purified glycerol market significantly as glycerol is a high-value and commercial chemical with thousands of applications [2].

Although extensive research has been carried out on the use of glycerol for various industrial applications, however, a compilation review on different approaches of glycerol production using homogenous and heterogeneous catalysts is scarce. The

present chapter focuses on compiling different state-of-the-art in glycerol manufacturing techniques with a special emphasis on homogeneous and heterogeneous catalysis approaches. Moreover, an attempt has also been made to review the application of glycerol in the production of various platform chemicals preferably using microbial pathways. A section has been dedicated on reviewing the application of glycerol in animal feed.

2. Glycerol production

Glycerol can be manufactured using a variety of chemical synthesis feedstocks. It can be produced, for example, by propylene synthesis by several methods [3], such as oil hydrolysis, or transesterification of fatty acids or oils. The following sections describe briefly about different glycerol production processes.

2.1 Glycerol production by propylene

As previously stated, several methods for producing glycerol from propylene can be used [4, 5]. In **Figure 1**, one of the major processes is shown, which includes the use of chlorination (Cl_2) [6].

2.1.1 Glycerol production via chlorination process

Propylene chlorination (**Figures 1 and 2**) produces allyl chloride at a temperature of 510°C in the presence of hypochlorous acid at 38°C . Glycerine dichlorohydrin is formed when allyl chloride reacts. The glycerol dichlorohydrin is then hydrolysed by sodium carbon oxide in a 6% sodium carbonate solution at 96°C or directly to glycerine, the epichlorohydrin being removed as an overhead in a stripping column. Finally, the epichlorohydrin is hydrated to glycerine using sodium hydroxide [4], resulting in a final glycerol yield of around 90% [6].

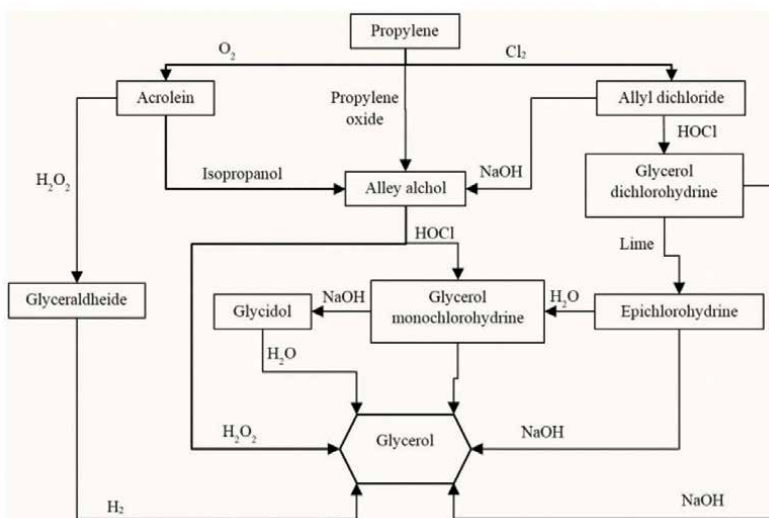


Figure 1. Flow diagram illustrating the production of glycerol from propylene [6].

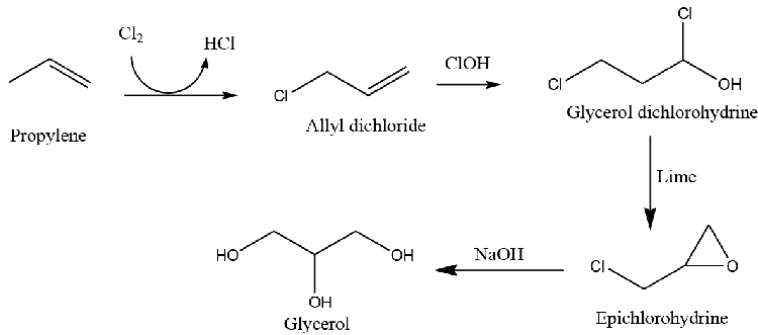


Figure 2.
 Reaction of the propylene chlorination process.

2.1.2 Glycerol production via oxygenation process

Figure 3 illustrates two paths to produce glycerol from propylene via oxygenation. Oxygen (O₂) reacts with propylene to produce acrolein, adding an aldehyde (HC=O). Acrolein can be converted to allyl alcohol with a reducing agent sodium borohydride (NaBH₄) in a presence of isopropanol as a solvent; peroxide is added to allyl alcohol to produce glycerol. In the other reactions, peroxide is added to acrolein which results in the formation of glyceraldehyde; the glyceraldehyde reacts with hydrogen to produce glycerol.

2.2 Saponification

In this reaction, sodium hydroxide (base) reacts with triglyceride as an ester to form glycerol and soap molecules. This method has been employed since 2800, and the first industrial factory was developed in 1860 [7]. As demonstrated in **Figure 4**, this reaction occurs between triglyceride and sodium hydroxide (caustic soda), producing glycerol and soap [6, 8].

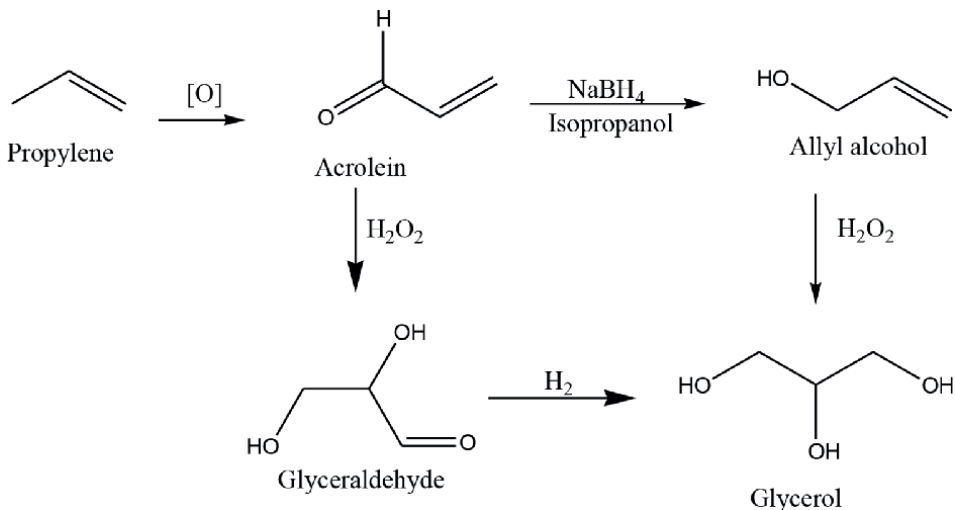


Figure 3.
 Production of glycerol from propylene oxygenation reaction.

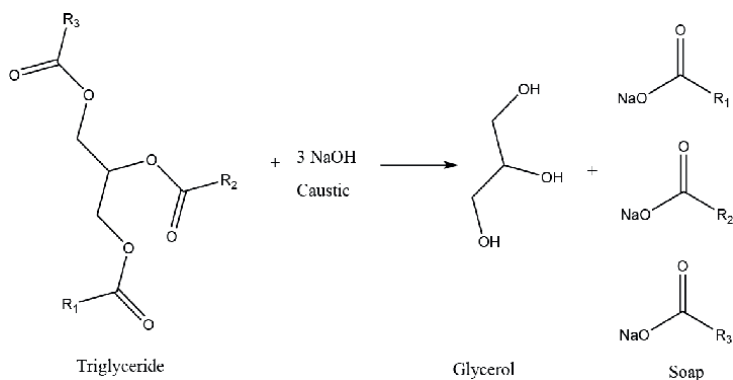


Figure 4. Illustrates the saponification reaction between triglyceride and sodium hydroxide (caustic soda) for the glycerol production [6].

2.3 Transesterification of the beaver oil

The transesterification reaction of beaver oil with ethanol to produce glycerol was carried out in 1864 [9, 10]. **Figure 5** shows the reaction in which methyl-esters from triglycerides (oils) and methanol (alcohol) combine to form glycerol and fatty esters (or biodiesel) [5, 6, 11, 12].

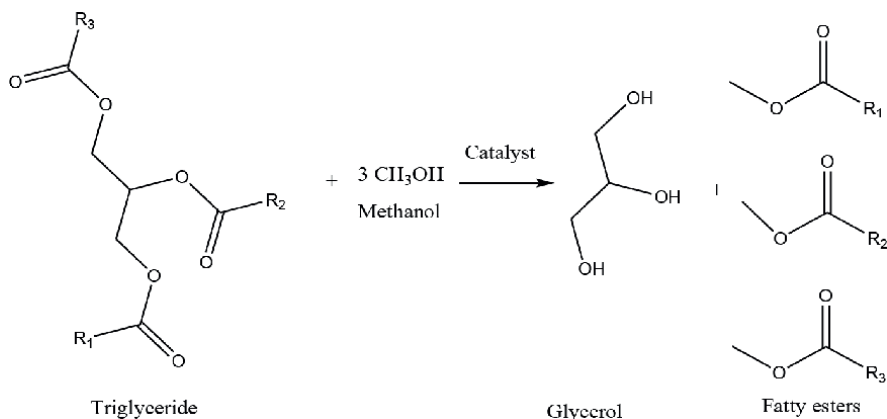


Figure 5. Glycerol production by a transesterification reaction [6].

Feedstock	Glycerol concentration (w/w %)	Methanol concentration (w/w %)	Soap concentration (w/w %)	Impurities (w/w %)	Ref.
Palm oil waste	87	—	—	6	[13]
Oil of Jatropa	19–22	14.5	29	11–21	[14]
Soybean oil	63	6.2	—	—	[15]
Soybean oil	22	10.9	26.2	23.5	[15]

Feedstock	Glycerol concentration (w/w %)	Methanol concentration (w/w %)	Soap concentration (w/w %)	Impurities (w/w %)	Ref.
Soybean oil	33	12.6	26.1	22.3	[15]
Vegetable oil waste	28	9	21	39	[15]
Palm oil	81	1	—	2.0	[16]
Seed oils	63–77	—	—	—	[17]
Used frying oil	85	—	—	15	[18]

Table 1. Different glycerol streams depending on initial feedstocks and production reactions.

Interestingly, the glycerol yield from transesterification was not only found to be dependent on different types of processes but also on the different type of oil feedstocks (Table 1) [13–18].

3. Glycerol catalysis

Transesterification of oil is accomplished using both homogenous as well as heterogeneous catalysts. Table 2 depicts glycerol production advantages and disadvantages of using different type of catalysts.

Moreover, depending on the type of catalyst used, the transesterification process can be categorised as homogeneous and heterogeneous catalysis to make biodiesel and subsequently glycerol.

Catalysts group	Type of catalyst	Advantages	Disadvantages
Homogeneous base catalyst	NaOH/KOH	<ul style="list-style-type: none"> Fast reaction rate, mild condition and less energy intensity. Catalysts are widely available and economical. 	<ul style="list-style-type: none"> If the usage limit for oil is less than 0.5 wt. % free fatty acid. Soap formation occurs as well if the free fatty acid content in the oil is more than 2 wt. %. Excessive soap formation reduces the glycerol yield and causes problems during product purification.
Heterogeneous base catalyst	CaO/MgO	<ul style="list-style-type: none"> Reaction conditions are mild and less energy-intensive, reuse and regenerating of a catalyst. Mild reaction condition and less energy intensive. 	<ul style="list-style-type: none"> Sensitive to free fatty acid content in the oil due to its basicity property. Excessive soap formation decreases the glycerol yield and causes problems during product refining.
Homogenous Acid catalyst	H ₂ SO ₄ /HCl	<ul style="list-style-type: none"> Affordable than base catalysed process. 	<ul style="list-style-type: none"> Very slow reaction rate. Not easy to separate the catalyst from products.

Table 2. Advantages and disadvantages of glycerol catalysts [19].

3.1 Homogeneous catalysis

During homogenous catalysis, the first stage comprises the reaction of vegetable oils with methanol in the presence of a catalyst, and then the separation of glycerol from the resultant mixture using a settler unit follows. The remaining flow is sent to a chamber that uses mineral acids to remove the catalytic component, resulting in two paths: a glycerol recovery chamber and an evaporator that separates biodiesel from the other products. The unit for purifying comprises three output units: the first with 80–95% glycerol; the second one with water, dissolved salts and unreacted methanol (it is then recycled back to the reactor); and one with fatty esters [12]. **Figure 6** depicts the glycerol manufacturing process employing homogeneous catalysts (namely, sodium hydroxide or sodium methylate) [6, 20, 21].

3.2 Heterogeneous catalysis

This type of catalysis procedure envisions two reaction phases to improve vegetable oil conversion; reactor 1 is supplied by vegetable oil and methanol. The product stream is sent through a heat exchanger to evaporate some of the residual methanol, and the remaining stream is directed to a decanter to separate polar and non-polar components such as glycerol and mainly vegetable oil and biodiesel, respectively. While, in reactor 2, the non-polar stream is reacted for the second time to boost biodiesel synthesis and recover methanol. The product stream travels through the heat exchanger, which takes out all unreacted methanol, and the decanter, which separates the biodiesel from polar components.

The polar streams from the first and second polar decanters are directed to another heat exchanger to recover the remaining methanol in the mixture, while the leftover fraction is delivered to a final decanter to separate vegetable oil and residual glycerol. **Figure 7** is a flowchart of triglyceride transesterification using heterogeneous catalysts such as aluminium and zinc oxide [6].

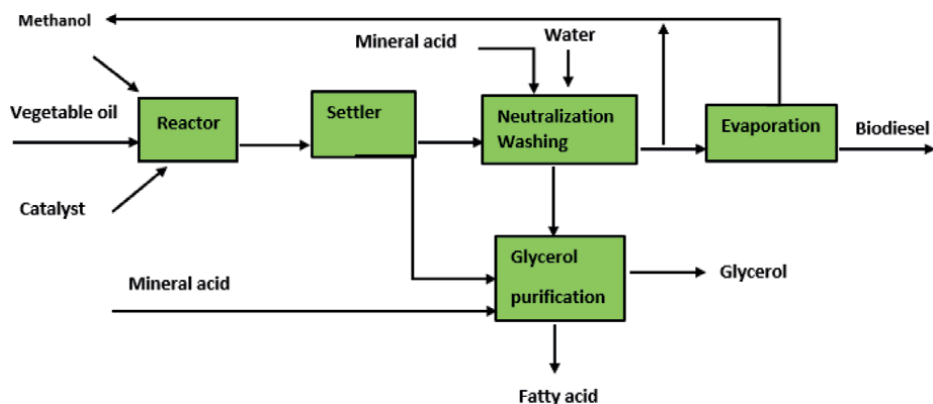


Figure 6. The production plant for biodiesel is based on a homogenous catalyst.

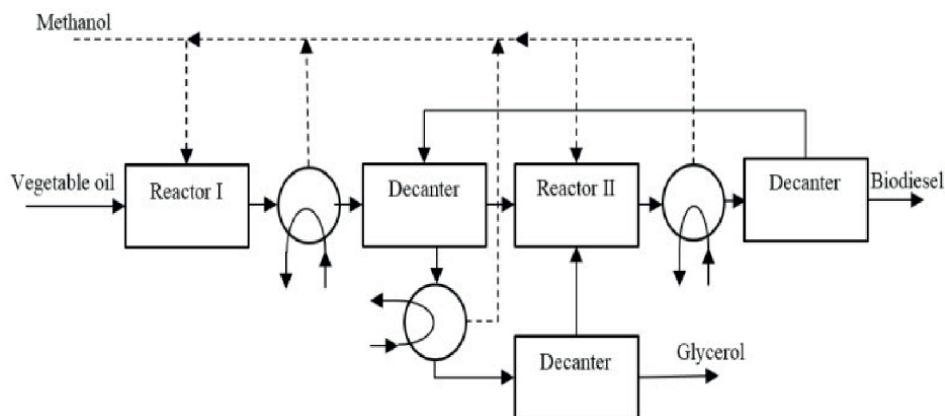


Figure 7.
 A heterogenous catalysis-based production plant flowchart [6].

4. Glycerol: a platform chemical

Synthesis of glycerol following microbial route has been known for over a century, however, new improvements in the biodiesel business have resulted in the production of large amounts of glycerol. During the biodiesel production process, approximately

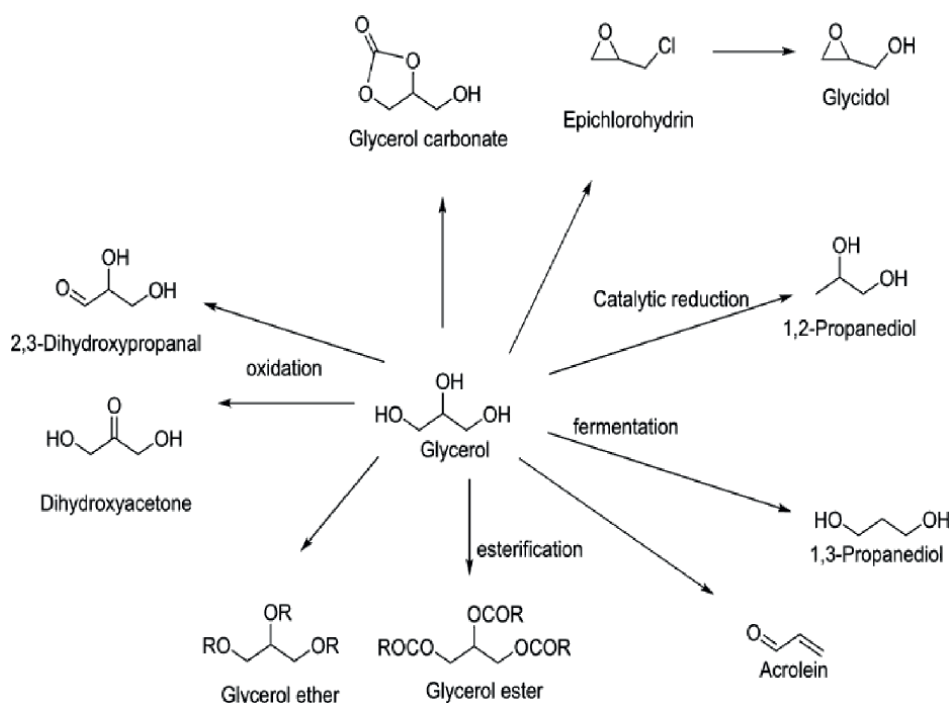


Figure 8.
 Glycerol as a platform chemical.

10% of glycerol is produced, accounting for about 90% of total glycerol produced [22]. Glycerol has gathered substantial interest in its conversion to higher value-added compounds due to its availability and potential to operate as a key building block in a biorefinery (**Figure 8**) [23].

Glycerol oxidation produces a wide range of compounds, such as glyceric acid dihydroxyacetone, glyceraldehyde, hydroxy-pyruvic acid, glycolic acid and others. Controlling reaction selectivity is a critical challenge in obtaining the desired molecules.

For example, glyceric acid is a crucial intermediary for more extensively oxidised compounds such as tartronic acid and mesoxalic acid. The catalytic aerobic oxidation of glycerol in a basic media has been extensively studied using monometallic or bimetallic catalysts such as Au, Pt and Pd.

Table 3 lists some of the most prominent catalysts used in this field [24–27, 30, 38–40]. Another approach for producing value-added compounds from glycerol is the reduction process. Lactic acid is produced by a reduction of glycerol in the presence of hydroxide bases [41]. This reaction is frequently carried out at medium to high pressures and temperatures ranging from 100 to 240°C using Cu- and Zn-based catalysts enhanced by sulphide Ru [28].

Glycerol carbonate is another derivative of glycerol that is formed by reaction between glycerol and urea, ethylene or propylene carbonate [22] or carbon dioxide [42]. It is also used in the commercial manufacture of epichlorohydrin. Epichlorohydrin is produced in a similar manner by Solvay and Dow Chemical Company [43]. When the principal hydroxyl groups in glycerol are selectively oxidised, the economically valuable chemicals glyceraldehyde [44], glyceric acid [45] and tartronic acid [46] are formed. Dihydroxyacetone (DHA) is produced by oxidation of the secondary hydroxyl group, whereas ketomalonic acid is produced by oxidation of all three hydroxyl groups [47].

Another glycerol derivative, glycidol, offers immense potential for the synthesis of industrially useful compounds such as epoxy resins, polyurethanes and polyglycerol esters. A bio-based technique for producing glycidol from glycerol was recently published [48]. The manufacture of acrolein from glycerol is an innovative, eco-friendly technology that has several advantages, such as less oil extraction and a minimal environmental impact [31]. In general, acrolein is synthesised from glycerol by acid-catalysed dehydrogenation over synthetic aluminium phosphate (AlPO_4), zeolites with varied channel configurations (HY and H-ZSM-5) and $\text{SiO}_2/\text{Al}_2\text{O}_3$ ratio [31, 49].

A novel synthetic approach for the synthesis of chlorohydrin was proposed, which involved reacting a polyhydroxy aliphatic hydrocarbon with a chlorination agent. Vitiello et al. [33] focused on the activity and selectivity of homologous chlorinated series of catalysts for glycerol halogenation, such as acetic acid, monochloro, dichloro and trichloroacetic acid.

Table 3 also includes information on one of the most significant glycerol conversion processes, esterification with acetic acid, which produces monoacylglycerol, diacylglycerol and glycerol carbonate. These materials are often used in cryogenics, biodegradable polyester and cosmetics [35, 36]. Sulphated-based superacids, heteropoly acid-based catalysts, tin chloride, zeolite, ZrO_2 -based solid acids and other significant acid catalysts can be used for glycerol esterification [35–37, 50–52].

Finally, pyrolysis of glycerol to produce syngas is another method of converting glycerol. The pyrolysis of biomass has been extensively studied in the specialist literature, although in most cases, only metal-based catalysts have been used. The microwave-assisted pyrolysis of glycerol over a carbonaceous catalyst is a unique approach

Reaction type	Reactant	Catalyst	Pressure (bar)	Temperature (°C)	Product	Ref.
Glycerol oxidation	O ₂	Pd–Ag/C	3	80	Dihydroxyacetone	[24]
	O ₂	Pt/NCNT	—	60		[25]
	O ₂	Pt/MCN	3	40	Glyceraldehyde	[26]
	O ₂	Pt/SiO ₂	1	100		[27]
	O ₂	Pt/MCN	3	40	Glyceric acid	[26]
	O ₂	Pt/SiO ₂	1	100		[27]
Glycerol reduction	H ₂	Ru/Al ₂ O ₃	25	180	1,2-propanediol	[28]
	H ₂	Ru/Al ₂ O ₃	25	200	Ethylene glycol	[29]
	H ₂	Ru/ZrO ₂	80	240		[30]
Glycerol dehydrogenation	—	AlPO ₄ –450	1	190–230	Acrolein	[31]
	—	HY(5.2)	1	170–230		[31]
	—	12 wt. % V ₂ O ₅ , V/P molar ratio of 0.2	1	325		[32]
Glycerol halogenation	HCl	Aspartic acid	4.5	100	1,3-dichloropropanol	[33]
	HCl	Glutamic acid	4.5	100		[33]
Glycerol esterification	Acetic acid	Sb ₂ O ₅	1	80–120	Monoglycerides	[34]
	Palmitic acid	ZrSBA-15	1	160–180	Diacylglycerol	[35]
	Acetic acid	Graphene oxide	1	120		[36]
	Acetic acid	ZSM-5	1	120		[36]
Glycerol pyrolysis	—	Bituminous carbon	1	400–900	Syngas	[37]
	—	Coconut shell	1	400–900		[37]

Table 3.
Compounds derived from traditional glycerol conversion under similar operating conditions.

for syngas generation in which the heating method and operating temperature (between 400 and 900°C) can impact the catalytic action of the activated carbons to optimise syngas production [37]. **Table 3** outlines some of the products derived from glycerol that may be transformed into other compounds with high added value.

5. Value-added products from glycerol via biological conversions

From 2004 to 2008, the global production of crude glycerol from biodiesel conversion increased from 200 thousand tonnes to 1.224 million tonnes [2, 19]. Meanwhile,

in 2005, the global market for purified glycerol was anticipated to be over 900,000 tonnes [53]. This provided a chance for scientists to discover new uses for refined and crude glycerol. Multiple publications on the direct use of crude glycerol from bio-diesel synthesis have been published.

5.1 1,3-Propanediol

The most promising alternative for the biological conversion of glycerol in anaerobic fermentative production is 1,3-propanediol [54], which indicates that crude glycerol could be employed directly for the manufacture of 1,3-propanediol in fed-batch cultures of *pneumoniae*.

Raw glycerol composition had less influence on the biological conversion and, therefore, a low fermentation cost could be predicted. However, using a response surface approach, the generation of 1,3-propanediol by *Klebsiella pneumoniae* was optimised. The highest concentration of 1,3-propanediol produced However, statistical optimisation along with genetic engineering approaches may be utilised to improve the 1,3-propanediol production [14, 55]. *K. pneumoniae* ATCC 15380 recently improved the synthesis of 1,3-propanediol from crude glycerol from *Jatropha* bio-diesel. The yield, purity and recovery of 1,3-propanediol obtained were 56 g/L, 99.7% and 34%, respectively [14]. In addition, a hollow fibre membrane was used to produce an integrated bioprocess that linked biodiesel generation by lipase with microbial production of 1,3-propanediol by *K. pneumoniae* [56].

5.2 Citric acid

Citric acid synthesis by *Yarrowia lipolytica* ACA-DC 50109 from raw glycerol was not only comparable to that obtained from sugar-based standard media [57] but also single-cell oil and citric acid were produced simultaneously [58, 59]. When acetate-negative mutants of the *Y. lipolytica* Wratislavia AWG7 strain were employed in a fed-batch fermentation to ferment crude glycerol, the final concentration of citric acid was 131.5 g/L, which was similar to that produced from pure glycerol (139 g/L). Similarly, *Y. lipolytica* LGAM S(7)1 has also shown the ability to convert crude glycerol to citric acid [60]. Interestingly, another strain *Y. lipolytica* N15 could produce large levels of citric acid, namely up to 98 g/L of citric acid and 71 g/L of citric acid from pure glycerol medium and crude glycerol medium, respectively [61].

5.3 Hydrogen and other lower molecule fuels

The photo-fermentative conversion of crude glycerol to hydrogen is one of the most fascinating approach to utilise glycerol. Both crude glycerol and pure glycerol can produce up to 6 moles of H₂ per mole of glycerol, representing 75% of the theoretical value. However, significant technological challenges, such as increasing the efficiency of light use by organisms and building effective photobioreactors, must be overcome before a viable method can be developed [62]. When *Enterobacter aerogenes* HU-101 was used, hydrogen and ethanol were synthesised at high yields and rates. However, in order to improve the rate of glycerol use, the crude glycerol should be diluted with a synthetic medium [63]. While Jitrwung and Yargeau [64] modified several media compositions of the *E. aerogenes* ATCC 35029 fermented crude glycerol procedure to maximise hydrogen generation.

5.4 Polyhydroxyalkanoates (PHB)

As an estimate, a biodiesel facility with a capacity of 10 million gallons per year could produce 20.9 tons of PHB [65]. The feasibility of using crude glycerol for PHB manufacture was investigated using *Paracoccus denitrificans* and *Cupriavidus necator* JMP134, and the resultant polymers were shown to be remarkably comparable to those generated from glucose. However, a high osmotic (sodium chloride-contaminated) crude glycerol was found to have harmful impact on PHB synthesis and needs to be taken care of. One way to handle the issue is combining crude glycerol from various producers to reduce the harmful effect of NaCl contamination [66]. In addition, for a large-scale PHB synthesis, a technique based on the *C. necator* DSM 545 fermentation of crude glycerol was developed [67]. Following this in the presence of NaCl, *Zobellella denitrificans* MW1 could use crude glycerol for growth and PHB synthesis at high concentrations. As a result, it was recommended as an appealing alternative for large-scale PHB manufacturing using crude glycerol [68]. Furthermore, when mixed microbial consortia (MMC) were utilised to produce PHA from crude glycerol, it was shown that methanol in the crude glycerol was converted to PHB by MMC.

5.5 Lipids as the sole carbon source

Crude glycerol might be used to manufacture lipids, which could be utilised to make a sustainable biodiesel feedstock. For example, raw glycerol might be used to culture *Schizochytrium limacinum* SR21 and *Cryptococcus curvatus*. However, the glycerol

Product	Reaction	Yield	Ref.
1,3-Propanediol	Fed-batch cultures of <i>Klebsiella pneumoniae</i> strain	1.7 g/L/h	[54]
	Maximum 1,3-propanediol production from <i>K. pneumoniae</i>	13.8 g/L	[55]
Citric acid	<i>Yarrowia lipolytica</i> strain ACA-DC 50109 (process modelling)	NA	[57]
	Acetate mutants of <i>Y. lipolytica</i> Wratislavia AWG7 strain; fed-batch operation	139 g/L	[74]
	<i>Y. lipolytica</i> strain LGAM S (7)1	35 g/L	[60]
Hydrogen	Photofermentative conversion process; <i>Rhodospirillum rubrum</i> strain	6 mol/mol glycerol	[62]
	<i>Enterobacter aerogenes</i> strain HU-101; continuous culture; porous ceramics as a support material to fix cells	63 mmol/L/h	[63]
Poly(hydroxyalkanoates) (PHAs)	<i>Pseudomonas oleovorans</i> NRRL B-14682 and <i>P. corrugata</i> 388 grew and synthesised PHB and mcl-PHA, respectively	NA	[75]
	Producing PHB; <i>Paracoccus denitrificans</i> and <i>Cupriavidus necator</i> JMP 134 strains	48%	[66]
Lipid	<i>Schizochytrium limacinum</i> SR21; batch culture	73.3%	[69]
	<i>Cryptococcus curvatus</i> ; two-stage fed-batch process	52%	[76]

Table 4.
 Biological conversion of crude glycerol.

Product	Reaction	Yield	Ref.
Acrolein	Fluidised bed, tungsten-doped zirconia catalyst	21%	[77]
Monoglyceride	Two-step process, purification of the monoglyceride produced from glycerolysis of palm stearin	~99% purity	[78]
	Glycerolysis of soybean oil	~42%	[79]
Gaseous products	Steam gasification with in situ CO ₂ removal	88 vol.% H ₂ purity	[80]
	Hydrothermal reforming of crude glycerol	~90 vol.% H ₂ purity	[81]

Table 5.
Conventional catalytic conversions of crude glycerol.

content over a certain threshold may prevent the rapid reproduction of cells. The best glycerol content for batch culturing of crude glycerol obtained from yellow grease were 25 and 35 g/L for untreated and treated crude glycerol, respectively, which may subsequently lead to cellular lipid content of approximately 75%. Methanol residues in crude glycerol may cause damage to the development of *S. limacinum* SR21 [69].

For lipid synthesis in *C. curvatus* yeast, fed-batch was preferable to batch; however, the addition of ammonium sulphate and Tween 20 improved the accumulation of lipids and carotenoids Saenge et al. [70] demonstrated that the oleaginous red yeast *Rhodotorula glutinis* TISTR 5159 generated lipids and carotenoids when grown on crude glycerol. *Chlorella protothecoides* was also capable of converting crude glycerol to lipids.

The lipid yield was 0.31 g lipids/g substrate [71]. Similarly, using *C. protothecoides* and crude glycerol (62% purity), Furthermore, Chatzifragkou et al. [72] did research, to investigate the ability of 15 eukaryotic micro-organisms to change crude glycerol to metabolic products. The results showed that yeast accumulated limited lipids (up to 22 wt.% in the case of *Rhodotorula*), whereas fungi collected greater levels of lipids in their mycelia (range between 18.1 and 42.6 wt.% of dry biomass). Interestingly, Chen and Walker [73] found that a fed-batch operation yielded a maximum lipid productivity of 3 g/L per day, which was greater than that generated by a batch procedure.

Tables 4 and **5** outline an overview of the conversions of crude glycerol to potential chemical through biological and catalytic conversions.

6. Application of crude glycerol in animal feedstock

Glycerol has been used as an animal feed additive since the 1970s [82]. However, the availability of glycerol has limited its application in diets [83], because of the rising corn prices and the oversupply of crude glycerol, the possibility of using crude glycerol from biodiesel in feeds has recently been examined.

6.1 Crude glycerol in non-ruminant diets

Crude glycerol is an excellent energy source due to its high absorption rates for non-ruminants such as broilers. Once ingested, the enzyme glycerol kinase converts it to glucose for energy generation in the liver of mammals [83]. Its samples from various biodiesel manufacturers were tested as energy sources. The digestible energy (DE) values for 85% of the crude glycerol samples ranged from 14.9 to 15.3 MJ/kg,

with metabolisable energy (ME) values ranging from 13.9 to 14.7 MJ/kg [84]. Overall, the use of crude glycerol derived from biodiesel process as an animal feed component offers significant potential for replacing maize in diets and is gaining popularity. However, the existence of potentially dangerous contaminants in biodiesel crude glycerol needs to be taken into consideration [85].

6.2 Crude glycerol in ruminant diets

Besides, the non-ruminants, crude glycerol may play a very significant role in the diets of ruminant animals as well. However, to improve its edibility, more emphasis should be placed on the crude glycerol produced by small-scale biodiesel plants that employ basic batch distillation or evaporation processes. There are several reports where use of crude glycerol has shown significant improvement in the overall performance of ruminants. Crude glycerol, at up to 15% dry matter in finishing lamb diets, might increase feedlot performance, particularly during the first 14 days, but had little influence on carcass attributes [86]. Diets for meat goats containing up to 5% crude glycerol were shown to be superior to medium-quality hay [87]. Nursing dairy cows can also be fed up to 15% of their dry matter diet without affecting feed intake, milk output or yield [88, 89]. When crude glycerol was added at 8% or less of dry matter in cow-finishing diets, its weight growth and feed efficiency were increased [90].

7. Summary and conclusions

Glycerol may be produced using various techniques and feedstocks, such as propylene synthesis by various routes, hydrolysis of fatty acid triglycerides, or transesterification of fatty acids or oils. The efficient use of crude glycerol is critical to the commercialisation and advancement of biodiesel synthesis. In the long run, using biomass-derived glycerol will not only help to reduce society's reliance on non-renewable resources, but it will also encourage the development of integrated biorefineries. This review focuses on the value-added prospects for crude glycerol derived from biodiesel production, primarily as a feed ingredient for animal feed and as a feedstock for chemicals.

For example, crude glycerol can be converted into 1,3-propanediol, citric acid, poly(hydroxyalkanoates), butanol, hydrogen, docosahexaenoic acid-rich algae, monoglycerides, lipids and syngas. Though many of the processes discussed have already been employed by the industries, they require additional research to minimise the manufacturing cost and be operationally practical for inclusion into biorefineries.

Furthermore, contaminants in crude glycerol can have a noticeable impact on the conversion of glycerol into other products. Pollutants in crude glycerol hinder cell and fungi's rapid reproduction, resulting in less production rates and product yields in many biological conversion processes (compared with pure or commercial glycerol under the same culture conditions). Contaminants, on the other hand, poison the catalysts in traditional catalytic conversions, boosting char generation and affecting product yield.

Many technologies need to be better understood and refined, such as optimising reaction parameters, production yields and fermentation conditions; generating mutant strains and efficient bioreactors for stable cultures and enhancing the activity and selectivity of catalysts.

Researchers have also obtained promising results on utilisation of crude glycerol as animal feed, particularly with non-ruminant animals such as pigs, laying hens and

broilers. But various precautions must be taken before this biomass-derived chemical may be used on a large scale in animal diets. To begin with, animal producers must exercise caution when deciding to incorporate crude glycerol as a component of animal feed diets, since the chemical composition of crude glycerol varies greatly depending on the processes and feedstocks used to manufacture biodiesel. Secondly, contaminants in crude glycerol affect feed performance to some extent. Finally, the amount of crude glycerol in feed formulations must be considered. It is advised that a crude glycerol feed standard be established so that it would be uniform for all producers, the resulting “standard” crude glycerol would have greater value.

There is a need to develop improved processes as well as other important value-added products. For example, among other renewable and bio-derived sources, glycerol has come up as an appealing possibility since it represents a relevant and alternative solution for producing hydrogen via reforming processes that may be carried out in both traditional and novel reactors.

Besides, catalytic process, though it is not yet introduced, the transesterification reaction using supercritical fluids has also gained noticeable attention. As one or two reaction stages are possible in a single-step supercritical fluid transesterification, the reaction occurs only once reactants are heated to critical temperatures and pressures with triglycerides [20, 21]. Triglycerides are initially transformed to free fatty acids and by-products in the hydrolysis reaction during the two-step subcritical-supercritical fluid transesterification. The acquired free fatty acids undergo esterification reaction, yielding fatty acid methyl esters in a supercritical fluid process [91, 92].

Conflict of interest

The authors declare no conflict of interest.

Author details

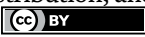
Anele Sibeko¹, Lethiwe D. Mthembu^{1*}, Rishi Gupta² and Nirmala Deenadayalu¹

1 Department of Chemistry, Durban University of Technology, Berea, Durban, South Africa

2 Anton Paar India Pvt. Ltd., Gurugram, Haryana, India

*Address all correspondence to: lethiwem@dut.ac.za

IntechOpen

© 2023 The Author(s). Licensee IntechOpen. This chapter is distributed under the terms of the Creative Commons Attribution License (<http://creativecommons.org/licenses/by/3.0>), which permits unrestricted use, distribution, and reproduction in any medium, provided the original work is properly cited. 

References

- [1] Yang F, Hanna MA, Sun R. Value-added uses for crude glycerol--a byproduct of biodiesel production. *Biotechnology for Biofuels*. 2012;**5**(1):1-10
- [2] Kerr BJ, Dozier WA III, Bregendahl K. Nutritional value of crude glycerin for nonruminants. In: *Proceedings of the 23rd Annual Carolina Swine Nutrition Conference*. Journal of Animal Science. Raleigh, NC; 2007. pp. 6-18
- [3] Shukla K, Srivastava VC. Synthesis of organic carbonates from alcoholysis of urea: A review. *Catalysis Reviews*. 2017;**59**(1):1-43
- [4] Ciriminna R, Pina CD, Rossi M, Pagliaro M. Understanding the glycerol market. *European Journal of Lipid Science and Technology*. 2014;**116**(10): 1432-1439
- [5] Matar S, Hatch LF. *Chemistry of Petrochemical Processes*. Elsevier; 2001
- [6] Bagnato G, Iulianelli A, Sanna A, Basile A. Glycerol production and transformation: A critical review with particular emphasis on glycerol reforming reaction for producing hydrogen in conventional and membrane reactors. *Membranes*. 2017;**7**(2):17
- [7] Hunt JA. A short history of soap. *The Pharmaceutical Journal*. 1999;**263**(7076):985-989
- [8] Marchetti J, Miguel V, Errazu A. Possible methods for biodiesel production. *Renewable and Sustainable Energy Reviews*. 2007;**11**(6):1300-1311
- [9] Formo M, Jungermann E, Norris F, Sonntag N. In: Swern D, editor. *Bailey's Industrial Oil and Fat Products*. New York, NY: John Wiley and Sons; 1979
- [10] Quispe CA, Coronado CJ, Carvalho JA Jr. Glycerol: Production, consumption, prices, characterization and new trends in combustion. *Renewable and Sustainable Energy Reviews*. 2013;**27**:475-493
- [11] Wang Z, Zhuge J, Fang H, Prior BA. Glycerol production by microbial fermentation: A review. *Biotechnology Advances*. 2001;**19**(3):201-223
- [12] Fukuda H, Kondo A, Noda H. Biodiesel fuel production by transesterification of oils. *Journal of Bioscience and Bioengineering*. 2001;**92**(5):405-416
- [13] Hidawati EN, Sakinah AM. "treatment of glycerin pitch from biodiesel production," *international journal of chemical and environmental Engineering*. 2011;**2**(5):309-313
- [14] Hiremath A, Kannabiran M, Rangaswamy V. 1,3-Propanediol production from crude glycerol from *Jatropha* biodiesel process. *New Biotechnology*. 2011;**28**(1):19-23
- [15] Hu S, Luo X, Wan C, Li Y. Characterization of crude glycerol from biodiesel plants. *Journal of Agricultural and Food Chemistry*. 2012;**60**(23):5915-5921
- [16] Liu Y-P, Sun Y, Tan C, Li H, Zheng X-J, Jin K-Q, et al. Efficient production of dihydroxyacetone from biodiesel-derived crude glycerol by newly isolated *Gluconobacter frateurii*. *Bioresource Technology*. 2013;**142**:384-389
- [17] Tan H, Aziz AA, Aroua M. Glycerol production and its applications as a raw material: A review. *Renewable and Sustainable Energy Reviews*. 2013;**27**:118-127

- [18] Bouaid A, Vázquez R, Martínez M, Aracil J. Effect of free fatty acids contents on biodiesel quality. Pilot plant studies. *Fuel*. 2016;**174**:54-62
- [19] Nomanbhay S, Hussain R, Rahman MM, Palanisamy K. Review paper integration of biodiesel and bioethanol processes: Conversion of low cost waste glycerol to bioethanol. *Advances in Natural and Applied Sciences*. 2012;**6**(6):802-818
- [20] Ilham Z, Saka S. Dimethyl carbonate as potential reactant in non-catalytic biodiesel production by supercritical method. *Bioresource Technology*. 2009;**100**(5):1793-1796
- [21] Goembira F, Saka S. Optimization of biodiesel production by supercritical methyl acetate. *Bioresource Technology*. 2013;**131**:47-52
- [22] Okoye P, Hameed B. Review on recent progress in catalytic carboxylation and acetylation of glycerol as a byproduct of biodiesel production. *Renewable and Sustainable Energy Reviews*. 2016;**53**:558-574
- [23] Schultz EL, de Souza DT, Damaso MCT. The glycerol biorefinery: A purpose for Brazilian biodiesel production. *Chemical and Biological Technologies in Agriculture*. 2014;**1**(1):1-9
- [24] Hirasawa S, Watanabe H, Kizuka T, Nakagawa Y, Tomishige K. Performance, structure and mechanism of Pd–Ag alloy catalyst for selective oxidation of glycerol to dihydroxyacetone. *Journal of Catalysis*. 2013;**300**:205-216
- [25] Ning X, Li Y, Yu H, Peng F, Wang H, Yang Y. Promoting role of bismuth and antimony on Pt catalysts for the selective oxidation of glycerol to dihydroxyacetone. *Journal of Catalysis*. 2016;**335**:95-104
- [26] Wang F-F, Shao S, Liu C-L, Xu C-L, Yang R-Z, Dong W-S. Selective oxidation of glycerol over Pt supported on mesoporous carbon nitride in base-free aqueous solution. *Chemical Engineering Journal*. 2015;**264**:336-343
- [27] Li Y, Zaera F. Sensitivity of the glycerol oxidation reaction to the size and shape of the platinum nanoparticles in Pt/SiO₂ catalysts. *Journal of Catalysis*. 2015;**326**:116-126
- [28] Lee S-H, Moon DJ. Studies on the conversion of glycerol to 1, 2-propanediol over Ru-based catalyst under mild conditions. *Catalysis Today*. 2011;**174**(1):10-16
- [29] Soares AV, Salazar JB, Falcone DD, Vasconcellos FA, Davis RJ, Passos FB. A study of glycerol hydrogenolysis over Ru–Cu/Al₂O₃ and Ru–Cu/ZrO₂ catalysts. *Journal of Molecular Catalysis A: Chemical*. 2016;**415**:27-36
- [30] Olmos CM, Chinchilla LE, Rodrigues EG, Delgado JJ, Hungría AB, Blanco G, et al. Synergistic effect of bimetallic Au-Pd supported on ceria-zirconia mixed oxide catalysts for selective oxidation of glycerol. *Applied Catalysis B: Environmental*. 2016;**197**:222-235
- [31] Estevez R, Lopez-Pedrajas S, Blanco-Bonilla F, Luna D, Bautista F. Production of acrolein from glycerol in liquid phase on heterogeneous catalysts. *Chemical Engineering Journal*. 2015;**282**:179-186
- [32] Cecilia J, García-Sancho C, Mérida-Robles J, Santamaría-González J, Moreno-Tost R, Maireles-Torres P. V and V–P containing Zr-SBA-15 catalysts for dehydration of glycerol to acrolein. *Catalysis Today*. 2015;**254**:43-52
- [33] Vitiello R, Russo V, Turco R, Tesser R, Di Serio M, Santacesaria E. Glycerol

chlorination in a gas-liquid semibatch reactor: New catalysts for chlorohydrin production. *Chinese Journal of Catalysis*. 2014;**35**(5):663-669

[34] Hu W, Zhang Y, Huang Y, Wang J, Gao J, Xu J. Selective esterification of glycerol with acetic acid to diacetin using antimony pentoxide as reusable catalyst. *Journal of Energy Chemistry*. 2015;**24**(5):632-636

[35] Yusoff MHM, Abdullah AZ. Catalytic behavior of sulfated zirconia supported on SBA-15 as catalyst in selective glycerol esterification with palmitic acid to monopalmitin. *Journal of the Taiwan Institute of Chemical Engineers*. 2016;**60**:199-204

[36] Gao X, Zhu S, Li Y. Graphene oxide as a facile solid acid catalyst for the production of bioadditives from glycerol esterification. *Catalysis Communications*. 2015;**62**:48-51

[37] Fernández Y, Arenillas A, Díez M, Pis J, Menéndez J. Pyrolysis of glycerol over activated carbons for syngas production. *Journal of Analytical and Applied Pyrolysis*. 2009;**84**(2):145-150

[38] Rodrigues EG, Pereira MF, Delgado JJ, Chen X, Órfão JJ. Enhancement of the selectivity to dihydroxyacetone in glycerol oxidation using gold nanoparticles supported on carbon nanotubes. *Catalysis Communications*. 2011;**16**(1):64-69

[39] Skrzyńska E, Zaid S, Girardon J-S, Capron M, Dumeignil F. Catalytic behaviour of four different supported noble metals in the crude glycerol oxidation. *Applied Catalysis A: General*. 2015;**499**:89-100

[40] Gil S, Marchena M, Fernández CM, Sánchez-Silva L, Romero A, Valverde JL. Catalytic oxidation of crude glycerol

using catalysts based on Au supported on carbonaceous materials. *Applied Catalysis A: General*. 2013;**450**:189-203

[41] Maris EP, Ketchie WC, Murayama M, Davis RJ. Glycerol hydrogenolysis on carbon-supported PtRu and AuRu bimetallic catalysts. *Journal of Catalysis*. 2007;**251**(2):281-294

[42] Ma J, Song J, Liu H, Liu J, Zhang Z, Jiang T, et al. One-pot conversion of CO₂ and glycerol to value-added products using propylene oxide as the coupling agent. *Green Chemistry*. 2012;**14**(6):1743-1748

[43] Bell BM, Briggs JR, Campbell RM, Chambers SM, Gaarenstroom PD, Hippler JG, et al. Glycerin as a renewable feedstock for epichlorohydrin production. The GTE process. *CLEAN–Soil, Air, Water*. 2008;**36**(8):657-661

[44] Kim HJ, Lee J, Green SK, Huber GW, Kim WB. Selective glycerol oxidation by electrocatalytic dehydrogenation. *ChemSusChem*. 2014;**7**(4):1051-1056

[45] Kondamudi N, Misra M, Banerjee S, Mohapatra S, Mohapatra S. Simultaneous production of glyceric acid and hydrogen from the photooxidation of crude glycerol using TiSi₂. *Applied Catalysis B: Environmental*. 2012;**126**:180-185

[46] Behr A, Eilting J, Irawadi K, Leschinski J, Lindner F. Improved utilisation of renewable resources: New important derivatives of glycerol. *Green Chemistry*. 2008;**10**(1):13-30

[47] Ciriminna R, Pagliaro M. One-pot homogeneous and heterogeneous oxidation of glycerol to ketomalonic acid mediated by TEMPO. *Advanced Synthesis & Catalysis*. 2003;**345**(3):383-388

[48] Bai R, Zhang H, Mei F, Wang S, Li T, Gu Y, et al. Retraction: One-pot synthesis

of glycidol from glycerol and dimethyl carbonate over a highly efficient and easily available solid catalyst NaAlO₂. Green Chemistry. 2016;**18**(22):6144-6144

[49] Jiang T, Zhou Y, Liang S, Liu H, Han B. Hydrogenolysis of glycerol catalyzed by Ru-Cu bimetallic catalysts supported on clay with the aid of ionic liquids. Green Chemistry. 2009;**11**(7):1000-1006

[50] Ishak ZI, Sairi NA, Alias Y, Aroua MKT, Yusoff R. Production of glycerol carbonate from glycerol with aid of ionic liquid as catalyst. Chemical Engineering Journal. 2016;**297**:128-138

[51] Munshi MK, Biradar PS, Gade SM, Rane VH, Kelkar AA. Efficient synthesis of glycerol carbonate/glycidol using 1,8-diazabicyclo [5.4. 0] undec-7-ene (DBU) based ionic liquids as catalyst. RSC Advances. 2014;**4**(33):17124-17128

[52] Liu J, Li Y, Zhang J, He D. Glycerol carbonylation with CO₂ to glycerol carbonate over CeO₂ catalyst and the influence of CeO₂ preparation methods and reaction parameters. Applied Catalysis A: General. 2016;**513**:9-18

[53] Nilles D. Combating the Glycerin Glut. Biodiesel Magazine; 2006 Available: <https://biodieselmagazine.com/articles/1123/combating-the-glycerin-glut/>

[54] Mu Y, Teng H, Zhang D-J, Wang W, Xiu Z-L. Microbial production of 1,3-propanediol by *Klebsiella pneumoniae* using crude glycerol from biodiesel preparations. Biotechnology Letters. 2006;**28**(21):1755-1759

[55] Oh B-R, Seo J-W, Choi MH, Kim CH. Optimization of culture conditions for 1,3-propanediol production from crude glycerol by *Klebsiella pneumoniae* using response surface methodology.

Biotechnology and Bioprocess Engineering. 2008;**13**(6):666-670

[56] Mu Y, Xiu Z-L, Zhang D-J. A combined bioprocess of biodiesel production by lipase with microbial production of 1,3-propanediol by *Klebsiella pneumoniae*. Biochemical Engineering Journal. 2008;**40**(3):537-541

[57] Papanikolaou S, Aggelis G. Modelling aspects of the biotechnological valorization of raw glycerol: Production of citric acid by *Yarrowia lipolytica* and 1,3-propanediol by *clostridium butyricum*. Journal of Chemical Technology & Biotechnology: International Research in Process, Environmental & Clean Technology. 2003;**78**(5):542-547

[58] Papanikolaou S, Fakas S, Fick M, Chevalot I, Galiotou-Panayotou M, Komaitis M, et al. Biotechnological valorisation of raw glycerol discharged after bio-diesel (fatty acid methyl esters) manufacturing process: Production of 1, 3-propanediol, citric acid and single cell oil. Biomass and Bioenergy. 2008;**32**(1):60-71

[59] Papanikolaou S, Aggelis G. Biotechnological valorization of biodiesel derived glycerol waste through production of single cell oil and citric acid by *Yarrowia lipolytica*. Lipid Technology. 2009;**21**(4):83-87

[60] Papanikolaou S, Muniglia L, Chevalot I, Aggelis G, Marc I. *Yarrowia lipolytica* as a potential producer of citric acid from raw glycerol. Journal of Applied Microbiology. 2002;**92**(4):737-744

[61] Kamzolova SV, Fatykhova AR, Dedyukhina EG, Anastassiadis SG, Golovchenko NP, Morgunov IG. Citric acid production by yeast grown on glycerol-containing waste from biodiesel industry. Food Technology and Biotechnology. 2011;**49**(1):65-74

- [62] Sabourin-Provost G, Hallenbeck PC. High yield conversion of a crude glycerol fraction from biodiesel production to hydrogen by photofermentation. *Bioresource Technology*. 2009;**100**(14):3513-3517
- [63] Ito T, Nakashimada Y, Senba K, Matsui T, Nishio N. Hydrogen and ethanol production from glycerol-containing wastes discharged after biodiesel manufacturing process. *Journal of Bioscience and Bioengineering*. 2005;**100**(3):260-265
- [64] Jitrwung R, Yargeau V. Optimization of media composition for the production of biohydrogen from waste glycerol. *International Journal of Hydrogen Energy*. 2011;**36**(16):9602-9611
- [65] Dobroth ZT, Hu S, Coats ER, McDonald AG. Polyhydroxybutyrate synthesis on biodiesel wastewater using mixed microbial consortia. *Bioresource Technology*. 2011;**102**(3):3352-3359
- [66] Mothes G, Schnorpfel C, Ackermann JU. Production of PHB from crude glycerol. *Engineering in Life Sciences*. 2007;**7**(5):475-479
- [67] Cavalheiro JM, de Almeida MCM, Grandfils C, Da Fonseca M. Poly (3-hydroxybutyrate) production by *Cupriavidus necator* using waste glycerol. *Process Biochemistry*. 2009;**44**(5):509-515
- [68] Ibrahim MH, Steinbüchel A. Poly (3-hydroxybutyrate) production from glycerol by *Zobellella denitrificans* MW1 via high-cell-density fed-batch fermentation and simplified solvent extraction. *Applied and Environmental Microbiology*. 2009;**75**(19):6222-6231
- [69] Liang Y, Sarkany N, Cui Y, Blackburn JW. Batch stage study of lipid production from crude glycerol derived from yellow grease or animal fats through microalgal fermentation. *Bioresource Technology*. 2010;**101**(17):6745-6750
- [70] Saenge C, Cheirsilp B, Suksaroge TT, Bourtoom T. Potential use of oleaginous red yeast *Rhodotorula glutinis* for the bioconversion of crude glycerol from biodiesel plant to lipids and carotenoids. *Process Biochemistry*. 2011;**46**(1):210-218
- [71] O'Grady J, Morgan JA. Heterotrophic growth and lipid production of *Chlorella protothecoides* on glycerol. *Bioprocess and Biosystems Engineering*. 2011;**34**(1):121-125
- [72] Chatzifragkou A, Makri A, Belka A, Bellou S, Mavrou M, Mastoridou M, et al. Biotechnological conversions of biodiesel derived waste glycerol by yeast and fungal species. *Energy*. 2011;**36**(2):1097-1108
- [73] Chen Y-H, Walker TH. Biomass and lipid production of heterotrophic microalgae *Chlorella protothecoides* by using biodiesel-derived crude glycerol. *Biotechnology Letters*. 2011;**33**(10):1973-1983
- [74] Rywinska A, Rymowicz W, Zarowska B, Wojtatowicz M. Biosynthesis of citric acid from glycerol by acetate mutants of *Yarrowia lipolytica* in fed-batch fermentation. *Food Technology and Biotechnology*. 2009;**47**(1):1-6
- [75] Ashby RD, Solaiman DK, Foglia TA. Bacterial poly (hydroxyalkanoate) polymer production from the biodiesel co-product stream. *Journal of Polymers and the Environment*. 2004;**12**(3):105-112
- [76] Liang Y, Cui Y, Trushenski J, Blackburn JW. Converting crude glycerol derived from yellow grease to lipids through yeast fermentation. *Bioresource Technology*. 2010;**101**(19):7581-7586

- [77] Sereshki BR, Balan S-J, Patience G, Dubois J-L. Reactive vaporization of crude glycerol in a fluidized bed reactor. *Industrial & Engineering Chemistry Research*. 2010;**49**(3):1050-1056
- [78] Chetpattananondh P, Tongurai C. "synthesis of high purity monoglycerides from crude glycerol and palm stearin," Songklanakarin. *Journal of Science & Technology*. 2008;**30**(4):515-521
- [79] Echeverri DA, Cardeño F, Rios LA. Glycerolysis of soybean oil with crude glycerol containing residual alkaline catalysts from biodiesel production. *Journal of the American Oil Chemists' Society*. 2011;**88**(4):551-557
- [80] Dou B, Dupont V, Williams PT, Chen H, Ding Y. Thermogravimetric kinetics of crude glycerol. *Bioresource Technology*. 2009;**100**(9):2613-2620
- [81] Dou B, Rickett GL, Dupont V, Williams PT, Chen H, Ding Y, et al. Steam reforming of crude glycerol with in situ CO₂ sorption. *Bioresource Technology*. 2010;**101**(7):2436-2442
- [82] Fisher L, Erfle J, Lodge G, Sauer F. Effects of propylene glycol or glycerol supplementation of the diet of dairy cows on feed intake, milk yield and composition, and incidence of ketosis. *Canadian Journal of Animal Science*. 1973;**53**(2):289-296
- [83] Mario Pagliaro MR. Royal Society of Chemistry (Great Britain), the Future of Glycerol: New Uses of a Versatile Raw Material. 2nd ed. Cambridge: Royal Society of Chemistry; 2008
- [84] Dasari M. Crude glycerol potential described. *Feedstuffs*. 2007;**79**(43):1-3
- [85] Cerrate S, Yan F, Wang Z, Coto C, Sacakli P, Waldroup P. Evaluation of glycerine from biodiesel production as a feed ingredient for broilers. *International Journal of Poultry Science*. 2006;**5**(11):1001-1007
- [86] Gunn P, Neary M, Lemenager R, Lake S. Effects of crude glycerin on performance and carcass characteristics of finishing wether lambs. *Journal of Animal Science*. 2010;**88**(5):1771-1776
- [87] Hampy K, Kellogg D, Coffey K, Kegley E, Caldwell J, Lee M, et al. Glycerol as a supplemental energy source for meat goats. *AAES Research Series*. 2008;**553**:63-64
- [88] Donkin SS. Glycerol from biodiesel production: The new corn for dairy cattle. *Revista Brasileira de Zootecnia*. 2008;**37**:280-286
- [89] Donkin S, Koser S, White H, Doane P, Cecava M. Feeding value of glycerol as a replacement for corn grain in rations fed to lactating dairy cows. *Journal of Dairy Science*. 2009;**92**(10):5111-5119
- [90] Parsons G, Shelor M, Drouillard J. Performance and carcass traits of finishing heifers fed crude glycerin. *Journal of Animal Science*. 2009;**87**(2):653-657
- [91] Saka S, Isayama Y, Ilham Z, Jiayu X. New process for catalyst-free biodiesel production using subcritical acetic acid and supercritical methanol. *Fuel*. 2010;**89**(7):1442-1446
- [92] Lam MK, Lee KT, Mohamed AR. Homogeneous, heterogeneous and enzymatic catalysis for transesterification of high free fatty acid oil (waste cooking oil) to biodiesel: A review. *Biotechnology Advances*. 2010;**28**(4):500-518

Chapter 3

Bioethanol Production

Chakali Ayyanna, Kuppusamy Sujatha, Sujit Kumar Mohanthy, Jayaraman Rajangam, B. Naga Sudha and H.G. Raghavendra

Abstract

In recent decades, usage of biofuels as fossil fuel substitutes has increased. One method for lowering both crude oil use and environmental pollution is the production of ethanol (bioethanol) from biomass. This report offers an examination of the existing state of affairs and future prospects for biomass-to-ethanol. We examine different conversion routes from a technological, economic, and environmental standpoint. The main focus of this study is on the yield of ethanol from molasses in relation to the dilution ratio and the quantity of yeast used for fermentation while maintaining a constant fermentation temperature and time. In this investigation, the feedstock is sugarcane molasses. A thick by-product of turning sugar cane into sugar is sugarcane molasses. Consequently, sugarcane molasses and other agricultural byproducts are desirable feedstock for the manufacture of bioethanol. Agricultural wastes are cheap, abundant, and renewable. The least expensive strain for the conversion of biomass substrate is *Saccharomyces cerevisiae*. As a conclusion, it was found that the ethanol yield increased with an increase in yeast quantity, reaching an optimal yeast quantity before ethanol yield started to drop. The ideal ratio of molasses to water was found to be 1:2. The amount of fermentable sugars contained in the biomass has a significant impact on the output of ethanol.

Keywords: bioethanol, fermentation, feedstock, *Saccharomyces cerevisiae*, sugarcane molasses

1. Introduction

The research for alternative energy sources is stimulated by the growth in the nation's renewable sources and the gradual depletion of oil resources [1]. Particularly, biomass is a renewable resource that is currently researched for the utilization of bioethanol as an additive or replacement with gasoline has been driven by concerns about global warming and the need to lower greenhouse gas emissions [2]. Bioethanol can also be used as a raw material in the manufacture of various chemicals, resulting in fully renewable chemical industry. Bioethanol is created by fermenting sugars derived from biomass. Sucrose (e.g., sugarcane, sugar beet) or starch (e.g., corn, wheat), or lignocellulosic material can be used as bioethanol feedstock (e.g., sugarcane bagasse, wood, and straw). The main ethanol producers in the world, the US and Brazil, employ corn and sugarcane as their respective feedstocks. The use of fossil fuels during the processing of sugarcane is far lower than that of corn, making it the most

effective raw material for the manufacturing of bioethanol to date [3]. Additionally, there is still room for improvement in the sugarcane-based bioethanol manufacturing process, and large energy savings are conceivable.

Brazil, one of the world's top ethanol producers, has been using sugarcane as a primary input for the production of huge amounts of bioethanol for more than 30 years [4]. Large amounts of sugarcane bagasse are often created during the sugarcane processing (about 240 kg of bagasse with 50% humidity per ton of sugarcane), and this bagasse are presently burned in boilers to produce steam and power. It is now possible to have a surplus of bagasse thanks to improved cogeneration and optimization techniques for the bioethanol production process [5], which can be used as a fuel source for power production or as a raw material for making bioethanol and other biobased products [6]. Although sugarcane bagasse and other lignocellulosic materials have been the subject of intense research over the past few decades, it is still not economically feasible to produce bioethanol on an industrial scale [2]. To make hydrolysis a competitive technique, more research that takes into account process integration, increased fermentation yields, and integration of unit operations is still required [7, 8]. Hemicellulose, a mixture of polysaccharides primarily made of glucose, mannose, xylose, arabinose, lignin, and cellulose makes up the majority of lignocellulosic materials [1]. Sugarcane bagasse needs to be treated to produce fermentable sugars in order to be used as a raw material for bioethanol production [9]. To improve cellulose hydrolysis, lignin and hemicellulose must be separated from cellulose, cellulose crystallinity must be reduced, and the bagasse's porosity must be increased [10]. The Organogold procedure with diluted acid hydrolysis is one approach that might be used to accomplish that [11].

2. Bioethanol production

A gasoline substitute known as bioethanol (grain alcohol; C_2H_5OH (EtOH)) was used for transportation [12]. Globally, the amount of bioethanol produced has drastically increased [13]. Worldwide production of bioethanol climbed to 51,3 billion liters in 2006 from 45,98 billion liters in 2005 [2, 12]. Biomass-derived ethanol has been shown to be competitive with other liquid fuels on a large scale. The production method was refined and made practical by cellulose's enzymatic hydrolysis [9]. The creation of bioethanol from biomass was one method for lowering oil consumption and environmental contamination [12].

The production use of bioethanol is relevant to major national concerns like permanence, global climate change, biodegradability, municipal contamination, coal sequestration, national security, and the farm economy. It was obvious that production should be assessed in terms of economic factors, including farm-gate prices for biomass, logistic costs (transport and storage of biomass), the direct economic value of feedstocks taking into account byproducts, employment creation or maintenance, water requirements, and water availability [2, 12].

The comparison of the feedstocks for a given production line took into account a number of factors, including the chemical makeup of the biomass, cultivation methods, land availability and land use practices, resource use, energy balance, emission of greenhouse gases, acidifying gases, and ozone-depleting gases, mineral absorption into water and soil, pesticide injection, soil erosion, contribution to biodiversity, and landscape value losses [12]. Agricultural leftovers (such as corn stover and wheat straw), wood, and energy crops were all desirable raw materials

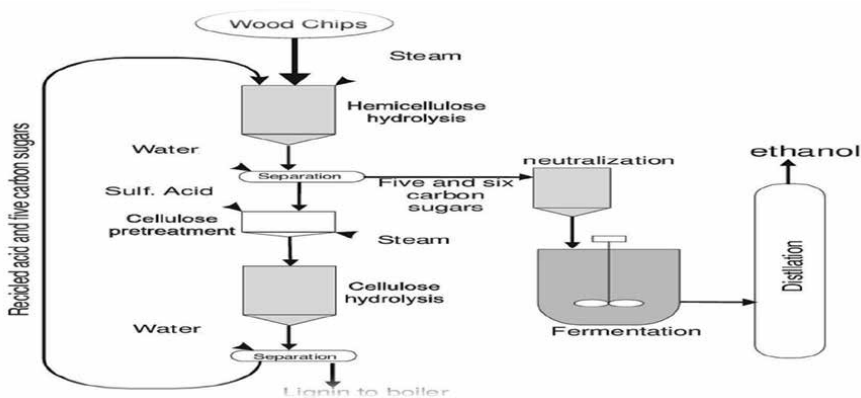
for the synthesis of bioethanol [12]. The total amount of bioethanol that might be produced from such biomass was nearly 16 times greater than what is currently produced globally [14].

Arable agricultural starch and sugars were mostly used to make ethanol. Because it was pricey, the quest for other materials that would work for this purpose started [15]. Different processes were utilized depending on the type of biomass used to produce the bioethanol. It was difficult to bio-convert lignocellulosic biomass into fermentable sugars. The bioconversion of starch to sugars for the creation of bioethanol was more efficient and popular [16].

Through the hydrolysis and fermentation of sugars, biomass can be transformed into ethanol. Biomass wastes contain a complex mixture of cellulose, hemicellulose, and lignin, three carbohydrate polymers found in plant cell walls. In order to get sugars from the biomass, the biomass is first pre-treated with acids or enzymes to reduce the size of the feedstock and to open up the plant structure. Enzymes or weak acids hydrolyze the cellulose and hemicellulose components to produce sucrose sugar, which is subsequently fermented to produce ethanol. The biomass, which also contains lignin, is typically burned in the boilers of ethanol manufacturing facilities. The three main techniques for extracting sugars from biomass are as follows.

3. Method of intense acid treatment

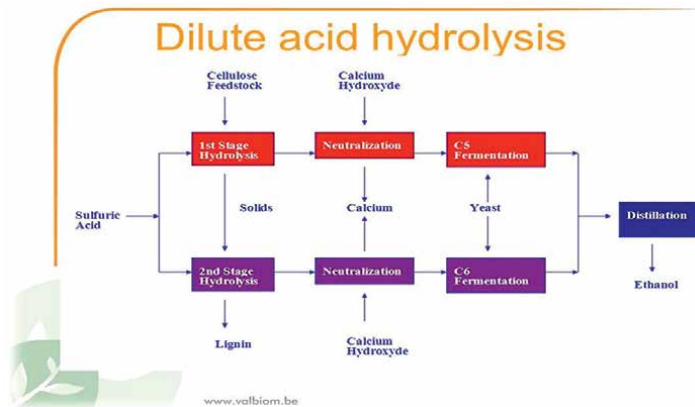
The biomass needs to first be dried to a moisture level of 10% before the Alkanol process can begin, which involves adding 70–77% sulfuric acid. The temperature is kept at 50°C and the acid is added at a ratio of 1.25 acid to 1 biomass. The mixture is then heated to 100°C for another hour after the water is added to dilute the acid to 20–30%. The gel that results from this combination is then compressed to produce an acid-sugar mixture, which is purified to use a chromatographic column.



3.1 Acid hydrolysis in dilutes

One of the earliest, simplest, and most effective processes for generating ethanol from biomass is dilute acid hydrolysis. The biomass is hydrolyzed to produce sugar using diluted acid. The hemicellulose included in the biomass is hydrolyzed in the first step using 0.7% sulfuric acid at 190°C. An improved second stage results in a more

robust cellulose fraction. By utilizing 0.4% sulfuric acid at 215°C, this is accomplished. Following neutralization, the liquid hydrolases are recovered from the process.

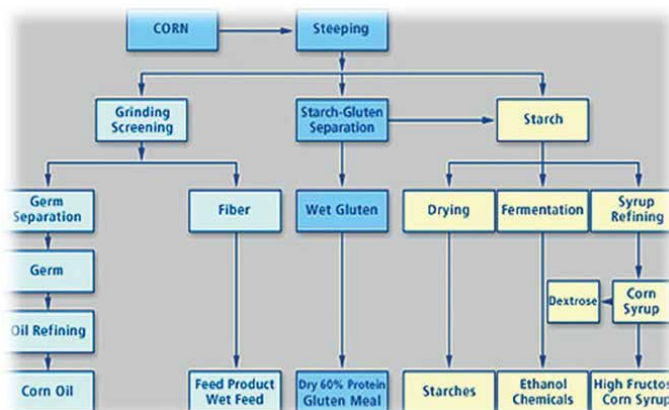


3.2 Enzymatic Hydrolysis

We can similarly break down the biomass using enzymes as opposed to utilizing acid to hydrolyze it into sugar. However, this procedure is still being developed and is highly expensive.

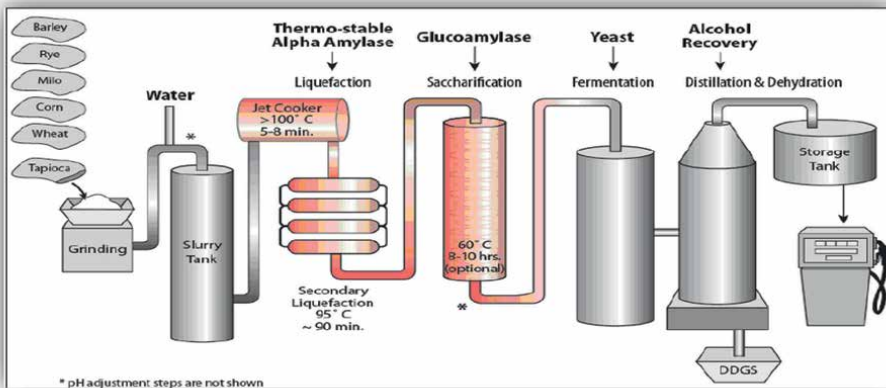
3.3 Wet milling processes

Corn can be processed into ethanol using either the dry milling or the wet milling method. The wet milling procedure involves soaking the maize kernel in warm water. This aids in the breakdown of the corn’s proteins, the release of its starch, and softening of the kernel in preparation for milling. Then, the ground maize is used to make products with starch, fiber, and germ. A gluten-wet cake is made from the starch fraction after it has been centrifuged and saccharified; maize oil is then made by removing the germ. The next step is to extract the ethanol using the distillation process. The wet milling method is commonly applied in businesses that generate several hundred million gallons of ethanol annually.



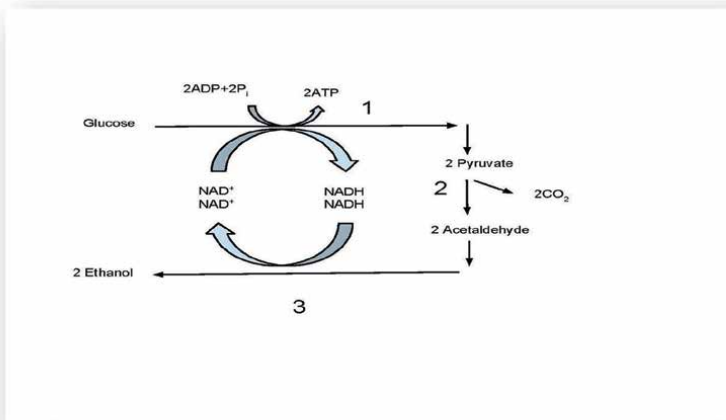
3.4 Dry milling process

Using a hammer mill, the maize kernel is cleaned and reduced to tiny pieces for dry milling. This results in a powder with a consistency similar to a coarse flour. Maize germ, starch, and fiber make up the powder. The combination is hydrolyzed, or changed into sucrose sugars, using enzymes or a moderate acid to create a sugar solution. After cooling, adding yeast causes the mixture to ferment into ethanol. In facilities that annually produce fewer than 50 million gallons of ethanol, dry milling is frequently employed.

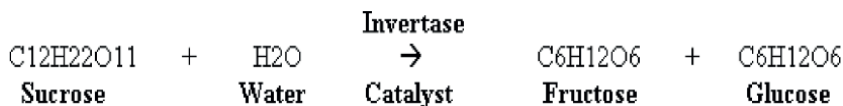


3.5 Sugar fermentation process

The cellulose component of biomass or corn is broken down during the hydrolysis process into sugar solutions, which can subsequently be fermented to produce ethanol. The mixture is heated after adding the yeast. Invertase, an enzyme found in yeast, serves as a catalyst and aids in the breakdown of sucrose carbohydrates into glucose and fructose (both $C_6H_{12}O_6$).

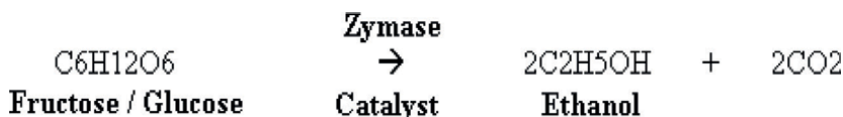


The chemical reaction is shown below



A second enzyme called zymase, which is also present in yeast, then reacts with the fructose and glucose carbohydrates to create ethanol and carbon dioxide.

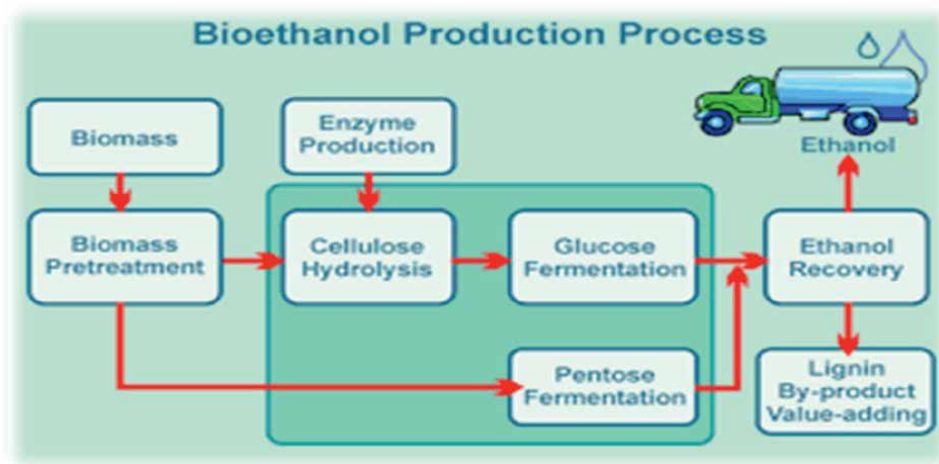
The chemical reaction is shown below:



Between 25°C and 30°C, the fermentation process is carried out over the course of around 3 days.

3.6 Fractional distillation process

The fermentation process results in the production of ethanol, but there is still a sizable amount of water present that needs to be removed. Utilizing the fractional distillation method, this is accomplished. The mixture of water and ethanol is heated during the distillation process. The fact that ethanol has a lower boiling point than water (78.3 vs. 100°C) means that it can be separated and condensed before water does.



4. The possibility of using bioethanol

The performance of the vehicle would not be affected if bioethanol were used as a pure fuel or in a blend with other fuels in sufficient quantities to replace conventional motor fuels [17]. Without any adjustments, the mixture might be burned in a conventional combustion process. Gasohol was the most popular bioethanol-petrol mixture

(E10). 10% bioethanol and 90% gasoline were combined to create gasohol. Most contemporary automobiles with internal combustion engines (ICEs) were capable of burning E10 [12, 17]. The fuel blend E85, which is composed of 15% gasoline and 85% bioethanol, may also contain bioethanol [18]. About 5% of the ethanol created biologically was water. This blend was azeotropic. Because of this, ordinary distillation was insufficient to clean it. Gasoline and diesel fuel were not entirely blended with hydrated ethanol.

Bioethanol and diesel could be blended together by employing the right emulsifiers. Diesohol is a mixture of hydrated alcohol with diesel oil with an emulsifier. Diesel, hydrated ethanol, and a 0.5 percent emulsifier were used to make diesohol [17]. Ethanol was used as gasohol or clean fuel in Brazil (24% bioethanol and 76% gasoline) [12, 19]. The EN228 standard allows for the use of bioethanol as a 5% blend of gasoline in the European Union [12, 20]. Bioethanol was an oxygenated fuel with 35% oxygen content. Lowering the amount of nitrogen oxide (NO_x) and particle pollutants produced during combustion. Utilizing a bioethanol-fuel combination allowed for the decrease in greenhouse gas (GHG) output and oil consumption [12]. It was possible to increase the fuel's oxygen content by adding bioethanol to conventional gasoline, which increased fuel combustion and reduced exhaust pollutants such as CO and unburned hydrocarbons [12, 16]. Bioethanol was added to gasoline to reduce environmental pollution and the use of fossil fuels. Because 1 liter of bioethanol could substitute for 0.72 liters of gasoline, using it as a gasoline substitute proved very cost-effective [14].

5. Conclusion

Bioethanol can be employed as a fuel source. Studies are now being done to advance biofuel producing technologies. Bioethanol manufacturing could be carried out using biomass as a raw source. The investigation mainly concentrated on the usage of biomass wastes. With the help of starch and lignocellulosic biomass, bioethanol was formed. Starch was transformed into bioethanol via three sequential steps: hydrolysis, fermentation, and product purification. Hydrolysis, fermentation, pretreatment, and purification were the four steps that were followed in order to produce bioethanol from lignocellulosic biomass. Pretreatment can be done physically, physiochemically, chemically and biologically. Each of these approaches has benefits and drawbacks. It played a crucial role in choosing the best pretreatment strategy. It was crucial to focus on the creation and application of suitable pretreatment techniques in addition to other phases of the synthesis of bioethanol.

Author details

Chakali Ayyanna^{1*}, Kuppusamy Sujatha², Sujit Kumar Mohanthy³,
Jayaraman Rajangam⁴, B. Naga Sudha⁵ and H.G. Raghavendra¹

1 Department of Pharmacology, CES College of Pharmacy, Kurnool, India

2 Department of Pharmaceutical Chemistry, Sri Ramachandra Institute of Higher Education and Research, Chennai, India


3 Department of Pharmaceutical Chemistry, Shri Vishnu College of Pharmacy, Bhimavaram, India

4 Department of Pharmacology, AMITY Institute of Pharmacy, AMITY University, Lucknow, India

5 Department of Pharmaceutical Chemistry, CES College of Pharmacy, Kurnool, India

*Address all correspondence to: ayyannac5@gmail.com

IntechOpen

© 2023 The Author(s). Licensee IntechOpen. This chapter is distributed under the terms of the Creative Commons Attribution License (<http://creativecommons.org/licenses/by/3.0>), which permits unrestricted use, distribution, and reproduction in any medium, provided the original work is properly cited. 

References

- [1] Saxena RC, Adhikari DK, Goyal HB. Biomass-based energy fuel through biochemical routes: A review. *Renewable and Sustainable Energy Reviews*. 2009;**13**:167-178
- [2] Balat M, Balat H, Öz C. Progress in bioethanol processing. *Progress in Energy and Combustion Science*. 2008;**34**(5):551-573
- [3] Macedo IC, Seabra JEA, Silva JEAR. Green house gases emissions in the production and use of ethanol from sugarcane in Brazil: the 2005/2006 averages and a prediction for 2020. *Biomass and Bioenergy*. 2008;**32**(7):582-595
- [4] Goldemberg J. Ethanol for a sustainable energy future. *Science*. 2007;**315**(5813):808-810
- [5] Ensinas AV, Nebra SA, Lozano MA, Serra LM. Analysis of process steam demand reduction and electricity generation in sugar and ethanol production from sugarcane. *Energy Conversion and Management*. 2007;**48**:2978-2987
- [6] Buddadee B, Wirojanagud W, Watts DJ, Pitakaso R. The development of multi-objective optimization model for excess bagasse utilization: A case study for Thailand. *Environmental Impact Assessment Review*. 2008;**28**:380-391
- [7] Cardona CA, Sánchez ÓJ. Fuel ethanol production: Process design trends and integration opportunities. *Bioresource Technology*. 2007;**98**:2415-2457
- [8] Zaldivar J, Nielsen J, Olsson L. Fuel ethanol production from lignocellulose: A challenge for metabolic engineering and process integration. *Applied Microbiology and Biotechnology*. 2001;**56**:17-34
- [9] Mosier N, Wyman C, Dale B, Elander R, Lee YY, Holtzapple M, et al. Features of promising technologies for pretreatment of lignocellulosic biomass. *Bio/Technology*. 2005;**96**:673-686
- [10] Kuo C-H, Lee C-K. Enhanced enzymatic hydrolysis of sugarcane bagasse by N-methylmorpholine-N-oxide pretreatment. *Bioresource Technology*. 2009;**100**:866-871
- [11] Rossell CEV, Lahr Filho D, Hilst AGP, Leal MRLV. Saccharification of sugarcane bagasse for ethanol production using the Organosolv process. *International Sugar Journal*. 2005;**107**:192-195
- [12] Balat M, Balat H. Recent trends in global production and utilization of bioethanol fuel. *Applied Energy*. 2009;**86**:2273-2282
- [13] Koh LP, Ghazoul J. Biofuels, biodiversity, and people: Understanding the conflicts and finding opportunities. *Biological Conservation*. 2008;**141**:2450-2460
- [14] Kim S, Dale BE. Global potential bioethanol production from wasted crops and crop residues. *Biomass and Bioenergy*. 2004;**26**:361-375
- [15] Enguádanos M, Soria A, Kavalov B, Jensen P. Techno-economic analysis of Bio-alcohol production in the EU: A short summary for decision-makers. 2002
- [16] Maria G, Chisti Y. Biotechnology-a sustainable alternative for chemical industry. *Biotechnology Advances*. 2005;**23**:471-499

[17] Demirbas A. Biofuels sources, biofuel policy, biofuel economy and global biofuel projections. *Energy Conversion and Management*. 2008;**49**(8):2106-2116

[18] De Oliveira MED, Vaughan BE, Rykiel EJ Jr. Ethanol as fuel: Energy, carbon dioxide balances, and ecological footprint. *Bioscience*. 2005;**55**(7):593-602

[19] Demirbas A. Importance of biodiesel as transportation fuel. *Energy Policy*. 2007;**35**:4661-4670

[20] Malca J, Freire F. Renewability and life-cycle energy efficiency of bioethanol and bio-ethyl tertiary butyl ether (bioETBE): Assessing the implications of allocation. *Energy*. 2006;**31**:3362-3380

Section 2

Conversion of Glycerol into
Aromatic Compounds

Sustainable Synthesis of Pyridine Bases from Glycerol

*Israel Pala-Rosas, José L. Contreras, José Salmones,
Ricardo López-Medina, Beatriz Zeifert and
Naomi N. González Hernández*

Abstract

Catalytic processes have been developed to obtain pyridine bases from glycerol, either by direct conversion or with acrolein as an intermediate. When producing acrolein as an intermediate, the reaction may proceed in a single reactor at temperatures above 400°C in co-feeding with ammonia. A system of two interconnected reactors can also be used: one reactor performs the catalytic dehydration of glycerol to acrolein, while in the second reactor acrolein reacts with ammonia to form pyridine bases. Both processes require the use of solid acid catalysts, for which ZSM-5 zeolite-based catalysts are the most studied. In the direct reaction between glycerol and ammonia, the most active catalysts were Cu/HZSM-5 and the composite zeolite HZSM-5/11. In the two-step systems, the dehydration of glycerol to acrolein over a HZSM-5 zeolite modified by alkali treatment or over a HZSM-22 zeolite modified by an alkali-acid treatment as catalysts in the first reactor, in combination with a Zn impregnated acid-treated-HZSM-5 zeolite have shown to be efficient catalyst pairs for the synthesis of pyridine bases from glycerol in two-step processes. When using acrolein or acrolein diacetals, the most active catalysts were a 4.6%Cu–1.0%Ru/HZSM-5 zeolite in the presence of hydrogen, and a ZnO/HZSM-5-At-acid zeolite.

Keywords: pyridine, picolines, alkylpyridines, lutidines, glycerol, acrolein, zeolite catalyst, ammonia

1. Introduction

Pyridine bases are a family of aromatic heterocyclic compounds of commercial interest since they found applications as solvents in organic reactions, and as precursors of drugs, polymers, insecticides, herbicides, dyes, and adhesives, being pyridine, the series of picolines (α -, β -, and γ -picoline) and some lutidines the most important [1, 2].

The pyridine (azabenzene) structure is defined by a six-membered ring consisting of five carbon atoms and one nitrogen atom (**Figure 1**). It can be considered as an analog of benzene in which one CH group is replaced by a nitrogen atom [3]. On the other hand, the simplest alkyl-substituted pyridines are α -picoline (2-methylpyridine), β -picoline (3-methylpyridine), and γ -picoline (4-methylpyridine), whose structures vary

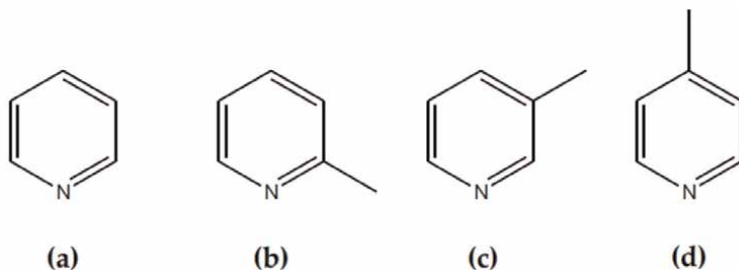


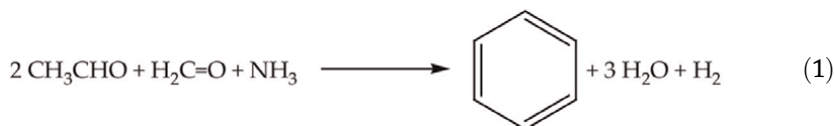
Figure 1. Chemical structures of (a) pyridine, (b) α -picoline, (c) β -picoline, and (d) γ -picoline.

according to the location where the methyl group is attached to the pyridine ring, either in position 2, 3, or 4 regarding the nitrogen atom. Physically, pyridine and picolines are considered to be dipolar, aprotic solvents, similar to dimethylformamide or dimethyl sulfoxide. They are colorless, flammable, irritating, toxic liquids with an unpleasant odor, and miscible in water and in most organic solvents [2, 3].

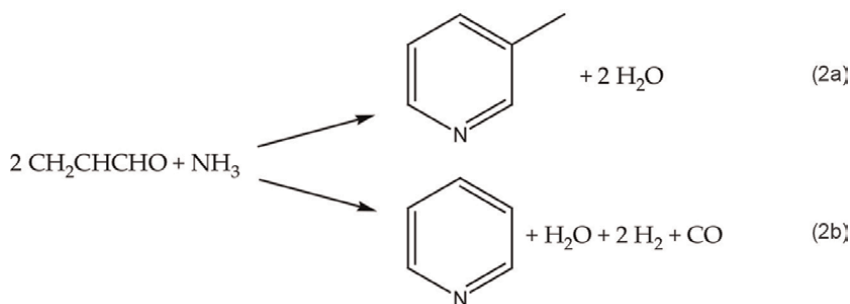
The chemical properties of pyridines are related to their structure, that is, ring aromaticity, presence of a basic ring nitrogen atom, π -deficient character of the ring, large permanent dipole moment, easy polarizability of the π -electrons, activation of functional groups attached to the ring, and presence of electron-deficient carbon atom centers at the α - and γ - positions. One or more of these factors can lead to different reactions of pyridine bases, namely electrophilic attack at nitrogen, electrophilic attack at carbon, nucleophilic attack at carbon or hydrogen, and free radical attack at carbon, besides varied substitution reactions of the carbon with N, O, S, halogen, or alkyl groups in the alkyropyridines [2].

The first industrial method for the production of pyridines was by their extraction from fossil sources such as coal tar, oil, and shale. However, it was only possible to obtain yields of less than 0.1% from a mixture of different pyridine bases and other organic compounds. In addition, the products obtained by this process had high sulfur contents, making it impossible to use them in pharmaceutical and agrochemical applications. So that, with a few exceptions, obtaining pyridine compounds by this method was expensive and had not been able to cover the industrial demand [3, 4].

Nowadays, the industrial synthesis of pyridine is based on the aminocyclization reaction (condensation/cyclization) between formaldehyde, acetaldehyde, and ammonia (NH_3) using a ZSM-5 catalyst as shown in Eq. (1). This method generates a mixture of α -, β -, and γ -picoline as byproducts [1].



Also, the reaction between acrolein and ammonia has been used for the synthesis of β -picoline and pyridine by means of two parallel reactions, as shown in stoichiometric Eqs. (2a) and (2b). This process allows to modulate the products selectivity, avoiding the formation of α - and γ -picoline, being β -picoline the main reaction product [1].



Despite these synthesis methods, the high demand of pyridine bases has led to research on the use of different raw materials, such as aldehydes, ketones, and alcohols, from renewable sources, to improve the yield of a desired product [5, 6].

On the other hand, glycerol has gained importance as raw material in several catalytic processes, namely hydrogenolysis, dehydration, oxidation, and esterification, since it is industrially obtained as byproduct in the production of biodiesel from vegetable and algae oils [7]. Specifically, the aminocyclization reaction between glycerol and ammonia represents a potential alternative to the current industrial process for the synthesis of pyridine compounds, based on petroleum-derived aldehydes [8–13]. In addition, the acrolein obtained by the catalytic dehydration of glycerol can also be used as feedstock for the production of pyridine bases [14–16].

In this context, this chapter presents the advances on the catalysts and reactor configurations employed for the synthesis of pyridine bases using glycerol and its derivatives, acrolein, and acrolein dialkyl acetals as raw materials.

2. Synthesis of pyridine bases from glycerol in single-step processes

The synthesis of pyridine compounds from glycerol, in batch and continuous one-pot systems, has been reported, under pyrolysis or microwave heating conditions [8]. In the batch pyrolysis, pure glycerol and an ammonium salt, such as $(\text{NH}_4)_2\text{HPO}_4$, $\text{NH}_4\text{H}_2\text{PO}_4$, $(\text{NH}_4)_2\text{SO}_4$, NH_4Cl , NH_4OAc , or $\text{H}_2\text{NNH}_2 \cdot \text{H}_2\text{SO}_4$, were packed into a glass tubular reactor. The system was heated to a desired temperature and the reaction was carried out for about 1.5 h. The reason for using ammonium salts was to provide an acidic environment required for the conversion of glycerol to acrolein. Additionally, under thermal conditions, ammonium salts would decompose and release gaseous ammonia for its condensation and cyclization with the acrolein produced from glycerol. A mixture of pyridine and β -picoline was obtained and the highest product yield (36%) was reached when reacting glycerol with $(\text{NH}_4)_2\text{HPO}_4$ at 450°C . However, glycerol also produced other volatile compounds, which polymerize with acrolein, resulting in tar formation and low product yields.

In the continuous system, an aqueous glycerol solution was fed to a tubular reactor, previously loaded with the ammonium salt and heated at 450°C . The best result (40% product yield) was obtained with $(\text{NH}_4)_2\text{HPO}_4$ and a mixture of 1 g glycerol and 7.2 ml H_2O . A mixture of pyridine, β -picoline, ethylpyridine, and ethylmethylpyridines was obtained, suggesting that during thermal degradation of glycerol, both acrolein and acetaldehyde were obtained as products. The low yield of pyridines was attributed to the uncontrolled formation and subsequent polymerization of acrolein at the reaction temperature [8].

For the microwave-assisted synthesis, glycerol and the ammonium salt were placed and closed into a glass vial, stirred, and subsequently irradiated by microwave energy to complete the reaction. The authors found that the addition of an organic acid, such as acetic acid, benzoic acid, or *p*-toluenesulfonic acid, improved the formation of pyridine bases [8].

On the other hand, the configuration of the continuous-flow fixed-bed reactor presented in **Figure 2** has been commonly used to evaluate the performance of solid catalysts for the gas-phase synthesis of pyridines from glycerol. The reactor, previously loaded with a certain amount of catalyst and heated at a required temperature, is fed at the top of the reactor with a gaseous stream composed of water, glycerol, and nitrogen (N_2) as carrier gas. At the same time, a flow of preheated ammonia is introduced to react with the glycerol stream by effect of the catalyst. The stream at the reactor outlet contains the pyridine bases and byproducts.

The direct synthesis of pyridine bases from glycerol was performed in a continuous-flow fixed-bed reactor in presence of zeolite catalysts, using ammonia as carrier gas and as the reactive nitrogen source [9]. It was found that the optimal conditions were 550°C, a weight-hourly space-velocity (WHSV) of glycerol of 1 h^{-1} , a NH_3 /glycerol molar ratio of 12/1, and HZSM-5 zeolite (Si/Al = 25) as a catalyst. Total conversion of glycerol was reached with a total yield of pyridines around 35.6%. Pyridine was the main reaction product with a selectivity of 70.7%, while α -, β -, and γ -picoline exhibited selectivities of 8.6%, 17.8%, and 2.9%, respectively. Gaseous compounds, such as CH_4 , C_2H_4 , C_3H_6 , and CO, added a yield of 49.3%, and aromatics were produced at around 2.2% yield. After five reaction/regeneration cycles, a slight deactivation of the catalyst was observed.

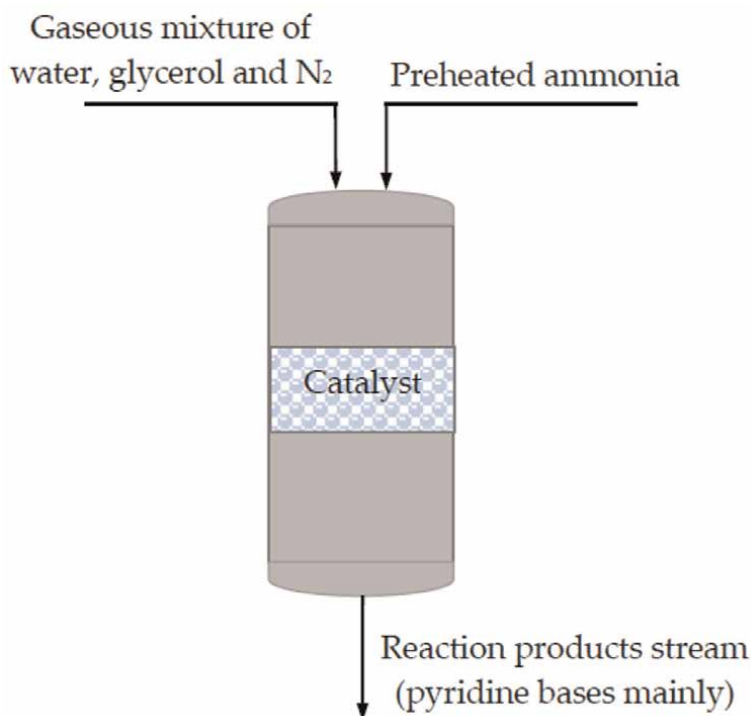


Figure 2. Continuous-flow fixed-bed reactor for the single-step gas-phase aminocyclization between glycerol and ammonia.

The gas-phase aminocyclization between glycerol and ammonia in presence of a Cu/HZSM-5 catalyst has also been reported [10]. The reaction was performed in a fixed-bed reactor using a catalyst with 4.6% Cu supported on HZSM-5 zeolite with a ratio Si/Al = 38. The identified products were pyridine, α -picoline, β -picoline, acetonitrile, propionitrile, acetaldehyde, propylene, ethylene, and CO₂. The best reaction conditions were 520°C, atmospheric pressure, a NH₃/glycerol molar ratio of 7/1, and a gas-hourly space-velocity (GHSV) of 300 h⁻¹, reaching a total yield of pyridines around 42.8%, 34.9% of pyridine yield, 2.4% of α -picoline, and 5.5% of β -picoline yield, respectively.

The synthesis of pyridine bases from glycerol over a series of modified ZSM-5 zeolites in a continuous fixed-bed reactor was reported [11]. The catalysts tested were a series of metal oxide-impregnated ZSM-5 zeolite (ZnO, La₂O₃, and Fe₂O₃), an alkali-treated zeolite (HZSM-5-At), and the alkali-acid treated ZSM-5 and ZSM-22 zeolites (HZSM-5-At-acid and HZSM-22-At-acid, respectively). The identified products in this process were pyridine, α -picoline, β -picoline, γ -picoline, small amounts of 3-ethylpyridine, 2-methyl-5-ethylpyridine, 3,5-dimethylpyridine, and benzene derivatives, as well as trace amounts of CO_x and C₁ – C₂ hydrocarbons. At 425°C; LHSV = 0.60 h⁻¹, glycerol concentration of 36 wt%, molar ratio NH₃/glycerol = 4/1, and time on stream (TOS) between 1 and 3 h, the HZSM-5-At-acid catalyst gave the highest total yield of pyridines (28.76%), with yields of pyridine, α -picoline, β -picoline, and γ -picoline around 15.67%, 1.90%, 10.02%, and 1.17%, respectively.

A composite zeolite HZSM-5/11 (SiO₂/Al₂O₃ = 78) has been synthesized and employed as a catalyst in the reaction between an aqueous solution of 20 wt% glycerol and ammonia in a fixed-bed reactor [12]. The products obtained using this catalyst were pyridine, α -picoline, β -picoline, acetonitrile, propionitrile, acetaldehyde, C₂H₄, and C₃H₆. The analysis of the process variables on the synthesis of pyridines revealed that the optimal reaction conditions were a reaction temperature of 520°C, a molar ratio NH₃/glycerol of 12/1, and a GHSV of 300 h⁻¹. At these conditions, glycerol reached total conversion and the total yield of pyridines was 40.8%, with selectivities of pyridine, α -picoline, and β -picoline around 27.7%, 2.6%, and 10.5%, respectively.

3. Synthesis of pyridine bases from glycerol in two-step processes with acrolein as intermediate

The conversion of glycerol to pyridine bases has also been carried out by first producing acrolein, and subsequently reacting it with ammonia [11, 13]. This process can be performed in a system with two coupled reactors. As shown in **Figure 3**, an aqueous solution of glycerol and a N₂ flow are mixed, preheated/vaporized and fed to the first reactor, which was previously loaded with a solid acid catalyst. In this first stage of the process, the catalytic dehydration of glycerol to acrolein takes place at temperatures between 280°C and 350°C.

Subsequently, the stream of dehydration products is introduced to the second reactor, which is simultaneously fed with preheated ammonia to carry out the aminocyclization reaction between acrolein and ammonia to produce pyridine bases in presence of an acid catalyst at temperatures between 375°C and 475°C. Both reactors can be loaded with the same or different acid catalyst. According to literature, this process allows to improve the total yield of pyridines by performing separately the dehydration and aminocyclization reactions at adequate temperatures [11, 13].

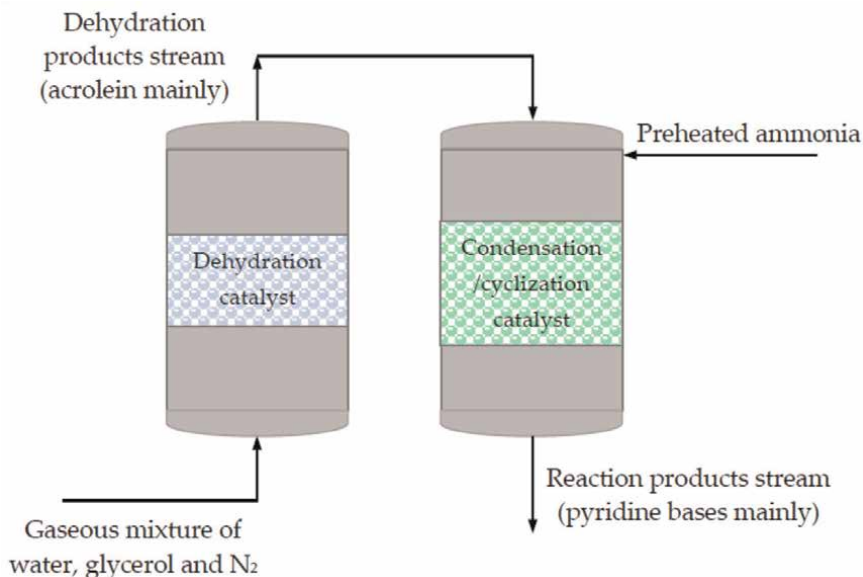


Figure 3. Continuous flow reaction system for the two-step gas-phase conversion of glycerol and ammonia to pyridine bases. Adapted from ref. [11].

Luo et al. [11] performed the synthesis of pyridines from glycerol in a two-step system comprised of a pair of reactors connected in series with different catalysts, denoted as a catalyst pair. The catalysts tested in the first reactor were the HZSM-5, HZSM-5-At, and HZSM-5-At-acid zeolites, while for the second reactor the HZSM-5-At-acid and the ZnO/HZSM-5-At-acid zeolites were evaluated. The reaction products identified in this process were pyridine, α -picoline, β -picoline, γ -picoline, 3-ethylpyridine, 2-methyl-5-ethylpyridine, 3,5-dimethylpyridine, benzene derivatives, trace amounts of CO_x, and C₁ – C₂ hydrocarbons. The best results were obtained with the catalyst pair (HZSM-5-At + ZnO/HZSM-5-At-acid) at 330°C for the first reactor; 425°C for the second reactor; LHSV = 0.45 h⁻¹; a glycerol concentration of 20 wt %; a molar ratio NH₃/glycerol = 5/1; and TOS between 1 and 3 h, obtaining a total yield of pyridine bases around 62.25%, without the formation of γ -picoline.

Similarly, Zhang et al. [13] performed the conversion of glycerol to pyridine bases in a system of two series-connected reactors. The catalytic dehydration of a 20 wt.% glycerol aqueous solution to acrolein was accomplished at 280°C in the first reactor over an alumina (γ -Al₂O₃) catalyst modified with Fe and P. The output stream from the first reactor was fed to the second one, previously loaded with a Cu_{4.6}Pr_{0.3}/HZSM-5 catalyst, which reacted with ammonia to produce pyridine compounds. The identified products were pyridine, α -picoline, β -picoline, 2,4-lutidine, acetonitrile, propionitrile, ethylene, propylene, butylene, and CO₂. At optimal reaction conditions, that is, 420°C in the second reactor, atmospheric pressure, GHSV = 300 h⁻¹, and NH₃/acrolein molar ratio of 7/1; glycerol achieved total conversion and the total yield of pyridines was 60.2%, while pyridine and β -picoline reached 39% and 20% yield, respectively. The impregnation of the zeolite with Cu and Pr resulted in the increase of the Lewis acidity and an improved dehydrogenation activity, enhancing the selectivity toward pyridine bases.

4. Synthesis of pyridine bases from acrolein and acrolein derivatives

Currently, the catalytic dehydration of glycerol, in the presence of a solid acid catalyst, is under research since it is considered a sustainable alternative method to the industrial process based on the partial oxidation of propylene for the synthesis of acrolein [14–16]. The use of acrolein for the synthesis of pyridine bases allows to modulate the products selectivity, enhancing the production of β -picoline and pyridine, without the formation of other pyridine compounds [3].

The synthesis of pyridine bases from acrolein in a batch process has been barely reported. The liquid-phase reaction of acrolein with ammonium acetate ($\text{CH}_3\text{COONH}_4$) over a $\text{SO}_4^{2-}/\text{ZrO}_2\text{-FeZSM-5}$ catalyst was reported [17]. The process requires the addition of a $\text{C}_2\text{-C}_6$ carboxylic acid, preferably acetic acid (CH_3COOH), as the reaction medium and solvent of acrolein. It was found that only β -picoline was generated, without the formation of any other pyridine compound. At the optimal conditions of 130°C as reaction temperature, a concentration of 14 wt% acrolein in the solution, a liquid flow of acrolein solution of 12 ml/h, and a catalyst usage of 0.7 g/g acrolein, the yield of β -picoline reached 60%. The presence of a carboxylic acid promoted the formation of β -picoline and retarded the polymerization of acrolein and its intermediate propylene imine.

Schematized in **Figure 4**, the gas-phase reaction between acrolein and ammonia in a continuous-flow fixed-bed reactor has also been reported [18–20]. Similarly, to the continuous single-step process described in Section 2, a preheated gaseous mixture of water, acrolein, and nitrogen is fed to the reactor previously loaded with a solid acid catalyst and heated to the reaction temperature. Simultaneously, a preheated flow of ammonia is introduced at the same end of the reactor as the acrolein stream, to come into contact with the catalytic bed and producing the pyridine bases.

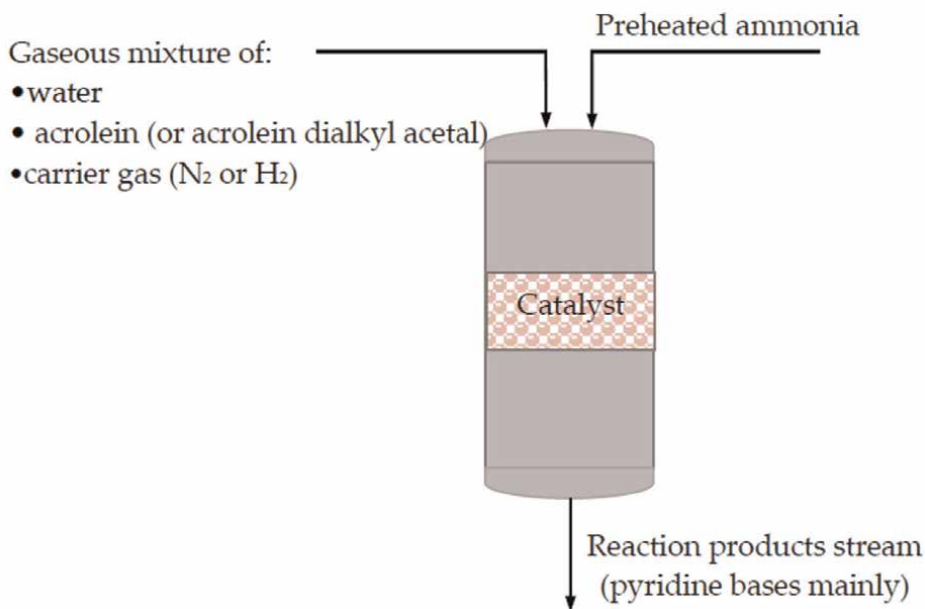


Figure 4. Continuous-flow fixed-bed reactor for the gas-phase aminocyclization between acrolein and ammonia.

This process has been studied with greater versatility than the direct reaction with glycerol, since the use of hydrogen as carrier gas has been explored, as well as the use of acrolein derivatives as raw material, specifically acrolein dialkyl acetals [21, 22].

The gas-phase reaction between acrolein and ammonia was studied by comparing the activity of a parent H-ZSM-5 catalyst and a series of zeolites modified with magnesium nitrate ($\text{Mg}(\text{NO}_3)_2$), hydrofluoric acid (HF), or both [18]. The reaction was performed at atmospheric pressure and 425°C in a fixed-bed reactor. When using the HF/MgZSM-5 catalyst, the total yield of pyridines achieved its maximum value (58.86%), with 30.38% being β -picoline and 26.59% being pyridine.

The use of hydrogen as a carrier gas in the synthesis of pyridine bases from acrolein and ammonia has been explored in presence of bimetallic copper-based ZSM-5 catalysts [19]. The identified products in this process were pyridine, α -picoline, β -picoline, 2,4-lutidine, acetonitrile, propionitrile, ethylene, propylene, butylene, and CO_2 . Among the tested catalysts, the 4.6%Cu–1.0%Ru/HZSM-5 zeolite produced the highest total yield of pyridines (69.4%) with pyridine and β -picoline yields around 27% and 37%, respectively, performing the reaction at 420°C, acrolein concentration of 20 wt.%, molar ratio $\text{NH}_3/\text{acrolein} = 3.5/1$, GHSV = 300 h^{-1} , and H_2 flow of 8.5 ml/min as optimal reaction conditions. The presence of Cu, Ru, and hydrogen enhanced the hydrogenation/dehydrogenation activity of the catalyst, promoting the conversion of acrolein to propionaldehyde, improving thus the formation of pyridine bases, notably of β -picoline. Additionally, the catalyst was stable with TOS, maintaining the total conversion of acrolein during 40 h, and decreasing gradually to 90.5% at 75 h of TOS.

The use of a catalyst other than ZSM-5 zeolite has been scarcely reported for the synthesis of pyridine bases from acrolein. Specifically, Y-type zeolites with different Si/Al composition has been reported as catalysts in the reaction between acrolein and ammonia at 360°C, pure acrolein, molar ratio $\text{NH}_3/\text{acrolein} = 2$, and GHSV = 4994 h^{-1} [20]. The best catalytic performance was obtained with the catalyst with an atomic ratio Si/Al = 45. The acrolein conversion was around 93% while the pyridine and β -picoline yields were 15% and 19.1%, respectively. However, formaldehyde and acetaldehyde were also detected as reaction products and the catalysts were rapidly deactivated. It was found that the total acidity of the catalysts was the key factor for the conversion of acrolein and the type of acid sites influenced the products selectivity.

Acrolein dialkyl acetals have also been used as reagents for the synthesis of pyridines [21, 22]. When performing the gas-phase reaction between acrolein diethyl acetal and ammonia in a continuous fixed-bed reactor, the ZnO/HZSM-5 zeolite has shown superior catalytic performance than ZnO/HY and ZnO/ α - Al_2O_3 catalysts. At 450°C; LHSV = 0.85 h^{-1} ; molar ratio of $\text{NH}_3/(\text{acrolein diethyl acetal}) = 4$; TOS between 1 and 3 h; and 1 wt.% of Zn loading, the total yield of pyridines was 61.14%, with pyridine and β -picoline yields of 26.87% and 34.27%, respectively [21].

Similarly, the reaction between acrolein dimethyl acetal and ammonia was performed over a series of ZSM-5 zeolites treated with $\text{Mg}(\text{NO}_3)_2$, NH_4F -HF, or both [22]. The reaction products were pyridine, α -picoline, β -picoline, and 3,5-dimethylpyridine. At 450°C, LHSV = 0.75 h^{-1} , molar ratio $\text{NH}_3/(\text{acrolein dimethyl acetal}) = 3.5/1$, TOS = 1–3 h, and F/Mg-ZSM-5 catalyst with small particle size; the highest total yield of pyridines was 55.4%, with 14.5% for pyridine, 0.9% of α -picoline, 34.2% of β -picoline, and 5.8% yield of 3,5-dimethylpyridine. The catalytic activity of the catalyst was related to an adequate concentration of total acid sites and a ratio B/L < 1.

5. The effect of catalyst acidic properties on the synthesis of pyridine bases from glycerol and acrolein

The reaction conditions and catalytic performance of representative zeolite catalysts reported in the literature for the gas-phase synthesis of pyridine bases from glycerol, acrolein, and acrolein dialkyl acetals in fixed-bed reactors are presented in **Table 1**.

The main features that affect the catalytic performance of these catalysts in the synthesis of pyridine bases are their acidic properties, namely the type and strength of acid sites. In the single-step process, the reaction between glycerol and ammonia takes place through a complex network of simultaneous and subsequent reactions, among which the most relevant for the synthesis of pyridine bases are the catalytic dehydration of glycerol to acrolein, and its subsequent condensation/cyclization with ammonia to produce pyridine bases. Both reactions proceed at the same time in the single

Catalyst	Feedstock composition ^a	T(°C) ^b	Space-velocity (h ⁻¹)	X (%) ^f	Y (%) ^g	TOS (h) ^h	Coke (wt. %) ⁱ	Ref.
HZSM-5	Pure gly, NH ₃ /gly = 12/1	550	1 ^c	100	Total = 36 Py = 25.2 αP = 3.1 βP = 6.3 γP = 1.0	—	10	[9]
4.6%Cu/HZSM-5	20 wt% gly aq. soln., NH ₃ /gly = 7/1	520	300 ^d	100	Total = 43 Py = 34.9 αP = 2.4 βP = 5.5	32	27.4	[10]
HZSM-5-At-acid	36 wt% gly aq. soln., NH ₃ /gly = 4/1	425	0.60 ^e	100	Total = 29 Py = 15.7 αP = 1.9 βP = 10.0 γP = 1.2	11	N.R.	[11]
HZSM-5/11	20 wt% gly aq. soln., NH ₃ /gly = 12/1	520	300 ^d	100	Total = 41 Py = 27.7 αP = 2.6 βP = 10.5	2	N.R.	[12]
Two-step process HZSM-5-At + ZnO/ HZSM-5-At-acid	20 wt% gly aq. soln., NH ₃ /gly = 5/1	T ₁ = 330 T ₂ = 425	0.45 ^e	100	Total = 62 Py = 35.8 αP = 0.06 βP = 25.8	11	N.R.	[11]
Two-step process FeP/γ-Al ₂ O ₃ Cu ₄ .6Pr _{0.3} / HZSM-5	20 wt% gly aq. soln., NH ₃ /gly = 7/1	T ₁ = 280 T ₂ = 420	300 ^d	100	Total = 60 Py = 39 βP = 20.2 2,4-L = 1	10	N.R.	[13]
HF/MgZSM-5	Molar ratio acr/H ₂ O/NH ₃ = 1/2/2	425	500 ^d	100	Total = 59 Py = 26.6 βP = 30.4	12	N.R.	[18]
4.6%Cu-1%Ru/ HZSM-5	20 wt% acr. aq. soln., NH ₃ /acr = 3.5/1	420	300 ^d	100	Total = 69 Py = 27 βP = 37 2,4-L = 5.4	75	14	[19]

Catalyst	Feedstock composition ^a	T(°C) ^b	Space-velocity (h ⁻¹)	X (%) ^f	Y (%) ^g	TOS (h) ^h	Coke (wt. %) ⁱ	Ref.
Y-45	Pure acr., molar ratio acr/ NH ₃ = 1/2	360	4994 ^d	92.9	Total = 34 Py = 15 βP = 19.1	0.75	22.5	[20]
1%Zn/ HZSM-5	Molar ratio (acr. Diethyl acetal)/ NH ₃ /H ₂ O = 1/4/1	450	0.85 ^e	100	Total = 61 Py = 26.9 βP = 34.3	11	8	[21]

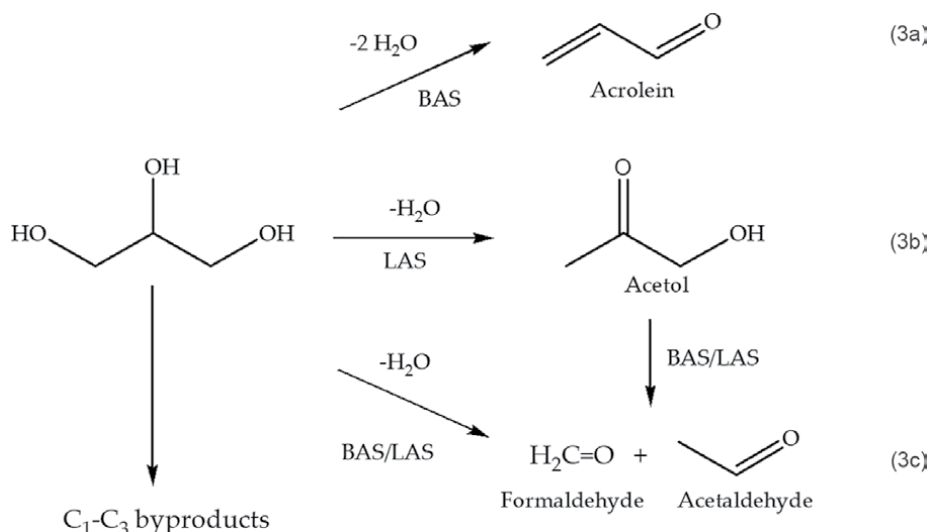
^a gly = glycerol, acr = acrolein, ^b T = reaction temperature, ^c WHSV = weight hourly space-velocity, ^d GHSV = gas hourly space-velocity, ^e LHSV = liquid hourly space-velocity, ^f X = feedstock conversion, ^g Y = product yield, Total = total yield of pyridine bases, Py = yield of pyridine, αP = yield of α-picoline, βP = yield of β-picoline, γP = yield of γ-picoline, 2,4-L = yield of 2,4-lutidine, 3,5-DMP = yield of 3,5-dimethyl pyridine, ^h TOS = time on stream, ⁱ N.R. = not reported.

Table 1.

Reaction conditions and catalytic performance of zeolite catalysts during the synthesis of pyridine bases from glycerol, acrolein, and acrolein dialkyl acetals in continuous systems.

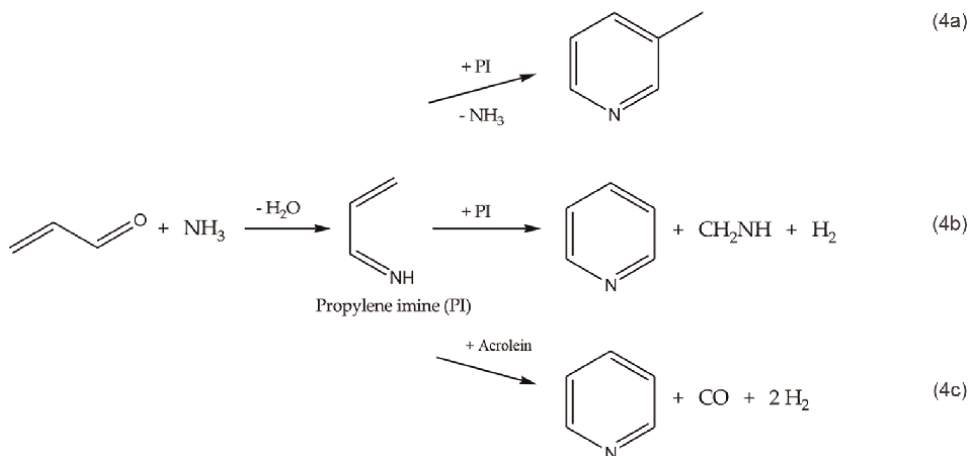
catalytic bed [9–12]. In the two-stage systems, these reactions occurred independently in interconnected reactors [11, 13].

As presented in Eq. (3a), the production of acrolein from glycerol occurs primarily over the Brønsted acid sites (BAS) of the catalyst. However, other dehydration products are obtained, that is, the conversion of glycerol to acetol proceeds over Lewis acid sites (LAS) as in Eq. (3b), while formaldehyde and acetaldehyde can be produced from glycerol (Eq. 3c) or acetol, either over BAS or LAS. Depending on the type of catalyst and the reaction conditions, minor amounts of byproducts, such as aldehydes, ketones, carboxylic acids, and alcohols, in the range of C₁–C₃ may be obtained from the glycerol dehydration reaction [14, 15].



Furthermore, the reaction between acrolein and ammonia proceeds in acid medium, that is, a carboxylic acid in homogeneous reactions or over a solid acid catalyst in heterogeneous systems, mostly a ZSM-5 catalyst. Infrared spectroscopy and

theoretical studies have demonstrated that acrolein can react with ammonia over LAS and BAS, producing propylene imine (prop-2-en-1-imine). This compound can undergo a Michael reaction over Brønsted or weak Lewis acid sites, condensing with another propylene imine, closing the ring structure, and producing β -picoline with the liberation of ammonia, as in Eq. (4a) [23, 24].



Additionally, as shown in Eqs. (4b) and (4c), the formation of pyridine takes place by a Diels-Alder reaction over strong Lewis sites, in which propylene imine condensates and cyclizes with acrolein or with another propylene imine, releasing CO or CH_2NH , respectively [23, 24]. Similar reaction steps and imine intermediates have been reported in the reaction between formaldehyde, acetaldehyde, and ammonia obtaining pyridine, α -picoline, β -picoline, and γ -picoline as products [24, 25].

Experimental studies have revealed the importance of catalyst acidity on the synthesis of pyridine bases. The effect of the Si/Al molar ratio of HZSM-5 zeolites on the reaction between glycerol and ammonia has been reported [9]. The increase of the Si/Al ratio from 25 to 80 decreased the total acidity from 580.6 to 92.4 $\mu\text{mol/g}$, resulting in the decrease of the total yield of pyridines with 26%, 22.85%, and 20.9% for Si/Al ratios of 25, 50, and 80, respectively. However, the pyridine selectivity increased from 67.3% to 69.3% and 72.3%, while the selectivity to β -picoline decreased from 21.4% to 17.9% and 16.1% in the same order.

The influence of acidity on the catalytic activity of a series of Cu/HZSM-5 zeolites, with Si/Al molar ratios of 25, 38, 50, 80, and 117, has been explored [10]. The total yield of pyridines increased from 40–43% with the change of Si/Al from 25 to 50. The further increase in the Si/Al ratio resulted in the decrease of the total yield of pyridines and pyridine. It was concluded that an appropriate proportion of BAS and LAS in the catalyst is a key factor for the synthesis of pyridine bases. However, the BAS/LAS ratio is not the only factor affecting the catalytic activity, but also the structure of HZSM-5 and the amount of Cu which enhanced the dehydrogenation/hydrogenation activity of the catalyst.

The acidity of a series of Mg- and HF-modified zeolites affected the gas-phase reaction between acrolein and ammonia [18]. The total yield of pyridines was 8.81%, 52.73%, and 58.86% for the MgZSM-5, HF/ZSM-5, and HF/MgZSM-5 catalysts, respectively. The MgZSM-5 zeolite presented a large quantity of acid sites and a low yield of pyridine bases, while the HF/ZSM-5 and HF/MgZSM-5 exhibited weaker and fewer acid sites and high yields of pyridine compounds. A certain concentration of

Brønsted acid sites and weak Lewis acid sites may promote the formation of β -picoline, while a high concentration of strong acid sites favored the synthesis of pyridine and polymers. It was concluded that the concentration and strength of acid sites promote the formation of pyridine bases, that is, proper amounts of BAS and weak LAS are necessary for the acrolein activation and pyridines formation, as well as the decrease in the formation of polymerization products (coke precursors).

A critical point of these processes is the catalyst deactivation by the deposition of carbonaceous compounds, which are formed by the polymerization of reaction products by the effect of the acid sites of the catalyst. Additionally, pyridine bases are strongly adsorbed on the acidic sites of the catalyst, being decomposed into carbon depositions [18, 20, 21]. In this sense, a proper amount and strength of acid sites can allow to control the polymerization reactions, and thus the catalyst deactivation.

In the direct reaction between glycerol and ammonia over molecular sieves, namely β -zeolite, MCM-41, and ZSM-5, the coke yield of the catalysts were 30.1%, 19.4%, and 13.7%, respectively, in agreement with the total acidity of the catalysts [9], as shown in **Figure 5**.

The comparison of HZSM-5 and ZnO/HZSM-5 catalysts in the reaction of acrolein diethyl acetal with ammonia, showed that both catalysts suffer a rapid deactivation resulting in the decrease of the total yield of pyridines. However, the ZnO/HZSM-5 zeolite, with a minor amount of total acid sites and a higher amount of weak acid sites than the HZSM-5 catalyst, exhibited the highest yield of pyridines even at longer TOS [21].

The characterization of the catalysts after reaction by ^{13}C NMR, FTIR, and Raman spectroscopies has suggested that the coke formed on the zeolites (Y and ZSM-5) was constituted by aliphatic species with alkoxy groups, as well as large polyaromatic compounds, when using formaldehyde, acetaldehyde, acrolein, and acrolein diethyl acetal as reactants for the synthesis of pyridine bases [20, 26, 27].

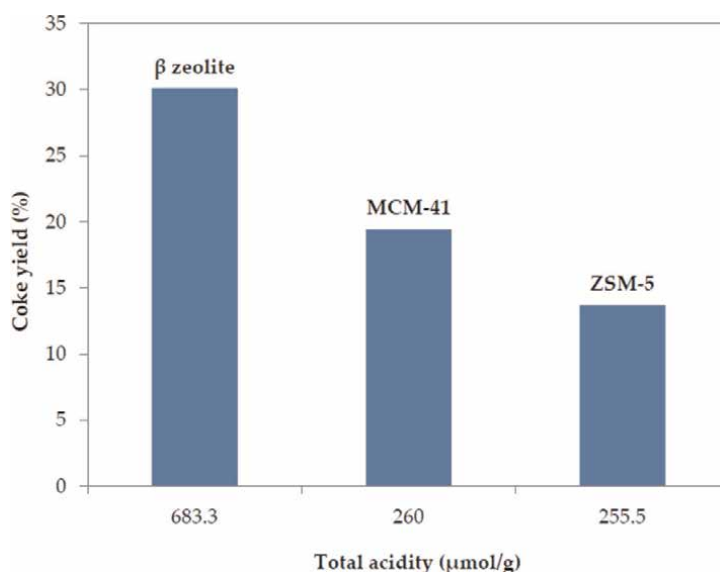


Figure 5. Effect of the total acidity on the coke yield of molecular sieve catalysts in the reaction between glycerol and ammonia. Adapted from ref. [9].

6. Conclusions

Pyridine bases can be obtained from glycerol and ammonia by an aminocyclization reaction, either in single-step or two-step processes. Glycerol derivatives, such as acrolein and acrolein dialkyl acetals, can also be used as raw materials for this reaction. The main process variables are the reaction temperature, the concentration of a reactant in water, the NH_3 /reactant molar ratio, and the space velocity in continuous fixed-bed reactors. When using glycerol as feedstock in the single-step process, the reactors operate usually at temperatures between 450°C and 550°C. The two-step process allows us to improve the total yield of pyridines by performing separately the dehydration and aminocyclization reactions at adequate temperatures, this is 280–350°C and 375–450°C for the first and second reactor, respectively. Single-step processes with acrolein or acrolein dialkyl acetals require reaction temperatures between 420°C and 450°C. The catalysts for the revisited processes are based on ZSM-5 zeolite. The most active catalyst for the direct synthesis from glycerol is Cu/HZSM-5, while for the two-step process, the catalyst pair (HZSM-5-At + ZnO/HZSM-5-At-acid) exhibits higher activity and selectivity. When using acrolein, the most active catalyst is a 4.6%Cu-1%Ru/HZSM-5 zeolite with hydrogen as a carrier gas, while a 1%Zn/HZSM-5 catalyst showed the highest yield of pyridines using acrolein diethyl acetal as raw material.

Acknowledgements

The authors acknowledge the Instituto Politécnico Nacional and the Universidad Autónoma Metropolitana for their support to develop this investigation. I. Pala-Rosas thanks the support of the company Síntesis y Aplicaciones Industriales S.A.

Conflict of interest

The authors declare no conflict of interest.

Author details


Israel Pala-Rosas¹, José L. Contreras^{2*}, José Salmones¹, Ricardo López-Medina², Beatriz Zeifert¹ and Naomi N. González Hernández²

1 Higher School of Chemical Engineering and Extractive Industries, National Polytechnic Institute, Mexico City, Mexico

2 CBI-Energy, Autonomous Metropolitan University-Azcapotzalco, Mexico City, Mexico

*Address all correspondence to: jlcl@azc.uam.mx

IntechOpen

© 2023 The Author(s). Licensee IntechOpen. This chapter is distributed under the terms of the Creative Commons Attribution License (<http://creativecommons.org/licenses/by/3.0>), which permits unrestricted use, distribution, and reproduction in any medium, provided the original work is properly cited. 

References

- [1] Shimizu S, Watanabe N, Kataoka T, Shoji T, Abe N, Morishita S, et al. Pyridine and pyridine derivatives. In: Ullmann's Encyclopedia of Industrial Chemistry. Weinheim, Germany: Wiley-VCH Verlag GmbH & Co. KGaA; 2012. pp. 557-589. DOI: 10.1002/14356007.a22_399
- [2] Scriven EFV, Murugan R. Pyridine and pyridine derivatives. In: Kirk-Othmer Encyclopedia of Chemical Technology. Vol. 21. Hoboken, New Jersey, United States of America: John Wiley & Sons, Inc.; March 2007. ISBN: 978-0-471-48496-7
- [3] Yurkanis BP. Organic Chemistry. Mishawaka, IN, USA: Prentice Hall; 2004
- [4] Weissberger A, Taylor EC. The Chemistry of Heterocyclic Compounds: Pyridine and its Derivatives, Part 1. Vol. 14. Hoboken, New Jersey, United States of America: John Wiley & Sons, Inc; 1974. Print ISBN: 9780471379133. DOI: 10.1002/9780470186633
- [5] Sagitullin RS, Shkil' GP, Nosonova II, Ferber AA. Synthesis of pyridine bases by the Chichibabin method (review). Chemistry of Heterocyclic Compounds. 1996;**32**(2):127-140. DOI: 10.1007/BF01165434
- [6] Lazdin'sh IY, Avots AA. Catalytic methods of obtaining pyridine bases (survey). Chemistry of Heterocyclic Compounds. 1979;**15**(8):823-837. DOI: 10.1007/BF00509781
- [7] Almena A, Bueno L, Díez M, Martín M. Integrated biodiesel facilities: Review of glycerol based production of fuels and chemicals. Clean Technologies and Environmental Policy. 2018;**20**:1639-1661. DOI: 10.1007/s10098-017-1424-z
- [8] Bayramoglu D, Gurel G, Sinag A, Gullu M. Thermal conversion of glycerol to value added chemicals: Pyridine derivatives by one-pot microwave-assisted synthesis. Turkish Journal of Chemistry. 2014;**38**:661-670. DOI: 10.3906/kim-1312-47
- [9] Xu L, Han Z, Yao Q, Deng J, Zhang Y, Fu Y, et al. Towards the sustainable production of pyridines via thermo-catalytic conversion of glycerol with ammonia over zeolite catalysts. Green Chemistry. 2015;**17**:2426-2435. DOI: 10.1039/c4gc02235a
- [10] Zhang Y, Yan X, Niu B, Zhao J. A study on the conversion of glycerol to pyridine bases over Cu/HZSM-5 catalysts. Green Chemistry. 2016;**18**: 3139-3151. DOI: 10.1039/c6gc00038j
- [11] Luo CW, Huang C, Li A, Yi WJ, Feng XY, Xu ZJ, et al. Influence of reaction parameters on the catalytic performance of alkaline-treated zeolites in the novel synthesis of pyridine bases from glycerol and ammonia. Industrial and Engineering Chemistry Research. 2016;**55**:893-911. DOI: 10.1021/ie504934n
- [12] Zhang Y, Zhai X, Zhang H, Zhao J. Enhanced selectivity in the conversion of glycerol to pyridine bases over HZSM-5/11 intergrowth zeolite. RSC Advances. 2017;**7**:23647-23656. DOI: 10.1039/c7ra02311a
- [13] Zhang Y, Zhang W, Zhang HY, Yin G, Zhao J. Continuous two-step catalytic conversion of glycerol to pyridine bases in high yield. Catalysis Today. 2019;**319**:220-228. DOI: 10.1016/j.cattod.2018.03.035
- [14] Galadima A, Muraza O. A review on glycerol valorization to acrolein over solid acid catalysts. Journal of the Taiwan Institute of Chemical Engineers. 2016;**67**: 29-44. DOI: 10.1016/j.jtice.2016.07.019

- [15] Pala Rosas I, Contreras Larios JL, Zeifert B, Salmones BJ. Catalytic dehydration of glycerine to Acrolein. In: Frediani M, Bartoli M, Rosi L, editors. *Glycerine Production and Transformation - An Innovative Platform for Sustainable Biorefinery and Energy*. London, UK, London, UK: IntechOpen; 2019. DOI: 10.5772/intechopen.85751
- [16] Liu L, Ye XP, Bozell JJ. A comparative review of petroleum-based and bio-based acrolein production. *ChemSusChem*. 2012;**5**:1162-1180. DOI: 10.1002/cssc.201100447
- [17] Zhang X, Luo CW, Huang C, Chen BH, Huang DG, Pan JG, et al. Synthesis of 3-picoline from acrolein and ammonia through a liquid-phase reaction pathway using $\text{SO}_4^{2-}/\text{ZrO}_2\text{-FeZSM-5}$ as catalyst. *Chemical Engineering Journal*. 2014;**253**:544-553. DOI: 10.1016/j.cej.2014.03.072
- [18] Zhang X, Wu Z, Liu W, Chao ZS. Preparation of pyridine and 3-picoline from acrolein and ammonia with HF/MgZSM-5 catalyst. *Catalysis Communications*. 2016;**80**:10-14. DOI: 10.1016/j.catcom.2016.02.011
- [19] Zhang W, Duan S, Zhang Y. Enhanced selectivity in the conversion of acrolein to 3-picoline over bimetallic catalyst 4.6%Cu–1.0%Ru/HZSM-5 (38) with hydrogen as carrier gas. *Reaction Kinetics, Mechanisms and Catalysis*. 2019;**127**:391-411. DOI: 10.1007/s11144-019-01558-0
- [20] Pala-Rosas I, Contreras JL, Salmones J, López-Medina R, Angeles-Beltrán D, Zeifert B, et al. Effects of the acidic and textural properties of Y-type zeolites on the synthesis of pyridine and 3-picoline from acrolein and ammonia. *Catalysts*. 2023;**13**:652. DOI: 10.3390/catal13040652
- [21] Luo CW, Li A, An JF, Feng XY, Zhang X, Feng DD, et al. The synthesis of pyridine and 3-picoline from gas-phase acrolein diethyl acetal with ammonia over ZnO/HZSM-5. *Chemical Engineering Journal*. 2015;**273**:7-18. DOI: 10.1016/j.cej.2015.01.017
- [22] Luo CW, Li A. Synthesis of 3-picoline from acrolein dimethyl acetal and ammonia over $\text{NH}_4\text{F-HF}$ treated ZSM-5. *Reaction Kinetics, Mechanisms and Catalysis*. 2018;**125**:365-380. DOI: 10.1007/s11144-018-1405-1
- [23] Zhang X, Wu Z, Chao Z. Mechanism of pyridine bases prepared from acrolein and ammonia by in situ infrared spectroscopy. *Journal of Molecular Catalysis A: Chemical*. 2016;**411**:19-26. DOI: 10.1016/j.molcata.2015.08.014
- [24] Jiang D, Wang S, Li W, Xu L, Hu X, Barati B, et al. Insight into the mechanism of glycerol dehydration and subsequent pyridine synthesis. *ACS Sustainable Chemistry & Engineering*. 2021;**9**:3095-3103. DOI: 10.1021/acssuschemeng.0c07460
- [25] Calvin JR, Davis RD, McAteer CH. Mechanistic investigation of the catalyzed vapor-phase formation of pyridine and quinoline bases using $^{13}\text{CH}_2\text{O}$, $^{13}\text{CH}_3\text{OH}$, and deuterium-labeled aldehydes. *Applied Catalysis A: General*. 2005;**285**:1-23. DOI: 10.1016/j.apcata.2004.10.021
- [26] Jin F, Li Y. The effect of H_2 on Chichibabin condensation catalyzed by pure ZSM-5 and Pt/ZSM-5 for pyridine and 3-picoline synthesis. *Catalysis Letters*. 2009;**131**:545-551
- [27] Luo CW, Feng XY, Liu W, Lia XY, Chao ZS. Deactivation and regeneration on the ZSM-5-based catalyst for the synthesis of pyridine and 3-picoline. *Microporous and Mesoporous Materials*. 2016;**235**:261-269

Catalytic Conversion of Glycerol to Bio-Based Aromatics

Patrick U. Okoye, Estefania Duque-Brito, Diego R. Lobata-Peralta, Jude A. Okolie, Dulce M. Arias and Joseph P. Sebastian

Abstract

Green application of biodiesel-derived glycerol will boost biodiesel production in terms of sustainability and economics. The glycerol to liquid fuels is a promising route that provides an additional energy source, which contributes significantly to energy transition besides biodiesel. This pathway could generate alkyl-aromatic hydrocarbons with a yield of ~60%, oxygenates, and gases. MFI Zeolites (H-ZSM-5) catalysts are mainly used to propagate the aromatization pathway. This chapter presents the pathways, challenges, catalytic design, influences of catalyst acidity, metal addition, reaction condition, and catalysts deactivation on glycerol conversion to hydrocarbon fuels and aromatics. Studies revealed that time on stream, temperature, and weight hourly space velocity (range of 0.1–1 h⁻¹) influences the benzene, toluene, and xylene BTX and benzene, toluene, ethylbenzene, and xylene BTEX yield. Acidity of the H-ZSM-5 could be tailored by metals, additives, and binders. Bronsted acidity promotes coke formation which results in reversible deactivation of the H-ZSM-5 catalyst. It is hoped that this study will promote intensified research on the use of glycerol for purposes of fuel generating and valuable products.

Keywords: BTX, BTEX, hydrodeoxygenation, hydrocarbon fuels, glycerol, biodiesel

1. Introduction

To achieve complete decarbonization, there is a need to transition from fossil fuels to renewable and sustainable alternative fuels. This is because fossil fuels are major sources of greenhouse gas emissions, which have contributed to rising earth temperatures and adverse climate change. Transportation sectors still rely heavily on fossil fuels and this trend must be discouraged to minimize the emission of noxious CO₂ emissions [1, 2]. Liquid fuels generated from renewable energy sources, for use in heavy-duty vehicles are a promising option to reduce the impact of fossil fuels. Amongst the commercialized fuels from renewable energy, biodiesel has enjoyed wide acceptability because of lower CO₂ and other greenhouse emissions, can directly be used in the current internal combustion engine without modifying the engine design, and requires facile production processes [3, 4]. More importantly, biodiesel can be obtained from natural sources including waste oil, second-generation non-edible seed oil, third-generation, microalgae and fungus, animal fats, etc. [5, 6].

The transesterification reaction of oils (triglycerides) and alcohol is a widely established route for the synthesis of biodiesel [7]. This route involves the reaction of a triglyceride and 3 mols of alcohol (preferably methanol) to produce 1 mol of fatty acid methyl ester (biodiesel) and glycerol as a byproduct. The glycerol produced in this process is about 10 g for every 100 g of biodiesel produced, which renders it abundant [8, 9]. The produced glycerol is cheap because of impurities of methanol, soap, and catalysts that require energy-intensive steps for purification [10, 11]. However, glycerol is a platform molecule with three hydroxyl groups which can be transformed into fuels and fine chemicals. Many reaction pathways such as acetylation [12], carboxylation [13], etherification [14], oxidation, dehydration, gasification, aromatization [15, 16], etc. have been adopted to valorize glycerol.

Conversion of glycerol to liquid hydrocarbon fuel is a very recent and notable research idea, which will boost the biodiesel process. This is because the hydrodeoxygenation and hydroisomerization of vegetable oils to green diesel is capital intensive. Hydrocarbon fuel is vital in energy transition because of its characteristics which include high density and ease of transportation. This liquid hydrocarbon contains mainly alkyl-aromatic hydrocarbons of cumene, xylene isomers, benzene, toluene, and traces of C₉+ compounds [16–18].

The feed has a significant influence on the aromatic product distribution, coke formation, and the type of aromatic products obtained. When the compounds with a H/C ratio is less than 2, for instance, glycerol with 0.67, are used as feed, increasing coke formation on the catalyst is generally observed. Hence, dilution with water or alcohol is employed. The dilution of glycerol with a solvent that has a H/C ratio of 2 increases the H/C ratio and presents improved catalyst stability. This preferred solvent for dilution is methanol with an effective H/C ratio of 2 [19, 20]. The conversion of glycerol and methanol to gasoline has emerged as a promising route to valorize glycerol [21, 22]. Increasing the methanol/glycerol ratio from 10 to 40% favored the production of oxygenated compounds instead of aromatics. Also, when methanol/glycerol are used as feeds, the formation of trimethylbenzenes and xylenes is obvious. These compounds can be transformed into heavy C₉ aromatics by dealkylation reaction to xylene and toluene (BTX). The use of higher alcohol like isopropanol and isobutanol for dilution results in the preferential generation of ethylmethylbenzenes, and ethylbenzene with xylenes and trimethylbenzenes (BTEX) from the alkylation of ethylene generated from the cracking of the alcohol or dehydration of ethanol [18].

Notably, benzene, toluene, and xylene (BTX) and/or benzene, toluene, ethylbenzene, and xylene (BTEX) have been the main focus of many researchers in this area of study because of the vast industrial applications of these aromatic compounds including their antiknocking characteristics [23]. In addition to the aromatic compounds, oxygenates such as propanal, hydroxyacetone, and propenal (acrolein) are the product of this process [24, 25]. Also, ethylene, methylene, and propylene gases could be derived from this process. The reaction is usually carried out in a fixed bed reactor at ~400°C under excess hydrogen, alcohols, and/or nitrogen gas flowrate at atmospheric pressure [18, 26, 27].

To promote this reaction, zeolites of ZSM-5 or protonated ZSM-5 have been widely used. However, the yield over these catalysts is generally low. To increase the catalytic activity, noble metals or transition metals have been functionalized on the ZSM-5 and used with remarkable performance [28, 29]. The noble metals of Pt, Pd, and Rh, promote the cleavage of C–O bonds of glycerol, which enhances the formation of hydrocarbons from polyols instead of H₂ and CO₂ gases [24, 30]. Another problem encountered

when ZSM-5 or H-ZSM-5 is used is rapid deactivation due to sintering, coking from reaction products, and attrition. This can be minimized by using a binder such as Al_2O_3 [31]. The binder stops irreversible deactivation and prolongs the catalyst life. In all these, control of the reaction conditions such as the temperature, catalyst amount, and sometimes the atmosphere, greatly influence the yield of bio-based aromatics. The operating reaction conditions also determine the operating cost of the process.

In this study, catalytic glycerol conversion to liquid hydrocarbon and bio-based aromatics are investigated with emphasis on the reaction mechanistic pathway and the influence of the reaction conditions such as temperature, time, and catalyst weight. The catalyst design, challenges, and deactivation mechanism are discussed. Prospects on bio-based aromatics are presented to reveal the knowledge gap and provide future guidelines for researchers and industries.

2. Mechanism of glycerol conversion to biobased BTX and BTEX

The mechanism of glycerol to liquid hydrocarbon follows two main routes namely hydrodeoxygenation (HDO), followed by aromatization reaction. Hydrodeoxygenation is an established method of removing oxygen from biomass. Glycerol hydrodeoxygenation is usually carried out to synthesize 1,2-propanediol, which is an oxygenate compound used in pharmaceutical, tobacco, and cryogenic industries. This pathway occurs through simultaneous C-O bond cleavage and hydrogen addition [27]. Usually, hydrogen is added from an external source, however, recent studies have shown that *in situ* hydrogen generation from hydrogen donors such as methanol, formic acid, 2-butanol, ethanol, etc. could eliminate the need for external hydrogen [25]. The hydrodeoxygenation also follows two parts of hydration-hydrogenation and dehydrogenation-hydration-hydrogenation, which is the most common pathway. The dehydration happens on the acid catalyst sites, whereas the hydrogenation is catalyzed by the noble metals or Cu, Zn, Ni, Sn, etc. This is because these metals promote the aqueous phase reforming of glycerol to

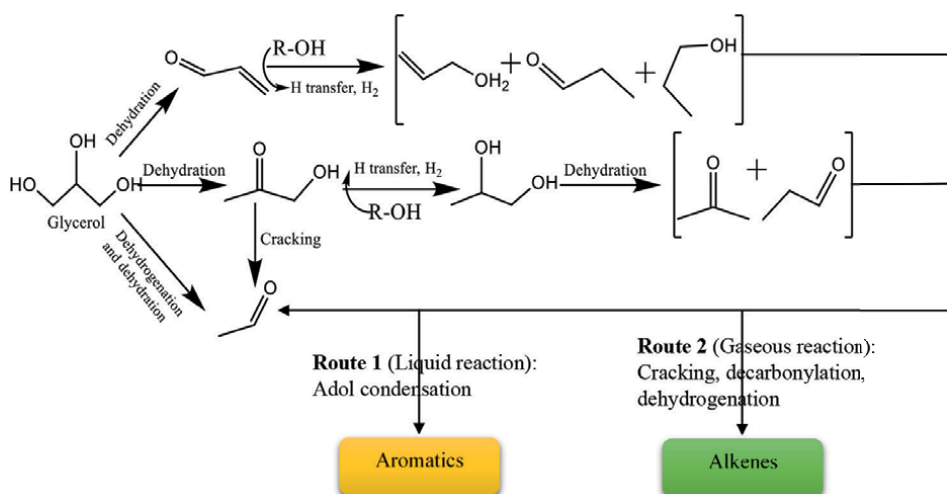


Figure 1. Reaction pathways for glycerol dehydration-hydrogenation and dehydrogenation-hydration-hydrogenation reaction to produce aromatics [17].

produce hydrogen that is consumed during the hydrogenation stage. **Figure 1** shows the liquid and gaseous steps for glycerol dehydration and dehydrogenation pathways.

Hydroxyacetone can be produced via dehydration or via another route that involves dehydration to obtain glyceraldehyde, followed by hydrogenation to hydroxyacetone [25, 27]. Also, there are other hydrocarbon mixtures of acetone, propenal, alcohols, ketone, paraffins, and olefins of ethylene and propylene. Both liquid and gaseous routes produce a hydrocarbon pool, which in the presence of a catalyst could be upgraded to benzene, toluene, and xylene (BTX) or benzene, toluene, ethylbenzene, and xylene (BTEX) and other oxygenate compounds [17]. Also, the hydrocarbon pool can be further cracked to light paraffin or olefins. Generally, the presence of strong acid sites results in the build up of heavy aromatics such as trimethylbenzene and tetra- methylbenzene, whereas the reduction in the strong catalytic sites that propagates cracking and cyclization reaction, inhibit the gas route. The liquid route however, is unaffected since the aldol condensation reaction requires weak acid sites [16, 17].

3. Effect of HZSM-5 acidity, metals addition, and reaction conditions

The unique three-dimensional cage-like crystalline structure and tunable acid properties of ZSM-5 render it a choice catalyst for many reactions including isomerization reaction, alkylation reaction, and aromatization reaction. Also, this catalyst possesses an appreciably high surface area and has been extensively used successfully to drive the reaction of methanol to aromatics. Studies on the glycerol to aromatics synthesis revealed that protonated ZSM-5 (H-ZSM-5) has been effective for BTX and BTEX production due to its acidity and shape-selective characteristics [32]. The H-ZSM-5 contains sinusoidal channels ($0.51 \times 0.5 \text{ nm}$) that are crossed with straight channels of the dimension ($0.53 \times 0.56 \text{ nm}$) with intersection channel of 0.9 nm size [33, 34]. However, the relatively large micropores of the catalysts limit the mass transport of large molecules and present a diffusion barrier, which ultimately results in undesired bulkier aromatics and cokes and eventual deactivation of the catalysts [35]. To correct this, hierarchical porous H-ZSM-5 catalysts with macro-meso- and micropores have been developed to ensure hitch-free diffusion of reactants. In the synthesis of hierarchical H-ZSM-5 catalyst, several factors should be considered (see **Figure 2**). These factors are the hydrophobicity of the catalyst since the reaction most times produce water, concentration, and strength of acid sites, presence of mesopores, and shape selectivity of the catalyst. Also, several metals have been added to stabilize the H-ZSM-5 and increase its acidity and efficiency [36]. This section presents the effect of acidity and the effects of metals used to functionalize H-ZSM-5 catalysts. Also, the influence of reaction conditions such as time on stream and reaction temperature was presented.

3.1 Effect of catalyst acidity

The acidity of the ZSM-5 and MFI (H-ZSM-5) is vital to promoting the aromatization or hydrodeoxygenation of glycerol. To determine the influence of the catalyst acidity, several analytical characterizations can be performed. A notable characterization technique employed is temperature desorption programming (TPD) using ammonia as a probe molecule [37]. Ammonia is used because it is basic and can easily interact with acid sites. The TPD can also be used to determine the number of active sites in mmol/g by deconvolution of the peaks using gamma distribution or the gaussian model [12]. The

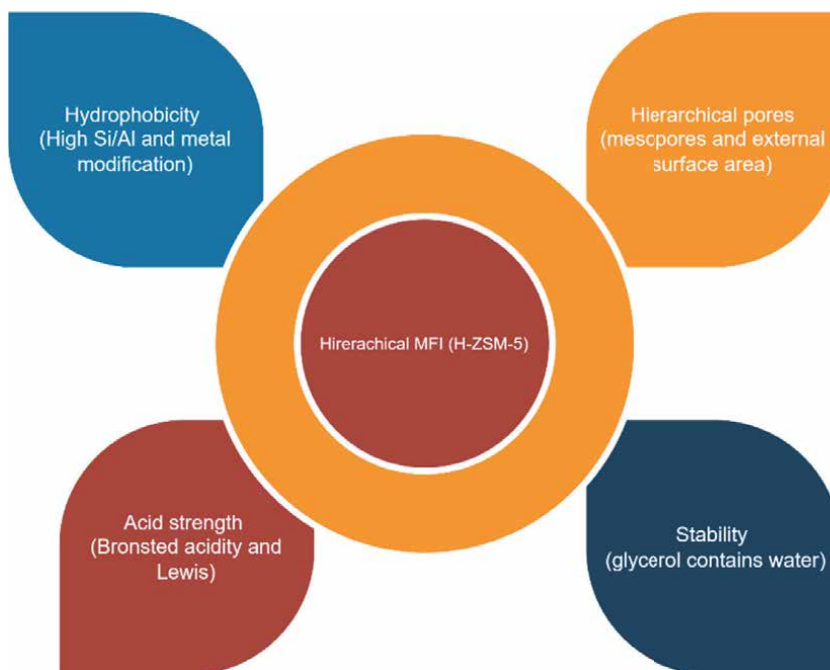


Figure 2.
Considered factors in the application of hierarchical porous H-ZSM-5 [34].

TPD peaks could be classified as weak, moderate, and strong peaks. The weak peak can be appreciated from 150 to 220°C, the moderate acid sites are around 300–350°C and the strong sites are from 400°C and above [38]. For zeolites, only weak and strong acid sites are usually identified [39]. Although weak and moderate peaks contribute to the deoxygenation and aromatization, mainly the strong acidity favors a higher yield of aromatics.

For instance, the yield of aromatics over catalyst of Zn/P/Si/ZSM-5 was lower than Zn/P/ZSM-5 catalyst by about 14.3% because the SiO₂ impregnation reduced the amount of the total acid sites by about 7.02% [38]. Also, the concentration of the surface acid sites is more vital than the total acid sites, because it is largely a surface dominated reaction. A similar study on atomic layer deposition (ALD) of Zn species on Sn/HZSM-5 zeolite revealed that above 20 cycles of ALD of Zn, precisely 40Zn, the interaction between the HZSM-5 and deposited Zn species were limited. Also, the strong acid sites reduced significantly, resulting in a reduction of BTX yield from close to C. 39% (for Sn/HZSM-5@20Zn) to C. 31% (for Sn/HZSM-5@40Zn) based on carbon yield [17]. Dealumination of HZSM-5 by steaming and acid leaching could produced different results. For instance, using 6 M nitric acid to remove extra-framework aluminum from the surface and channels of HZSM-5 and steaming to achieve the same purpose revealed significantly lower Brønsted acidity in steam treated HZSM-5. Whereas the concentration of the strong acid sites for the acid treated HZSM-5 remained almost unchanged. However, the weak acid sites decreased significantly, resulting in reduced total acidity. Likewise, BTX aromatic yield was higher for acid treated HZSM-5 (C. 28.1%) compared to the steam treated zeolite (C. 18.3%) [16].

To evaluate the type and concentration of the acid site, Fourier transforms infrared (FTIR) of adsorbed pyridine are normally used [40]. The pyridine IR is usually conducted by heating a known mass of the catalyst at around 150°C for 3 h, followed

by pyridine adsorption for 2 h and subsequent desorption of the pyridine at 200°C under vacuum [41–43].

From pyridine DRIFTS analysis, the types of acid sites normally encountered with ZSM-5 zeolites are Brønsted and Lewis acid sites. Due to high pressure and temperature conditions of the glycerol to liquid fuels and aromatics compounds, high coke selectivity and consequent deactivation often occur for this type of catalyst. Particularly, the strong acid sites, which are mainly Brønsted acids promote the undesired coke formation, because the coke deposits preferentially on these sites through different proton transfer steps that occur on the Brønsted acid sites [26]. It is important to mention that understanding of acidity types of the zeolite catalyst can be appreciated from the Si/Al ratio [44]. Tuning of the acid strength [41] and reduction in the acid density [45] are two notable strategies to reduce coke deposits. The tuning of the acid strength and concentration can be achieved by modifying the zeolite tetrahedral framework Al content of the H-ZSM-5 or exchanging the protons that compensate for the negative charge of the Al sites tetrahedral framework. The strategy adopted over the years to accomplish these are either post-synthesis modification (top-down) or in situ modification during synthesis (bottom-up) [26, 32]. For instance, the synthesis of H-ZSM-5 with different Si/Al ratios is a common bottom-up strategy to evaluate the effect of acidity. For the bottom-up strategy, the total acid sites increase when the Si/Al ratio decreases. Top-down strategies include dealumination by acid extraction or steam treatment and isomorphic substitution of Al or Si atom with Zr, Fe, Ga, In, etc. [21, 46–48], other metals, heteroatoms of phosphorus, sulfur, and alkali metals, and alkaline earth metals [16, 40, 43]. Although these substitution strategies, which focus on the framework tetrahedral sites have been successful, however, they often result in the damage of the framework or defects of the crystalline structure, which adversely impacts the reactants and products diffusion to and from the cage-like zeolite structure. Also, the accurate introduction of these metals could be very problematic and can lead to uncertainty in the pore dimension [26].

Evaluation of the H-ZSM-5 acidity after dealumination via washing with HNO₃ and steaming revealed that the weak acid sites decreased, whereas the strong acid sites were unaffected. It is important to note that ZSM-5 zeolites have amorphous extra framework aluminum, which contributes significantly to the weak acid sites (although it could contribute slightly to the medium and strong acid sites with other silanols (Si-(OH)-Al) species), whereas the framework aluminum species are more related to the strong acid sites. Hence, the reduction in weak acid sites after dealumination can be attributed to the removal of the extra framework aluminum. The steaming treatment, however, resulted in a remarkable reduction of the acid concentration and strength, which shows the dealumination of the framework and extra-framework aluminum [16].

3.2 Effect of metal addition

Metal addition on H-ZSM-5 is bifunctional to provide stability as well as promote the dehydration/dehydrogenation reaction of glycerol to aromatics. A conducted study using only H-ZSM-5 reveal that predominantly oxygenates namely acrolein were obtained with about 11% of C₆ – C₉ compounds [30]. In this same study, the addition of metals (platinum and palladium), provided bifunctional properties, which promoted the C – O, C – H, O – H, and C – C bonds cleavages to achieve deoxygenation of the oxygenates [24]. Palladium however showed better performance in the conversion of the oxygenates to aromatics because of the higher H/metal ratio.

Notably, noble metals are preferred for fast kinetic activation of hydroxyl groups of glycerol and hydrogen dissociative adsorption [49]. Depending on the operating temperature they generally promote the hydrocarbon formation instead of the CO and H₂ pathway.

Apart from noble metals, which are usually expensive and can impact the overall production cost of liquid hydrocarbon and biobased aromatics from glycerol, other metals have been used with appreciable performance. Binders such as Al₂O₃ have been used to prolong the H-ZSM-5 catalyst life. The mesopores of the Al₂O₃ provided a higher capacity to store coke deposits in amorphous form. Also, the binder promoted a high total BTX yield compared to H-ZSM-5 [31]. Another study investigated the incorporation of tin (Sn) species in ZSM-5 catalysts. The composite catalysts were treated hydrothermally using sodium hydroxide, followed by ion exchange with ammonium chloride. The H[Sn, Al] ZSM-5/0.3AT composite catalysts after ion exchange reaction showed a slight decrease in crystallinity, a decrease in total Bronsted acid sites with an increase in Lewis acid sites [36]. Also, the Sn incorporation replaced some medium and strong acid sites and new acid sites were formed. The addition of the Sn did not destroy the H-ZSM-5 morphology, and the composite catalyst showed intra-mesopores and micropores, which benefits mass transfer of reactants and products. Overall, the catalyst showed a higher carbon yield of BTX (C 32.1%) compared to H-ZSM-5 (C 17.8%). The H[Sn, Al] ZSM-5/0.3AT could sustain about 13 h of time on stream reaction (H-ZSM-5 sustained the reaction for only 3 h with severe deactivation due to coke deposits), which was attributed to the mesopores and tuned Lewis acid and Bronsted acid sites due to alkali post-treatment. Similar studies have demonstrated the effect of binary material of Sn, Zn incorporated on H-ZSM-5 with appreciable BTX yield and longer catalyst life [17]. The Zn has been reported to promote high BTX formation by suppressing H-transfer reactions and light paraffins [29].

3.3 Effect of temperature

Catalytic pyrolysis is employed to achieve glycerol to aromatics and liquid hydrocarbons conversion. The operating temperature is very vital because glycerol to aromatics is a consecutive reaction steps that involves dehydration, oligomerization, cyclization, aldol condensation, cracking, and dehydrogenation. Since these reaction pathways occur simultaneously and parallel, different product distributions could be obtained at different reaction temperatures. An effect of reaction temperature on glycerol to aromatics shows that at a low temperature of ~200°C, O – H and C – H bonds could be easily broken due to their lower activation energy. This activation could be prevented by a possible hydrogenation reaction that is propagated by high H₂ content. An increase in temperature in the range of 300–400°C facilitated the bond cleavages of C – C and C – O species, which could happen simultaneously due to their similar activation energy [24]. However, breaking of the C – C bond at this temperature results in the formation of coke deposits, which could be graphitic or amorphous. Hence, the temperature should be tuned properly with the right amount of catalyst acidity to achieve the breaking of C – O bonds, while minimally avoiding the C – C bond. At 450°C, more of the liquid products are further cracked to gases, and syngas formation and methanation reactions are promoted [30]. Hence, the aromatics yield decreases, whereas the gaseous product increases as shown in **Figure 3** [30]. Most studies adopted 400°C as the optimum temperature to achieve the glycerol to aromatic conversion [18, 32, 50].

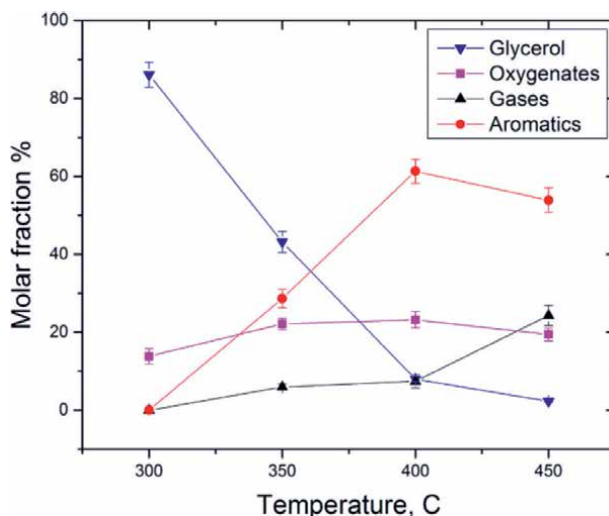


Figure 3. Effect of pyrolysis temperature using Pd/H-ZSM-5 catalyst. Conditions: 1 atm, H₂/glycerol molar ratio of 10, and 6 g cat-h/g glycerol (copyright obtained <https://pubs.acs.org/doi/full/10.1021/acscenergylett.6b00421>).

3.4 Effect of time on stream

Time on stream for glycerol conversion to bio-based aromatics could be categorized into induction time, steady-state reaction time, and deactivation time [16]. Selectivity of the products is a clear function of the reaction time on stream; hence, it is important to optimize this factor. This has been generally established based on the yield of the aromatic intermediates in the cage structure of the H-ZSM-5 zeolite during aromatization. A study revealed that polymethyl benzenes and olefines, which is a very vital active hydrocarbon pools, were formed over the H-ZSM-5 cages as a product of the dehydration of the glycerol (oxycarbides) in the induction period [17]. This results in improved aromatic yields with a decrease in oxycarbides. After the induction period in a continuous reaction set-up, aromatization of glycerol proceeds via multiple steps of autocatalytic non-stop reaction of alkylation/dealkylation, oligomerization, and H-transfer. This stage usually has a relatively constant BTX and BTEX yield because the consumed hydrocarbon species are replenished. As the reaction time on stream is prolonged, the dealkylation step is suppressed with a corresponding decrease in lighter aromatic yield (toluene) and a buildup of heavier hydrocarbon species [38]. This was attributed to the coverage of the strong active sites by the heavier autocatalytic species, which suppresses the cracking and cyclization pathways propagated by the strong acid sites [51]. Hence, the gaseous route is mitigated allowing for the liquid synthesis. Further extension of the time on stream for continuous reaction set-up facilitates the conversion of the heavier intermediates (heavier hydrocarbon species) into carbon by a condensation reaction [52]. Eventually, the carbon formed blocks the micropores and the acid sites resulting in the catalyst deactivation. In the deactivation phase, the BTX and BTEX yields drop drastically, however, unconverted glycerol, acetol, acetaldehyde, and acrolein remained in the product [15]. **Table 1** shows the reported catalysts for glycerol conversion to aromatics and reaction conditions with selectivity towards BTX.

Catalyst	Conditions	Glycerol conv. (%)	Selectivity of aromatics (%)	Ref.
Dealuminated H-ZSM-5 (MFI) with initial Si/Al = 25	T = 400°C, glycerol/methanol = 40 wt.%, P = 0.1 MPa, WHSV: 0.71 h ⁻¹ .	Ca. 98	ca.32 (C% BTX)	[16]
ZSM-5 (SiO ₂ /Al ₂ O ₃ = 30)	T = 400°C, WHSV = 0.8 h ⁻¹ .	100	>30 (C% BTX)	[18]
H-ZSM-5 (Si/Al ₂ = 200)	T = 400°C, WHSV = 0.9 h ⁻¹ .	100	18	[36]
Hierarchical Sn-ZSM-5	T = 400°C, WHSV = 0.9 h ⁻¹ .	100	32 BTX	[36]
H-ZSM-5/Al ₂ O ₃ (60/40 wt%)	T = 550°C, WHSV = 1 h ⁻¹ , TOS = 0–12 h.	—	19.5 (C% BTX)	[31]
H-ZSM-5/Al ₂ O ₃ catalysts (60/40 wt%)	T = 550°C, glycerol/oleic acid = 30/70 wt.%, TOS = 12 h, catalyst = 10 g.	—	26.7 (C% BTX)	[53]
H-ZSM-5 (SiO ₂ /Al ₂ O ₃ = 23)	T = 400°C, WSHV = 1 h ⁻¹ , TOS = 5 h, 0–5 mbar.	—	28.1 (C% BTX)	[50]
Nano-sized H-ZSM-5 modified with carboxymethylcellulose sodium, NaCl, and sodium alginate	T = 400°C, WHSV = 0.9 h ⁻¹ , catalyst = 1.2 g, glycerol/methanol = 40 wt.%.	—	35 (C% BTX)	[33]
Nano-sized H-ZSM-5 produced with sodium alginate (S-HZSM-5–0.75)	T = 400°C, WHSV = 0.96 h ⁻¹ , catalyst = 1.2 g, glycerol/methanol = 40 wt.%.	100	35.06 (C% BTX)	[39]
Zn and Sn modified H-ZSM-5 (Si/Al = 25)	T = 400°C, WHSV = 0.71 h ⁻¹ , glycerol/methanol = 40 wt.%, TOS = 1.5 ~ 2 h.	—	Ca. 35.7 (C% BTX)	[17]

Table 1.
 Reported catalysts for glycerol conversion to aromatics.

4. Deactivation of catalysts

Deactivation of catalyst is the loss of performance over time, and the difference in catalyst life depends on the contaminant and application. There are several mechanisms by which a catalyst can be deactivated including fouling, poisoning, sintering, leaching of active surface, and mechanical attrition. Thermal degradation deactivation could be found with catalysts used in petroleum cracking or polymers [54]. Poisoning is a deactivation mechanism whereby a contaminant is loosely or strongly adsorbed on the active sites of the catalyst, which prevents access to the reactant species. This type of deactivation could be reversible or irreversible. A notable poisoning mechanism is coking, which results in carbon deposits, which could mask the surface of the active sites or even block the catalyst pores (pore mouth-filling). Coke formation can be investigated by temperature gravimetric analysis and visual inspection to observe a color change, usually from off-white to black. In general, catalyst deactivation is inevitable, however, careful catalyst design and operation under mild conditions could prolong the catalyst life in any given application. The design of a suitable shape-selective catalyst with tunable acid properties could increase the peak BTX yield, and total productivity and prolong the catalyst life.

Aromatization reaction occurs through a series of consecutive reaction steps that involves aldol condensation, oligomerization, cracking, cyclization, dehydrogenation, dehydration, aromatization, etc. The strength and concentration of the acid sites influence the yield of BTX and BTEX; specifically, the amount of Bronsted and Lewis acids could propagate the deactivation of the catalysts. The Bronsted acid sites promote cracking, H-transfer, and oligomerization reaction and it is principally responsible for coke generation since it promotes the C – C bond breaking. A Survey of the literature shows that coke deposition is the main deactivation mechanism of the H-ZSM-5. The coking deactivation is considered reversible because the coke can be removed by oxidative treatment. The spent catalyst is subjected to high-temperature calcination in the air to decompose the coke deposits. For instance, the stability analysis for H-ZSM-5/Al₂O₃ and H-ZSM-5 catalysts used in the synthesis of BTX showed that the Al₂O₃ binder had more coke accommodation capacity than only H-ZSM-5. This was attributed to the mesoporous nature of Al₂O₃. Besides, the coke formation on the H-ZSM-5/Al₂O₃ was amorphous, whereas that of H-ZSM-5 was graphitic [50, 55]. This implies that the decomposition temperature would vary widely and the graphitic coke obviously would result in irreversible deactivation [31].

There are other forms of deactivation of H-ZSM-5 related to the deformation of the structure, reduction of crystallinity, acid strength, and reduction of microporosity. As stated before, this type of structural defect can manifest during the top-down approach. A situation whereby the acidity is reduced by chemical treatment or steaming. In particular, the hydrophobicity and spatial constraints of some chemical agents such as CH₃ONa and NaOH, in high concentrations could promote rapid desilication of the H-ZSM-5, which results in the damage of the catalyst microporous structure, diminished cage-like walls of the H-ZSM-5, and a drastic reduction in the crystallinity [52]. This situation presents a deformed H-ZSM-5 catalyst with low catalytic

Catalyst	Total acidity ($\mu\text{mol NH}_3$ g^{-1} cat fresh sample)	Total coke content (wt.%)	No. of reuse	catalyst lifetime (h)	Ref.
H-ZSM-5/Al ₂ O ₃ (60/40 wt%)	1051	16.0	5	8.5	[31]
ZSM-5	—	—	—	8	[19]
H-ZSM-5	1466	12	1	4	[15]
3 h 500°C/HZSM-5	413	—	—	8.5	[16]
H-ZSM-5/Al ₂ O ₃	1051	16.8	5	12	[53]
3 h 450°C/0.3 M NaOH/ HZSM-5	615	22.82	—	3	[35]
S-HZSM-5-0.75	1240	1123.90 ⁱ	3	11.5	[39]
Sn/HZSM-5@20Zn	878	—	3	11	[17]
H-ZSM-5/ Al ₂ O ₃	1238	15	1	5.3	[56]
H-ZSM-5/SiO ₂	1286	9	1	3.66	[56]
H-ZSM-5/ Kaolinite	1318	13	1	4	[56]

ⁱ is the peak area of the coke determined by the TPO method at 395°C.

Table 2.

Reported H-ZSM-5-based catalysts, coke content, acidity, and number of reuse.

performance towards the aromatization reaction of glycerol. Another study reported in situ deactivation due to the conditions of the pyrolysis and reaction intermediates. He et al. [56] in their study to produce bio-based aromatics from glycerol revealed that dealumination of H-ZSM-5 occurred, which severely affected the crystallinity and acidity of the catalyst. This dealumination was attributed to catalyst exposure to steam generated by glycerol dehydration and the framework interaction with intermediate oxygenates. These types of deactivation are irreversible and eventually result in the complete deactivation of the catalyst. **Table 2** shows the total acidity of some reported catalysts, total coke content, and catalyst lifetime.

5. Prospects of catalytic glycerol to bio-aromatics

The conversion of glycerol to liquid fuels and aromatics is a notable research effort towards the production of “green” drop-in fuels that can be used as aviation fuel or bio-based chemicals. The glycerol is subjected to pyrolysis and sometimes in situ hydrotreating to reduce the oxygenates under heterogeneous catalysts. Zeolites of MFI (ZSM-5) have been widely applied because of the shape-selective nature, tunable acidity, and structure of the catalyst that promotes dehydration and hydrodeoxygenation reaction to produce hydrocarbon pools. In particular, protonated ZSM-5 (H-ZSM-5) has been synthesized for this synthesis with different modifications to evolve hierarchical pores and moderate the Bronsted acidity. However, there are continuous improvements to this strategy to increase the yield of BTX and BTEX from glycerol pyrolysis.

Notable about this is the modification of the H-ZSM-5 with metals and steaming to dealuminate the catalyst or alkaline treatment. These techniques are deployed to stabilize the zeolite and achieve higher selectivity of BTX. Conducted studies have evidenced that most strategies used to achieve dealumination or functionalization with metals are invasive, i.e., the crystallinity is sometimes affected significantly [44]. Hence, it is pertinent to look for non-invasive methods, such as low-temperature plasma techniques and isomorphous substitution methods [46, 48]. These methods are capable of achieving grafting metals on the H-ZSM-5 with minimal damage to the crystallinity or the framework structure. Also, the synthesis of the zeolite with pore-templating agents to evolve hierarchical pores would benefit the mass transport of reactants and products from the catalyst active sites. Another aspect that needs further insights is the optimization of reaction conditions such as the temperature, time on stream, weight hourly space velocity (WHSV), and methanol/glycerol ratio. Optimization of these reaction influencing parameters will result in minimal operation cost and provide insights into the mechanistic pathways involved.

Wholistic study of the deactivation mechanism of the unmodified H-ZSM-5 based on time and spaced resolved analysis suggested that coke deposit increases with the time on stream. The longer time on stream, the more coke accumulation. The mechanism proposed for this scenario posits that initially, coke is formed at the microporous channel of the H-ZSM-5 catalyst, followed by accumulation on the external surface of the zeolite as the time on stream increases [15]. The primary cause of the coke formation is the strong acid sites of the H-ZSM-5 catalysts, which have been improved by the design of shape-selective catalysts [35], metals, additive addition [33], and dealumination [43]. It is important to search for more binders that are capable of accumulating coke in amorphous form as opposed to the graphitic form, which is energy-intensive to regenerate.

6. Conclusions

Conclusively, the aromatization of glycerol via pyrolysis methods could be promoted using MFI zeolites (HZSM-5 and ZSM-5) catalysts. The acid form of ZSM-5 (H-ZSM-5) possesses appropriate crystallinity and acidity to tailor the reaction to produce benzene, toluene, and xylene (BTX) and/or benzene, toluene, ethylbenzene, and xylene (BTEX) with some oxygenates. The crystalline cage-like structure, acidity, pore size, and channel of the H-ZSM-5 catalysts influence the product's yield and distribution. Also, the reaction conditions such as temperature, time on stream, weight hourly space velocity significantly influence the product distribution and the carbon yield (BTX and BTEX). Also, these factors impact the coke formation mechanism, especially the time on stream and reaction temperature. The addition of metals like Zn, noble metals, Sn, binders (Al_2O_3), and additives (heteroatoms) influence the H-ZSM-5 acid concentration, acid strength, and acid type. These chemical modifications of the H-ZSM-5 catalysts substitute the framework aluminum responsible for high Bronsted acidity, which promotes coke formation and stabilizes the catalysts. Deactivation caused by dealumination techniques and *in situ* reaction conditions destroys the crystalline cage-like zeolite framework and is irreversible. Whereas reversible coke deposition is removed by energy-intensive oxidation that could impact the porosity and crystalline structure of the catalyst.

Hence, it is recommended that further studies should be conducted on the synthesis of shape-selective and hierarchical porous H-ZSM-5 catalyst with moderate Bronsted acidity to minimize coke formation and promote mass transport. Non-invasive modification methods such as plasma techniques should be adopted to achieve metal and heteroatoms incorporation into the cage-like structure of the H-ZSM-5 without damage to the framework. An in-depth study on the techno-economic analysis and life cycle analysis of the aromatization reaction will provide insights on the associated costs for comparison and the environmental impact of this process. Also, machine learning methods should be deployed to optimize the reaction conditions.

Acknowledgements

This work was financially supported by Dirección General de Asuntos del Personal Académico, Mexico under Programa de Apoyo a Proyectos de Investigación e Innovación Tecnológica (DGAPA-PAPIIT) Project Nos: IA102522, IG100217, and IA203320. PhD fellowship was granted to D.R. Lobato-Peralta by Consejo Nacional de Ciencia y Tecnología, Mexico (CONACYT).

Conflict of interest

The authors declare no conflict of interest.

Author details


Patrick U. Okoye^{1*}, Estefania Duque-Brito¹, Diego R. Lobata-Peralta¹, Jude A. Okolie², Dulce M. Arias¹ and Joseph P. Sebastian¹

1 Instituto de Energías Renovables, Universidad Nacional Autónoma de México, Temixco, Morelos, Mexico

2 Gallogly College of Engineering, University of Oklahoma, USA

*Address all correspondence to: ugopaok@ier.unam.mx

IntechOpen

© 2022 The Author(s). Licensee IntechOpen. This chapter is distributed under the terms of the Creative Commons Attribution License (<http://creativecommons.org/licenses/by/3.0>), which permits unrestricted use, distribution, and reproduction in any medium, provided the original work is properly cited. 

References

- [1] Scrucca F, Rotili A, Presciutti A, Fantozzi F, Bartocci P, Zampilli M. Energy valorization of bio-glycerol: Carbon footprint of Co-pyrolysis process of crude glycerol in a CHP plant. In: Muthu SS, editor. *Carbon Footprints: Case Studies from the Energy and Transport Sectors*. Singapore: Springer Singapore; 2019. pp. 19-46. DOI: 10.1007/978-981-13-7912-3_2
- [2] Li C, Zhang X, Wang K, Su F, Chen CM, Liu F, et al. Recent advances in carbon nanostructures prepared from carbon dioxide for high-performance supercapacitors. *Journal of Energy Chemistry*. 2021;54:352-367
- [3] Gouran A, Aghel B, Nasirmanesh F. Biodiesel production from waste cooking oil using wheat bran ash as a sustainable biomass. *Fuel*. 2021;295:120542
- [4] Madhuvilakku R, Piraman S. Biodiesel synthesis by TiO₂-ZnO mixed oxide nanocatalyst catalyzed palm oil transesterification process. *Bioresource Technology*. 2013;150:55-59
- [5] Ilham Z, Haque NF. Quantitative priority estimation model for evaluation of various non-edible plant oils as potential biodiesel feedstock. *AIMS Agriculture and Food*. 2019;4(2):303-319
- [6] Ambat I, Srivastava V, Sillanpää M. Recent advancement in biodiesel production methodologies using various feedstock: A review. *Renewable and Sustainable Energy Reviews*. 2018;90:356-369
- [7] Ideris F, Shamsuddin AH, Nomanbhay S, Kusumo F, Silitonga AS, Ong MY, et al. Optimization of ultrasound-assisted oil extraction from *Canarium odontophyllum* kernel as a novel biodiesel feedstock. *Journal of Cleaner Production*. 2021;288:125563. DOI: 10.1016/j.jclepro.2020.125563
- [8] Ortiz Olivares RD, Okoye PU, Ituna-Yudonago JF, Njoku CN, Hameed BH, Song W, et al. Valorization of biodiesel byproduct glycerol to glycerol carbonate using highly reusable apatite-like catalyst derived from waste Gastropoda Mollusca. *Biomass Conversion and Biorefinery*. Springer; 2020. DOI: 10.1007/s13399-020-01122-0
- [9] Aghbashlo M, Tabatabaei M, Rastegari H, Ghaziaskar HS. Exergy-based sustainability analysis of acetins synthesis through continuous esterification of glycerol in acetic acid using Amberlyst®36 as catalyst. *Journal of Cleaner Production*. 2018;183:1265-1275. DOI: 10.1016/j.jclepro.2018.02.218
- [10] Das B, Mohanty K. A green and facile production of catalysts from waste red mud for the one-pot synthesis of glycerol carbonate from glycerol. *Journal of Environmental Chemical Engineering*. 2019;7(1):102888. DOI: 10.1016/j.jece.2019.102888
- [11] Okoye PU, Abdullah AZ, Hameed BH. A review on recent developments and progress in the kinetics and deactivation of catalytic acetylation of glycerol—A byproduct of biodiesel. *Renewable and Sustainable Energy Reviews*. 2017;74:387-401. DOI: 10.1016/j.rser.2017.02.017
- [12] Okoye PU, Abdullah AZ, Hameed BH. Synthesis of oxygenated fuel additives via glycerol esterification with acetic acid over bio-derived carbon catalyst. *Fuel*. 2017;209(July):538-544. DOI: 10.1016/j.fuel.2017.08.024
- [13] Aresta M, Dibenedetto A, Nocito F, Pastore C. A study on the

carboxylation of glycerol to glycerol carbonate with carbon dioxide: The role of the catalyst, solvent and reaction conditions. *Atmospheric Environment*. 2007;**41**(2):407-416

[14] Dominguez CM, Romero A, Santos A. Improved etherification of glycerol with tert-butyl alcohol by the addition of dibutyl ether as solvent. *Catalysts*. 2019;**9**(4):378. DOI: 10.3390/catal9040378

[15] He S, Goldhoorn HR, Tegudeer Z, Chandel A, Heeres A, Stuart MCA, et al. A time- and space-resolved catalyst deactivation study on the conversion of glycerol to aromatics using H-ZSM-5. *Chemical Engineering Journal*. 2022;**434**(Jan):134620. DOI: 10.1016/j.cej.2022.134620

[16] Wang F, Chu X, Zhu F, Wu F, Li Q, Liu B, et al. Producing BTX aromatics-enriched oil from biomass derived glycerol using dealuminated HZSM-5 by successive steaming and acid leaching as catalyst: Reactivity, acidity and product distribution. *Microporous and Mesoporous Materials*. 2019;**277**(November 2018):286-294. DOI: 10.1016/j.micromeso.2018.11.015

[17] Wang F, Kang X, Zhou MX, Yang XH, Gao LJ, Xiao GM. Sn and Zn modified HZSM-5 for one-step catalytic upgrading of glycerol to value-added aromatics: Synergistic combination of impregnated Sn particles, ALD introduced ZnO film and HZSM-5 zeolite. *Applied Catalysis A: General*. 2017;**539**(April):80-89. DOI: 10.1016/j.apcata.2017.04.005

[18] Jang HS, Bae K, Shin M, Kim SM, Kim CU, Suh YW. Aromatization of glycerol/alcohol mixtures over zeolite H-ZSM-5. *Fuel*. 2014;**134**(2014):439-447. DOI: 10.1016/j.fuel.2014.05.086

[19] Luo G, McDonald AG. Conversion of methanol and glycerol into gasoline via ZSM-5 catalysis. *Energy and Fuels*. 2014;**28**(1):600-606

[20] Gayubo AG, Valle B, Aguayo AT, Olazar M, Bilbao J. Attenuation of catalyst deactivation by cofeeding methanol for enhancing the valorisation of crude bio-oil. *Energy and Fuels*. 2009;**23**(8):4129-4136

[21] Han Z, Zhou F, Liu Y, Qiao K, Ma H, Yu L, et al. Synthesis of gallium-containing ZSM-5 zeolites by the seed-induced method and catalytic performance of GaZSM-5 and AlZSM-5 during the conversion of methanol to olefins. *Journal of the Taiwan Institute of Chemical Engineers*. 2019;**103**:149-159. DOI: 10.1016/j.jtice.2019.07.005

[22] Valle B, Gayubo AG, Alonso A, Aguayo AT, Bilbao J. Hydrothermally stable HZSM-5 zeolite catalysts for the transformation of crude bio-oil into hydrocarbons. *Applied Catalysis B: Environmental*. 2010;**100**(1-2):318-327. DOI: 10.1016/j.apcatb.2010.08.008

[23] Lok CM, Van Doorn J, Aranda AG. Promoted ZSM-5 catalysts for the production of bio-aromatics, a review. *Renewable and Sustainable Energy Reviews*. 2019;**113**(June):109248. DOI: 10.1016/j.rser.2019.109248

[24] Liu B, Greeley J. Decomposition pathways of glycerol via C-H, O-H, and C-C bond scission on Pt(111): A density functional theory study. *Journal of Physical Chemistry C*. 2011;**115**(40):19702-19709

[25] Yfanti VL, Lemonidou AA. Effect of hydrogen donor on glycerol hydrodeoxygenation to 1,2-propanediol. *Catalysis Today*. 2020;**355**(May 2019):727-736. DOI: 10.1016/j.cattod.2019.04.080

- [26] Xian X, He M, Gao Y, Bi Y, Chu Y, Chen J, et al. Acidity tuning of HZSM-5 zeolite by neutralization titration for coke inhibition in supercritical catalytic cracking of n-dodecane. *Applied Catalysis A: General*. 2021;**623**(April)
- [27] Yfanti VL, Lemonidou AA. Mechanistic study of liquid phase glycerol hydrodeoxygenation with in-situ generated hydrogen. *Journal of Catalysis*. 2018;**368**:98-111. DOI: 10.1016/j.jcat.2018.09.036
- [28] Wang F, Xiao W, Gao L, Xiao G. Enhanced performance of glycerol to aromatics over Sn-containing HZSM-5 zeolites. *RSC Advances*. 2016;**6**(49):42984-42993
- [29] Tamiyakul S, Ubolcharoen W, Tungasmita DN, Jongpatiwut S. Conversion of glycerol to aromatic hydrocarbons over Zn-promoted HZSM-5 catalysts. *Catalysis Today*. 2015;**256**:325-335
- [30] Xiao Y, Varma A. Conversion of glycerol to hydrocarbon fuels via bifunctional catalysts. *ACS Energy Letters*. 2016;**1**(5):963-968
- [31] He S, Kramer TS, Klein FGH, Chandel A, Tegudeer Z, Heeres A, et al. Improved catalyst formulations for the conversion of glycerol to bio-based aromatics. *Applied Catalysis A: General*. 2022;**629**(September 2021):118393. DOI: 10.1016/j.apcata.2021.118393
- [32] Wang F, Li Q, Chu X, Zhu F, Zhao P, Wu F, et al. The synergistic effect of hydroxylated carbon nanotubes and ultrasound treatment on hierarchical HZSM-5 in the selective catalytic upgrading of biomass derived glycerol to aromatics. *Catal Letters*. 2021;(0123456789). DOI: 10.1007/s10562-021-03823-1
- [33] Xu W, Gao L, Xiao G. Effects of additives and metals on crystallization of nano-sized HZSM-5 zeolite for glycerol aromatization. *Catalysts*. 2019;**9**(11):899. DOI: 10.3390/catal9110899
- [34] Muraza O. Peculiarities of glycerol conversion to chemicals over zeolite-based catalysts. *Frontiers in Chemistry*. 2019;**7**(Apr):1-11
- [35] Wang F, Chu X, Zhao P, Zhu F, Li Q, Wu F, et al. Shape selectivity conversion of biomass derived glycerol to aromatics over hierarchical HZSM-5 zeolites prepared by successive steaming and alkaline leaching: Impact of acid properties and pore constraint. *Fuel*. 2020;**262**(November 2019):116538. DOI: 10.1016/j.fuel.2019.116538
- [36] Yang X, Wang F, Wei R, Li S, Wu Y, Shen P, et al. Synergy effect between hierarchical structured and Sn-modified H[Sn, Al]ZSM-5 zeolites on the catalysts for glycerol aromatization. *Microporous and Mesoporous Materials*. 2018;**257**:154-161. DOI: 10.1016/j.micromeso.2017.08.039
- [37] Aptel G, Petrakis D, Jones D, Roziere J, Pomonis P. Mesoporous Al-Fe-P-O solids prepared in non-aqueous medium: Structure and surface acid catalytic behaviour. *Studies in Surface Science and Catalysis*. 1998;**118**:931-939
- [38] Zhang J, Qian W, Kong C, Wei F. Increasing Para-xylene selectivity in making aromatics from methanol with a surface-modified Zn/P/ZSM-5 catalyst. *ACS Catalysis*. 2015;**5**(5):2982-2988
- [39] Xu N, Pan D, Wu Y, Xu S, Gao L, Zhang J, et al. Preparation of nano-sized HZSM-5 zeolite with sodium alginate for glycerol aromatization. *Reaction Kinetics, Mechanisms and Catalysis*. 2019;**127**(1):449-467. DOI: 10.1007/s11144-019-01566-0

- [40] Almutairi SMT, Mezari B, Pidko EA, Magusin PCMM, Hensen EJM. Influence of steaming on the acidity and the methanol conversion reaction of HZSM-5 zeolite. *Journal of Catalysis*. 2013;**307**:194-203. DOI: 10.1016/j.jcat.2013.07.021
- [41] Auepattana-aumrung C, Suriye K, Jongsomjit B, Panpranot J, Praserttham P. Inhibition effect of Na⁺ form in ZSM-5 zeolite on hydrogen transfer reaction via 1-butene cracking. *Catalysis Today*. 2020;**358**(August 2019):237-245. DOI: 10.1016/j.cattod.2019.08.012
- [42] Xiao W, Wang F, Xiao G. Performance of hierarchical HZSM-5 zeolites prepared by NaOH treatments in the aromatization of glycerol. *RSC Advances*. 2015;**5**:63697-63704. Available from: <http://xlink.rsc.org/?DOI=C5TC02043C>
- [43] Fan Y, Bao X, Lin X, Shi G, Liu H. Acidity adjustment of HZSM-5 zeolites by dealumination and realumination with steaming and citric acid treatments. *The Journal of Physical Chemistry. B*. 2006;**110**(31):15411-15416
- [44] Silva DSA, Castelblanco WN, Piva DH, de Macedo V, Carvalho KTG, Urquieta-González EA. Tuning the Brønsted and Lewis acid nature in HZSM-5 zeolites by the generation of intracrystalline mesoporosity—Catalytic behavior for the acylation of anisole. *Molecular Catalysis*. 2020;**492**(February):111026. DOI: 10.1016/j.mcat.2020.111026
- [45] Yabushita M, Kobayashi H, Neya A, Nakaya M, Maki S, Matsubara M, et al. Precise control of density and strength of acid sites of MFI-type zeolite nanoparticles: Via simultaneous isomorphous substitution by Al and Fe. *CrystEngComm*. 2020;**22**(44):7556-7564
- [46] Wloch J. Influence of isomorphous substitution in MFI-type materials on the diffusion of n-hexane: Molecular dynamic studies. *Applied Surface Science*. 2007;**253**(13 SPEC. ISS):5692-5695
- [47] Jin L, Fang Y, Hu H. Selective synthesis of 2,6-dimethylnaphthalene by methylation of 2-methylnaphthalene with methanol on Zr/(Al)ZSM-5. *Catalysis Communications*. 2006;**7**(5):255-259
- [48] Morgan CI, Paredes SP, Flores SO, Alfaro S. Single gel hydrothermal synthesis and characterization of vanadium isomorphously modified silicalite-1 and ZSM-5. *Materials Letters*. 2017;**209**:513-516. DOI: 10.1016/j.matlet.2017.08.074
- [49] Harris J, Andersson S. H₂ dissociation at metal surfaces. *Physical Review Letters*. 1985;**55**(15):1583-1586
- [50] He S, Zuur K, Santosa DS, Heeres A, Liu C, Pidko E, et al. Catalytic conversion of pure glycerol over an un-modified H-ZSM-5 zeolite to bio-based aromatics. *Applied Catalysis B: Environmental*. 2021;**281**(August 2020):119467. DOI: 10.1016/j.apcatb.2020.119467
- [51] Hoang TQ, Zhu X, Sooknoi T, Resasco DE, Mallinson RG. A comparison of the reactivities of propanal and propylene on HZSM-5. *Journal of Catalysis*. 2010;**271**(2):201-208. DOI: 10.1016/j.jcat.2010.01.017
- [52] Wang F, Zhou MX, Yang XH, Gao LJ, Xiao GM. The effect of hierarchical pore architecture on one-step catalytic aromatization of glycerol: Reaction routes and catalytic performances. *Molecular Catalysis*. 2017;**432**:144-154. DOI: 10.1016/j.mcat.2017.01.017
- [53] He S, Klein FGH, Kramer TS, Chandel A, Tegudeer Z, Heeres A, et al.

Catalytic co-conversion of glycerol and oleic acid to bio-aromatics: Catalyst deactivation studies for a technical H-ZSM-5/Al₂O₃ catalyst. *Applied Catalysis A: General*. 2022;**632**(January)

[54] Okoye PU, Hameed BH. Review on recent progress in catalytic carboxylation and acetylation of glycerol as a byproduct of biodiesel production. *Renewable and Sustainable Energy Reviews*. 2016;**53**:558-574. DOI: 10.1016/j.rser.2015.08.064

[55] He S, Kramer TS, Santosa DS, Heeres A, Heeres HJ. Catalytic conversion of glycerol and co-feeds (fatty acids, alcohols, and alkanes) to bio-based aromatics: Remarkable and unprecedented synergetic effects on catalyst performance. *Green Chemistry*. 2022;**24**(2):941-949

[56] He S, Goldhoorn HR, Tegudeer Z, Chandel A, Heeres A, Liu C, et al. Catalytic conversion of glycerol to bio-based aromatics using H-ZSM-5 in combination with various binders. *Fuel Processing Technology*. 2021;**221**(May):106944. DOI: 10.1016/j.fuproc.2021.106944

Section 3

Applications

Chapter 6

Ethanol Inhalation in Treatment and Prevention of Coronavirus Disease (COVID-19)

Ali Amoushahi

Abstract

The goal of this study was to determine if nebulized ethanol (EtOH) is safe and effective in treating COVID-19. A randomized controlled trial was carried out on 99 symptomatic and RT-PCR-positive patients admitted to a hospital that were given Remdesivir and Dexamethasone. They were randomly given either a 35% EtOH spray (intervention group, IG) or distilled water spray (control group, CG). For a week, each group underwent three nebulizer puffs every 6 hours. Global Symptomatic Score (GSS) comparisons between the two groups at the initial visit and on days 3, 7, and 14. Secondary outcomes include the readmission rate and the Clinical Status Scale (CSS), a seven-point ordinal scale that ranges from death to full recovery. The intervention and control groups, respectively included 44 and 55 patients. The GSS and CSS considerably improved in the IG, despite the fact that there was no difference at admission ($p = 0.016$ and $p = 0.001$, respectively) (Zero vs. 10.9%; $P = 0.02$). The IG readmission rate was much reduced. Inhaled-nebulized EtOH responds well in quickly improving the clinical status and limiting the need for further therapy. Further investigation into the therapeutic and preventative properties of EtOH is advised due to its affordability, availability, and lack of/tolerable side effects.

Keywords: ethanol, inhalation, nebulizer, COVID-19, blood oxygen saturation

1. Introduction

Deaths from cytokine storms are frequently caused by COVID-19. Alcohol has been shown to have in vitro antiviral effects on coronavirus glycoprotein destruction [1] and the breakdown of the fat layer [2]. Ethyl alcohol (EtOH) has been shown to have antiviral effects on extracellular surfaces in the past [3]. Inflammatory factors such TLR, interleukin-6, and TL9, as well as TNF-mRNA protein and mitogen-activated protein kinase, have been proven in immunological investigations to have immunomodulatory effects on the innate immune system and to attenuate cytokine storm [4, 5]. Additionally, it promotes bronchoalveolar macrophages' chemotaxis [6]. Other effects of ethanol include the prevention of viral multiplication through RNA-dependent polymerase inhibition [7], bronchial dilatation by relaxing involuntary smooth muscles [8], patient sedation and relaxation [9], and analgesic effects

on muscles [10]. Methanol poisoning [11], fat embolism [12], premature labor prevention [13], preeclampsia [14], and pulmonary edema [15] have all been treated with ethanol-specific treatments in the past. Castro-Balado et al. [16] have shown the histological safety of inhalation ethanol treatment on rats' lungs and respiratory systems. Ethanol was authorized by the Food and Drug Administration. Can ethanol inhalation treatment be beneficial in treating COVID-19? Given the effects of ethanol on virus wall breakdown, proliferation inhibition, and immunological hyperactivity inhibition, the use of inhaled ethanol as a COVID-19 treatment is still unknown. One month following the COVID-19 epidemic in Iran, this concept was initially put forth and published [17, 18]. Later, a paper explaining the justification for ethanol usage in this area was presented [19]. Recent research on the combined administration of dimethyl sulfoxide and ethanol in healthcare professionals, demonstrated positive effects on COVID-19 prevention [20]. We conducted a randomized clinical study to assess the impact of ethanol treatment on the clinical condition and prognosis of a predetermined group of patients in an effort to discover the solution. The Medical University of Isfahan Research and Ethics Committee accepted the study, which was then registered at <https://irct.ir/trial/58201>.

2. Materials and methods

Study Design and Oversight (**Figure 1**). The Isabn-e-Maryam Hospital (Christian hospital) at the Medical University of Isfahan in Iran, where this study was carried out in September 2021, was the site of a randomized double-blind clinical trial with a control group and parallel design. The patients were matched one to one at random. The study was initially intended to be conducted on hospitalized patients, but because the country's policy had been changed to allow for the establishment of respiratory

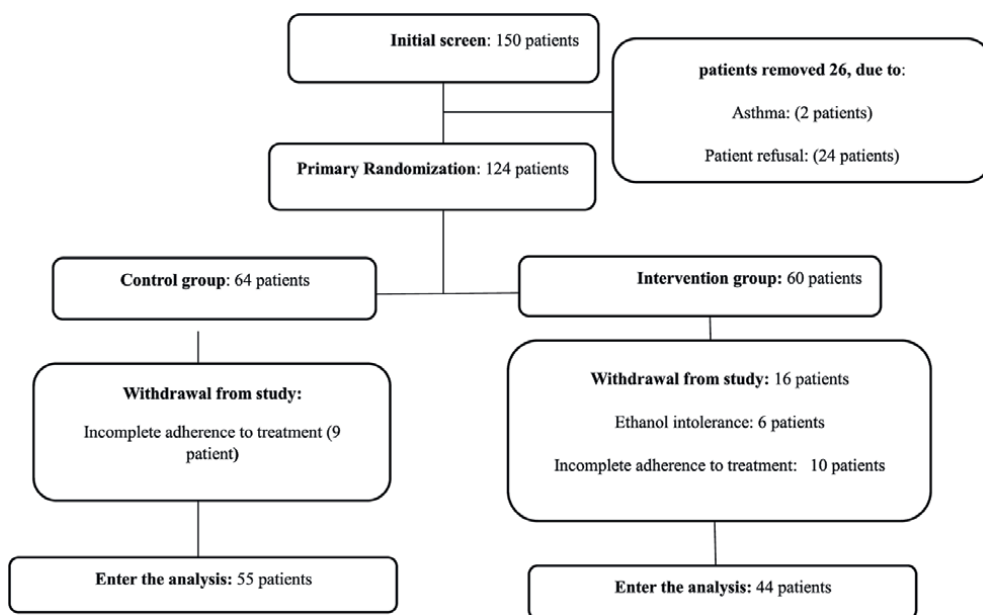


Figure 1.
Flowchart of the study.

clinics in hospitals and the prescription of Remdesivir and Dexamethasone to patients with moderate COVID-19, the study was instead carried out in this clinic. The referral of the patient to the respiratory clinic and this report were shared with the doctors of patients who were being treated in hospitals.

2.1 Patients

Patients who tested positive for SARS-CoV-2-RT-PCR are the foundation of the study population. They were admitted to the hospital's respiratory clinic because they had moderate COVID-19 (based on the national guideline for managing COVID-19, O₂Sat 90–94% or lung involvement [21]). The following criteria were required for inclusion: informed consent, age of at least 12 years old, no pregnancy, no history of epilepsy, alcoholism, or asthma, no contraindications to ethanol usage, and no use of ethanol-interacting medications. Intolerance to inhaled ethanol and incomplete or partial therapy were the exclusion criteria. To investigate possible allergies to alcohol, a skin test with ethanol was performed. In this study, the patient's arm was linked to a gauze pad with an ethanol drop on it. Symptoms including skin redness, swelling, or itching were seen after around 7 minutes. These signs may be indicative of an alcohol allergy or intolerance.

2.2 Intervention

According to Iran's national clinical norms, both the control and intervention groups were enrolled in the standard medical treatment [21]. The national standard treatment included intramuscular Dexamethasone, 8 mg/day (5 days), and 200 mg of Remdesivir intravenously on day 1, followed by 100 mg of Remdesivir once daily for 4 days, infused over 30–60 minutes. Patients received normal care as per routine and were then randomly allocated to either the control group (distilled water spray) or the intervention group (35% ethanol spray). The delivery of two 100 ml sets of spray was done in accordance with randomization. Each patient was told to spray the mask three times per day (every 6 to 8 hours) and inhale deeply. We stressed that, depending on the duration of symptoms, this procedure had to be repeated for 7 days. Patients were guided through the process by nurses until they were able to do it on their own. At each appointment for referrals and follow-up care, patient compliance was evaluated. Failure to follow the protocol (spray not used or used incorrectly) resulted in removal from the trial.

3. Clinical and laboratory monitoring

The demographic and clinical information were separated into different sections on the data collecting sheet. A qualified nurse performed the data-collecting checklist based on clinical symptoms, clinical outcomes, and clinical examination after obtaining demographic data from the patient's records. Up to discharge, information on study variables, such as blood oxygen saturation measured by pulse oximetry, the requirement for supplementary care or hospital readmission, and clinical complaints in both groups, was gathered.

3.1 Study outcomes

Primary outcomes: The global symptomatic score (GSS), which is calculated by adding up the cumulative scores of clinical signs and symptoms like anorexia, fever,

headache, body aches, sore throat, runny nose, chills, coughing, and loss of taste and smell, is regarded as a gauge of a patient's clinical condition. This index was created to provide a concise list of clinical symptoms. Using a pulse oximeter, oxygenation status was tracked and documented each day. The patient was not receiving any additional oxygen at the time of the measurement and was breathing room air with a fixed pulse oximeter. Changes in blood C-reactive protein (CRP) levels were used to characterize the presence of inflammation.

Secondary outcomes: On day 14 of the treatment period for the investigation, clinical conditions were evaluated using a modified 7-point ordinal scale [22].

There are seven indicators in this scale:

1. Death.
2. A patient in a hospital receiving invasive mechanical ventilation.
3. High-flow oxygen or non-invasive ventilation systems used in hospitals.
4. Hospitalized and in need of low-flow oxygen.
5. Hospitalized for any cause, requiring continuous medical care (whether linked to COVID-19 or not), and requiring home oxygen supplementation.
6. Continued signs or symptoms of COVID-19 without requiring supplemental oxygen, no longer require ongoing medical care.
7. Both groups reported and dealt with full recovery as well as any potential side effects.

The necessity for critical care unit admission, adverse medication reactions, clinical symptoms, and death in the research samples were noted and tracked in both groups. The last follow-up was scheduled on the day fourteenth of the illness. Physical examinations, history-taking, phone calls, reviews of patient records, and documents from the hospital information system were all used during follow-up. After receiving informed consent, side effects were documented. The main endpoints have undergone some alterations. This was due to the study's implementation restrictions, which coincided with the disease's peak in Iran, and the fact that patients who required hospitalization were followed up on an outpatient basis in the respiratory clinic. We informed the sponsor and institutional review board in great detail of the protocol revisions. The length of stay was the key anticipated result. This index was replaced with a more detailed clinical status since all moderate patients were treated on a 5-day regimen during the surge.

3.2 Sampling

An easy random sample technique was used to do the sampling. Random assignment was performed using a computerized random number table. The order of the random distributions was decided by one nurse. Each participant who was qualified and gave their agreement to participate in the experiment was randomly assigned from a list that she kept confidential. One by one, a different nurse added 100 ml of diluted distilled water or ethanol-35% to the sprays (nebulizers) and labeled them

with the numbers from the list. Each spray was given to a participant, who was then instructed on how to use it by their family or companion. Blinding was carried out by analysts, nurses, and clinicians.

4. Statistical analysis

Using a 2-sided significance level of 0.05, we calculated that 88 patients (44 in each group) would offer higher than 90% power to detect an odds ratio of 3 for the ethanol group vs. the placebo group. The analysis was restricted to individuals who, in accordance with the research protocol and inclusion criteria, got full treatments and contributed to the outcomes, as per the “treatment-on” or “per-protocol” method. Means, standard deviations, and percentages (%) were used to report both quantitative and qualitative information. The chi-square test was used to evaluate qualitative characteristics between the two groups, and a mixed model was used to compare SpO₂ readings and GSS on days 1, 3, 7, and 14. Repeated-measures analysis was used to calculate the average changes from baseline values. With the use of Mauchly’s statistics and the Geisser-Greenhouse adjustment, the sphericity hypothesis was disproved. The cumulative odds ordinal logistic regression with proportional odds was used to compare clinical status between the two groups on day 14, and the two test was used to determine the proportion of patients in each group who required additional medical care after 14 days. These tests were carried out at 0, 3, and 14 days after the intervention. For the intervention group compared to the usual care group, an odds ratio larger than 1 showed changes in clinical status across all categories toward category 7. For clinical status, if a patient recovered, the ordinal score was recorded as 7 on the day of recovery and all subsequent days unless the patient was hospitalized for COVID-19-related reasons or others; all statistical analyses were performed using SPSS software version 22 (SPSS Inc., Chicago, IL, USA), and $p < 0.05$ was considered significant. The outcome markers were adjusted for the patient’s gender.

5. Results

Patient Characteristics from September to November 2021, 150 patients from the COVID-19 Respiratory Outpatient Clinic of the Isabn-e-Maryam Hospital of the Isfahan University of Medical Sciences were assessed for participation in the research based on the positive outcome of the RT-CPR test. A total of 24 patients disagreed with the research, and 2 patients did not meet the inclusion requirements. Randomly, 124 more patients were divided into two groups (Intervention and Control). In the next days, 25 participants were removed from the trial due to intolerance to ethanol inhalation (6 patients); their intolerance was mostly caused by hiccups, eye irritation, coughing, shortness of breath, sneezing, and the unpleasant odor of alcohol. On the other hand, 19 patients (9 in the control group and 10 in the intervention group) were disqualified from the trial because of irregularities or failure to adhere to the suggested procedure. Finally, 99 patients entered the analysis: 44 patients in the IG and 55 patients in the CG (**Table 1**).

Table 1 summarizes the baseline characteristics and demographics of the two groups of patients. The male-to-female patient ratio was 43/56 (42.4/56.6%). The patients were 46.4 years old on average. A total of 38 patients had multiple conditions. Diabetes mellitus was the most prevalent underlying condition in both groups, with 6

Index	Control group N = 55	Intervention group N = 44	P value
Age (years) (Mean ± SD)	46.15 ± 13.15	45.91 ± 12.58	0.928
BMI (Kg/m ²) (Mean ± SD)			
Normal weight	16 (29.1)	9 (20.5)	0.804
Overweight	25 (45.5)	22 (50)	
Obesity	10 (20)	10 (22.7)	
Excessive obesity	3 (5.5)	3 (6.8)	
Gender N (%)			
Female	37 (67.3)	19 (43.2)	0.024
Male	18 (32.7)	25 (56.8)	
Education Level N (%)			
Illiterate and Elementary	3 (5.4)	8 (16.3)	0.251
Secondary	8 (14.3)	7 (14.3)	
Diploma	28 (50)	16 (32.7)	
Bachelor-higher	16 (26.8)	16 (30.6)	
Unknown	2 (3.6)	3 (6.1)	
Risk factors for disease N (%)			
Not any	23 (52.3)	38 (69.1)	0.614
1 risk factor	19 (43.2)	12 (21.8)	
2 risk factors	2 (4.5)	4 (7.3)	
3 risk factors	0	1 (1.8)	

Table 1.
Demographic characteristics in two research groups.

(14.3%) in the intervention group and 4 (7%) in the control group. Seven individuals had high blood pressure and seven others had additional cardiovascular issues. The two groups' mean ages, weights, levels of education, and total number of risk variables did not significantly differ from one another.

5.1 Clinical signs and symptoms at the time of admission

The interval between the onset of symptoms and admission, lung involvement, and early clinical signs and symptoms at baseline did not substantially differ among the patients. The clinical signs and symptoms of the patient's fundamental characteristics are listed in **Table 2**.

Cough, body pains, chills, and headaches were the intervention group's main clinical complaints. The control group had a higher prevalence of anorexia, olfactory disturbance, and cough. There was no discernible change in symptoms. Overall Symptom Score The GSS was evaluated at the start of therapy, 3, 7, and 14 days afterward in two groups. The results are shown in **Figure 2**.

The GSS of the two groups was equal at the start of the research, according to statistical analysis, but in the IG group, clinical symptoms reduced more quickly than in the placebo group. The statistical significance of this difference was ($p = 0.016$).

5.2 Blood oxygen saturation

At the time of the trial, there was no noticeable change in the two groups' blood oxygen saturation levels (92.07 ± 4.6 in the control group vs. 91.56 ± 3.39 in the intervention group). As seen in **Figure 3**.

Characteristic	Control group N = 55	Intervention group N = 44	P value
Distance from onset of symptoms to Start treatment (Mean ± SD)	9.36 ± 5.13	8.50 ± 3.52	0.338
Pulmonary Involvement (CT scan) N (%)			
Less than 30%	22 (40)	19 (43.2)	0.153
30–49%	25 (45.5)	15 (34.1)	
50% and above	2 (3.6)	2 (4.5)	
Unknown	6 (10.9)	8 (18.2)	
Fever N (%)	21 (38.2)	25 (56.8)	0.072
Chills N (%)	35 (63.6)	30 (68.2)	0.675
Cough N (%)	49 (89.1)	41 (95.3)	0.262
Headache N (%)	35 (63.6)	30 (68.2)	0.636
Short Breath N (%)	37 (67.3)	24 (54.5)	0.196
Sore throat N (%)	27 (49)	16 (36.4)	0.204
Rhinorrhea N (%)	18 (32.7)	9 (20.5)	0.173
Body pain N (%)	36 (65.5)	36 (65.5)	0.069
Anorexia N (%)	38 (69.1)	29 (65.9)	0.737
Anosmia N (%)	39 (70.9)	26 (59.1)	0.219
Lack of taste N (%)	32 (58.2)	27 (61.4)	0.749
Global Symptomatic Score (GSS)	6.67 (2.09)	6.72 (2.07)	0.910

Table 2. Preliminary characteristics of signs and symptoms, risk factors, and laboratory values in baselines.

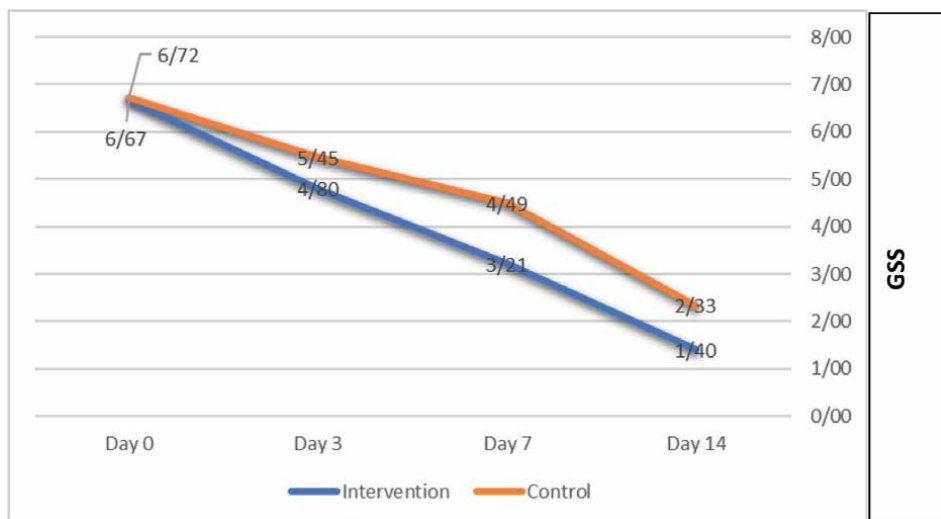


Figure 2. Comparison of global symptomatic score (GSS) in the intervention and control groups at the beginning of admission, days 3, 7 and 14 after admission.

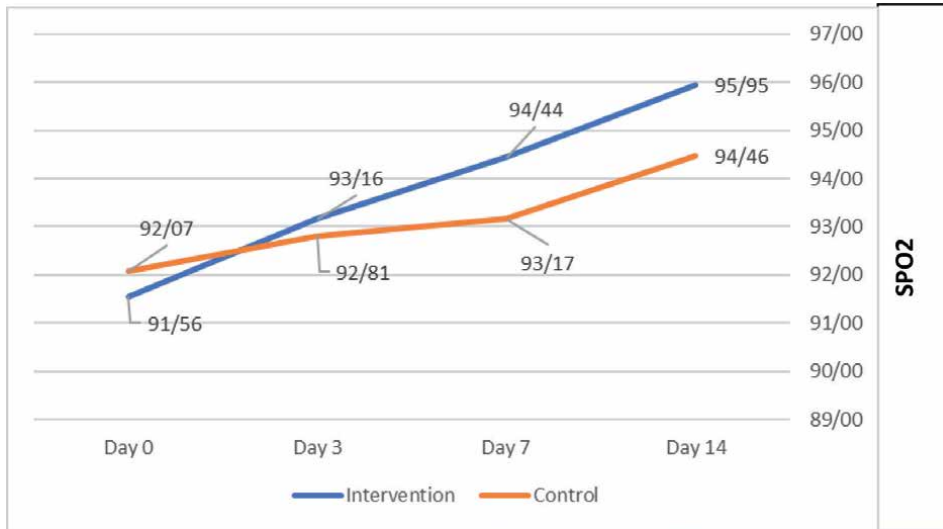


Figure 3. Comparison of mean blood oxygen saturation (SPO₂) in intervention and control groups at the beginning of admission, days 3, 7 and 14 after patient admission.

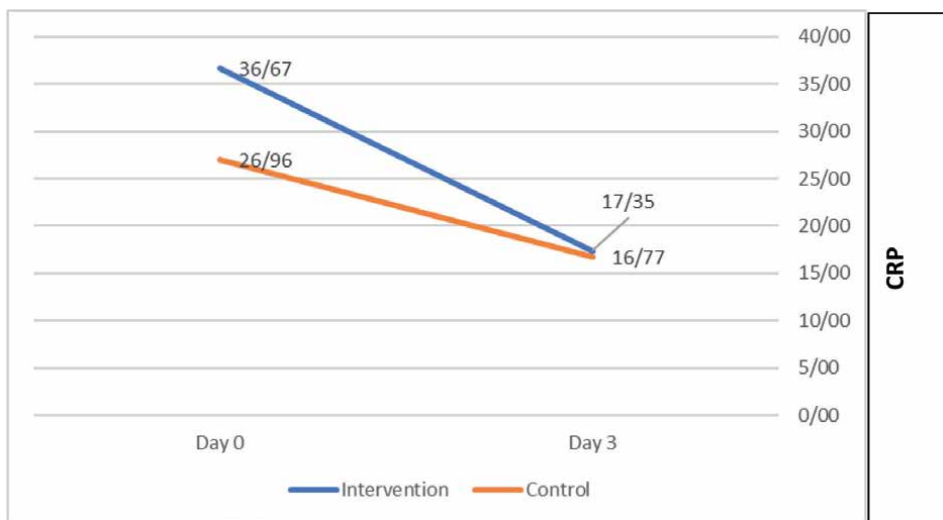


Figure 4. Comparison of CRP (C-reactive protein) in the intervention and control groups at the beginning of admission and three days after patient admission.

Both groups had an improvement in blood oxygenation, however, the ethanol group’s slope of oxygenation was greater. The change is not statistically significant, though ($p = 0.097$) inflammatory factor (CRP) Multiple assessments and statistical comparisons between the two groups revealed a declining trend in CRP (**Figure 4**).

However, the rate of reduction was much faster and more intense in the IG ($p = 0.05$). Two sets of CSS based on the modified 7-point ordinal scale were compared. On day 14, the intervention group had 5.7 times the chance of having superior

Characteristic and Score N (%)	Intervention N = 44	Control N = 55
1. Death	0	0
2. Hospitalized, on invasive mechanical ventilation	0	0
3. Hospitalized, on non-invasive ventilation or high flow oxygen devices	0	0
4. Hospitalizations for any reason and need oxygen	0 (0)	2 (3.63)
5. Requiring ongoing medical care or supplemental oxygen at home	2 (4.54)	10 (18.18)
6. Continue signs or symptoms without requiring supplemental oxygen - no longer requires ongoing medical care	13 (29.54)	29 (52.72)
7. Complete recovery	29 (65.90)	14 (25.45)

Table 3.
 Comparison of clinical status scale (CSS) of intervention and control groups on the 14th day of admission.

CSS than the control group (95% CI, 2.47–13.19), which is a statistically significant difference (Wald 2 (1) =16.67, $p = 0.001$). **Table 3** provides details.

Six patients (10.9%) from the control group were readmitted after the therapy period had ended in order to obtain further care or hospitalization. None of the patients were readmitted to the ethanol group ($p = 0.02$).

5.3 Adverse events and safety

Six out of 50 patients in the ethanol group (12%) quit taking it due to adverse effects that started as soon as inhalation began, and we eliminated them from the research. Only one instance of each negative effect was noted, and it vanished after ethanol consumption was discontinued. Hiccups, eye discomfort, coughing, shortness of breath, sneezing, and a strong alcohol odor were a few of the undesirable side effects.

6. Discussion

The impact of adding nebulized Ethanol inhalation has been researched in this clinical study on patients having positive RT-PCR test results, mild clinical symptoms, and suitability for Remdesivir and Dexamethasone treatment, according to the Iran Ministry of Health protocol. The rationale for the use of EtOH in COVID-19 has been well discussed [19]. There is no question regarding the ability of ethanol in killing or making SARS-CoV-2 inactive, even at concentrations as low as 30% v/v and for only 30 seconds [23]. The virus's fat layer is broken down by the virucidal effects of EtOH, which then stop the virus from multiplying. EtOH has also been demonstrated to reduce the immune system's hyperactivity during COVID-19. It seems likely that ethanol is ineffective against intracellular viruses. It is crucial to continue ethanol inhalation for at least 3 days since viral multiplication happens within 48–72 hours, followed by cellular death and shedding. Additionally, ethanol is fundamentally effective against all SARS-CoV-2 variants and other “enveloped” viruses due to its non-specificity. The abnormal presence of *Mycoplasma salivarium* in the lower tract or the lack of *Clostridia* in the upper tract was linked to worse outcomes in ICU patients [24]. It is interesting to note that ethanol completely inactivates *Mycoplasma*

and SARS-CoV-2 (Eterpi et al.) [25]. Additionally, certain strains of Clostridia synthesize endogenous ethanol [26]. According to a hypothetical scenario, the lack of nasopharyngeal Clostridia would prevent the local generation of ethanol, which would prevent or drastically limit the inactivation of SARS-Cov-2 at this level, allowing the virus to propagate to the lower respiratory tract. A lot of concern has been expressed regarding the potential mucosal harm that breathed ethanol might cause. Castro-Balado et al. careful research [16] appears to have completely dispelled these concerns. It should be noted that spraying into the mask prolongs the action of the nebulized liquid and maintains its efficiency by reducing the dispersion and evaporation of the liquid. The different smells of the two solutions indicate a potential inherent bias. Patients could only recognize that one spray was different from another since they were unaware of the actual ingredient in the spray. To put it differently, the medication may have been in an odorless spray. Dexamethasone and Remdesivir are administered intramuscularly as part of the COVID-19 standard therapy [21]. According to a recent trial, introducing early antibiotic therapy for COVID-19 pneumonia had no positive effects on 30-day mortality [27]. Despite what was predicted [28, 29], the authors [27] did not discover any appreciable vaccination benefit in reducing illness severity and death among patients with COVID-19 pneumonia. The GSS fell more in the Intervention group than in the control group, according to our findings, and these data reached a statistically significant level ($p = 0.016$). Nebulized EtOH inhalation had positive effects on lowering CRP levels, which was a significant advantage ($p = 0.05$). This result supports EtOH's positive immune-modulation effects [3]. On the other hand, blood oxygenation increased more quickly and had a greater slope in the ethanol than it did in the control group. Regarding blood oxygenation, between the two groups, there was, however, no statistically significant difference ($p = 0.097$). In terms of CSS, the intervention responded better than the control since no patient had to be readmitted, as opposed to the control where 6 patients (10.8%) had to repeat the normal therapy or be hospitalized. These results provide credibility to EtOH's virucidal properties.

7. Conclusions

Overall, recovery from moderate COVID-19 is greatly improved by adding EtOH to the conventional therapy (Remdesivir+Dexamethasone). It is advised to do more research and invest more in order to assess ethanol's therapeutic and preventative effects in the early stages of COVID-19 given its accessibility, low cost, and lack of substantial adverse events. The patients in this experiment were far from our rigorous oversight and switched to other treatments, which was one of its shortcomings. The healthcare system is also concerned about unpleasant alcohol consumption and the potential for non-inhaled alcohol intake. This study is constrained by chance (due to the small sample size), confounding factors (due to the imbalance in gender distribution), and low power, among other things. The randomization sequence is broken by a per-protocol analysis, which also introduces bias into the study.


Author details

Ali Amoushahi

Department of Anesthesiology and Intensive Care Unit, Isabn-e-Maryam Hospital,
Isfahan University of Medical Sciences, Isfahan, Iran

*Address all correspondence to: aliamoushah@gmail.com

IntechOpen

© 2023 The Author(s). Licensee IntechOpen. This chapter is distributed under the terms of the Creative Commons Attribution License (<http://creativecommons.org/licenses/by/3.0>), which permits unrestricted use, distribution, and reproduction in any medium, provided the original work is properly cited. 

References

- [1] Lai MM, Cavanagh D. The molecular biology of coronaviruses. *Advances in Virus Research*. 1997;**48**:1-100. DOI: 10.1016/S0065-3527(08)60286-9
- [2] Singh D, Joshi K, Samuel A, et al. Alcohol-based hand sanitizers as first line of defence against SARS-CoV-2: A review of biology, chemistry and formulations. *Epidemiology & Infection*. 2020;**148**:e229
- [3] Moorer W. Antiviral activity of alcohol for surface disinfection. *International Journal of Dental Hygiene*. 2003;**1**:1601-5037. DOI: 10.1034/j.1601-5037.2003.00032.x
- [4] Mörs K, Hörauf J-A, Kany S, et al. Ethanol decreases inflammatory response in human lung epithelial cells by inhibiting the canonical NF- κ B-pathway. *Cellular Physiology and Biochemistry*. 2017;**43**:17-30
- [5] Chandrasekar A, Olde Heuvel F, Palmer A, et al. Acute ethanol administration results in a protective cytokine and neuroinflammatory profile in traumatic brain injury. *International Immunopharmacology*. 2017;**51**:66-75
- [6] Boé DM, Nelson S, Zhang P, et al. Acute ethanol intoxication suppresses lung chemokine production following infection with *Streptococcus pneumoniae*. *The Journal of infectious diseases*. 2001;**184**:1134-1142
- [7] Berres ME, Garic A, Flentke GR, et al. Transcriptome profiling identifies ribosome biogenesis as a target of alcohol teratogenicity and vulnerability during early embryogenesis. *PLoS One*. 2017;**12**:0169351
- [8] Sakihara C, Jones KA, Lorenz RR, et al. Effects of primary alcohols on airway smooth muscle. *The Journal of the American Society of Anesthesiologists*. 2002;**96**:428-437. DOI: 10.1097/00000542-200202000-00031
- [9] Acevedo SF, Gonzalez DA, Rodan AR, et al. S6 kinase reflects and regulates ethanol-induced sedation. *Journal of Neuroscience*. 2015;**35**:15396-15402. DOI: 10.1523/JNEUROSCI.1880-15.2015
- [10] Aroust CA, Perrino AC Jr, Ralevski E, et al. Effect of intravenous ethanol on capsaicin-induced hyperalgesia in human subjects. *Alcoholism: Clinical and Experimental Research*. 2016;**40**:1425-1429
- [11] Ekins BR, Rollins DE, Duffy DP, et al. Standardized treatment of severe methanol poisoning with ethanol and hemodialysis. *Western Journal of Medicine*. 1985;**142**:337-1306022
- [12] Myers R, Taljaard J. Blood alcohol and fat embolism syndrome. *The Journal of bone and joint surgery American volume*. 1977;**59**:878-880
- [13] Haas DM, Morgan AM, Deans SJ, et al. Ethanol for preventing preterm birth in threatened preterm labor. *Cochrane Database of Systematic Reviews*. 2015;**2015**:CD011445
- [14] Teran E, Racines-Orbe M, Vivero S, et al. Preeclampsia is associated with a decrease in plasma coenzyme Q10 levels. *Free Radical Biology and Medicine*. 2003;**35**:1453-1456
- [15] Gootnick A, Lipson HI, Turbin J. Inhalation of ethyl alcohol for pulmonary edema. *New England Journal of Medicine*. 1951;**245**:842-843. DOI: 10.1056/NEJM195111292452202

- [16] Castro-Balado A, Mondelo-García C, Barbosa-Pereira L, et al. Development and characterization of inhaled ethanol as a novel pharmacological strategy currently evaluated in a phase II clinical trial for early-stage SARS-CoV-2 infection. *Pharmaceutics*. 2021;5:342-317
- [17] Amoushahi A. A suggestion on ethanol therapy in COVID-19? *EC Anaesthesia*. 2020;6:1-2
- [18] Ezz A, Amoushahi A, Rashad A. Disinfection of SARS-COV-2 (COVID-19) in human respiratory tract by controlled ethanol vapor inhalation combined with Aspirin. *Journal of Vaccines & Vaccination*. 2021;12:454
- [19] Salvatori P. The rationale of ethanol inhalation for disinfection of the respiratory tract in SARS-CoV-2-positive asymptomatic subjects. *The Pan African Medical Journal*. 2021;40:201
- [20] Hosseinzadeh A, Tavakolian A, Kia V, et al. Combined application of dimethyl sulfoxide and ethanol nasal spray during COVID-19 pandemic may protect healthcare workers: A randomized controlled trial. *Iranian Red Crescent Medical Journal*. 2022;24:8. DOI: 10.32592/ircmj.2022.24.8.1640
- [21] Rahmanzade R, Rahmanzadeh R, Hashemian SM, et al. Iran's approach to COVID-19: Evolving treatment protocols and ongoing clinical trials. *Frontiers in Public Health*. 2020;4:551889-551810. DOI: 10.3389/fpubh.2020.551889
- [22] Spinner C, Gottlieb R, Criner G, et al. Effect of Remdesivir vs standard care on clinical status at 11 days in patients with moderate COVID-19: A randomized clinical trial. *JAMA*. 2020;324:1048
- [23] Kratzel A, Todt D, V'kovski P, et al.: Inactivation of severe acute respiratory syndrome coronavirus 2 by WHO-recommended hand rub formulations and alcohols. *Emerging Infectious Diseases* 2020, 26: 1592-1595. 10.3201/eid2607.200915
- [24] Sulaiman I, Chung M, Angel L, et al. Microbial signatures in the lower airways of mechanically ventilated COVID19 patients associated with poor clinical outcome. *MedRxiv*. 2021;26:10-1101. DOI: 10.1038/s41564-021-00961-5
- [25] Eterpi M, McDonnell G, Thomas V. Decontamination efficacy against mycoplasma. *Letters in Applied Microbiology*. 2011;52:21198694. DOI: 10.1111/j.1472-765X.2010.02979.x
- [26] Ruuskanen MO, Åberg F, Mannistö V, et al. Links between gut microbiome composition and fatty liver disease in a large population sample. *Gut Microbes*. 2021;13:1
- [27] Choi YJ, Song JY, Hyun H, et al. Prognostic factors of 30-day mortality in patients with COVID-19 pneumonia under standard remdesivir and dexamethasone treatment. *Medicine*. 2022;23:30474. DOI: 10.1097/MD.000000000000304741
- [28] Lopez Bernal J, Andrews N, Gower C, et al. Effectiveness of the Pfizer-BioNTech and Oxford-AstraZeneca vaccines on covid-19 related symptoms, hospital admissions, and mortality in older adults in England: Test negative case-control study. *BMJ*. 2021;373:1088. DOI: 10.1136/bmj.n1088
- [29] Tenforde MW, Self WH, Adams K, et al. Association between mRNA vaccination and COVID-19 hospitalization and disease severity. *Journal of the American Medical Association*. 2021;326:54. DOI: 10.1001/jama.2021.19499

Nebulized Ethanol: An Old Treatment for a New Disease

Steven W. Stogner

Abstract

Ethyl alcohol (ethanol) is known to inactivate SARS-CoV-2, and therefore, direct delivery to the upper and lower respiratory tracts hypothetically would inhibit the progression of COVID-19. After informed consent, nebulized EtOH was given to inpatients admitted with COVID-19, and outcomes were retrospectively compared to randomly selected controls. Benefits of nebulized EtOH included decreased average length of stay, improved inpatient survival, decreased intubation rate and need for transfer to intensive care, improvement in hypoxemia, and decreased need for transfer to another facility for ongoing post-acute care. Also, fewer patients required supplemental home oxygen after discharge to home. Interpretation: Nebulized EtOH is beneficial in the treatment of COVID-19. Further study is warranted.

Keywords: inhaled ethanol, COVID-19, SARS-CoV-2, hypoxemia, virucide

1. Introduction

The virus that causes COVID-19 Disease (designated SARS-CoV-2, Severe Acute Respiratory Syndrome Coronavirus 2) has caused severe morbidity and mortality around the world. In addition to the human toll of disease, the pandemic triggered stark social as well as economic disruption around the world, affecting a global recession [1]. Supply shortages (including food), travel restrictions, business restrictions and closures, workplace hazard controls, quarantines, testing systems, and tracing contacts of the infected has been costly in not only financial terms as governments attempted to control the pandemic but also in societal customs and “norms” as well. Near-global lockdowns of educational institutions and other entities were partially or completely closed in many areas, as well as the postponement of needed surgeries placed major stress on communities across the globe, often resulting in a political uproar. In truth, the world has not experienced a similar pandemic and its results since the 1918 Flu Pandemic (February 1918 until April 1920 in four successive waves affecting 500 million people) [2, 3].

As of August 2022, COVID-19 has infected more than 600 million people and caused almost 6.5 million confirmed deaths worldwide—one of the deadliest in history [3]. First identified in Wuhan, China, in December 2019, the COVID-19 virus outbreak was identified by the World Health Organization (WHO) as a public health emergency of international concern on January 30, 2020, and the astronomical

trajectory continued with it being declared a global pandemic only 2 weeks later [4]. In March of that year, hospitals and outpatient clinics alike found themselves overwhelmed with astonishing volumes of patients which stressed healthcare resources to the edge, to the point of having to contemplate the rationing of care [5], including intensive care beds and mechanical ventilators.

In addition to inadequate resources at the onset of the pandemic—other than standard treatment measures for respiratory failure, including ARDS—specific treatment for the COVID-19 virus did not exist. Healthcare workers found themselves having to care for critically ill and dying patients who were most often isolated from their loved ones. Saddled with the grim fact of no specific treatment, the apprehension of becoming infected themselves and transmission of the virus to their own loved ones at home, and the emotional (and *ethical*) nightmarish thoughts which occurred as the potential of rationing healthcare loomed, it is no shock the common *burn-out* of healthcare workers that ensued [6].

2. COVID-19: the disease

The degree of disease caused by COVID-19 ranges from undetectable to lethal, but most commonly includes fever, nonproductive cough, fatigue, and loss of taste and/or smell in 40 percent of cases [7]. While severe illness such as organ failure occurs most frequently in elderly patients, it is also seen in younger patients with certain comorbidities such as chronic obstructive pulmonary disease, heart failure, malignancy, obesity, chronic steroid or immunosuppressive use, etc. [8]. Transmission occurs when people inhale droplets of airborne particles containing the virus, but also when viral-contaminated fluids reach the eyes, nose, mouth, and even contaminated objects (i.e. hands, etc.).

3. Pathogenesis: a clue for an effective treatment

The COVID-19 virus contains genetic material (RNA) packaged in a protein coat which is surrounded by an envelope composed of a lipid bilayer derived from the host cell membrane [9–11]. SARS-CoV-2 affects the upper and lower respiratory tracts, where its entry genes are highly expressed in epithelial cells of the nasal cavity and into the alveolar cells. Thus, the portal of entry of SARS-CoV-2 is the upper respiratory tract where the acute infection begins, then subsequently travels to the alveoli by viral aspiration. A “*cytokine storm*” can then ensue, likely due to an interleukin-6 amplifier resulting in a hyper-activation process that regulates the nuclear factor kappa B (NF- κ B) [12–14]. Ultimately, this cascade of events can be fatal in 75% of cases due to the development of ARDS and other acute organ failures including thrombotic complications [15].

4. Nebulized ethanol: potential benefits and risks

Potential benefits: Direct delivery of a drug with viricidal activity against SARS-CoV-2 (or other susceptible respiratory viruses, i.e., influenza) to the epithelial cells of the upper and lower respiratory tracts in an effort to destroy the virus before severe disease can ensue seem advantageous—and is logical. Ethanol/ethyl alcohol/

EtOH suits this purpose. Ethanol is volatile and has long been used as an antiseptic/disinfectant, and constitutes the basis for many hand rubs and disinfectants used in healthcare settings [16, 17] as well as by the general public. Ethanol and other alcohols are known to inactivate many enveloped viruses like SARS-CoV-2 by dissolving the virus' lipid membrane causing its destruction [18–20]. Notably, alcohol-based hand rub solutions have been shown to inactivate SARS-CoV-2 in as little as 30 s [21]. In addition to coronavirus, the effective viricidal activity of ethanol against many other common viruses (i.e., influenza, adenovirus, etc.) as well as Zika and Ebola has been demonstrated [22].

Ethanol is presently used worldwide as a generally nontoxic antiseptic and disinfectant and has been effectively and safely used in medicine for methanol poisoning [23], and as late as the 1950s as an inhalational treatment of pulmonary edema [24, 25] and alcohol withdrawal [26, 27].

Published reports suggest promise for the use of inhaled ethanol in the treatment of ARDS [28]. Ethanol is a well-known efficient surfactant (wetting agent), as it is an amphiphilic chemical compound possessing both hydrophilic and lipophilic properties. Surfactant proteins are critical components of alveolar function, and laboratory studies on animal lungs indicate ethanol has the potential to restore surfactant activity in experimentally-induced non-compliant lungs (produced with nebulized saline) [29]. Notably, analysis of SARS-CoV-2-infected lung tissues has revealed that surfactant proteins are indeed severely downregulated in infected lungs, causing respiratory distress [30].

Ethanol has mediator effects on inflammation [31] and thus could potentially have a beneficial effect on the prevention of cytokine storms [13]. In addition, there may be a possible benefit with ethanol in the prevention of thrombus formation shown by autopsy findings to frequently occur in COVID-19 [15, 32, 33]. Ordinarily, cutting of the fibrin mesh by plasmin enzyme leads to the production of circulating fragments that are cleared by other proteases or by the kidney and liver. Tissue plasminogen activator (t-PA) and urokinase then convert plasminogen to the active plasmin, allowing normal fibrinolysis to occur. Ethanol has been shown to “upregulate” the urokinase receptor in human endothelial cells and thus may be helpful in the elimination of thrombi [34].

Potential risks: Ethanol is flammable and combustible, and if ignited, can cause severe injury or even death. Appropriate cautionary measures are absolutely mandatory with its usage.

The risks and negative health effects on the immune, cardiovascular, pulmonary, gastrointestinal-hepatic, and neurologic systems of chronic oral consumption of ethanol are well-known [35]. Even acute oral consumption of large amounts is known to have the potential for serious health consequences, including even fatal toxicity. Vaporized ethanol used recreationally (*AWOL* = “alcohol without liquid”) appears to some extent becoming more prevalent, and serious concerns have appropriately been raised about its acute and unknown long-term health consequences, especially in young adults. However, a review of the literature fails to show any significant acutely negative effects of the short-term intake of small amounts of ethanol on the immune system or other organ systems [36–40].

Inhaled ethanol can irritate the eyes, as well as the nose, throat, and plausibly the lungs [41, 42]. In one small study, a decrease in ventilator flow rates on partial expiratory flow volumes [43] was found up to ninety minutes after inhalation, but no significant change in FEV₁ (forced expiratory volume) occurred compared to placebo (inhaled saline solution). Interestingly, pretreatment with disodium cromoglycate considerably diminished the acute reductions of flow rates caused by ethanol

inhalation, suggesting that ethanol in some persons may act, at least partly, through the release of mediators with bronchoconstrictive action.

As with any nebulized treatment, nebulized ethanol poses a risk for aerosolization of respiratory viruses like SARS-CoV-2 and transmission of the disease. Appropriate infection control precautions must be strictly followed when such conditions exist.

In the swarm of patients requiring inpatient care for acute hypoxemic respiratory failure due to SARS-CoV-2 in March 2020, those patients who deteriorated necessitating intubation for adult respiratory distress syndrome (ARDS) were having mortality exceeding 75% [3]. While governments were scrambling to issue emergency-use authorization for experimental treatments as well as civil protections for healthcare providers trying to best care for these patients, patients continued to literally smother ultimately requiring intubation and mechanical ventilation. The situation was not only grim, but it seemed hopeless. The urgency to find an effective treatment for this novel virus had never before been witnessed in the lives of most medical professionals. While some treatments were showing promise (i.e., remdesivir, dexamethasone, etc.), there remained an existential need for an effective readily available treatment. Given its proven viricidal efficacy, history of harmless use in the treatment of other medical conditions, as well as a lack of evidence for acute detrimental health effects when used in mild, non-chronic, non-excessive intake, the reasoning that nebulized ethanol may prove beneficial in the treatment of COVID-19 is rational.

5. Nebulized ethanol for treatment of COVID-19: results of a clinical study

In March 2020, at Forrest General Hospital (a non-profit community hospital in Hattiesburg, Mississippi) due to the emergent onslaught of this lethal and “untreatable” disease, and out of necessity and companionate care, a novel treatment regimen of nebulized ethanol was developed to offer patients with COVID-19 who required inpatient treatment for acute hypoxemia as a sole or supplemental treatment option, at the discretion of their attending physicians. While Shintake [44] had proposed the potential use of inhaled ethanol to eradicate the virus in the respiratory tract, extensive research of the medical literature otherwise revealed no reports of inhaled ethanol for treatment of COVID-19 infection¹ (or any other viral respiratory infection for that matter).

As a sole or additional option, a protocolized order set for the administration of nebulized ethanol was made available to hospital physicians in the electronic medical record beginning in April 2020. Education of all involved healthcare personnel was conducted prior to making the order set available. Administration of all nebulized treatments was performed by respiratory therapists, who in addition to nurses, monitored the patients. Access to and dispensing of the ethanol was meticulously controlled by the hospital pharmacy, which also confirmed that all of the following criteria were met prior to dispensing:

1. Admission for COVID-19 with dyspnea and/or hypoxemia;
2. Non-intensive care unit admission (general medical floor);

¹ The results of this study have not been published elsewhere.

3. Positive PCR (polymerase chain reaction test) via nasopharyngeal swab;
4. Pulmonary infiltrates typical of COVID-19 on chest radiographs or chest tomography (CT);
5. No contraindication to the intake of ethanol;
6. Informed consent.

5.1 Dose and administration

Ninety-five percent pure grain ethanol was used for a three-day regimen (3 total doses). Each daily dose was weight-based (actual body weight): female patients = 0.31 g/kg, and males = 0.33 g/kg. An equal volume of sterile water was mixed with the ethanol for a final concentration of 47.5%, and given continuously via face mask over approximately 60–75 min using a standard large-volume nebulizer driven by wall oxygen or air (determined by the patient's pre-treatment supplemental oxygen requirement) at a flow rate of 10 l/min. An anti-viral filter was connected to the exhalation port of the face mask. Respiratory therapists closely observed the patients and monitored SpO₂ (oxygen saturation via pulse oximetry) during treatments, and nurses recorded pre-treatment blood pressure, pulse and respiratory rates, and temperature, as well as every 15 min during and for one-hour post-treatment. No other persons were allowed in the room during or post-nebulization except per hospital policy, which included strict adherence to isolation precautions and protection measures such as personal protection equipment.

5.2 Data collection, statistical analysis, and outcomes

Demographic, clinical, and outcomes data were collected by retrospective review of the medical records of three hundred-six patients admitted for COVID-19 with respiratory disease from April through December 2020. Patients who completed the three-day regimen (Ethanol Group) were compared to randomly selected patients (Control Group) who had been admitted to the general medical floor during the same time-period but had received only “standard” therapy for COVID-19 (i.e., no ethanol treatment). Statistical analysis was performed using the T-Test and Fisher's Exact Test, with a statistical significance of p-value < 0.05.

5.3 Demographics

Ninety-one patients received one or more doses of nebulized ethanol, while two hundred twenty-five randomly selected “control” patients were identified. Of the ninety-one patients who received any ethanol treatment, eighty-one (89%) completed the three-day regimen. (*Note: The total number of patients who were offered but refused treatment with alcohol is not known.*)

5.4 Severity of hypoxemia

The severity of hypoxemia was assessed in all patients before receiving any COVID-19 treatment, at 96 h after the first treatment, and again at the time of discharge from the hospital, using the SFR (SpO₂/FiO₂ ratio; “normal” ≥ 4.57) [45–47].

5.5 Outcome metrics

The following data and clinical outcomes of the two groups were collected and compared:

1. Change in level of SFR from admission to discharge;
2. Need for transfer to ICU for progression of disease severity;
3. Need for intubation for invasive mechanical ventilation;
4. Inpatient mortality and survival;
5. The average length of stay (ALOS);
6. Discharge disposition: home, need for supplemental home oxygen, home health services, hospice, or post-hospitalization admission/transfer to another health-care facility, i.e., nursing home, skilled-nursing facility, rehabilitation center, or long-term acute care center.

5.6 Results

Eighty-one patients completed the three-day regimen (Ethanol Group), and were compared to the Control Group (225). Ten patients (11%) who initially gave informed consent to try inhaled ethanol treatment did not complete the three-dose regimen and were not included in the final data analysis. One was in the respiratory extremis prior to starting the first treatment and received an unknown quantity before requiring emergent intubation and immediate transfer to the ICU, and received no further ethanol treatments. This patient subsequently expired after a prolonged hospital stay on mechanical ventilation. The other nine (9.9%) did not complete the first treatment dose or refused the second dose due to a universally reported side effect of immediate mild coughing and / or burning sensation in the naso-oropharynx. Two of these nine patients (22.2%) later required transfer to ICU and intubation for disease progression, and both subsequently expired. Seven of the nine patients (77.8%) improved after prolonged hospital stays and were subsequently discharged from the hospital with home health or to a skilled nursing facility.

As shown in **Table 1**, average age of both groups was similar: 63.6 years (median 64; range 41–96) in the Ethanol Group, compared to 65.5 years (median 62; range 28–99) in the Control Group ($p = 0.50$). Gender distribution was also comparable between the two groups: 42% (34) females and 58% (47) males, 51.6% (116) females and 48.4% (109) males in the Control Group ($p = 0.15$). Average BMI (body mass index = kg/m^2) was similar: 35.3 (median 34), compared to 33.4 (median 34) in the Control Group ($p = 0.06$).

Likewise, the presence of one or more significant co-morbidities was similar in both groups, including diabetes mellitus, chronic obstructive pulmonary disease, drug-induced immunosuppression (i.e., chemotherapy for cancer), obesity, hypertension, end-stage renal disease, and autoimmune disease (i.e., rheumatoid arthritis): 92.5% (75) in the Ethanol Group, and 87.1% (196) in the Control Group, ($p = 0.22$). The average pre-treatment SFR was statistically *worse* ($p < 0.001$) in the Ethanol Group (2.86) compared to the Control Group (3.83).

Demographic	Ethanol group (n = 81)	Control group (n = 225)	p-value*
Average age (years)	63.6	65.5	0.50
Median; range	64; 41–96	62; 28–99	
Gender	M = 58% (47)	M = 48.4% (109)	0.15
M = male; F = female	F = 42% (34)	F = 51.6% (116)	
Average BMI**	35.3	33.4	0.06
Median	34.5	34	
Comorbidities ≥ 1***	92.6% (75)	87.1% (196)	0.22
Average Pre-treatment SFR****	2.86	3.83	<0.001
Range	2.65–3.07	3.33–3.93	

*Statistical significance: $p < 0.05$.
 **BMI = body mass index, kg/m^2 .
 ***Comorbidities include diabetes mellitus, chronic obstructive pulmonary disease, drug-induced immunosuppression (i.e. chemotherapy for cancer), obesity, hypertension, end-stage renal disease, and autoimmune disease (i.e. rheumatoid arthritis).
 ****SFR = $\text{SpO}_2/\text{FiO}_2$ Ratio (Example: “normal” SFR: $\text{SpO}_2 0.98/0.21 = 4.67$).

Table 1.
 Demographic data.

Table 2 shows the use of “standard” (non-ethanol) treatments in both groups were similar, with all patients having received one or more of the following drugs: remdesivir, tocilizumab, azithromycin, intravenous steroids (dexamethasone or methylprednisolone), and convalescent plasma. The most frequent in both groups were remdesivir and intravenous steroids, but no statistical difference was found between both groups for anyone “standard” treatment ($p = 0.07$ – 0.86).

Table 3 shows pre-treatment SFR, and average post-treatment SFRs for both groups. In the ethanol group, the average SFR at 96 h (2.89) compared to pre-treatment (2.86) was unremarkable. Notable, the average SFR at 96 h in the Control Group had *decreased* from 3.83 to 3.69, but not statistically significant from the Ethanol Group ($p = 0.21$). Although not quite statistically significant ($p = 0.06$), the Ethanol Group had considerable improvement (21.7%) from the average pre-treatment SFR

Medication*	Ethanol group (n = 81)	Control group (n = 225)	p-value**
Remdesivir	45.7% (37)	56.4% (127)	0.22
Tocilizumab	4.9% (4)	8.9% (20)	0.34
Convalescent Plasma	17.3% (14)	16.4% (37)	0.86
Intravenous Steroids***	55.6% (45)	70.2% (158)	0.26
Hydroxychloroquine****	6.2% (5)	53.3% (12)	0.78
Azithromycin	28.4% (23)	14.7% (33)	0.07

*All patients in both groups received vitamins C, D3, and zinc.
 **Statistical significance: $p < 0.05$; no statistical difference was found between the two groups.
 ***Dexamethasone or methylprednisolone.
 ****Removed from hospital “COVID-19 Formulary” in July 2020.

Table 2.
 “Standard” COVID-19 medications received.

Time of SFR [†]	EtOH group Average SFR (Range)	Control group Average SFR (Range)	p-value
Pre-treatment	2.86 (2.65–3.07)	3.83 (3.33–3.93)	<0.001
96 h post-treatment	2.89	3.69	0.21
Discharge from hospital	3.48 (3.28–3.68)	3.88 (3.87–3.89)	0.13
Δ pre-treatment versus 96 h	+1%	–3.7	0.23
Δ pre-treatment versus discharge	+21.7%	+1.3	0.06

[†]SFR = SpO₂/FiO₂ ratio; “normal” SFR: SpO₂ 0.98/0.21 = 4.67.

Table 3.
Pre- and post-treatment SPO₂/FIO₂ ratios.

(2.86) to discharge (3.48), compared to the Control Group which had a minor increase (1.3%) from the average pre-treatment SFR (3.83) to discharge (3.88).

Comparison of clinical outcomes is shown in **Table 4**. Progression (e.g., worsening) of COVID-19 disease requiring transfer to the intensive care unit (ICU) occurred less in the Ethanol Group compared to the Control Group: 8.6% (7), and 14.7% (33), respectively (p = 0.18), equating to a 41% less chance of requiring transfer to ICU for disease progression in the Ethanol Group. Intubation was necessary for all seven patients in the Ethanol Group who required transfer to ICU, compared to 82% (27) in

Clinical metric	EtOH group (n = 81)	Control group (n = 225)	p-value
Transfer to ICU	8.6% (7)*	14.7% (33)	0.18
Intubation	8.6% (7)	82% (27)	0.57
ALOS (days)	6.88	9.98	0.03
Median	5.5	8	
Range	4–27	6–33	
Inpatient overall mortality	7.4% (6)	17.8% (40)	0.03
Overall survival	92.6% (75)	82.2% (185)	0.03
ICU mortality	71.4% (5)	48.5% (16)	0.41
Home	81.4% (66)	40.9% (92)	<0.001
Home oxygen	45.7% (37)	64.4% (82)	0.15
Home health	34.6% (28)	28.9% (65)	0.40
DC to another facility**	6.2% (5)	38.2% (86)	<0.001
Hospice	4.9% (4)	3.1% (7)	0.49

*One patient developed hospital-acquired pneumonia and progressive shock due to *S. marcescens* on day 5. hospitalization; another required intubation for sudden cardiac arrest the day after 3rd EtOH treatment. **Facility = long-term acute care, nursing home, other skilled nursing, or rehabilitation. Abbreviations: ALOS = average length of inpatient stay; DC = discharge from hospital.

Table 4.
Clinical outcomes.

the Control Group but was not statistically significant ($p = 0.57$). Notably, one of the seven patients in the Ethanol Group who required transfer to ICU had developed progressive respiratory failure and sepsis due to hospital-acquired pneumonia (*Serratia marcescens*) on day five of admission (two days post-third ethanol treatment), requiring intubation and vasopressor support for shock, and subsequently expired in ICU. Another patient expired having required transfer to ICU after emergent intubation for sudden cardiac arrest the day following the third EtOH treatment, although having been stable pre-arrest with no worsening hypoxemia or hemodynamic instability.

ALOS was less in the Ethanol Group (6.88 days, median 5.5, range 4–27) versus the Control Group, (9.98, median 8, range 6–33) and was statistically significant ($p = 0.03$).

Inpatient mortality was also statistically less in the Ethanol Group (6) compared to the Control Group (40): 7.4% and 17.8%, respectively ($p = 0.03$), translating to a significantly improved survival in the Ethanol Group of 92.6% (75) compared to 82.2% (185) in the Control Group ($p = 0.03$). The mortality rates of patients who required transfer to ICU because of disease progression were not statistically different between the two groups ($p = 0.41$), although a larger percentage of patients in the Ethanol Group (71%; $n = 5$) died compared to the Control Group (48.5%; $n = 16$).

Note: Post-discharge mortality rate is not known at this time.

Interestingly, and statistically significant, 81.4% (66) in the Ethanol Group were able to be discharged to their homes compared to 40.9% (92) in the Control Group ($p < 0.001$), and only five (6.2%) in the Ethanol Group required discharge/transfer and admission to another healthcare facility for ongoing care (i.e. long-term acute care, nursing home, skilled nursing, or rehabilitation) compared to 38.2% (86) in the Control Group ($p < 0.001$). Four survivors (4.9%) in the Ethanol Group were discharged to hospice care, comparable to 7 (3.1%) in the Control Group ($p = 0.49$). The need for home health services post-discharge was similar: 34.6% (28) in the Ethanol Group, and 28.9% (65) in the Control Group ($p = 0.40$). Considerably fewer patients required supplemental home oxygen in the Ethanol Group (45.7%; $n = 37$) versus the Control Group (64.4%; $n = 82$), though not statistically significant ($p = 0.15$).

5.7 Discussion

The results of this study suggest a number of positive benefits of inhaled ethanol in the treatment of COVID-19 in non-ICU patients with acute hypoxemia. Statistically significant benefits included decreased ALOS, improved survival, and increased chance of discharge to home as opposed to requiring post-hospital treatment in long-term acute care, extended care facility (i.e., nursing home), or other skilled nursing facility (i.e. rehabilitation center, etc.). Other benefits included the decreased need for transfer to ICU due to disease progression, decreased need for intubation and decreased need for home oxygen. If such outcomes are confirmed in larger studies, the benefits to patients and healthcare systems worldwide would be incredible.

The science is sound as noted by other researchers [48, 49] regarding the potential use of inhaled ethanol as a treatment for COVID-19. Ethanol is rapidly absorbed in the respiratory tract and then transported via the circulatory system to other tissues. Nebulization into the nares (and mouth) has the benefit of direct deposition and contact with the virus in the upper and lower respiratory tissues, from which it can then circulate to other tissues where the virus has been shown to be present in autopsy findings [12], allowing ethanol to circumvent the “first pass” metabolism by alcohol dehydrogenase in the liver. The hypothesis is logical: direct deposition of ethanol

on respiratory tissues may inactivate the virus in the respiratory epithelium thereby inhibiting viral replication and thus decreasing the viral load—and the risk of the inflammatory response (i.e., cytokine storm) which is responsible for organ failure (i.e., ARDS, acute kidney injury, etc.). The clinical results in this study support the hypothesis.

Obviously, while ethanol is known to inactivate SARS-CoV-2 on skin surfaces, the amount needed to inactivate SARS-CoV-2 in the respiratory tract (and other human tissues) is not known. The dose in this regimen was weight-based (0.31 g/kg for females, and 0.33 g/kg for males), estimated to produce a blood alcohol concentration of less than 0.08 mg %. Five ounces or 148 ml of wine is 12% EtOH by volume and contains about 14 g of EtOH, or 0.095 g/ml, whereas 95% EtOH contains 0.75 g/ml. Thus, in this regimen, for example, a 70 kg male would receive a nebulized dose of EtOH of about 23 cc of EtOH or about 17 g of EtOH—3 g more than that in one glass of wine [50]. (Of note, serum EtOH levels were not detectable 1-h post nebulization treatments.) While the dosing of EtOH in this study showed benefits, the optimal dosing and method of administration need further study. Plausibly, different dosing, frequency, and duration of therapy may prove even more beneficial, and it may prove more beneficial if initiated earlier, or within a specified time period of the initial onset of COVID-19 symptoms. (*Note: In this study, the duration of symptoms before seeking treatment is not available.*)

This regimen proved safe and was well tolerated in the great majority (89%) of patients who were known to have been offered the treatment. No severe adverse or untoward events were reported or discovered on review of the medical records. No patient reported a feeling of intoxication, and none became noticeably intoxicated during observance by medical personnel. All patients had onset of a temporary minor cough and/or burning sensation in the nasopharynx and throat, which lasted about 2 min, but these were the reasons given by those who initially gave consent to try the nebulized EtOH but refused subsequent treatments. No patient who received any or all of the three-day regimen was found to have physical evidence of naso-oropharyngeal mucosal inflammation. Likely, dilution of the nebulized weight-based dose with sterile water by one-half is beneficial in reducing the mild cough and/or burning sensation.

6. Where we currently stand

The ability of COVID-19 to cause widespread morbidity, mortality, and profound stress on healthcare systems worldwide has been harrowing. Not only increased costs of healthcare due to COVID-19 on the world economy, but this pandemic has had major negative effects on the entire well-being of society—previously unseen for many decades. No other disease has affected the current generation of medical professionals (or the world) like COVID-19. While other diseases exist for which there is no effective treatment, the mere volume of cases of COVID-19 has made its indelible mark.

From its beginning, the entire world felt the urgent need to find an effective treatment for this novel virus, and the discovery and development of new treatments for SARS-CoV-2 have been remarkable. Published data suggest definite benefits with a variety of medications including antivirals, monoclonal antibodies [51, 52], and high-titer convalescent plasma [51]. Based on COVID-19 pathogenesis, therapies that attack the virus itself are more likely to work *early* in the course of infection, whereas

treatments that restrain the immune response (*cytokine storm*) may have more influence later in the disease [13, 14, 53]. Unfortunately, these medications are costly, and the prescriber of such treatments as the antiviral nirmatrelvir-ritonavir must also consider the potential for significant adverse reactions and interactions with a wide variety of other common medications that are highly dependent on *CYP3A* for clearance and for which elevated concentrations are associated with serious and or life-threatening reactions [54].

Obviously, as new COVID-19 variants arise, current therapy guidelines will need to be amended. For example, bebtelovimab has activity against Omicron *BA.2*, but there is a paucity of good clinical data showing an associated reduction in COVID-19 mortality [55, 56]. Monoclonal antibody therapies like sotrovimab, casirivimab-imdevimab, and bamlanivimab-etesevimab have shown a reduction in death and the need for hospitalization in outpatients who have a non-severe disease but at risk for progression [57, 58]. However, these formulations are not appropriate for use in areas where COVID-19 infection is most probably due to SARS-CoV-2 variants that are not susceptible (i.e., Omicron, subvariants, etc.) [59].

Beyond question, prevention of this devastating disease is of utmost importance, and vaccines are very promising. Several COVID-19 vaccines are available globally, but unfortunately, there are areas and populations of people who do not have access to vaccinations [60, 61]. In addition, as with current therapeutic treatments (e.g., anti-virals, monoclonal antibodies, etc.), the existing and future effectiveness of vaccines is a genuine concern given the recurrent mutations already witnessed in the SARS-CoV-2 genome. However, while vaccinations are a mainstay of prevention, *there will always remain a need for efficacious treatment for those who become acutely infected.*

6.1 Final comments

The results of this novel study should not be ignored. Not to downplay the importance of new treatments and vaccines which have been developed since the start of the COVID-19 Pandemic, unfortunately for the foreseeable future as new variants arise, the proclivity of SARS-CoV-2 to mutate and cause widespread infection and wreckage to the health of individuals and society alike remains a global health concern. The world needs an effective, safe, widely-available, and inexpensive treatment for COVID-19—and inhaled ethanol may well be that needed treatment. Extensive studies are needed to confirm and better define the use of inhaled ethanol in combatting this disease—and other susceptible respiratory viruses (i.e. influenza, etc.). If confirmed, inhaled ethanol has the potential to prevent morbidity, and save lives, healthcare resources, and economies the world over. Extensive research is needed to confirm the findings herein, but the results must not be unheeded.²


² Addendum: Since this writing, data that suggests the benefits of inhaled ethanol in the treatment of COVID-19 has been published, and supports the findings in this study [62].

Author details

Steven W. Stogner
Hattiesburg Clinic Pulmonary Medicine, Hattiesburg, MS, USA

*Address all correspondence to: sstogner@forrestgeneral.com

IntechOpen

© 2023 The Author(s). Licensee IntechOpen. This chapter is distributed under the terms of the Creative Commons Attribution License (<http://creativecommons.org/licenses/by/3.0>), which permits unrestricted use, distribution, and reproduction in any medium, provided the original work is properly cited. 

References

- [1] Dong E, Ratcliff J, Goyea TD, Katz A, Lau R, Ng TK, et al. The Johns Hopkins University Center for Systems Science and Engineering COVID-19 Dashboard: data collection process, challenges faced, and lessons learned. *The Lancet Infectious Diseases*. Dec 2022;**22**(12):e370-e376. DOI: 10.1016/S1473-3099(22)00434-0. Epub 2022 Aug 31. Erratum in: *Lancet Infect Dis*. 2022 Nov;**22**(11):e310. PMID: 36057267; PMCID: PMC9432867
- [2] Viboud C, Lessler J. The 1918 influenza pandemic: Looking back, looking forward. *American Journal of Epidemiology*. 2018;**187**(12):2493-2497. DOI: 10.1093/aje/kwy207
- [3] COVID-19 surpasses 1918 flu as deadliest pandemic in U.S. history. *National Geographic*. September 21, 2021
- [4] Cucinotta D, Vanelli M. WHO declares COVID-19 a pandemic. *Acta Biomedica*. 2020;**91**(1):157-160. DOI: 10.23750/abm.v91i1.9397
- [5] Rockwood K. Rationing care in COVID-19: If we must do it, can we do better? *Age and Ageing*. 2021;**50**(1):3-6. DOI: 10.1093/ageing/afaa202
- [6] Amanullah S, Ramesh SR. The impact of COVID-19 on physician burnout globally: A review. *Healthcare (Basel)*. 2020;**8**(4):421. DOI: 10.3390/healthcare8040421
- [7] Agyeman A et al. Smell and taste dysfunction in patients with COVID-19: A systematic review and meta-analysis. *Mayo Clinic Proceedings*. 2020;**95**(8):1621-1631
- [8] Kompaniyets L, et al. Underlying medical conditions and severe illness among 540,667 adults hospitalized with COVID-19, March 2020–March 2021. *Preventing Chronic Disease*. Available from: <https://www.cdc.gov/pcd/issues/2021/21>
- [9] Yao H et al. Molecular architecture of the SARS-CoV-2 virus. *Cell*. 2020;**183**(3):730-738.e13. DOI: 10.1016/j.cell.2020.09.018
- [10] Sungnak W, Huang N, Becavin C, et al. SARS-CoV-2 entry factors are highly expressed in nasal epithelial cells together with innate immune genes. *Nature Medicine*. 2020;**26**:681-687. DOI: 10.1038/s41591-020-0868-6
- [11] Severe acute respiratory syndrome-related coronavirus: classifying 2019-nCoV and naming it SARS-CoV-2. *Coronaviridae Study Group of the International Committee on Taxonomy of Viruses*. *Nature Microbiology*. 2020;**5**(4):536
- [12] Polak SB, Van Gool IC, Cohen D, et al. A systematic review of pathological findings in COVID-19: a pathophysiological timeline and possible mechanisms of disease progression. *Modern Pathology*. 2020;**33**:2128-2138. DOI: 10.1038/s41379-020-0603-3
- [13] Singh E et al. Management of COVID-19-induced cytokine storm by Keap1-Nrf2 system: a review. *Inflammopharmacology*. 2021;**29**(5):1347-1355. DOI: 10.1007/s10787-021-00860-5
- [14] Mousavizadeh L, Ghasemi S. Genotype and phenotype of COVID-19: Their roles in pathogenesis. *Journal of Microbiology, Immunology, and Infection*. 2021;**54**(2):159-163. DOI: 10.1016/j.jmii.2020.03.022

- [15] Alnima T, Mulder MMG, van Bussel BCT, Ten Cate H. COVID-19 Coagulopathy: From Pathogenesis to Treatment. *Acta Haematologica*. 2022;**145**(3):282-296. DOI: 10.1159/000522498
- [16] Kratzel A et al. Efficient inactivation of SARS-CoV-2 by WHO-recommended hand rub formulations and alcohols. *bioRxiv*. 2020. DOI: 10.1101/2020.03.10.986711
- [17] Meyers C et al. Ethanol and isopropanol inactivation of human coronavirus on hard surfaces. *The Journal of Hospital Infection*. 2021;**107**:45-49. DOI: 10.1016/j.jhin.2020.09.026
- [18] Kampf G. Efficacy of ethanol against viruses in hand disinfection. *Journal of Hospital Infection*. 2018;**98**(4):331-338
- [19] Gold NA, Mirza TM, Avva U. Alcohol Sanitizer. [Updated 2022 Jun 21]. In: StatPearls [Internet]. Treasure Island (FL): StatPearls Publishing; 2022. Available from: <https://www.ncbi.nlm.nih.gov/books/NBK513254>
- [20] Singh D, Joshi K, Samuel A, Patra J, Mahindroo N. Alcohol-based hand sanitizers as first line of defense against SARS-CoV-2: a review of biology, chemistry and formulations. *Epidemiology and Infection*. 2020;**(148)**:e229. DOI: 10.1017/S0950268820002319
- [21] Sauerbrei A. Bactericidal and viricidal activity of ethanol and povidone-iodine. *Microbiology*. 2020;**9**(9):e1097. DOI: 10.1002/mbo3.1097
- [22] Siddhartha A et al. Viricidal activity of World Health Organization-recommended formulations against enveloped viruses, including Zika, Ebola, and emerging coronaviruses. *The Journal of Infectious Diseases*. 2017;**215**:902-906
- [23] Barceloux DG et al. American Academy of Clinical Toxicology Ad Hoc Committee on the Treatment Guidelines for Methanol Poisoning. American Academy of Clinical Toxicology practice guidelines on the treatment of methanol poisoning. *Journal of Toxicology. Clinical Toxicology*. 2002;**40**(4):415-446. DOI: 10.1081/clt-120006745
- [24] Gootnick A, Lipson HI, Turbin J. Inhalation of ethyl alcohol for pulmonary edema. *New England Journal of Medicine*. 1951;**245**:842-843
- [25] Luisada A, Ruth W, Goldmann M. Alcohol Vapor by Inhalation in the Treatment of Acute Pulmonary Edema. *Circulation*. 1952;**5**:363-369. DOI: 10.1161/01.CIR.5.3.363
- [26] Zhang P et al. Inhalation of alcohol vapor driven by oxygen is a useful therapeutic method for postoperative alcohol withdrawal syndrome in a patient with esophageal cancer: a case report. *Alcohol and Alcoholism*. 2011;**46**(4):424-426. DOI: 10.1093/alcalc/agr037
- [27] Dillard R et al. Ethanol infusion for alcohol withdrawal prophylaxis does not cause intoxication. *The Southwest Respiratory and Critical Care Chronicles*. 2016;**4**(16):11-18
- [28] Takahashi G, Endo S. Improvement of acute respiratory distress syndrome with ethyl alcohol infusion into the airway: A case report. *Pulmonary and Respiratory Medicine*. 2018;**8**:464. DOI: 10.4172/2161-105X.1000464
- [29] Mcclenahan JB, Mussenden R, Ohlsen JD. Effect of ethanol on surfactant of ventilated lungs. *Journal of Applied Physiology*. 1969;**27**(1). DOI: 10.1152/jappl.1969.27.1.90

- [30] Leng L et al. Pathological features of COVID-19-associated lung injury: a preliminary proteomics report based on clinical samples. *Signal Transduction and Targeted Therapy*. 2020;**5**:240. DOI: 10.1038/s41392-020-00355-9
- [31] Mörs K et al. Ethanol decreases inflammatory response in human lung epithelial cells by inhibiting the canonical NF- κ B-pathway. *Cellular Physiology and Biochemistry*. 2017;**43**:17-30. DOI: 10.1159/000480313
- [32] Elsoukkary SS et al. Autopsy findings in 32 patients with COVID-19: A single-institution experience. *Pathobiology*. 2021;**88**(1):56-68. DOI: 10.1159/000511325
- [33] Iba T et al. The unique characteristics of COVID-19 coagulopathy. *Critical Care*. 2020;**24**(1):360. DOI: 10.1186/s13054-020-03077-0
- [34] Tabengwa EM et al. Ethanol-induced up-regulation of candidate plasminogen receptor annexin II in cultured human endothelial cells. *Alcoholism, Clinical and Experimental Research*. 2000;**24**(6):754-761
- [35] Centers for Disease Control and Prevention (CDC). Alcohol and Public Health: Alcohol-Related Disease Impact (ARDI); 2020. Available from: <https://nccd.cdc.gov>.
- [36] Simet SM, Sisson JH. Alcohol's Effects on Lung Health and Immunity. *Alcohol Research: Current Reviews*. 2015;**37**(2):199-208
- [37] Goral J, Karavitis J, Kovacs EJ. Exposure-dependent effects of ethanol on the innate immune system. *Alcohol*. 2008;**42**(4):237-247. DOI: 10.1016/j.alcohol.2008.02.003
- [38] Sarkar D et al. Alcohol and the immune system. *Alcohol Research: Current Reviews*. 2015;**37**(2):153-155
- [39] Watzl B, Bub A, Briviba K, Rechkemmer G. Acute intake of moderate amounts of red wine or alcohol has no effect on the immune system of healthy men. *European Journal of Nutrition*. 2002;**41**(6):264-270. DOI: 10.1007/s00394-002-0384-0
- [40] Jerrells TR. Immunodeficiency Associated with Ethanol Abuse. In: Friedman H, Specter S, Klein TW, editors. *Drugs of Abuse, Immunity, and Immunodeficiency, Advances in Experimental Medicine and Biology*. Vol. 288. Boston, MA: Springer; 1991. DOI: 10.1007/978-1-4684-5925-8_26
- [41] MacLean RR, Valentine GW, Jatlow PI, Sofuoglu M. Inhalation of alcohol vapor: Measurement and implications. *Alcoholism, Clinical and Experimental Research*. 2017;**41**(2):238-250. DOI: 10.1111/acer.13291
- [42] Valentine GW et al. The effects of alcohol-containing e-cigarettes on young adult smokers. *Drug and Alcohol Dependence*. 2016;**159**:272-276. DOI: 10.1016/j.drugalcdep.2015.12.011
- [43] Žuškin E, Bouhuys A, Šari M. Lung function changes by ethanol. *Frontiers in Immunology*. 1981. DOI: 10.1111/j.1365-2222.1981.tb01590.x
- [44] Tsumoru Shintake (2020). "Possibility of Disinfection of SARS-CoV-2 (COVID-19) in Human Respiratory Tract by controlled Ethanol Vapor Inhalation. Available from: <https://arxiv.org/abs/2003.12444> (Cornell University).
- [45] Boyle AJ, Sweeney RM, McAuley DF. Pharmacological treatments in ARDS; a state-of-the-art update. *BMC Medicine*. 2013;**11**:166. DOI: 10.1186/1741-7015-11-166
- [46] Festic E, Bansal V, Kor DJ, Gajic O. US Critical Illness and Injury Trials

Group: Lung Injury Prevention Study Investigators (USCIITG–LIPS). SpO₂/FiO₂ ratio on hospital admission is an indicator of early acute respiratory distress syndrome development among patients at risk. *Journal of Intensive Care Medicine*. 2015;**30**(4):209-216. DOI: 10.1177/0885066613516411

[47] Rice TW et al. National Institutes of Health, National Heart, Lung, and Blood Institute ARDS Network. Comparison of the SpO₂/FIO₂ ratio and the PaO₂/FIO₂ ratio in patients with acute lung injury or ARDS. *Chest*. 2007;**132**(2):410-417

[48] Salvatori P. The rationale of ethanol inhalation for disinfection of the respiratory tract in SARS- CoV-2-positive asymptomatic subjects. *The Pan African Medical Journal*. 2021;**40**:201. DOI: 10.11604/pamj.2021.40.201.31211

[49] Amoushahi A, Padmos A. A Suggestion on Ethanol Therapy in COVID-19? Available from: <https://www.ecronicon.com/ecan/pdf/ECAN-06-00229.pdf>

[50] Campbell L, Wilson HK. Blood alcohol concentrations following the inhalation of ethanol vapor under controlled conditions. *Journal of the Forensic Science Society*. 1986;**26**(2):129-135. DOI: 10.1016/S0015-7368(86)72458-4

[51] Infectious Diseases Society of America Guidelines on the Treatment and Management of Patients with COVID-19. Available from: <https://www.idsociety.org/practice-guidelines-and-management>.

[52] WHO Solidarity Trial Consortium, Pan H, Peto R, et al. Repurposed antiviral drugs for Covid-19—Interim WHO solidarity trial results. *The New England Journal of Medicine*. 2021;**384**:497

[53] Libster R et al. Early high-titer plasma therapy to prevent severe Covid-19 in older adults. *The New England Journal of Medicine*. 2021;**384**(7):610

[54] US FDA. Remdesivir letter of EUA. Available from: <https://www.fda.gov/media>

[55] National Institutes of Health. The COVID-19 Treatment Guidelines Panel's statement on potential drug-drug interactions between ritonavir-boosted nirmatrelvir (Paxlovid®) and concomitant medications. Available from: <https://www.covid19treatmentguidelines.nih.gov/therapies/statement-on-paxlovid-drug-drug-interactions>

[56] US Food and Drug Administration. Fact sheet for healthcare providers: Emergency Use Authorization for bebtelovimab. Available from: <https://www.fda.gov/media/156152>.

[57] O'Brien MP et al. Effect of Subcutaneous Casirivimab and Imdevimab Antibody Combination vs Placebo on Development of Symptomatic COVID-19 in Early Asymptomatic SARS-CoV-2 Infection: A Randomized Clinical Trial. *JAMA*. 2022;**327**(5):432

[58] US Food and Drug Administration. Coronavirus (COVID-19) update: FDA limits use of certain monoclonal antibodies to treat COVID-19 due to the Omicron variant. January 2022. Available from: <https://www.fda.gov/news-events/press-announcements/coronavirus-covid-19-update-fda-limits-use-certain-monoclonal-antibodies-treat-covid-19-due-omicron>.

[59] National Institutes of Health. COVID-19 treatment guidelines: What's new in the guidelines. Available from: <https://www.covid19treatmentguidelines.nih.gov/about-the-guidelines/whats-new>.

[60] Malik JA et al. The SARS-CoV-2 mutations versus vaccine effectiveness: New opportunities to new challenges. DOI: 10.1016/j.jjiph.2021.12.014

[61] WHO. Draft landscape of COVID-19 candidate vaccines. Available from: <https://www.who.int/publications/m/item/draft-landscape-of-covid-19-candidate-vaccine>

[62] Amoushahi A, Moazam E, Tabatabaei A, et al. (December 05, 2022) Efficacy and Safety of Inhalation of Nebulized Ethanol in COVID-19 Treatment: A Randomized Clinical Trial. *Cureus* 14(12): e32218. doi:10.7759/cureus.32218

Theoretical Bases for the Disinfection of the SARS-CoV-2-Contaminated Airways by Means of Ethanol Inhalation

Pietro Salvatori

Abstract

Ethyl alcohol, or ethanol (EtOH), is a linear alkyl chain alcohol, whose condensed structural formula is $\text{CH}_3\text{CH}_2\text{OH}$. Besides the common industrial and recreational uses (spirits, cosmetics, fuelling, etc.), EtOH is considered a medicament and listed in the European and US Pharmacopeias. Medically, EtOH is mainly employed as an antidote in methanol and ethylene glycol poisoning, as an excipient in many medications, as a sclerosant agent, and as a powerful disinfectant. Less recently, EtOH was shown to be both effective and safe in the treatment of pulmonary edema and cough. This chapter deals with EtOH use in SARS-CoV-2 infection and COVID-19 treatments.

Keywords: SARS-CoV-2, COVID-19, ethanol, inhalation, public health

1. Introduction

This section resumes and adequately updates as of September 4, 2022 my published article [1].

The SARS-CoV-2 outbreak has hit the global community and we are experiencing the third wave after the first phase—and likely, a fourth one—as well as more aggressive variants surge (Delta and Epsilon, Omicron, Centaurus). To this day, no specific therapy has been identified as effective. While mass immunization campaigns take a long time, and pose questions about their effectiveness against new variants and long-lasting protection, they are very likely to dramatically improve disease control. As consequence, attempts to understand the cold chain and potential active eradication of the virus become of the highest significance and the emphasis on prevention over pandemic control grows. In fact, the main objective still to be achieved for the control of any contagious disease is the individuation and—possibly—treatment of spreading subjects. According to this, research has been done on conjunctival cells, upper respiratory tract goblet cells, type 2 pneumocytes, and enterocytes as the main targets of the virus-binding receptors. Actually, epithelial cells of the nasal cavity and lower respiratory tract, including alveolar cells, are associated with SARS-CoV-2

entry factors, mainly angiotensin-converting enzyme 2 (ACE2) receptors [2] and therefore, COVID-19 infection occurs initially in the epithelial layer of the upper respiratory tract, followed by transfer to the lower respiratory tract [3]. According to Madas et al. [4], pneumonia may be prevented by stopping or significantly limiting the transit of viruses into the acinar airways during the gap between the start of early symptoms and any potential clinical worsening. As a result, even non-specific therapies like disinfecting the mouth, nose, and throat successfully keep the viral load in the upper airways low enough to stop or delay the disease's progression. A very comprehensive study [5] on Wuhan's population (about 10,000,000 individuals) demonstrates that, following a period of isolation, the incidence of symptomatic individuals was reduced to 0.00303%, providing an indication of the success of containment. Many of these infected individuals do not have any clinical manifestations of the disease; they are also known as "asymptomatic positives" or PAS (healthy carriers?). Observations show that PASs have a noticeable SARS-CoV-2 viral load, and this surely draws attention to their contribution to the epidemic's progression. Among a group of students, Nelson et al. [6] recently discovered that, in said group, contacts of people who tested positive returned positive at rates of 10.4 and 4.8% after 3 and 9 days, respectively. One of the latest researches by Atripaldi et al. [7] discovered that asymptomatic patients had a noticeable SARS-CoV-2 viral load. This highlighted the importance of asymptomatic (and pre-symptomatic) individuals in the development of the epidemic.

There still are no established criteria for identifying asymptomatic patients who will spread the infection to other subjects; thus, all of them should be regarded as being suitable for disinfection. Thus, early detection and potential treatment of asymptomatic positive people are of major importance. The goal is to terminate the transmission chain and reduce or even end confinement time (and the related financial, social, and psychological costs), and promptly reintroduce recovered patients back in society. The 14-day quarantine is undoubtedly the only option that now is currently given to asymptomatic positive patients. It may be deduced from Liu et al.'s [8] study of SARS-CoV-2 contamination in quarantine rooms that unless the patient lives alone, or each person present in the household has their own private rooms, the strategy is likely to be unsuccessful. The objective is to highlight the extent of the issue, illustrate available solutions, and investigate the effectiveness and toxicological aspects that would support the use of inhaled ethanol (or ethyl alcohol) for airway disinfection in SARS-CoV-2-infected patients who are asymptomatic. For research publications published up to July 29, 2021, databases such as MEDLINE, Embase, Europe PubMed Central, medRxiv, and bioRxiv, as well as the gray literature, have been examined. Key findings were covered in our case reports (with five or more participants), cohort studies, randomized controlled trials, and records of trial registration:

- epidemiological data highlighting the extent of the problem;
- ongoing efforts in disinfection of SARS-CoV-2-positive asymptomatic patients;
- the ability of ethanol to eliminate or inactivate viruses, and SARS-CoV-2 more specifically.
- potentially positive effects of ethanol on the airways.

- ethanol's both local and general harmful effects when ingested or inhaled.
- data allowing the identification of the therapeutic window for ethanol inhalation.

The explanation for the suggested novel technique was supported (or rejected) based on reliable data.

2. Results

2.1 Extension of the problem

As of now (September 4, 2022), the world's active cases are 610,144,519 and total deaths reached 6,503,374 [9]. Thus, lethality accounts for 1.07%. Between 17 and 20% of positives are asymptomatic (healthy carriers) [10]. Within 8 days (mean), 43% of asymptomatic positive patients develop symptoms (of any kind) [11]. As even more nations implement some form of quarantine laws, the effects on the social and economic sectors are extremely detrimental. The mean viral load elimination time for the upper and lower respiratory tracts, respectively is 14 days and 17 days, according to a fairly recent meta-analysis [12]. Interestingly, no live virus has ever been found 9 days after the sickness first appears. Patients who were asymptomatic and those who had symptoms were compared, and the results for the elimination time between the two groups were inconsistent. Among health workers, Bongiovanni [13] reports an average viral load elimination time of 22 days, which may be explained by their propensity to receive a higher viral load in their work environment, compared to the average population.

2.2 Current efforts

Metformin, ivermectin, and fluvoxamine have been studied in less severe COVID-19 infections [14].

Protease inhibitors are currently used in high-risk patients [15].

Highly specialized medications such as monoclonal and polyclonal antibodies are now being studied and used, but their high cost and possibility for effectiveness loss caused by the spread of new variations severely restrict their potential advantages [16].

It is necessary to investigate the potential of nonspecific medications in the absence of particular, well-established therapies for respiratory disinfection. Guenezan et al. [17] made an effort to disinfect positive but asymptomatic individuals. Povidone iodine mouthwash and nasal spray both significantly increased viral titer in a single small-randomized clinical study, although they had no impact on the lower respiratory tract.

According to a recent randomized clinical trial [18], medical professionals could significantly reduce their risk of contracting COVID-19 by using a nasal spray solution composed of dimethyl sulfoxide and ethanol.

2.3 Ethanol efficiency

Ethyl alcohol or ethanol is widely used in disinfection procedures. Additionally, a substantial amount of integrated evidence shows that ethanol does indeed have

antiviral properties, which may be related to the solvent's effects on lipids (pericapsid) and the denaturation of proteins (capsid) [19]. The temperature and phase in which the pericapsid is located (which derives from the cell membrane of the infected host) affect the outcome. The effectiveness of ethanol in an aqueous solution of 35.2% by weight (equivalent to 44% by volume) is the highest at about 50°C (crystalline phase) and diminished or rendered ineffective at about 25°C (gel phase) [20]. It is possible to assume an intermediate impact at human body temperature. Human coronaviruses, including Severe Acute Respiratory Syndrome Coronavirus (SARS), Middle East Respiratory Syndrome (MERS), and Human Endemic Coronavirus, have been demonstrated to be significantly affected by ethanol where, on surfaces such as plastic and glass, these viruses can survive for days. Disinfectants, such as EtOH, have been demonstrated to diminish the coronavirus's infectiousness in a short amount of time. The said demonstrations showed a 62–71% effectiveness. Thankfully, SARS-CoV-2 is an enveloped virus that is extremely sensitive to ethanol; current experimental data show that an ethanol concentration of 30% v/v is able to inactivate SARS-CoV-2 in 30 seconds [21].

- The quantity of alcohol required to reduce the SARS-CoV-2 viral load affecting the lungs was determined by Manning et al. [22].
- According to estimates, COVID-19 has a viral load of 20 million copies per milliliter of lung tissue.
- Adult lung tissue contains 120×10^9 (billions) (rounded to 200×10^9 (billions)) virus particles, many of which are infected cells.
- It is estimated that 10×10^6 million molecules of ethanol are required to disinfect or render a virus particle inactive.
- Ethanol has a density of around 0.8 g/ml = 800 g/l = 800,000 mg/l = 80,000 mg/dl = 800 mg/ml. Its molar mass is 46 g/mol. A mole contains $N = 6.02252 \times 10^{23}$ molecules, which is equal to Avogadro's number.
- To remove 200×10^9 (billions) of viruses, $(10 \times 10^6) \times (200 \times 10^9) = 2 \times 10^{18}$ molecules of ethanol will be needed (molar mass = 46 g/mol).
- $(2 \times 10^{18} \text{ EtOH}) / (N \times 10^{23} \text{ EtOH/mol}) = 3.3 \times 10^{-6}$ moles of ethanol
- $(3.3 \times 10^{-6}) \times (46 \text{ g/mol}) = 0.000153 \text{ gr} = 153 \text{ }\mu\text{g}$ of ethanol or 191.25 μL

2.4 Effects of ethanol on respiratory cells and microbiota

1. The relationship between alcohol exposure time and dose and the effect it has on respiratory hairy cells is bimodal. Sisson [23] demonstrated (*in vitro*) that ethanol (10 mM concentration = 0.46 mg/ml) caused a 40% increase in beat frequency (6 Hz to 8.5 Hz) after only 10 minutes of treatment. A mechanism that is dependent on nitrogen oxide is responsible for this result. However, the same experiment performed with ethanol at a greater concentration (1 M = 46 mg/ml) resulted in a decrease in the beat frequency, demonstrating that ethanol could have a harmful impact by desensitizing ciliary motility, which makes it

stimulation-resistant (a process known as Alcohol-Induced Ciliary Dysfunction mediated by oxidative stress) [24].

2. Up to the 1950s, inhalations of EtOH were proven to be both safe and effective for treating coughs and pulmonary edema [25–28].
3. Up to 9 mg of ethanol per actuation is frequently used as an excipient in inhalation treatment for asthma and chronic obstructive pulmonary disease [29].

It is possible that EtOH might have a harmful effect on the respiratory microbiome, but there is no solid evidence of this in the medical literature. In contrast, some helpful remarks could emerge from this. As a matter of fact, Sulaiman et al. [30] discovered that a poor clinical outcome was connected to an enrichment of the lower respiratory tract's microbiota with an oral commensal (*Mycoplasma salivarium*) and an enhanced SARS-CoV-2 virus load in a group of patients intubated with COVID-19. Intensive care patients with SARS-CoV-2 showed full depletion of *Bifidobacterium* and *Clostridium*, according to Rueca et al.'s [31] study of the nasal/oropharyngeal microbial flora.

2.5 Ethanol toxicity

The toxicity of acute inhalation of ethanol has mostly been researched in four real-world scenarios. From a toxicological perspective, there is a significant difference between ingested and inhaled ethanol, since the latter bypasses the first necessary metabolic step of ingested ethanol and instead travels straight to the left ventricle of the heart and the brain [32].

Surgical disinfection of the hands. Bessonneau [33] has demonstrated that the cumulative dose of ethanol inhaled in 90 seconds while surgically disinfecting hands with a gel containing ethanol at a concentration of 700 g/l is 328.9 mg. The blood alcohol content would be 203.9 mg, giving blood alcohol content (BAC) of 40.6 mg/L because the inhalation/absorption rate (i.e., the amount of ethanol that passes from the alveoli to the bloodstream) is 62%. Hypothetically, even if ethanol absorption was to happen instantly (rather than during 90 seconds), the blood alcohol level would still be well below the limit that is deemed toxic (500 mg/L in Italy and 800 mg/L in the majority of the United States). Healthcare workers may disinfect their hands up to 30 times per day [34], which results in a daily dose of inhaled ethanol of 9.86 grams, depending on the frequency of surgical hand disinfection associated with appropriate care activities with a high risk of contamination (for instance, by washing incontinent patients).

Liquid contained in some “e-cigarettes” (electronic cigarettes) may contain ethanol in various proportions. The usage of electronic cigarettes containing 23.5% ethanol and utilized with various suction mechanisms is reported in the study by More [35] along with statistics on ethanol absorption. The said statistics showed that the absorption of ethanol never exceeded 0.85 mg/l. The calculated blood alcohol content never went over 0.85 mg/l. The estimated blood alcohol level by projecting to triple or quadruple concentrations should be $0.85 \text{ mg/l} \times 3 = 2.55 \text{ mg/L}$ in the first hypothesis and 3.4 mg/L in the second, which are both substantially below the toxic limit.

Patients with COVID-19-pneumonia are now being researched to see if ethanol inhalation could be a viable therapy option [36].

Additionally, a phase II clinical trial has been filed to assess the effectiveness and safety of inhaled ethanol in the early stage of COVID-19 therapy. The trial is now actively recruiting new participants [37, 38].

In rodents breathing, 65% v/v ethanol for 15 min every 8 hours (3 times a day), for five consecutive days (flow rate: 2 L/minute), Castro-Balado et al. [38] examined the mucosal or structural damages to EtOH in the lung, trachea, and esophagus. The calculated absorbed dosage was 1.2 g/kg/day. Under the same conditions, this dosage in humans would be equivalent to 151 g per day. Notably, neither the treated animals nor the controls' histology samples showed any signs of damage.

Numerous studies suggest that industrial exposure is not a problem in reproductive medicine (Irvine) [39] nor in oncology (Bevan) [40], despite the toxicity of chronic ethanol inhalation. In Bevan's [40] research, the occupational exposure limit (OEL) for the United Kingdom was examined (1000 ppm of ethanol = 1910 mg/m³ over an 8-hour shift). It was also determined that ingesting 10 g of ethanol (roughly one glass of alcohol) per day would be perfectly in line with the occupational exposure limit (OEL). These numbers are in perfect agreement with Bessonneau's [33] and Boyce's [34] reports.

Chronic ethanol use is not the same as chronic ethanol abuse, which can result in lung damage (alveolar macrophage dysfunction, increased susceptibility to bacterial pneumonia, and tuberculosis) [41].

The greatest amount of ethanol that can be instantly administered to a healthy adult is 2.5 g, given that the blood volume is roughly 5 L and the maximum permissible blood level of ethanol is 500 mg/L.

Elimination of ethanol occurs at a rate of 120 to 300 mg/L/hour [42]. Alcohol dehydrogenase breaks down 95% of EtOH that has been consumed (or breathed), while the remaining 5% is removed—unaltered—by exhaled air, urine, perspiration, saliva, and tears.

2.6 Inhaled ethanol therapeutic window

On this subject, no focused research was found.

The highest permitted ethanol dose or concentration, however, will be determined using previous data from regulatory reports [40].

Each type of inhalation treatment is potentially more effective compared to any other mode of delivery for treating airway diseases [22].

3. Discussion

3.1 Dimension of the problem

The SARS-CoV-2 outbreak pattern exhibits a rather steady trend combined with local upsurges, most likely as result of variant selection and superspreader events [43]. In addition to the immeasurable worth of the suffering and lives lost (4,203,776 to date), the world's lost economic output has tremendously increased to roughly 3.94 trillion U.S. Dollars [44]. These findings logically support the intensive treatment of positive asymptomatic people in an effort to limit or, ideally, stop the spread of the infection.

3.2 Current efforts

In a study evaluating metformin, ivermectin, and fluvoxamine, none of the drugs were effective in avoiding hypoxemia, ER visits, hospital stays, or deaths related to COVID-19 [14].

Protease inhibitors seem to have the potential to cause a rebound infection and appear to be ineffective against some SARS-CoV-2 strains [45, 46].

There is currently no published research on the regular use of monoclonal antibodies to treat SARS-CoV-2 positive and asymptomatic individuals. Furthermore, their high price and the probable loss of efficacy owing to variants seem to substantially restrict any benefit.

In the pharynx and oral cavity, povidone-iodine [17] has demonstrated excellent efficiency in lowering the viral titer. Povidone-iodine gargles, however, does not reach the lower respiratory tract, which is a notable limitation. However, as it focuses on the management of a crucial stage in the chain of viral transmission, this work deserves special attention. Of course, inhaling ethanol removes the previously mentioned limitation.

Actually, the experience of Hosseinzadeh [18] has shown that ethanol (together with dimethyl sulfoxide) can be delivered as a nasal spray in a safe and efficient way. In this randomized clinical trial involving volunteer healthcare providers without a history of SARS-CoV-2 infection or COVID-19, it has been clearly demonstrated that such a prophylactic measure can considerably prevent COVID-19 in the treated group. Namely, the risk of COVID-19 was about eightfold higher in those who used routine care than in those who used dimethyl sulfoxide-ethanol spray.

3.3 Ethanol efficiency

There is no question regarding ethanol's ability to kill or inactivate SARS-CoV-2, even at concentrations as low as 30% v/v in just 30 seconds, according to experimental and clinical data [21].

Alcohol is probably ineffective against intracellular viruses. It is crucial to extend ethanol inhalation by at least 3 days, since viral multiplication happens in 48–72 hours, which is then followed by cellular death and shedding. Additionally, ethanol is fundamentally effective against all SARS-CoV-2 variants and other “enveloped” viruses due to its non-specificity. This particular characteristic broadens the ethanol's range of activity against the SARS-CoV-2 pandemic and suggests its use in potential future viral epidemics.

The determined theoretical lowest dose of ethanol (= 153 µg) required to eradicate the fictitious virus load is relatively low when compared to daily exposure to many different jobs.

3.4 Ethanol effects on respiratory cells and microbiota

Alcohol's impact on respiratory hairy cells has been demonstrated by Sisson [23] to be a bimodal function of both exposure time and dosage. Low concentrations of ethanol (10 mM = 0.46 mg/ml) cause an increase in ciliary clearance, which may help to speed up the viral load's elimination once it has, theoretically, been made inactive by ethanol's own physicochemical features.

There is currently not enough research on how short-term ethanol administration affects respiratory microbiome. On the other hand, certain recommendations can be made in this regard. In fact, patients in the intensive care unit who had abnormally high levels of *M. salivarium* in the lower tract or low levels of clostridia in the upper tract had worse outcomes. It is noteworthy that ethanol totally inactivates SARS-CoV-2, mycoplasma, and SARS-CoV-2 (Eterpi et al.) [47]. Additionally, certain strains of clostridia are known to independently produce ethanol on their

own [48]; this ability has been used in commercial ABE fermentation to create acetone, butanol, and ethanol [49]. The lack of nasopharyngeal clostridia may hypothetically result in decreased or nonexistent local ethanol production, which would then let SARS-Cov-2 remain active at this level and move to the lower respiratory tract [3].

3.5 Ethanol toxicity

Rules governing acute ethanol exposure vary by nation or state and are subject to laws. The maximum Blood Alcohol Concentration (BAC) for the general public in the USA is between 500 and 800 mg/L. The regulation also restricts the maximum amount of chronic ethanol exposure in the workplace. For instance, the occupational exposure limit (OEL) for ethanol in the United Kingdom is 1000 parts per million (ppm) of ethanol, or 1910 mg/m³, during an 8-hour shift, which is equivalent to consuming 10 g of ethanol (about one glass of alcohol) daily, according to estimates [40]. These numbers much exceed the amount that would theoretically be needed to reduce the virus load in the respiratory tract. There have been many and vocal concerns made concerning the potential mucosal harm that inhaled ethanol might cause. These worries appear to have been completely dispelled by the thorough study by Castro-Balado et al. [38]. Interestingly, in the RCT from Hosseinzadeh [18], collateral effects are not mentioned, perhaps because were lacking or minimal and tolerable.

3.6 Inhaled ethanol therapeutic window

One must inevitably connect to the current experience because no focused research on this subject was found [33, 40].

Therefore, it appears acceptable and rational to declare that the hazardous risk of such acute inhalation—that is, about 330 mg—may be viewed as negligible [33]. This is because surgical cleaning with 70% ethanol for 90" is a daily habit and should generally be suggested and implemented. In reality, even if this dose was administered instantaneously to a healthy adult, the amount of ethanol in the air patients would inhale would be 0.078 mg/ml or 330 mg/5 L (airway volume). This quantity is significantly lower than both the legal limit of 500 mg/L (0.5 mg/ml) and the experimentally determined threshold of alcohol-induced ciliary dysfunction, which is 46 mg/ml [23]. Given that the lung and blood volumes are similar, equivalent numbers for the blood's ethanol concentration—which is far lower than the 500 mg/L legal lethal dose— could be derived.

However, this dose is a thousand times greater than the minimal dose of 153 µg needed to inactivate the calculated viral load in the lungs [22].

Each type of inhalation treatment is potentially more successful than any other method of administration for treating airway diseases [22]. Aerosol treatment enables lower doses, access to “hidden” regions, improved targeting of certain cells or compartments, etc., all of which boost the bioavailability of medications.

The size of the particles generated—classified according to the Aerodynamic Median Mass Diameter, or AMMD—well relates to the site to be treated. For the purpose of this chapter, the AMMD of the aerosol particles should be 5 µm.

Because of the relatively fresh technique suggested in this chapter, it is expected that there are little consolidated data in medical literature.

Focusing on the issue's dimension revealed that, in terms of threats to personal and societal health as well as associated economic costs, the disinfection of asymptomatic positive patients is crucial. There are currently no viable or affordable solutions to the issue.

Within a well-defined framework, the review and update of information attest to the high effectiveness and tolerable toxicity of inhaled ethanol. As a result, it is appropriate to administer inhaled ethanol to SARS-CoV-2-positive patients who are asymptomatic. A clinical trial should be carried out to examine its efficacy and tolerance in particular scenarios, as already suggested by Prof. Shintake [50] on March 17, 2020, and Dr. Amoushahi et al. [51] on May 25, 2020. Certainly, the research would be speedy, affordable, and straightforward to carry out.

The Authors post the following propositions:

It must be made clear that ethanol treatment is not believed to be an alternative to vaccination but rather must be considered complementary with it because vaccination appears to not prevent infection and disease from subintra variants [52]. IF IT IS FOUND THAT THIS TREATMENT IS EFFECTIVE, THE FOLLOWING HEALTH BENEFITS COULD BE EXPECTED:

reduction of the viral load on the respiratory tract, if not elimination, in a period of time much less than the duration of the normal cycle.

lowering the viral pressure on the immune system of the infected person to decrease the disease's course.

decrease in the quantity of virus that is actively released when someone coughs or sneezes.

reduction in the spread of the infection.

Minimal biological/health consequences (lethality, pulmonary fibrosis, psychiatric disorders, etc.).

4. Proposal for a study

4.1 Aim and scope

A study in which ethanol is administered as an inhaled vapor to SARS-CoV-2-positive asymptomatic patients.

The aim is to eradicate or, at the very least, lower the viral load of the respiratory tract, of course, in a span of time much shorter than the natural one.

The predicted health advantages include the following:

- Reduction of the viral pressure on the infected subject's immune system to halt the disease's progression.
- A decrease in the quantity of virus that is actively released when someone coughs or sneezes.
- A reduction in the infection's spread.
- Less biological/health harm (lethality, pulmonary fibrosis, psychiatric disorders, etc.)

4.2 Dosage and timing

Given that the lowest concentration of ethanol that is effective against SARS-CoV-2 is 30% v/v (Kratzel) [20], it is considered reasonable and wise to use a concentration that is between the one mentioned above and the one used for surgical disinfection (70%) [33].

In essence, the following dose is suggested: 1 ml of normal saline solution at 50% v/v (galenic preparation) = 390 mg (i.e., 50% by volume = 39% by weight, then 1 ml = 390 mg), in 2 at 5 minutes. Although the proposed dose is in absolute terms slightly higher than the dose inhaled during surgical disinfection, it can be assimilated because it is delivered over a longer time.

4.3 Delivery system

Each type of inhalation treatment is potentially more successful than any other method of administration for treating airway illnesses [22]. Aerosol treatment enables lower doses, access to “hidden” areas, improved targeting of certain cells or compartments, etc., all of which boost the bioavailability of medications.

According to the Aerodynamic Median Mass Diameter, or MMAD, the size of the particles produced is closely tied to the area that has to be treated.

1. It is advised that patients utilize a nebulizer, a medical aerosol device, and a mask that covers their mouth and nose. The patient should start nasal inhalation with the mask at a comfortable distance from the face, gradually lowering this distance as much as possible to avoid or reduce the initial (moderate) burning sensation. According to the distillation curve, the ethanol breathed in the beginning is at a higher concentration (approximately 65% v/v) while nearing the ending of the session, in obedience of the distillation curve.
2. The mass median aerodynamic diameter (MMAD) of the aerosol particles should be 5 μm .

4.4 Scheduling

Every 8 hours (6- to 10-hour intervals), for 7 days, there will be one activation (treatment), for a total of 21 administrations. When two-thirds of the solution has been administered, the administration might be terminated, according to the distillation curve.

4.5 Candidates

1. Individuals that turned a positive rapid antigenic test or RT-PCR for COVID-19.
2. Absence of symptoms (fever, anosmia, ageusia, cough, ultrasound, or CT associated with infiltrating/interstitial pneumonia, diarrhea) at the time of testing positive. The potential development of symptoms while undergoing the administration is not a requirement for exclusion.

4.6 Inclusion criteria

Age > 18 years old; ability to give informed consent.

4.7 Exclusion criteria

Alcoholism or a history of adverse reactions to ethanol, drug addiction or previous treatment for alcoholism/drug addiction, currently on disulfiram or cimetidine, non-drinkers of alcohol (no absolute criteria), any liver disease, uncontrolled diabetes, acute or chronic pancreatitis, serious respiratory diseases, tuberculosis or other mycobacterial infections, confirmed or suspected pregnancy, active psychosis, inability to give legally valid informed consent.

4.8 Measures

- After 1 week or at least 10 ethanol doses, nasopharyngeal antigen and molecular swabs (RT-PCR) should be collected. Depending on the current quarantine laws of local, regional, and national health authorities, values are articulated as either positive or negative dichotomies.
- A negative sample must be taken at the conclusion of the quarantine or just before the individual is readmitted in community, all of this, depending on local regulations.
- Determination of viral strain is considered a plus.

4.9 Type of study

Randomized clinical trial.

Arm A: treatment as above, quarantine as prescribed.

Arm B: no treatment, quarantine as prescribed.

4.10 Sample size

This is to be estimated with accuracy using biostatistical knowledge. Although the predicted difference between the two groups (treatment and controls) is projected to be roughly 60%, if we anticipate recruiting 150 participants in total, we are not far from very concrete evidence.

4.11 Primary outcome

Reduction of the mean time to eliminate the viral load (see MEASURES) from 17 to 7 days.

4.12 Secondary outcome

- A decrease in the mean time to viral load eradication (see MEASURES), from 17 to 5 days.
- A decrease in the mean time to viral load eradication (see MEASURES), from 17 to 3 days.
- Reduction in the rate (below 43%, at least) of asymptomatic subjects who will develop symptoms.

- Comparison of the mean timeframes for viral load (see *MEASURES*) decreases in the general population and among medical professionals.

If the proposed treatment were successful in improving health, tremendous benefits could be anticipated:

- Reduction in the financial burden caused by decreased (if not complete interruption) labor productivity (the global GNP (Gross Domestic Product) decline for 2020 is close to 10%) and medical expenses. Savings should be in the number of billions of euros.
- Faster return to normal life (school, work, sports, travel, reduction of measures restricting personal freedom, etc.).
- Ethanol is potentially active no matter the variant in circulation thanks to its nonspecific action mechanism.
- Additionally, it could be effective against “enveloped” viruses that could be the origin of upcoming epidemic outbreaks.
- The pressure on the vaccination campaign can be reduced thanks to the viral circulation’s slowing down.
- Even nations with limited financial resources may control the SARS-Cov-2 outbreak effectively thanks to the wide availability and inexpensive cost of ethanol.

Abbreviations

PAS	positive asymptomatic subjects
ACE2	angiotensin-converting enzyme 2
EtOH	ethanol
SARS	Severe Acute Respiratory Syndrome Coronavirus
MERS	Middle East Respiratory Syndrome
HcoV	Human Endemic Coronavirus
OEL	occupational exposure limit
ABE	acetone, butanol, ethanol
BAC	blood alcohol concentration
AMMD	aerodynamic median mass diameter


Author details

Pietro Salvatori

Head & Neck Surgeon, former Head of the ENT Department at the Humanitas San Pio X Hospital, Milan, Italy

*Address all correspondence to: pietro.salvatori@me.com

IntechOpen

© 2023 The Author(s). Licensee IntechOpen. This chapter is distributed under the terms of the Creative Commons Attribution License (<http://creativecommons.org/licenses/by/3.0>), which permits unrestricted use, distribution, and reproduction in any medium, provided the original work is properly cited. 

References

- [1] Salvatori P. The rationale of ethanol inhalation for disinfection of the respiratory tract in SARS-CoV-2-positive asymptomatic subjects. *The Pan African Medical Journal*. 2021;**40**:201. DOI: 10.11604.pamj.2021.40.201.31211
- [2] Sungnak W, Huang N, Bécavin C, Berg M, Queen R, Litvinukova M, et al. SARS-CoV-2 entry factors are highly expressed in nasal epithelial cells together with innate immune genes. *Nature Medicine*. 2020;**26**:681-687. DOI: 10.1038/s41591-020-0868-6
- [3] Polak SB, Van Gool IC, Cohen D, von der Thüsen JH, van Paassen J. A systematic review of pathological findings in COVID-19: A pathophysiological timeline and possible mechanisms of disease progression. *Modern Pathology*. 2020;**33**:2128-2138. DOI: 10.1038/s41379-020-0603-3
- [4] Madas BG, Füre P, Farkas A, Nagy A, Czitrovsky A, Balásházy I, et al. Deposition distribution of the new coronavirus (SARS-CoV-2) in the human airways upon exposure to cough-generated droplets and aerosol particles. *Scientific Reports*. 2020;**10**(1):22430. DOI: 10.1038/s41598-020-79985-6
- [5] Cao S, Gan Y, Wang C, Bachmann M, Wei S, Gong J, et al. Post-lockdown SARS-CoV-2 nucleic acid screening in nearly ten million residents of Wuhan, China. *Nature Communications*. 2020;**11**(1):5917. DOI: 10.1038/s41467-020-19802-w
- [6] Nelson EJ, McKune SL, Ryan KA, Lednický JA, PhD CSR, Myers MJG Jr. SARS-CoV-2 Positivity on or after 9 days among quarantined student contacts of confirmed cases. *JAMA*. 2021;**325**(15):1561-1562. DOI: 10.1001/jama.2021.2392
- [7] Atripaldi L, Sale S, Capone M, Montesarchio V, Parrella R, Bot G, et al. Could asymptomatic carriers spread the SARS-CoV-2 infection? Experience from the Italian second wave. *Journal of Translational Medicine*. 2021;**19**:93. DOI: 10.1186/s12967-021-02762-0
- [8] Liu J, Liu J, He Z, Yang Z, Yuan J, Wu H, et al. The duration of SARS-CoV-2 positive in the environments of quarantine rooms: A perspective analysis. *International Journal of Infectious Diseases*. 2021;**105**:68-74
- [9] Worldometer - real time world statistics [Internet]. COVID Live Update: 234,869,049 Cases and 4,802,852 Deaths from the Coronavirus – Worldometer. Available from: <https://www.worldometers.info/coronavirus/> [Accessed: September 17, 2021].
- [10] Byambasuren O, Cardona M, Bell K, Clark J, McLaws ML, Glasziou P. Estimating the extent of asymptomatic COVID-19 and its potential for community transmission: Systematic review and meta-analysis. *JAMMI*. 2020;**5**(4):223-234. DOI: 10.3138/jammi-2020-0030
- [11] Yu C, Zhou M, Liu Y, Guo T, Ou C, Yang L, d, et al., Characteristics of asymptomatic COVID-19 infection and progression: A multicenter, retrospective study, *Virulence*. 2020; **11**(1):1006-1014
- [12] Cevik M, Tate M, Lloyd O, Maraolo AE, Schafers J, Ho A. SARS-CoV-2, SARS-CoV, and MERS-CoV viral load dynamics, duration of viral shedding, and infectiousness: A

- systematic review and meta-analysis. *Lancet Microbe*. 2021;**2**(1):e13-e22
- [13] Bongiovanni M, Marra AM, De Lauretis A, Bini F, Di Carlo D, Manes G, et al. Natural history of SARS-CoV-2 infection in healthcare workers in northern Italy. *Journal of Hospital Infection*. 2020;**106**:709-712. DOI: 10.1016/j.jhin.2020.08.027
- [14] Bramante CT, Huling JH, Tignanelli C, et al. Randomized trial of metformin, Ivermectin, and fluvoxamine for Covid-19. *The New England Journal of Medicine*. 2022;**387**:599-610. DOI: 10.1056/NEJMoa2201662
- [15] Ganatra S, Dani SS, Ahmad J, Kumar A, Shah AGM, DP MQ, et al. Oral Nirmatrelvir and ritonavir in non-hospitalized vaccinated patients with Covid-19. *Clinical Infectious Diseases*. 2022;**76**:563-572. DOI: 10.1093/cid/ciac673
- [16] Chen RE, Zhang X, Case JB, et al. Resistance of SARS-CoV-2 variants to neutralization by monoclonal and serum-derived polyclonal antibodies. *Nature Medicine*. 2021;**27**(4):717-726. DOI: 10.1038/s41591-021-01294-w
- [17] Guenezan J, Garcia M, Strasters D, Jousselin C, Lévêque N, Frasca D, et al. Povidone iodine mouthwash, gargle, and nasal spray to reduce nasopharyngeal viral load in patients with COVID-19: A randomized clinical trial. *JAMA Otolaryngology. Head & Neck Surgery*. 2021;**147**(4):400-401
- [18] Hosseinzadeh A, Tavakolian A, Kia V, Ebrahimi H, Sheibani H, Binesh E, et al. Combined application of dimethyl sulfoxide and ethanol nasal spray during COVID-19 pandemic may protect healthcare workers: A randomized controlled trial. *Iranian Red Crescent Medical Journal*. 2022;**24**(8):e1640,1-6. DOI: 10.32592/ircmj.2022.24.8.1640
- [19] Kampf G. Efficacy of ethanol against viruses in hand disinfection. *The Journal of Hospital Infection*. 2018;**98**(4):331-338
- [20] Eslami H, Das S, Zhou T, Müller-Plathe F. How alcoholic disinfectants affect coronavirus model membranes: Membrane fluidity, Permeability, and Disintegration, *J Phys Chem B*. 2020;**124**(46):10374-10385
- [21] Kratzel A, Todt D, V'kovski P, Steiner S, Gultom M, Nhu Thao TT, et al. Inactivation of severe acute respiratory syndrome coronavirus 2 by WHO-recommended hand rub formulations and alcohols. *Emerging Infectious Diseases*. 2020;**26**(7):1592-1595
- [22] Manning TJ, Thomas-Richardson J, Cowan M, Thomas-Richardson G. Should ethanol be considered a treatment for COVID-19? *Revista da Associação Médica Brasileira*. 2020;**66**(9):1169-1171
- [23] Sisson JH, Pavlik JA, Wyatt TA. Alcohol stimulates ciliary motility of isolated airway axonemes through a nitric oxide, cyclase and cyclic nucleotide-dependent kinase mechanism. *Alcoholism, Clinical and Experimental Research*. 2009;**33**(4):610-616
- [24] Simet SM, Pavlik JA, Sisson JH. Dietary antioxidants prevent alcohol-induced ciliary dysfunction. *Alcohol*. 2013A;**47**:629-635. DOI: 10.1016/j.alcohol.2013.09.004
- [25] Gootnick A, Lipson HI, Turbin J. Inhalation of ethyl alcohol for pulmonary edema. *New England Journal of Medicine*. 1951;**245**:842-843
- [26] Luisada AA, Weyl R, Goldmann MA. Treatment of pulmonary edema. *Journal*

- of the American Medical Association. 1954;**1**(154):62. DOI: 10.1001/jama.1954.02940350064019
- [27] Calesnick B, Vernick HQ. Antitussive activity of ethanol. *Journal of Studies on Alcohol*. 1971;**32**(2):434-441
- [28] PJQ B. A new rapid treatment for the useless cough in the postoperative patient. *Quarterly Bulletin of the Northwestern University Medical School*. 1954;**28**(1):76-78
- [29] Available from: <https://www.sps.nhs.uk/artcles/ethanol-content-of-inhalers-what-is-the-significance/>
- [30] Sulaiman I, Chung M, Angel L, Tsay JJ, Wu BG, Yeung ST, et al. Microbial signatures in the lower airways of mechanically ventilated COVID19 patients associated with poor clinical outcome. *Res. Sq*. 29 Mar 2021;**266050**:1-42
- [31] Rueca M, Fontana A, Bartolini B, Piselli P, Mazzarelli A, Copeti M, et al. Investigation of nasal/oropharyngeal microbial community of COVID-19 patients by 16S rDNA sequencing. *International Journal of Environmental Research and Public Health*. 2021;**18**(4):2174. DOI: 10.3390/ijerph18042174
- [32] MacLean RR, Valentine GW, Jatlow PI, Sofuoglu M. Inhalation of alcohol vapor: Measurement and implications. *Alcoholism, Clinical and Experimental Research*. 2017;**41**(2):238-250. DOI: 10.1111/acer.13291
- [33] Bessonneau V, Thomas O. Assessment of exposure to alcohol vapor from alcohol-based hand rubs. *International Journal of Environmental Research and Public Health*. 2012;**9**(3):868-879
- [34] Boyce JM, Pitet D. Guideline for hand hygiene in health-care settings. *American Journal of Infection Control*. 2002;**30**:1-46
- [35] More SL, Thornton SA, Maskrey JR, Sharma A, de Gandiaga E, Cheng TJ, et al. PBPK modeling characterization of potential acute impairment effects from inhalation of ethanol during e-cigarette use. *Inhalation Toxicology*. 2020;**32**(1):14-23
- [36] Available from: <https://clinicaltrials.gov/ct2/show/NCT04554433>
- [37] Available from: <https://www.clinicaltrialsregister.eu/ctr-search/search?query=2020-001760-29>
- [38] Castro-Balado A, Mondelo-Garcia C, Barbosa-Pereira L, Varela-Rey I, Novo-Veleiro I, Vázquez Agra N, et al. Development and Characterization of inhaled ethanol as a novel pharmacological strategy currently evaluated in a phase II clinical trial for early-stage SARS-CoV-2 infection. *Pharmaceutics*. 2021;**13**:342. DOI: 10.3390/pharmaceutics13030342
- [39] Irvine LFH. Relevance of the developmental toxicity of ethanol in the occupational setting: A review. *Journal of Applied Toxicology*. 2003;**23**(5):289-299
- [40] Bevan RJ, Slack RJ, Holmes P, Levy LS. An assessment of potential cancer risk following occupational exposure to ethanol. *Journal of Toxicology and Environmental Health, Part B, Critical Reviews*. 2009;**12**(3):188-205
- [41] Yeligar SM, Chen MM, Kovacs EJ, Sisson JH, Burnham EL, Brownf LAS. Alcohol and lung injury and immunity. *Alcohol*. 2016;**55**:51-59. DOI: 10.1016/j.alcohol.2016.08.005

- [42] Winek CL, Murphy KL. The rate and kinetic order of ethanol elimination. *Forensic Science International*. 1984;**25**(3):159-166
- [43] Majra D, Benson J, Pitts J, Stebbing J. SARS-CoV-2 (COVID-19) superspreader events. *Journal of Infection*. 2021;**82**(1):36-40. DOI: 10.1016/j.jinf.2020.11.021
- [44] Szmigiera M. Impact of the Coronavirus Pandemic on the Global Economy. *Statistics & Facts*; 2021. Available from: https://www.statista.com/topics/6139/covid-19-impact-on-the-global-economy/#topicHeader__wrapper
- [45] Sai M, Heilmann E, Moraes SN, Kearns FL, von Laer D, Amaro RE, et al. Transmissible SARS-CoV-2 variants with resistance to clinical protease inhibitors. *bioRxiv*. 26 Dec 2022;**503099**:1-33. DOI: 10.1101/2022.08.07.503099
- [46] Wang L, Volkow ND, Davis PB, Berger NA, Kaelber DC, Xu R. COVID-19 rebound after Paxlovid treatment during omicron BA.5 vs BA.2.12.1 subvariant predominance period. *MedRxiv*. 04 Aug 2022;**2227845**:1-5. DOI: 10.1101/2022.08.04.22278450. PMID: 35794889; PMCID: PMC9258292
- [47] Eterpi M, McDonnell G, Thomas V. Decontamination efficacy against mycoplasma. *Letters in Applied Microbiology*. 2011;**52**(2):150-155
- [48] Ruuskanen MO, Åberg F, Mannistö V, Havulinna AS, Méric G, Liuh Y, et al. Links between gut microbiome composition and fatty liver disease in a large population sample. *Gut Microbes*. 2021;**13**(1):e1888673 (22 pages). DOI: 10.1080/19490976.2021.1888673
- [49] Seo SO, Lu T, Jin YS, Blaschek HP. A comparative phenotypic and genomic analysis of *Clostridium beijerinckii* mutant with enhanced solvent production. *Journal of Biotechnology*. 2021;**329**:49-55
- [50] Shintake T. Possibility of disinfection of SARS-CoV-2 (COVID-19) in human respiratory tract by controlled ethanol vapor inhalation. *arXiv:2003.12444v1 [physics.med-ph]*. 15 Mar 2020:1-12. DOI: 10.48550/arXiv.2003.12444
- [51] Amoushahi A, Padmos A. A Suggestion on Ethanol Therapy in COVID-19?. *EC Anaesthesia*; 2020;**6**(6):1-2
- [52] CDC. Laboratory-confirmed COVID-19-associated hospitalizations among adults during SARS-CoV-2 omicron BA.2 variant predominance — COVID-19-associated hospitalization surveillance network, 14 states, June 20, 2021–may 31, 2022. *Morbidity and Mortality Weekly Report*. 2022;**71**(34):1085-1091

Ethanol as a Subgroup of the UNIFAC Model in the Prediction of Liquid-Liquid Equilibrium in Food and Fuel Systems

Jacqueline M. Ortega Bacicheti, Guilherme D. Machado, Fábio Nishiyama, Vladimir F. Cabral and Donato Aranda

Abstract

Ethanol has been employed as a solvent in biodiesel production and vegetable oil refining since it is more economically attractive and less toxic than methanol and hexane. Furthermore, ethanol has demonstrated easy recovery, good selectivity, and distribution coefficient for free fatty acids (FFA), which is the primary target in the refining process since high acidity oil can lead to the formation of side products. As the knowledge of phase equilibrium behavior of fatty systems is essential to design and optimize the extraction of FFA, this chapter will present two new UNIFAC subgroups for ethanol: EtOH-B, focused on biodiesel production; and EtOH-D, focused on the deacidification process. Except for ethanol and water subgroups fitted in this study, all remaining UNIFAC parameters were taken from the literature. The new EtOH-B and EtOH-D parameters provide a considerably lower mean square error (1.20% and 0.87%) than the other works available in the literature. The results show that new ethanol subgroups and the developed methodology are valuable tools in predicting liquid-liquid phase equilibrium for ethyl biodiesel and vegetable oil deacidification systems considered, resulting in reduced computational calculations and a relatively small split with the complex dataset established by the UNIFAC-LL model.

Keywords: biodiesel, deacidification, ethanol, liquid-liquid equilibrium, vegetable oil, UNIFAC

1. Introduction

Several studies have introduced ethanol as a solvent for liquid-liquid extraction, resulting in a satisfactory reduction of free fatty acid (FFA) content in oils [1–4]. High acidity level vegetable oils need to be refined either for human consumption or for fuel production. In this way, ethanol can act both as a solvent for oil deacidification by liquid-liquid extraction and as a reagent for transesterification reaction.

Considering edible vegetable oil, high levels of FFA have been associated with digestive problems for consumers, autoimmune disorders, and various types of cancer [5–8]. Besides health problems, the content of pigments, phosphatides, odoriferous molecules, and free fatty acids in edible vegetal oil is detrimental to the oil quality, oxidative stability, and consumer acceptance. Among these impurities, FFA is the most detrimental because they increase the acidity of the oil, inducing an undesirable rancid flavor [9]. In order to reduce neutral oil losses and production of undesired compounds, caused by unwanted chemical reactions [10], liquid-liquid extraction using ethanol as a solvent can replace the conventional physical and chemical refining processes.

Besides deacidification of edible vegetable oils, ethanol can be employed in biodiesel production. The conventional biodiesel production process requires the use of a feedstock with reduced acidity; however, residual oils are characterized by a high FFA content, which promotes soap production with the alkali homogeneous catalysts used in transesterification [11]. Thus, feedstock purification processes, such as oil deacidification, through solvent extraction are needed. Using residual oils for biodiesel production can provide several advantages when compared to the conventional process with refined oils, such as the minimization of environmental impacts related to the disposal of waste oils, a noncompetitive relationship with the food crops, and availability of the feedstock supply, which accounts for over 70% of the refined oil biodiesel production costs [12].

In order to correctly design, operate and optimize extraction columns and the subsequent additional purification or solvent recovery units, liquid-liquid phase equilibrium (LLE) data are necessary to determine the thermodynamic properties of the systems composed of oil, solvent, and FFA [3, 13]. In general, most of the phase equilibrium data for biodiesel systems use methanol as the reacting alcohol [14], studies regarding systems with ethanol are more recent [15]. Some advantages of using ethanol as a solvent are its high affinity for FFAs at ambient temperature, low toxicity when compared to methanol, and its easy removal under mild conditions [16, 17].

Thermodynamic modeling can be used to predict or correlate the experimental behavior of fatty acid systems described through LLE data. The approach using excess Gibbs energy models is widely applied to describe biodiesel and vegetable oil systems through thermodynamic models, such as NRTL [18–22], UNIQUAC [18, 22–24], and UNIFAC [25–28]. Although thermodynamic models, such as UNIQUAC and NRTL, are capable of accurately representing the experimental data, both are restricted to the specificity of the type of vegetable oil used, as the phase equilibrium parameters are adjusted solely for the system described in the experimental data used for the LLE data fitting. Numerous types of refined or residual feedstocks are available for biodiesel production or require deacidification to be safe for human consumption. Thus, the use of a predictive group-contribution method, such as UNIFAC, to describe the phase behavior of the variety of biodiesel reaction systems or deacidification of edible vegetable oil systems is motivated, as larger number of systems would be useful.

In the UNIFAC model, alcohols, such as methanol and propanol, used to be represented by a specific group. As stated by Magnussen et al. [29] in their work, 1-propanol ($\text{CH}_3\text{CH}_2\text{CH}_2\text{OH}$) can be represented, in principle, by the CH_3 , CH_2 , and OH subgroups. However, the fitting of these parameters in the UNIFAC parameter table depends on several other molecules that present these subgroups. An approach that represents molecules by a subgroup of their own, as in the case of methanol (CH_3OH), can provide more accurate property calculations.

On account of the growing tendency of substitution of environmentally damaging chemicals for less impactful compounds, added to its availability and price in the context of biofuels in Brazil and other countries, the use of ethanol as a solvent or reactant is expected to vastly increase. Therefore, the study of the possibility of using ethanol as UNIFAC subgroup must also be evaluated.

In the literature, the thermodynamic modeling of these systems focuses on the UNIQUAC and NRTL models. Reipert et al. [30] correlated the LLE experimental data of refined babassu oil, lauric acid, and hydrated ethanol using the NRTL model. The mass fraction root mean square error (RMSD) between the observed and estimated compositions was 0.85%. Gonçalves et al. [31] applied NRTL and UNIQUAC models to correlate LLE experimental data for corn oil with a hydrated ethanol solvent system at room temperature and atmospheric pressure. The RMSD of 0.89% and 0.92%, respectively. Rodrigues et al. [32] investigated the LLE of Brazil nut oil or Macadamia nut oil + commercial oleic acid + ethanol + water, at 298.2 K. They reported RMSD not higher than 1.5% using the NRTL and UNIQUAC models. Basso et al. [19] determined LLE data for glycerol + ethanol + fatty acid ethyl ester from crambe oil system and adjusted parameters for NRTL model. The RMSD between experimental and calculated values by the NRTL model was less than 0.82%. The authors verified the prediction capacity of the UNIFAC model by testing two different sets of UNIFAC binary interaction parameters and obtained a RMSD of 2.27% and 3.97%, respectively. Da Silva et al. [20] established experimental data for *Jatropha curcas* oil + oleic acid + ethanol + water systems at (288.15, 298.15, 308.15, and 318.15) K and correlated the experimental data by the nonrandom two-liquid (NRTL) model with temperature-dependent binary parameters. For all systems, the RMSD was lower than 0.96%. Basso et al. [33] obtained LLE experimental data of systems containing glycerol + ethanol + ethyl biodiesel from macauba pulp oil, performed thermodynamic modeling, and simulated the settling step of this biodiesel using simulation software. Binary interaction parameters were adjusted for NRTL and UNIQUAC models and the RMSD between experimental data and calculated values were 0.44%, 1.07%, 3.52%, and 2.82%, respectively, using the NRTL, UNIQUAC, UNIFAC-LLE, and UNIFAC-Dortmund models.

All the aforementioned studies indicate that the NRTL and UNIQUAC models can reproduce the experimental liquid-liquid behavior of the systems involving vegetable oil + fatty acids + ethanol + water and biodiesel + glycerol + ethanol. However, although these thermodynamic models represent satisfactorily the experimental data, the NRTL and UNIQUAC parameters obtained in these studies are specific to these systems, consequently, they are restricted to the specific vegetable oil used in the parameter correlation. Considering the numerous types of vegetable oils that need deacidification, and different triacylglycerides matrices that can be used for biodiesel production, new parameter-fitting procedures are required for other systems, and new experimental databanks are required [9, 17, 30]. However, the new parameter-fitting procedures required for new systems are not mandatory if we consider the group contribution method. UNIFAC (UNIQUAC Functional-group Activity Coefficient) model [34] is a group contribution method established by Fredenslund, Jones e Prausnitz in 1975, that can predict the liquid-liquid behavior of systems containing fatty acids using the activity coefficient calculation, which considers the interaction between the subgroups that form the molecules. Fredenslund et al. [34] proposed a group contribution method that could use experimental data available in the literature to predict the LLE of systems with no disposable experimental data.

Models based in group contribution concept estimate the properties of a mixture considering it as a solution of different functional groups that forms the molecule in the

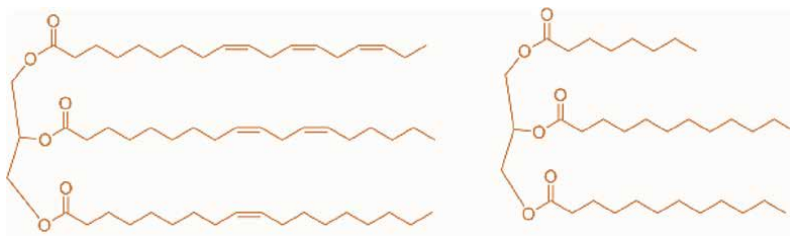


Figure 1.
Soybean oil (left) and coconut oil (right) molecular structures.

mixture. As can be seen in **Figure 1**, soybean and coconut oils are different molecules, but the same chemical compounds are encountered in these molecules. Considering these few functional groups as building blocks, a vast array of vegetable oil can be represented, as all vegetable oils present the same functional groups only differing in quantities.

This type of predictive model applicable to a larger number of systems would be useful and important in the food industry and biofuel industry, respectively, given the diversity of raw materials and the fact that most systems are multicomponent, and the variety of generated biodiesel systems.

Physical and chemical properties are considered as a sum of all contributions made by each one of the functional groups. These contributions are quantified according to the interaction parameters, adjusted by experimental data.

This model was extensively applied to study the liquid-liquid equilibrium of vegetable oils.

Batista et al. [2] applied UNIFAC and ASOG (analytical solution of groups) group contribution methods to correlate interaction parameters of triolein + oleic acid + ethanol and triolein + stearic acid + ethanol systems. The parameters were validated for canola, corn, and Spanish oil and the root mean square deviation between experimental and calculated molar fractions were 1.31% and 1.32% for the UNIFAC and ASOG models, respectively.

Bessa et al. [35] tested the predictive capability of the original UNIFAC model parameters and then modified them in terms of new readjusted binary interaction parameters. Due to inadequate results obtained by UNIFAC model without any changes in its subgroups, the authors introduced a new group (“OHgly”) and two matrices of parameters were adjusted. The authors obtained good predictions and a significant improvement in the performance of this group contribution model has been achieved.

Noriega and Narvaez [28] proposed a new set of UNIFAC group interaction parameters to describe the LLE for all the systems involved in biodiesel production. The parameters presented a RMSD up to 2.07%.

In the UNIFAC model, the activity coefficient is given in terms of a combinatorial contribution taking into account entropy effects arising from differences in molecular size and shape, and a residual contribution taking into account energetic interactions between the functional groups in the mixture. To achieve a better description of the experimental data composed by the molecules presented in **Table 1**, the chosen subgroups to represent the studied fatty systems were as follows: CH₃, CH₂, CH, CH=CH, COOH, CH₂COO, OH, H₂O, and the new proposed group EtOH.

Therefore, this chapter proposes the adjustment of thermodynamic parameters of the UNIFAC model considering a new ethanol subgroup in order to predict the LLE for systems containing food or fuel. The fact that vegetable oils present different types

Molecule	Subgroups
Ethanol	1 EtOH
Water	1 H ₂ O
Glycerol	2 CH ₂ , 1 CH, 3 OH
Fatty acid	n CH ₃ , n CH ₂ , COOH
Triacylglycerol	n CH ₃ , n CH ₂ , nCH, nCH=CH, CH ₂ COO
Biodiesel	n CH ₃ , n CH ₂ , nCH, nCH=CH, CH ₂ COO

Table 1.
 Chosen subgroups to represent the studied fatty systems.

of constituent fatty acids but with similarity in their structure makes it possible to use a predictive approach that represents the interactions between groups based on UNIFAC thermodynamic model in the proper representation of the LLE for industrial separation processes. Thus, this study aims to present such methodology in the prediction of food systems containing FFA to be separated as well as systems containing fuels, focusing on biodiesel produced from vegetable oils.

2. Methodology

The isofugacity criterion for phase equilibrium is conventionally used to describe a condition at which the chemical potential of each component is equal in the phases among which this component can distribute. If fugacities are expressed in terms of activity coefficients, the LLE using an excess Gibbs energy model is represented by Eq. (1) [34].

$$x_i^{AP} \gamma_i^{AP} = x_i^{OP} \gamma_i^{OP} \quad (1)$$

where x_i^{AP} and x_i^{OP} are the molar fractions of component i in the alcohol and oil phases, respectively, and γ_i^{AP} and γ_i^{OP} are the activity coefficients of component i in the alcohol and oil phases, respectively.

In this chapter, the activity coefficients are calculated through UNIFAC model [34], which considers the combinatorial and residual contributions, Eq. (2).

$$\ln \gamma_i = \ln \gamma_i^C + \ln \gamma_i^R \quad (2)$$

The combinatorial contribution γ_i^C (Eq. (3)) is related to the difference in size and shape of molecules. The volume fraction ϕ_i and surface fraction θ_i of each molecule i are obtained using Eq. (5) and (6), respectively.

$$\ln \gamma_i^C(x) = \ln \frac{\phi_i}{x_i} + \frac{Z}{2} q_i \ln \frac{\theta_i}{\phi_i} + l_i - \frac{\phi_i}{x_i} \sum_{j=1}^{n_c} x_j l_j, \quad (3)$$

$$l_i = \frac{z}{2} (r_i - q_i) - (r_i - 1); Z = 10. \quad (4)$$

$$\varnothing_i = \frac{r_i x_i}{\sum_{j=1}^{n_c} r_j x_j} \quad (5)$$

$$\theta_i = \frac{q_i x_i}{\sum_{j=1}^{n_c} q_j x_j} \quad (6)$$

where x_i is the mole fraction of component i and r_i and q_i are the measures of molecular van der Waals volumes and molecular surface areas, respectively. They are calculated as the sum of the group volume and group area parameters, R_k and Q_k .

$$r_i = \sum_{k=1}^{n_g} \nu_{ki} R_k \quad (7)$$

$$q_i = \sum_{k=1}^{n_g} \nu_{ki} Q_k \quad (8)$$

where ν_{ki} is the number of groups of type k in molecule i . Here, we use the values of R_k and Q_k reported by Magnussen *et al.* [29]. Os valores R_k e Q_k são calculados a partir do volume e área superficial dos grupos de Van der Waals (V_{wk} e A_{wk} , respectivamente), retratado por Bondi (1968):

$$R_k = \frac{V_{wk}}{15,17} \quad (9)$$

$$Q_k = \frac{A_{wk}}{2,5 \times 10^9} \quad (10)$$

The residual contribution γ_i^R , described through Eq. (11), is due to group areas and group interaction parameters. Γ_k and $\Gamma_k^{(i)}$ are the residual activity coefficient from group k in the solution and in a solution containing only molecules of type i , respectively.

$$\ln \gamma_i^R(T, x) = \sum_k \nu_{ki} \left(\ln \Gamma_k - \ln \Gamma_k^{(i)} \right) \quad (11)$$

By Eq. 12 it is possible to calculate the residual activity coefficient.

$$\ln \Gamma_k = Q_k \left[1 - \ln \left(\sum_m^k \theta_m \psi_{mk} \right) - \sum_m \left(\frac{\theta_{dm} \psi_{km}}{\sum_n \theta_n \psi_{nm}} \right) \right] \quad (12)$$

where θ_m is the area fraction of group m given by:

$$\theta_m = \frac{Q_m X_m}{\sum_n Q_n X_n}, \# \quad (13)$$

and X_m is the molar fraction of the group m in the mixture.

$$X_m = \frac{\sum_j^n Q_m X_m}{\sum_j \sum_n \nu_{nj} x_j} \quad \# \quad (14)$$

The group interaction parameter ψ_{nm} between groups n and m is given by:

$$\psi_{mn} = \exp\left(-\frac{a_{mn}}{T}\right), \# \quad (15)$$

where a_{mn} is an adjustable parameter of the binary interaction between groups m and n , and it has units of kelvins. Each group-group interaction possesses two parameters: a_{nm} , a_{mn} , and $a_{nm} \neq a_{mn}$. These parameters were obtained from a database using a wide range of experimental phase-equilibrium results.

The parameter fitting procedure was applied separately to fit the EtOH interaction parameters for biodiesel separation and deacidification systems. In deacidification process, the presence of water in ethanol solvent increases the polarity of the solution. This feature and the presence of glycerol in biodiesel system makes the behavior of EtOH subgroup different in deacidification systems from that in biodiesel systems, even assuming that the subgroups of both systems were similar (the CH₃, CH₂, CH, CH = CH, COOH, CH₂COO), and accepting that UNIFAC model is a group contribution method that can predict the liquid-liquid behavior considering the interaction between the subgroups that form the molecules.

As the ethanol parameters calculated for the biodiesel system are not adequate for deacidification process, the UNIFAC parameters for new ethanol subgroup were fitted for the biodiesel process separately from deacidification process. As result, this study will present UNIFAC interaction parameters for ethanol subgroup in biodiesel systems (EtOH-B) and in deacidification systems (EtOH-D). The UNIFAC parameters were fitted considering the phase compositions in molar fractions and binary interaction parameters in 1/K.

A data bank containing 56 systems was compiled. We used a total of 88 tie-lines from eight biodiesel types from vegetable oils with ethanol, and 246 tie-lines for the 14 types of vegetable oils with hydrated ethanol, at temperatures ranging from 288.15 to 333.15 K, all systems studied at atmospheric pressure. **Table 2** shows a summary of the equilibrium systems used in the parameter fitting and validation procedure.

For biodiesel separation fitted ethanol-related parameters, the LLE database of seven ethyl systems of vegetable oils (soybean, canola, palm, *jatropha curcas*, cottonseed, crambe, and sunflower) at different temperatures were used to fit the interaction parameters of the ethanol subgroups. The fitted ethanol-related parameters were validated against data for the macauba (*Acrocomia aculeata*) biodiesel system. Lastly, the results obtained are compared with those obtained by the UNIFAC-LL parameters [29] and parameters available from literature work [35].

For deacidification fitted ethanol-related parameters, the LLE database of 13 systems of vegetable oils (brazil nut, corn, cottonseed, garlic, grapeseed, *jatropha curcas*, palm, peanut, rice bran, sesame, soybean, and sunflower) at different temperatures were used to fit the interaction parameters of the ethanol subgroups. The validation procedure was performed using canola oil system and a total of five tie-lines at 303.15 K, and it is worth mentioning that canola oil was not included in the parameter estimation process. Lastly, the results obtained are compared with those obtained by the UNIFAC-LL parameters [29] and parameters available from literature work [26, 28, 43].

The system is composed of biodiesel, ethanol, and glycerol.			
Vegetable oil source	Tie-lines	T (K)	References
Soybean	10	293.15, 323.15	[36]
Canola	5	303.15	[1]
Palm	15	298.15, 323.15	[37]
<i>Jatropha curcas</i>	12	303.15, 318.15, 333.15	[14]
Macauba pulp	6	298.15	[33]
Cottonseed	18	293.15, 313.15, 333.15	[38]
Crambe	18	298.15, 318.15, 338.15	[19]
Sunflower	12	298.15, 313.15	[36]
The system is composed of vegetable oil, free fatty acids (FFA), ethanol, and water.			
Vegetable oil source	Tie-lines	T (K)	References
Brazil nut	6	298.15	[32]
Canola	5	303.15	[18]
Corn	21	298.15	[31]
Cottonseed	21	298.15	[4]
Garlic	21	298.15	[39]
Grapeseed	22	318.15	[39]
<i>J. curcas</i>	40	288.15, 298.15, 308.15, 318.15	[20]
Macadamia	15	298.15	[32]
Palm	10	318.15	[40]
Peanut	7	298.15	[9]
Rice bran	17	298.15	[41]
Sesame	14	298.15	[39]
Soybean	16	323.15	[42]
Sunflower	32	298.15	[3]

Table 2.
LLE database of the systems involved in the correlation process.

The software Microsoft Excel was used in the parameter fitting procedure coupled to XSEOS [44] and SOLVER® add-ins. The XSEOS add-in, an open-source code programmed in visual basic for applications (VBA) with several excess Gibbs energy models and equations of state, was employed to evaluate the activity coefficient of the UNIFAC model, while the SOLVER® add-in with the generalized reduced gradient (GRG) method [45] was used as the numerical calculation tool.

The parameter fitting was performed by minimizing the objective function (Eq. 16) using the generalized reduced gradient (GRG) nonlinear solving method.

$$\text{OF} = \sum_n^{NL} \sum_i^{NCn} \left(W_{i,n}^{OPexp} - W_{i,n}^{OPcalc} \right)^2 + \left(W_{i,n}^{APexp} - W_{i,n}^{APcalc} \right)^2 \quad (16)$$

where NLa and NCn represent the total number of tie-lines in each group and the total number of components or pseudo components in tie-line n , respectively. $W_{i,n}$ correspond to the mass fraction of the component or pseudo component i in the tie-line n in the oil phase (OP) or alcohol phase (AP), while the superscripts exp and $calc$ the experimental or calculated values, respectively. During the parameter fitting procedure, the minimization of eq. (16) is constrained by the isofugacity condition expressed by Eq. (1), and the calculated mass fraction sum, which must be equal to 1.

In order to evaluate the capability of the ethanol interaction parameters [27, 43] to describe LLE in systems containing FFA accurately, the percentual mass fraction root mean square deviation between the experimental and calculated phase composition values (RMSD), Eq. (17), was compared to the results obtained using parameters available in the literature (UNIFAC-LL from Magnussen et al. [46], Bessa et al. [35], Noriega and Narváez [28], Hirata et al. [26]).

$$RMSD = 100 \cdot \sqrt{\frac{\sum_n^{NLa} \sum_i^{NCn} (W_{i,n}^{OPexp} - W_{i,n}^{OPcalc})^2 + (W_{i,n}^{APexp} - W_{i,n}^{APcalc})^2}{2 \cdot NLa \cdot NCn}}{\#}} \quad (17)$$

The subgroups chosen to represent the fatty acids systems were as follows: CH_3 , CH_2 , CH , $CH = CH$, $COOH$, CH_2COO , H_2O , and ethanol, $EtOH$. Only the binary interaction parameters corresponding to water and ethanol were estimated in this study.

In order to reduce the number of components considered in the interaction parameter estimation methodology, the pseudo-component approach can be used to characterize a complex mixture as a single component [9]. Several authors had successfully applied this approach assuming the vegetable oil as a single pseudo component with an average molar mass and average physical-chemical properties [4, 9, 17, 19, 20, 26, 28, 30–32, 35, 39–43].

Based on the results of the reported studies, it is assumed that the use of the described methodology does not cause expressive deviations in the thermodynamic modeling of deacidification and biodiesel separation systems. Therefore, each vegetable oil was replaced by a pseudo component, and the same approach was used for commercial fatty acids. The pseudo component is a thermodynamic tool applied to represent the edible oil as a single TAG and FFAs as a unique FFA. A weighted average of the vegetable oil and FFA molar masses and subgroup numbers was applied to each pseudo component, considering the fatty acid profile of each vegetable oil, [2–4, 20, 31, 32, 39–42]. The molar mass data of the components were obtained from the NIST Chemistry WebBook database.

3. Results and discussion

For biodiesel separation system, the methodology was initially applied to fit parameters for the new interaction subgroup representing the ethanol molecule ($EtOH-B$), while the UNIFAC-LL for the subgroups forming the other components of the system (ethyl biodiesel and glycerol) remained unchanged. The fitting process used seven ethyl biodiesel from soybean, canola, palm, *jatropha curcas*, cottonseed, crambe, and sunflower oils available in the literature. **Table 3** summarizes the UNIFAC-LL parameters [29] used and the interaction parameters fitted for the new $EtOH-B$ subgroup proposed [43].

Subgroup	CH3	CH2	CH	CH=CH	OH	CH2COO	EtOH-B
Rk	0.90	0.67	0.45	1.12	1.00	1.68	2.11
Qk	0.85	0.54	0.23	0.87	1.20	1.42	1.97
CH3	0.00	0.00	0.00	74.54	644.60	972.40	3582.81
CH2	0.00	0.00	0.00	74.54	644.60	972.40	3582.81
CH	0.00	0.00	0.00	74.54	644.60	972.40	3582.81
CH=CH	292.30	292.30	292.30	0.00	724.40	-577.50	241.75
OH	328.20	328.20	328.20	470.70	0.00	195.60	5299.17
CH2COO	-320.10	-320.10	-320.10	485.60	180.60	0	-395.51
EtOH-B	-53.92	-53.92	-53.92	-4658.24	-550.58	106.42	0.00

Table 3. UNIFAC interaction parameters for CH₃, CH₂, CH, CH = CH, COOH, CH₂COO, H₂O, and EtOH subgroups.

The bold numbers are the fitted one.

Figures 2 and 3 show the experimental points and calculated tie-lines obtained using the new interaction parameters summarized in Table 3 for different types of biodiesel. For all diagrams presented in this chapter, the following classification is valid:

- △ and ▲ for experimental and calculated points, respectively;
- and ■ for experimental and calculated overall composition, respectively;
- - - and — for experimental and calculated tie-lines;
- . - for experimental binodal line;

The tie-lines overlapping seen in Figures 2 and 3 suggest that the fitted UNIFAC parameters for the proposed EtOH subgroup can predict the behavior of the systems considered with high accuracy.

In order to validate these new fitted EtOH parameters, we perform a liquid-liquid equilibrium prediction for ethyl biodiesel from macauba pulp, which was not used during the parameter fitting process.

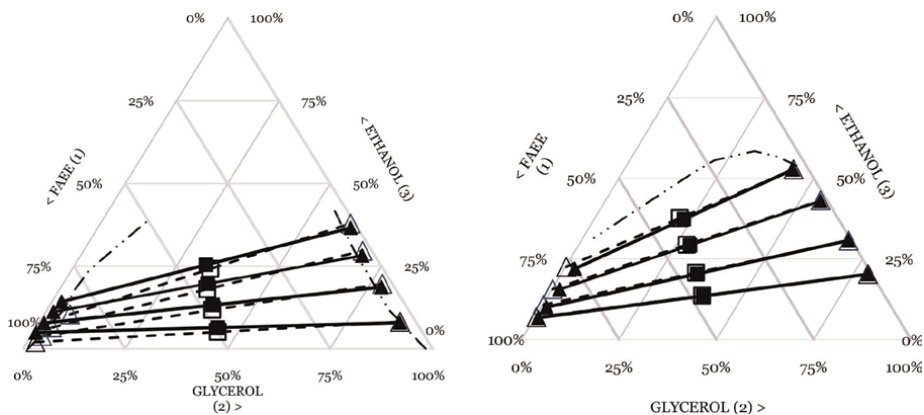


Figure 2. Ternary LLE diagram for the ethyl biodiesel from soybean oil system at 293.15 K (left) and jatropha curcas oil at 318.15 K (right). Experimental data from [14, 36], respectively.

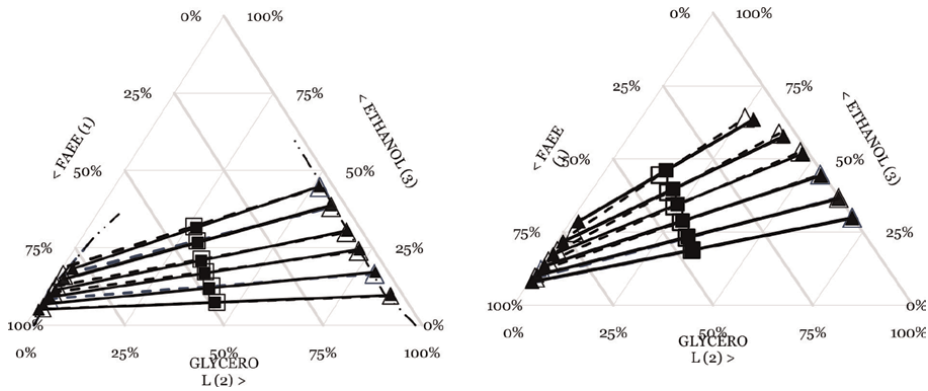


Figure 3. Ternary LLE diagram for the ethyl biodiesel from cottonseed oil system at 333.15 K (left) and crambe oil at 298.2 K (right). Experimental data from [19, 38], respectively.

Figure 4 shows the results of this prediction in the form of a ternary diagram, which exhibit small deviations from the experimental data, thus validating the methodology used.

The results obtained in the fitting and validation processes were then compared with UNIFAC parameters proposed by Magnussen et al. [29] and Bessa et al. [35]. The UNIFAC-LL database fitted by Magnussen et al. [29] in 1981 is extensively widespread and applied to describe fatty systems equilibrium [47–49]. A more recent research by Bessa and collaborators [35] refitted all interaction parameters of the UNIFAC-LL and proposed a new OH subgroup used to represent uniquely this subgroup present in the glycerol molecule, thus having to fit 42 interaction parameters.

Table 4 shows the percentage mean square error (MSE%). The results using the parameters proposed by Machado et al. [43] are always better than those using the Magnussen et al. [29] and Bessa et al. [35] parameters.

Figure 5 shows ternary LLE diagrams for the ethyl biodiesel from macauba pulp oil system comparison with Bessa et al. [35] fitted parameters (left) and with UNIFAC-LL parameters (right).

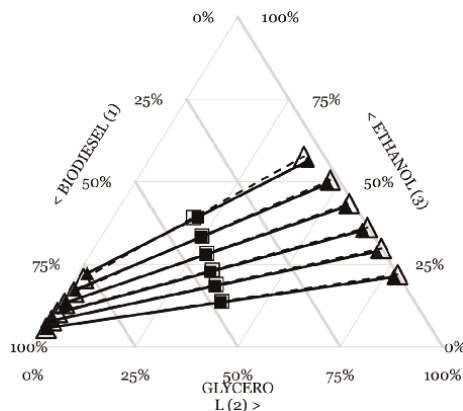


Figure 4. Ternary LLE diagram for the ethyl biodiesel from macauba pulp oil system at 298.15 K for validation procedure. Experimental data from [33].

Biodiesel	T (K)	MSE (%)		
		UNIFAC-LL [29]	Bessa et al. [35]	Machado et al. [43]
Soybean	293.15	21.07	4.68	0.98
	323.15	30.30	2.77	2.08
Canola	303.15	4.41	2.75	2.13
Palm	298.15	4.62	3.25	0.73
	323.15	4.61	2.54	0.76
<i>Jatropha curcas</i>	303.15	5.62	4.04	1.34
	318.15	5.83	4.01	0.85
	333.15	15.33	5.09	1.55
Macauba pulp	298.15	5.22	3.49	0.87
Cottonseed	293.15	5.16	4.49	1.20
	313.15	5.72	4.45	0.96
	333.15	5.59	4.13	0.87
Crambe	298.15	11.00	4.76	1.50
	318.2	10.07	5.69	1.14
Sunflower	298.15	3.53	2.99	0.92
	313.15	4.17	3.54	1.23
MSE%		8.89	3.92	1.20

Table 4. Comparative percentage mean square error (MSE%) for this study's fitting and the literature (EtOH).

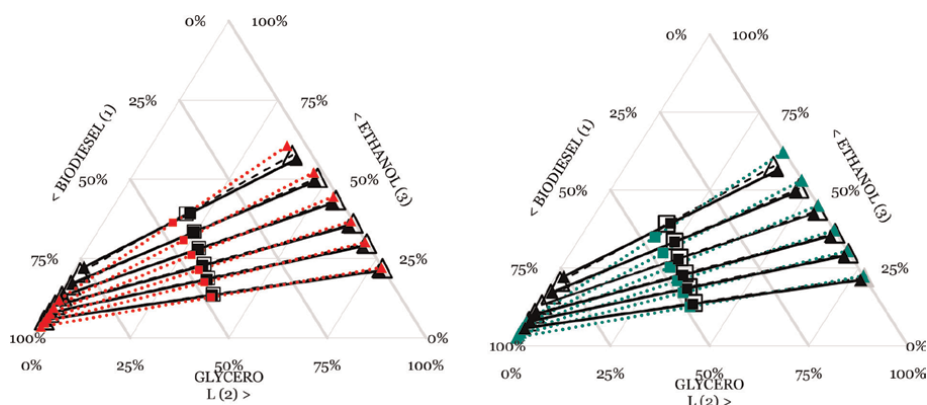


Figure 5. Ternary LLE diagram for the ethyl biodiesel from macauba pulp oil system at 298.15 K comparison with the Bessa et al. [35] (left, red tie-lines); and with the UNIFAC-LL [29] data (right, green tie-lines). Experimental data from ref. [19].

Figure 5 (right) shows that the UNIFAC-LL results have large deviations and the use of such parameters to predict equilibrium between the glycerol-rich phase and the biodiesel-rich phase for the systems considered by Machado et al. [43] is not

recommended. Although the parameters fitted by Bessa et al. [35] could better describe the LLE than the UNIFAC-LL [29] parameters, still there is considerable discrepancy between the predictions and the experimental data. Such observations corroborate the results shown in **Table 4**. **Figure 4** shows that ethanol subgroup fitting tie-lines represent considerably better the equilibrium of the biodiesel-rich phase with the glycerol-rich phase. It is worth mentioning that, only eight parameters were fitted, while Bessa et al. [35] considered 42 adjustable parameters in their study.

For deacidification system, the methodology was initially applied to fit parameters for the new interaction subgroup representing the ethanol molecule (EtOH-D) and H₂O subgroups, while the UNIFAC-LL for the subgroups forming the other components of the system (vegetable oil and free fatty acids—FFA) remained unchanged. The fitting process used experimental LLE data of 17 (Brazil nut, corn, cottonseed, garlic, grapeseed, *jatropha curcas*, macadamia, palm, peanut, rice bran, sesame, soybean, and sunflower) different vegetable oils available in the literature. **Table 5** shows the original UNIFAC-LL [29] parameters used and the interaction parameters fitted for the water (H₂O) and EtOH-D subgroups.

Figures 6 and **7** show the experimental points and calculated tie-lines obtained using the new interaction parameters summarized in **Table 5** for corn and soybean oil. Due to the systems presenting different water contents added to the ethanol solvent, ethanol and water were used as a mixed solvent to represent the pseudo-quaternary systems in a triangular diagram.

Analyzing **Figures 6** and **7** it can be noted an inversion in the tie-line slopes as water is added to the solvent. This phenomenon occurs because water decreases the solubility between oil and ethanol; hence, it increases the two-liquid phase regions [30, 32, 39, 42].

The ternary diagrams presented in **Figures 6** and **7** show that the calculated results are very close to the experimental data. Therefore, the H₂O and EtOH-D adjusted interaction parameters using the UNIFAC model correlated with the high accuracy of the LLE behavior of the considered system containing fatty acids.

Table 6 compares the RMSD from the experimental mass fraction data from the calculated data obtained by UNIFAC modeling using the parameters fitted by Bacicheti et al. [27] for EtOH-D subgroup with those obtained using parameters available in the literature (UNIFAC-LL from Magnussen et al. [29]), Noriega and Narváez [28], Hirata et al. [26]). **Table 6** still presents the RMSD between experimental and calculated data obtained using Machado et al. [43] parameter set.

Subgroup	CH ₃ , CH ₂ , CH	CH=CH	H ₂ O	COOH	CH ₂ COO	ETOH-D
CH ₃ , CH ₂ , CH	0	74.54	962.89	139.40	972.40	624.24
CH=CH	292.30	0	6337.07	1647.00	-577.50	537.49
H ₂ O	94.39	-134.08	0	363.72	-609.05	-277.75
COOH	1744.00	-48.52	-250.67	0	-117.60	-283.55
CH ₂ COO	-320.10	485.60	1716.74	1417.00	0	867.81
EtOH-D	-44.17	-61.21	8003.65	1117.01	-493.44	0

Table 5. UNIFAC-LL [29] parameters and 18 interaction parameters fitted for H₂O and EtOH-D subgroups.

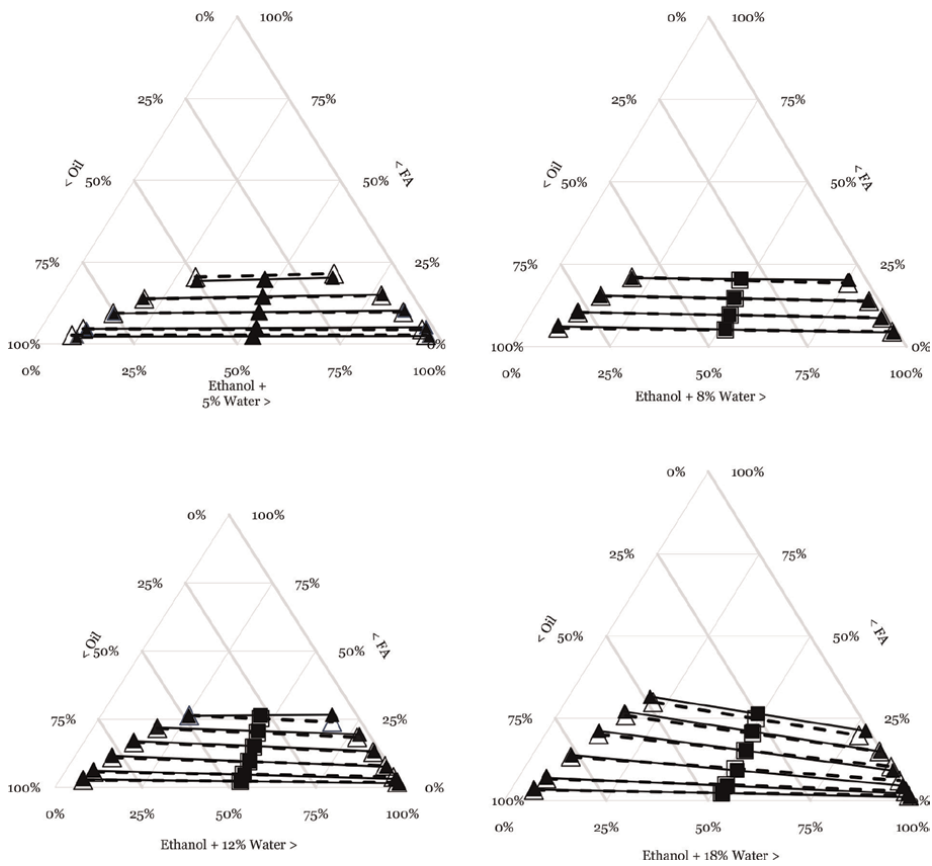


Figure 6. LLE diagram for corn oil + commercial oleic acid 1 + and solvent (ethanol + %water) system at 298.15 K [31]. All compositions are on a mass basis.

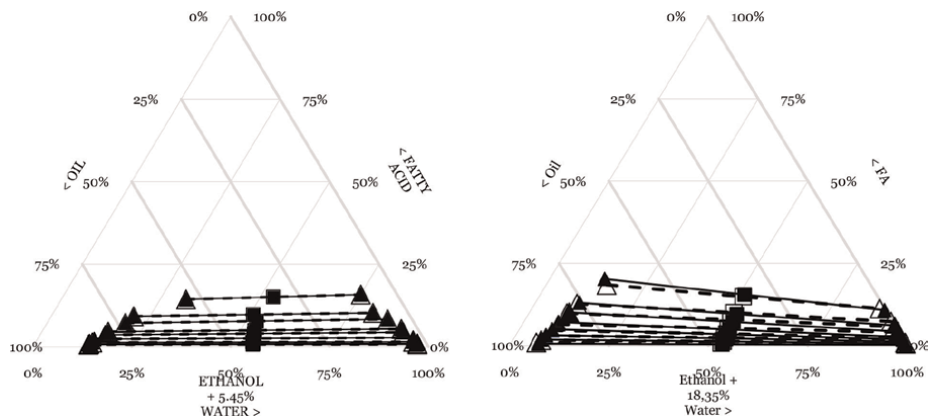


Figure 7. LLE diagram for soybean oil + commercial linoleic acid 1 + and solvent (ethanol + water) system at 323.15 K [42]. All compositions are on a mass basis.

Oil	T (K)	RMSD (by mass)				
		UNIFAC-LL [29]	Noriega and Narváez [28]	Hirata et al. [26]	Machado et al. [43]	Bacicheti et al. [27]
Brazil nut	298.15	5.95	11.49	0.72	10.90	0.52
Corn	303.15	10.11	14.25	0.93	9.94	0.78
Cottonseed	298.15	9.59	13.63	2.59	12.13	0.90
Garlic	298.15	11.81	12.98	0.63	11.32	0.58
Grapeseed	318.15	7.75	11.90	1.85	12.58	0.77
Jatropha	288.15	9.37	11.05	0.73	11.46	0.89
	298.15	11.99	16.02	0.67	10.31	0.76
	308.15	13.91	16.83	0.64	9.27	0.86
	318.15	15.19	11.49	0.75	8.90	0.59
Macadamia	298.15	5.28	12.11	1.97	10.06	1.77
Palm	318.15	3.74	15.45	0.46	7.19	1.63
Peanut	298.15	11.15	14.04	1.15	11.36	0.72
Rice bran	298.15	10.56	16.46	1.12	11.43	0.59
Sesame	298.15	8.57	12.23	1.42	11.62	0.75
Soybean	323.15	4.74	18.73	1.34	10.18	0.60
Sunflower (O)	298.15	5.53	10.27	2.29	12.27	0.97
Sunflower (L)	298.15	11.63	9.35	2.13	12.72	1.01
Global RMSD%		9.24	13.43	1.27	10.81	0.87

Table 6. Root mean square deviation (RMSD for fittings in this chapter and the literature.

As commented previously, Noriega and Narvaez [28] fitted 30 UNIFAC parameters of the subgroups related to pseudo-ternary and pseudo-quaternary systems of biodiesel + alcohol + glycerol and oil + fatty acid + alcohol + water. Hirata et al. [26] used plenty of pseudo-quaternary data available in the literature to fit all the 30 UNIFAC interaction parameters of interest for fatty systems. The present study adjusted only 16 interaction parameters for pseudo-ternary biodiesel systems and adjusted only 18 interaction parameters for pseudo-quaternary deacidification systems.

The global RMSD displayed in **Table 6** shows that the parameters set proposed by UNIFAC-LL [29] and Noriega and Narváez [28] are not suitable to describe the liquid-liquid equilibrium of deacidification and biodiesel-related systems. The global RMSD using UNIFAC-LL and Noriega and Narváez [28] were 9.24 and 13.43, respectively, while using the parameters fitted by Bacicheti et al. [27] resulted in a global RMSD of 0.87.

The considerable difference in RMSD between experimental and calculated data applying Machado et al. [43] parameter set (10.81%) and Bacicheti et al. [27] parameter set (0.87%) subgroup parameters emphasize the difference in ethanol subgroup in biodiesel separation and deacidification systems due to water and glycerol molecules in the system.

It was expected that Noriega and Narváez [28] parameters and Machado et al. [43] parameter set resulted in slightly high deviations (**Table 6**) since they were adjusted to biodiesel systems. But we were expecting that the other UNIFAC subgroups (CH_3 , CH_2 , CH , $\text{CH} = \text{CH}$, COOH , CH_2COO) would be able to represent the liquid-liquid equilibrium behavior, giving a fair and enough performance of UNIFAC model. However, the presence of water is too sharp, turning the whole systems distinct and the deviations significant, despite having similar UNIFAC subgroups.

In contrast to results obtained by the other UNIFAC parameter matrices, the RMSD obtained by using Hirata et al. [26] proposed parameters were closer to this study's parameters performance. It is worthy to quote that, although using a similar databank, this chapter ensues in lower RMSD between experimental and calculated data and, moreover, it has the upgrade of adjusting only 18 interaction parameters, resulting in a considerable faster procedure and relatively lower computational calculations than Hirata et al. [26] that fitted 30 interaction parameters.

The validation procedure of the parameters was taken for canola oil system, which was not used in the parameter fitting process. **Table 7** lists the RMSD between the experimental and calculated molar fractions using Bacicheti et al. [27] parameter set with those obtained using UNIFAC-LL from Magnussen et al. [29]), Noriega and Narváez [28], and Hirata et al. [26]). As previously stated, canola oil [18] data did not take part in this study's parameter fitting, but it was used by Hirata et al. [26] in their parameter fitting procedure, resulting in alike RMSD.

According to **Table 7**, the Bacicheti et al. [27] parameter set exhibits lower RMSD values than those obtained by applying the parameter matrix from the previously cited authors; hence the EtOH-D subgroup can successfully describe the deacidification systems of vegetable oils.

Figure 8 exhibits the ternary diagrams for the validation with canola oil data. Bacicheti et al. [27] parameter set exhibited small deviations from the experimental data than the other parameter matrices. In contrast, the results using the Machado et al. [43] parameter set and the parameters of Noriega and Narváez [28] have a considerable deviation from the experimental data, and thus, they are not recommended for quantitatively predicting the equilibrium of deacidification of vegetable oils.

As shown in **Figure 8**, Machado et al. [43] and Noriega and Narváez [28] parameter set, and UNIFAC-LL [29] present the highest average deviation from the experimental points. The average deviation values between the experimental and calculated data obtained using the interaction parameters from Hirata et al. [26] were close to

Oil	T(K)	RMSD% (by mass)				
		UNIFAC-LL [29]	Noriega and Narváez [28]	Hirata et al. [26]	Machado et al. [43]	Bacicheti et al. [27]
Canola	303.15	8.92	11.16	0.46	9.86	0.40

Table 7.

RMSD between experimental and calculated data mass fraction for the validation system composed of canola oil + commercial oleic acid 3 + ethanol + water at 303.15 K.

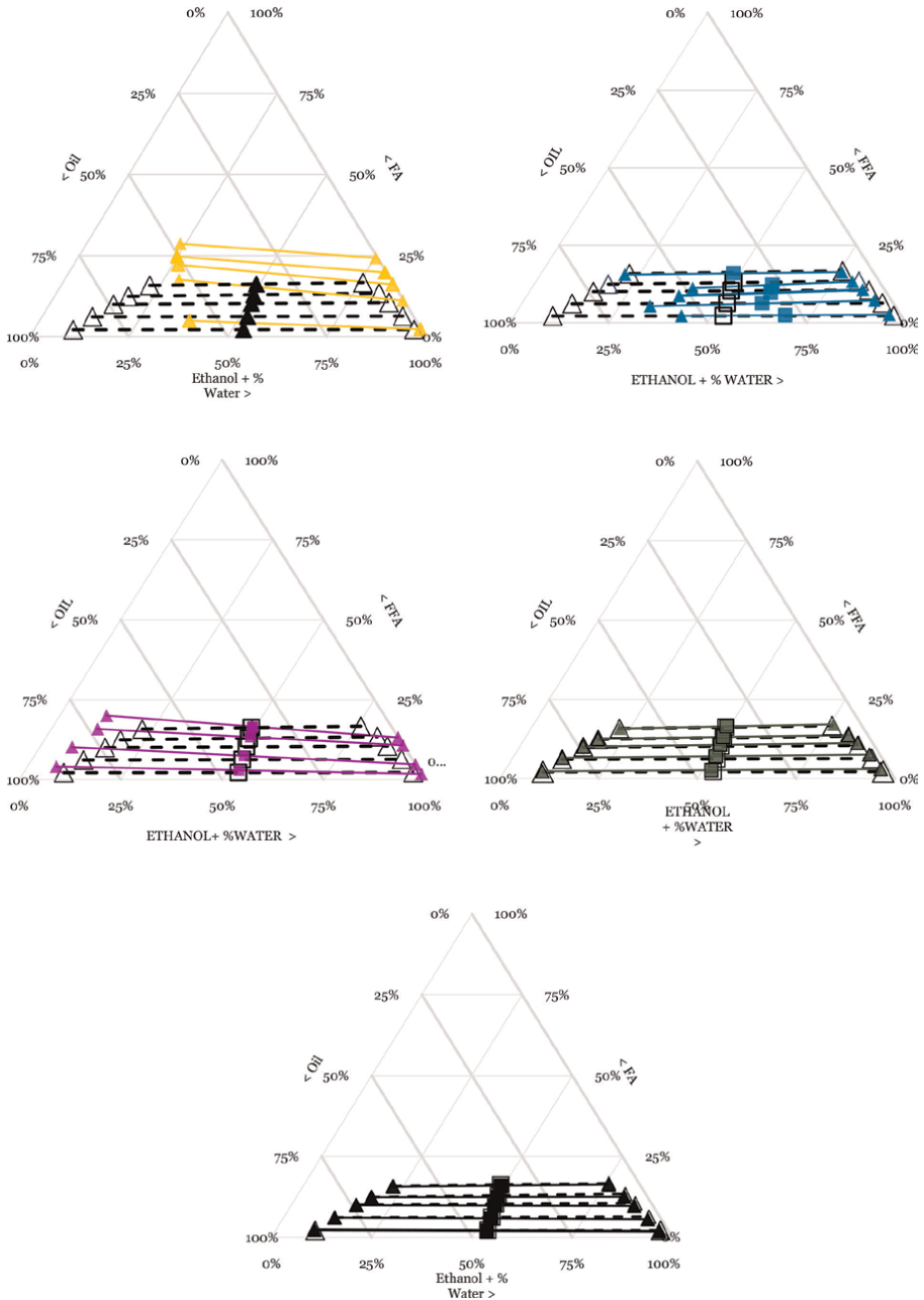


Figure 8. LLE diagram for validation procedure with canola oil system [18]. Comparison between literature data (traced line) with predictions using parameters from Bacicheti et al. [27] (black lines), Noriega and Narváez [28] (yellow lines), Machado et al. [43] (blue lines), UNIFAC-LL [29] (purple lines), and Hirata et al. [26] (green lines). All compositions are on a mass basis.

those obtained by Bacicheti et al. [27]. However, Bacicheti et al. [27] only refitted 18 parameters, taking fewer computational calculations than those required by Hirata et al. [26], who readjusted all of them.

4. Conclusions

The new ethanol subgroups for the UNIFAC model presented in this chapter could correctly and accurately describe the liquid-liquid phase equilibrium of deacidification and biodiesel systems. The ethanol binary interaction parameters were fitted using a data bank of LLE available in the literature for biodiesel vegetable oil systems.

Using relatively few computational calculations and aiming to result in a relatively small split with the complex data set established by the UNIFAC-LL model, Bacicheti et al. [27] maintain CH_3 , CH_2 , CH , $\text{CH} = \text{CH}$, COOH and CH_2COO subgroups parameters, and refitted just water and ethanol UNIFAC interaction parameters. Ethanol-fitted parameters were then validated with very small deviations in the prediction of macauba pulp oil biodiesel for EtOH-B and canola oil for EtOH-D. The overall deviation calculated in the validation of these new UNIFAC parameters was 1.20% for biodiesel systems and 0.87% for deacidification systems.

When compared to prediction results for biodiesel systems using UNIFAC-LL parameters and those fitted by Bessa et al. [35], Machado et al. [43] had better results for the tie-lines, despite the small number of parameters fitted. The same results were obtained considering deacidification systems of vegetable oils, which ethanol interaction parameters proposed by Bacicheti et al. [27] exhibited small deviations from the experimental data and lower deviations than Noriega and Narváez [28], UNIFAC-LL [29], and Hirata et al. [26].

The method applied can contribute to a better description of the phase behavior of fatty systems involved in the deacidification of vegetable oil using liquid-liquid extraction and biodiesel separation process, as this biofuel is subject to strict composition and purity regulations. Moreover, taking into account the lower root mean square deviation between the experimental and calculated molar fractions obtained here and the relatively low computational calculations for the parameter fitting procedure, this chapter presents an easier and faster alternative approach instead to refitting all UNIFAC parameters.

The results show that the methodology employed is consistent and may be useful in predicting equilibrium when experimental equilibrium data are not available.

Funding

This work was supported by the Brazilian agencies CAPES [88887.486092/2020–2100] and CNPq [grant number 421930/2016–0].

Author details

Jacqueline M. Ortega Bacicheti^{1,2}, Guilherme D. Machado^{2,3*}, Fábio Nishiyama^{2,3}, Vladimir F. Cabral^{1,2} and Donato Aranda³


1 Food Engineering Program, State University of Maringá, Maringá, PR, Brazil

2 Chemical Engineering Program, State University of Maringá, Maringá, PR, Brazil

3 Department of Chemical Engineering, Federal Technologic University of Paraná-UTFPR, Londrina, PR, Brazil

*Address all correspondence to: guilhermed@utfpr.edu.br

IntechOpen

© 2023 The Author(s). Licensee IntechOpen. This chapter is distributed under the terms of the Creative Commons Attribution License (<http://creativecommons.org/licenses/by/3.0>), which permits unrestricted use, distribution, and reproduction in any medium, provided the original work is properly cited. 

References

- [1] Sérgio MBO, Soletti BJI, Carvalho SHV, Queimada AJ, Coutinho JAP. Liquid–liquid equilibria for the canola oil biodiesel +ethanol+glycerol system. *Fuel*. 2011;**90**: 2738-2745. DOI: 10.1016/j.fuel.2011.03.017
- [2] Batista E, Monnerat S, Stragevitch L, Pina CG, Gonçalves CB, Meirelles AJA. Prediction of liquid–liquid equilibrium for Systems of Vegetable Oils, fatty acids, and ethanol. *Journal of Chemical & Engineering Data*. 1999;**44**:1365-1369. DOI: 10.1021/jc9900169
- [3] Cuevas MS, Rodrigues CEC, Gomes GB, Meirelles AJA. Vegetable oils Deacidification by solvent extraction: Liquid–liquid equilibrium data for systems containing sunflower seed oil at 298.2 K. *Journal of Chemical & Engineering Data*. 2010;**55**:3859-3862. DOI: 10.1021/jc900791w
- [4] Rodrigues CEC, Reipert ÉCD, de Souza AF, Filho PAP, Meirelles AJA. Equilibrium data for systems composed by cottonseed oil+commercial linoleic acid+ethanol+water+tocopherols at 298.2K. *Fluid Phase Equilibria*. 2005;**238**: 193-203. DOI: 10.1016/j.fluid.2005.09.027
- [5] Tripathy D, Mohanty P, Dhindsa S, Syed T, Ghanim H, Aljada A, et al. Elevation of free fatty acids induces inflammation and impairs vascular reactivity in healthy subjects. *Diabetes*. 2003;**52**:2882-2887. DOI: 10.2337/diabetes.52.12.2882
- [6] Röhrig F, Schulze A. The multifaceted roles of fatty acid synthesis in cancer. *Nature Reviews. Cancer*. 2016;**16**: 732-749. DOI: 10.1038/nrc.2016.89
- [7] Scoville EA, Allaman MM, Adams DW, Motley AK, Peyton SC, Ferguson SL, et al. Serum polyunsaturated fatty acids correlate with serum cytokines and clinical disease activity in Crohn's disease. *Scientific Reports*. 2019;**9**:2882. DOI: 10.1038/s41598-019-39232-z
- [8] Tsoukalas D, Fragoulakis V, Sarandi E, Docea AO, Papakonstaninou E, Tsilimidos G, et al. Targeted Metabolomic analysis of serum fatty acids for the prediction of autoimmune diseases. *Frontiers in Molecular Biosciences*. 2019;**6**:120. DOI: 10.3389/fmolb.2019.00120
- [9] Rodrigues CEC, Meirelles AJA. Extraction of free fatty acids from Peanut oil and avocado seed oil: Liquid–liquid equilibrium data at 298.2 K. *Journal of Chemical & Engineering Data*. 2008;**53**:1698-1704. DOI: 10.1021/jc7007186
- [10] Rodrigues CEC, Gonçalves CB, Marcon EC, Batista EAC, Meirelles AJA. Deacidification of rice bran oil by liquid–liquid extraction using a renewable solvent. *Separation and Purification Technology*. 2014;**132**:84-92. DOI: 10.1016/j.seppur.2014.05.009
- [11] Lu W, Xu Z, Li M, Ma Y, Xiao Z. Deep eutectic solvent (DES) assisted deacidification of acidic oil and retaining catalyst activity: Variables optimization and catalyst characterization. *Industrial Crops and Products*. 2022;**183**:114990. DOI: 10.1016/j.indcrop.2022.114990
- [12] Hajjari M, Tabatabaei M, Aghbashlo M, Ghanavati H. A review on the prospects of sustainable biodiesel production: A global scenario with an emphasis on waste-oil biodiesel utilization. *Renewable and Sustainable Energy Reviews*. 2017;**72**:445-464. DOI: 10.1016/j.rser.2017.01.034

- [13] Mu T, Rarey J, Gmehling J. Group contribution prediction of surface charge density profiles for COSMO-RS(OI). *AIChE Journal*. 2007;**53**:3231-3240. DOI: 10.1002/aic.11338
- [14] Silva JRF, Mazutti MA, Voll FAP, Cardozo-Filho L, Corazza ML, Lanza M, et al. Thermophysical properties of biodiesel and related systems: (liquid+liquid) equilibrium data for *Jatropha curcas* biodiesel. *The Journal of Chemical Thermodynamics*. 2013;**58**:467-475. DOI: 10.1016/j.jct.2012.10.006
- [15] Mazutti MA, Voll FAP, Cardozo-Filho L, Corazza ML, Lanza M, Priamo WL, et al. Thermophysical properties of biodiesel and related systems: (liquid+liquid) equilibrium data for soybean biodiesel. *The Journal of Chemical Thermodynamics*. 2013;**58**: 83-94. DOI: 10.1016/j.jct.2012.10.026
- [16] Bou Orm R, Citeau M, Comitis A, Savoie R, Harscoat-Schiavo C, Subra-Paternault P, et al. Walnut oil deacidification by liquid-liquid extraction with ethanol in a single- and multistage crossflow process. *OCL*. 2020;**27**:35. DOI: 10.1051/ocl/2020029
- [17] Mohsen-Nia M, Modarress H, Nabavi HR. Measuring and modeling liquid-liquid equilibria for a soybean oil, oleic acid, ethanol, and water system. *Journal of the American Oil Chemists' Society*. 2008;**85**:973-978. DOI: 10.1007/s11746-008-1288-9
- [18] Batista E, Monnerat S, Kato K, Stragevitch L, Meirelles AJA. Liquid-liquid equilibrium for Systems of Canola oil, oleic acid, and short-chain alcohols. *Journal of Chemical & Engineering Data*. 1999;**44**:1360-1364. DOI: 10.1021/jc990015g
- [19] Basso RC, de Almeida Meirelles AJ, Batista EAC. Liquid-liquid equilibrium of pseudoternary systems containing glycerol+ethanol+ethylic biodiesel from crambe oil (*Crambe abyssinica*) at T/K= (298.2, 318.2, 338.2) and thermodynamic modeling. *Fluid Phase Equilibria*. 2012; **333**:55-62. DOI: 10.1016/j.fluid.2012.07.018
- [20] da Silva CAS, Sanaiotti G, Lanza M, Meirelles AJA, Batista EAC. Liquid-liquid equilibrium data for systems containing *Jatropha curcas* oil + oleic acid + anhydrous ethanol + water at (288.15 to 318.15) K. *Journal of Chemical & Engineering Data*. 2010;**55**:2416-2423. DOI: 10.1021/jc900831p
- [21] da Silva AE, Lanza M, Batista EAC, Rodrigues AMC, Meirelles AJA, da Silva LHM. Liquid-liquid equilibrium data for systems containing palm oil fractions + fatty acids + ethanol + water. *Journal of Chemical & Engineering Data*. 2011;**56**:1892-1898. DOI: 10.1021/jc1009015
- [22] Mohsen-Nia M, Dargahi M. Liquid-liquid equilibrium for systems of (corn oil + oleic acid + methanol or ethanol) at (303.15 and 313.15) K, *Journal of Chemical & Engineering Data* 52 (2007) 910-914. doi:10.1021/jc700051j
- [23] Serres JDS, Soares D, Corazza ML, Krieger N, Mitchell DA. Liquid-liquid equilibrium data and thermodynamic modeling for systems related to the production of ethyl esters of fatty acids from soybean soapstock acid oil. *Fuel*. 2015;**147**:147-154. DOI: 10.1016/j.fuel.2015.01.059
- [24] Mohsen-Nia M, Khodayari A. De-acidification of sunflower oil by solvent extraction: (liquid+liquid) equilibrium data at T=(303.15 and 313.15) K. *The Journal of Chemical Thermodynamics*. 2008;**40**:1325-1329. DOI: 10.1016/j.jct.2008.01.029

- [25] Ferreira MC, Bessa LCBA, Abreu CRA, Meirelles AJA, Caldas Batista EA. Liquid-liquid equilibrium of systems containing triolein + (fatty acid/partial acylglycerols/ester) + ethanol: Experimental data and UNIFAC modeling. *Fluid Phase Equilibria*. 2018; **476**:186-192. DOI: 10.1016/j.fluid.2018.07.030
- [26] Hirata GF, Abreu CRA, Bessa LCBA, Ferreira MC, Batista EAC, Meirelles AJA. Liquid-liquid equilibrium of fatty systems: A new approach for adjusting UNIFAC interaction parameters. *Fluid Phase Equilibria*. 2013; **360**:379-391. DOI: 10.1016/j.fluid.2013.10.004
- [27] Bacicheti JMO, Machado GD, Cabral VF. Liquid-liquid equilibrium calculations of systems containing vegetable oil + fatty acids + ethanol + water using new parameters for the unifac subgroups of ethanol and water. *Fluid Phase Equilibria*. 2021; **548**:113182. DOI: 10.1016/j.fluid.2021.113182
- [28] Noriega MA, Narváez PC. UNIFAC correlated parameters for liquid-liquid equilibrium prediction of ternary systems related to biodiesel production process. *Fuel*. 2019; **249**:365-378. DOI: 10.1016/j.fuel.2019.03.124
- [29] Magnussen T, Rasmussen P, Fredenslund A. UNIFAC parameter table for prediction of liquid-liquid equilibria. *Industrial & Engineering Chemistry Process Design and Development*. 1981; **20**:331-339. DOI: 10.1021/i200013a024
- [30] Reipert ÉCD, Rodrigues CEC, Meirelles AJA. Phase equilibria study of systems composed of refined babassu oil, lauric acid, ethanol, and water at 303.2K. *The Journal of Chemical Thermodynamics*. 2011; **43**:1784-1790. DOI: 10.1016/j.jct.2011.05.039
- [31] Gonçalves CB, Batista E, Meirelles AJA. Liquid-liquid equilibrium data for the system corn oil + oleic acid + ethanol + water at 298.15 K. *Journal of Chemical & Engineering Data*. 2002; **47**: 416-420. DOI: 10.1021/je010273p
- [32] Rodrigues CEC, Silva FA, Marsaioli A, Meirelles AJA. Deacidification of Brazil nut and macadamia nut oils by solvent extraction: Liquid-liquid equilibrium data at 298.2 K. *Journal of Chemical & Engineering Data*. 2005; **50**:517-523. DOI: 10.1021/je049687j
- [33] Basso RC, da Silva CAS, de Sousa CO, de Meirelles AJA, Batista EAC. LLE experimental data, thermodynamic modeling and sensitivity analysis in the ethyl biodiesel from macauba pulp oil settling step. *Bioresource Technology*. 2013; **131**:468-475. DOI: 10.1016/j.biortech.2012.12.190
- [34] Fredenslund A, Jones RL, Prausnitz JM. Group-contribution estimation of activity coefficients in nonideal liquid mixtures. *AIChE Journal*. 1975; **21**:1086-1099. DOI: 10.1002/aic.690210607
- [35] Bessa LCBA, Ferreira MC, Abreu CRA, Batista EAC, Meirelles AJA. A new UNIFAC parameterization for the prediction of liquid-liquid equilibrium of biodiesel systems. *Fluid Phase Equilibria*. 2016; **425**:98-107. DOI: 10.1016/j.fluid.2016.05.020
- [36] Mesquita FMR, Feitosa FX, Sombra NE, de Santiago-Aguiar RS, de Sant'Ana HB. Liquid-liquid equilibrium for ternary mixtures of biodiesel (soybean or sunflower) + glycerol + ethanol at different temperatures. *Journal of Chemical & Engineering Data*. 2011; **56**:4061-4067. DOI: 10.1021/je200340x

- [37] de Rocha EGA, Follegatti-Romero LA, Duvoisin S, Aznar M. Liquid-liquid equilibria for ternary systems containing ethylic palm oil biodiesel+ethanol +glycerol/water: Experimental data at 298.15 and 323.15K and thermodynamic modeling. *Fuel*. 2014;**128**:356-365. DOI: 10.1016/j.fuel.2014.01.074
- [38] Mesquita FMR, Bessa AMM, de Lima DD, de Sant'Ana HB, de Santiago-Aguiar RS. Liquid-liquid equilibria of systems containing cottonseed biodiesel +glycerol+ethanol at 293.15, 313.15 and 333.15K. *Fluid Phase Equilibria*. 2012;**318**: 51-55. DOI: 10.1016/j.fluid.2012.01.016
- [39] Rodrigues CEC, Filipini A, Meirelles AJA. Phase equilibrium for systems composed by high unsaturated vegetable oils + linoleic acid + ethanol + water at 298.2 K. *Journal of Chemical & Engineering Data*. 2006;**51**:15-21. DOI: 10.1021/jc0495841
- [40] Gonçalves CB, Meirelles AJA. Liquid-liquid equilibrium data for the system palm oil + fatty acids + ethanol + water at 318.2K. *Fluid Phase Equilibria*. 2004;**221**:139-150. DOI: 10.1016/j.fluid.2004.05.002
- [41] Rodrigues CEC, Antoniassi R, Meirelles AJA. Equilibrium data for the system Rice bran oil + fatty acids + ethanol + water at 298.2 K. *Journal of Chemical & Engineering Data*. 2003;**48**: 367-373. DOI: 10.1021/jc0255978
- [42] Rodrigues CEC, Peixoto ECD, Meirelles AJA. Phase equilibrium for systems composed by refined soybean oil +commercial linoleic acid+ethanol +water, at 323.2K. *Fluid Phase Equilibria*. 2007;**261**:122-128. DOI: 10.1016/j.fluid.2007.07.021
- [43] Machado GD, Castier M, Voll AP, Cabral VF, Cardozo-Filho L, Aranda DAG. Ethanol and methanol Unifac subgroup parameter estimation in the prediction of the liquid-liquid equilibrium of biodiesel systems. *Fluid Phase Equilibria*. 2019;**488**:79-86. DOI: 10.1016/j.fluid.2019.01.012
- [44] Castier M, Amer MM. XSEOS: An evolving tool for teaching chemical engineering thermodynamics. *Education for Chemical Engineers*. 2011;**6**:e62-e70. DOI: 10.1016/j.ece.2010.12.002
- [45] Lasdon LS, Waren AD, Jain A, Ratner M. Design and testing of a generalized reduced gradient code for nonlinear programming. *ACM Transactions on Mathematical Software*. 1978;**4**:34-50. DOI: 10.1145/355769.355773
- [46] Magnussen T, Rasmussen P, Fredenslund A. UNIFAC parameter table for prediction of liquid-liquid equilibria. *Industrial & Engineering Chemistry Process Design and Development*. 1981;**20**:331-339. DOI: 10.1021/i200013a024
- [47] Homrich POB, Ceriani R. Phase equilibria for systems containing refined soybean oil plus Cosolvents at different temperatures. *Journal of Chemical & Engineering Data*. 2018;**63**:1937-1945. DOI: 10.1021/acs.jced.7b01051
- [48] Homrich POB, Dias LG, Mariutti LRB, Bragagnolo N, Ceriani R. Liquid-liquid equilibria and density data for pseudoternary systems of refined soybean oil + (hexanal, or heptanal, or butyric acid, or valeric acid, or caproic acid, or caprylic acid) + dimethyl sulfoxide at 298.15 K. *The Journal of Chemical Thermodynamics*. 2019;**131**: 149-158. DOI: 10.1016/j.jct.2018.10.030
- [49] Kanda LR, Voll FAP, Corazza ML. LLE for the systems ethyl palmitate (palmitic acid)(1)+ethanol(2)+glycerol (water)(3). *Fluid Phase Equilibria*. 2013;**354**:147-155. DOI: 10.1016/j.fluid.2013.06.027



*Edited by Rampal Pandey, Israel Pala-Rosas,
José L. Contreras and José Salmones*

Due to their unique physicochemical properties, low cost, and wide availability, ethanol and glycerol have gained attention for their use as alternative feedstocks in the sustainable production of several commodity and specialty products. As a result, during the last decades, there has been intense research aimed at developing the potential applications of these biomass-derived compounds. *Ethanol and Glycerol Chemistry - Production, Modelling, Applications, and Technological Aspects* discusses recent advances and different aspects of the production, direct applications, and processing of ethanol and glycerol from a multidisciplinary perspective that includes the medical field, fuels, and chemical synthesis.

Published in London, UK

© 2023 IntechOpen
© Perception7 / iStock

IntechOpen

